STEPHANIE SANTOS SUEHIRO ARCOS

Estudo das atividades antitumorais de peptídeos presentes no veneno do escorpião amarelo *Tityus serrulatus*

Dissertação apresentada ao Programa de Pós-Graduação Interunidades em Biotecnologia da Universidade de São Paulo, Instituto Butantan e Instituto de Pesquisas Tecnológicas, para obtenção de Título de de Mestre em Biotecnologia.

São Paulo
2022

STEPHANIE SANTOS SUEHIRO ARCOS

Estudo das atividades antitumorais de peptídeos presentes no veneno do escorpião amarelo *Tityus serrulatus*

Dissertação apresentada ao Programa de Pós-Graduação Interunidades em Biotecnologia da Universidade de São Paulo, Instituto Butantan e Instituto de Pesquisas Tecnológicas, para obtenção de Título de Mestre em Biotecnologia.

Área de concentração: Biotecnologia

Orientador: Dr Leo Kei Iwai

Coorientadora: Dra Fernanda C. V. Portaro

Versão corrigida. A versão original eletrônica, encontra-se disponível tanto na Biblioteca no ICB quanto na Biblioteca Digital de Teses e Dissertações da USP (BDTD).

São Paulo
2022

CATALOGAÇÃO NA PUBLICAÇÃO (CIP)
Serviço de Biblioteca e Informação Biomédica do
Instituto de Ciências Biomédicas da Universidade de São Paulo

Ficha Catalográfica elaborada pela autora

Arcos, Stephanie Santos Suehiro
Estudo das atividades antitumorais de peptídeos presentes no veneno do escorpião amarelo *Tityus srrulatus* / Stephanie Santos Suehiro Arcos; Orientador: Dr Leo Kei Iwai; Coorientadora: Dra Fernanda Calheta Vieira Portaro. – São Paulo, 2022
154 p.

Dissertação (mestrado) – Universidade de São Paulo. Instituto de Ciências Biomédicas, Programa de Pós-Graduação Interunidades em Biotecnologia USP/IPT/Instituto Butantan. Área de concentração: Biotecnologia. Linha de pesquisa: Toxinas e sistemas biológicos.

Versão do título para o inglês: Study of the antitumor activities of peptides present in the venom of the yellow scorpion *Tityus serrulatus*

1. Peptídeo 2. Tityus serrulatus 3. Peçonha de escorpião 4. Câncer 5. Linhagens celulares I. Iwai, Dr Leo Kei II.Portaro, Dra Fernanda Calheta Vieira. III. Estudo das atividades antitumorais de peptídeos presentes no veneno do escorpião amarelo *Tityus serrulatus*

UNIVERSIDADE DE SÃO PAULO
Programa de Pós-Graduação Interunidades em Biotecnologia
Universidade de São Paulo, Instituto Butantan, Instituto de Pesquisas Tecnológicas

Candidata: Stephanie Santos Suehiro Arcos

Título da dissertação: Estudo das atividades antitumorais de peptídeos presentes no veneno do escorpião amarelo *Tityus serrulatus*.

Orientador: Prof. Dr Leo Kei Iwai.

A Comissão Julgadora dos trabalhos de Defesa da Dissertação, em sessão pública realizada a / / , considerou a candidata:

( ) Aprovada ( ) Reprovada

Examinador(a) Assinatura:.....

Nome:.....

Instituição:.....

Examinador(a) Assinatura:.....

Nome:.....

Instituição:.....

Examinador(a) Assinatura:.....

Nome:.....

Instituição:.....

Presidente: Assinatura:.....

Nome:

Instituição:

INSTITUTO BUTANTAN
A serviço da vida

Comissão de Ética no Uso de Animais

São Paulo, 06 de julho de 2022
CEUAx N 6893040219

Ilmo(a). Sr(a).
Responsável: Leo Kei Iwai E Fernanda Portaro
Executor: Stephanie Santos Suehiro Arcos
Área: Biotecnologia

Título do projeto: " Estudo das atividades antitumorais de peptídeos presentes no veneno de escorpião amarelo Tityus serrulatus".

Parecer Consubstanciado da CEUA IB

A Comissão de Ética no Uso de Animais da Instituto Butantan, na reunião de 20/02/2019, **ANALISOU** e **APROVOU** o protocolo de estudo acima referenciado. A partir desta data, é dever do pesquisador:

1. Comunicar toda e qualquer alteração do protocolo.
2. Comunicar imediatamente ao Comitê qualquer evento adverso ocorrido durante o desenvolvimento do protocolo.
3. Os dados individuais de todas as etapas da pesquisa devem ser mantidos em local seguro por 5 anos para possível auditoria dos órgãos competentes.
4. **Relatórios parciais** de andamento deverão ser enviados **anualmente** à CEUA até a conclusão do protocolo.

Maria Leonor Sarno de Oliveira
Coordenador da Comissão de Ética no Uso de Animais
Instituto Butantan

Nancy Oguiura
Vice-Coordenadora da Comissão de Ética no Uso de Animais
Instituto Butantan

INSTITUTO BUTANTAN
A serviço da vida

Comissão de Ética no Uso de Animais

São Paulo, 6th July 2022

CERTIFIED

We certify that the Research "Study of the antitumor activities of peptides derived from Tityus serrulatus scorpion", protocol number CEUAx 6893040219 (ID 000166), under the responsibility Leo Kei Iwai E Fernanda Portaro and Stephanie Santos Suehiro Arcos agree with Ethical Principles in Animal Research adopted by Ethic Committee in the Use of Animals of Butantan Institute, and was approved in the meeting of day February 20, 2019.

Certificamos que o protocolo do Projeto de Pesquisa intitulado " Estudo das atividades antitumorais de peptídeos presentes no veneno de escorpião amarelo Tityus serrulatus", protocolado sob o CEUAx nº 6893040219, sob a responsabilidade de Leo Kei Iwai E Fernanda Portaro e Stephanie Santos Suehiro Arcos está de acordo com os princípios éticos de experimentação animal da Comissão de Ética no Uso de Animais da Instituto Butantan, e foi aprovado na reunião de 20 de fevereiro de 2019.

Maria Leonor Sarno de Oliveira
Coordenador da Comissão de Ética no Uso de Animais
Instituto Butantan

Nancy Oguiura
Vice-Coordenadora da Comissão de Ética no Uso de Animais
Instituto Butantan

Aos meus pais, amigos, namorado e vários bichinhos de estimação. Sem eles, eu nunca teria terminado.

AGRADECIMENTOS

Agradeço a todos e tudo que fez eu conseguir ter forças para concluir essa etapa da minha vida. Não foi fácil. Esse caminho não foi uma escolha totalmente própria, portanto foi muito mais sofrido do que eu imaginava.

Agradeço à minha mãe, Edicléia, por sempre me suportar quando eu chegava estressada e me aconselhava, sempre se interessou pelo meu trabalho, seja ele qual fosse. Agradeço ao meu pai, Ricardo, por proporcionar sempre tudo na medida do possível para todos em casa, além de proporcionar um dos melhores momentos da minha vida, que foram as viagens que fizemos em família. Agradeço aos meus irmãos, Gabriel e Rodrigo, por existirem, sem vocês eu não seria quem eu sou hoje, mesmo com todas as brigas. Agradeço também ao meu falecido tio, Ednilson, sinto muito a sua falta e de como você tinha orgulho da sua sobrinha bióloga! Agradeço a todas as outras pessoas da minha família, Aline, tia Gi, tia Edna, Juliana, Leo, Phill, Thi, minha vó Elena, Kadota, Frank e a mais nova luz, Giovanna. Obrigada por existirem, amo todos vocês!

Agradeço ao meu namorado, Gabriel, por abrir meus olhos e me fazer querer ir atrás do que eu realmente quero fazer da vida. Por ter me apoiado nas decisões, mesmo que tenhamos brigado muitas vezes pelo meu estresse com o mestrado. Amo você.

Obrigada a todos os meus animais de estimação por serem os melhores bichinhos do mundo, Dimitri, Bonnie, Amora, Bolinha, Sidney, Branquinha, Zorro, Pescoço, Bebê, Kenai e Kiara.

Agradeço a uma pessoa muito especial, que teve paciência e me apoiou nas decisões malucas que eu tive, Dr. Carlos, o melhor advogado que tem!

Obrigada aos meus melhores amigos, Jennifer, Amanda, Rodrigo, Marcus e Matheus, por ouvirem meus desabafos e aguentarem muitas vezes meu choro. Amo vocês demais.

Agradeço ao meu orientador Dr. Leo Kei Iwai e à coorientadora Dra. Fernanda Calheta Vieira Portaro por terem paciência com todas as mudanças que aconteceram ao longo desse projeto, por me ensinarem e guiarem pelos árduos caminhos da pós-graduação.

Obrigada a todos os colegas e amigos de laboratório (LETA, CeTICS, CENTD) que me ajudaram muito ao longo dessa jornada, Dr. Pedro Ismael da Silva Junior, Dra. Solange Maria de Toledo Serrado, e em especial Carol, Fábio, Wellington, Hamida, Kimberly, Patrícia, Thiago, Dani, Carolzona, Norton, Soraia, Pedro, Ismael e Dona Lídia.

Um agradecimento especial à Dra. Rosangela Aparecida Wailemann Mansano e à Dra. Luciana Rodrigues Gomes que me ajudaram demais enquanto eu não podia frequentar o laboratório, principalmente na manutenção da cultura de células. Sem vocês, muita coisa não teria acontecido.

Agradeço à equipe do Grupo Fleury, em especial ao Dr. Valdemir Melechco Carvalho, que nos auxiliou bastante na corrida das amostras no espectrômetro de massas.

Obrigada também ao Núcleo Estratégico de Venenos e Antivenenos do Instituto Butantan, por ter disponibilizado a peçonha de *T. serrulatus* para a pesquisa.

Agradeço a toda secretaria do programa de pós de Biotecnologia pela paciência e condução do programa de excelência.

Agradeço ao Programa de Pós-Graduação Interunidades em Biotecnologia da Universidade de São Paulo (USP), Instituto Butantan e Instituto de Pesquisas Tecnológicas (IPT), à Universidade de São Paulo (USP) e ao Instituto Butantan por deixarem este projeto ser desenvolvido.

Agradeço ao Conselho Nacional de Desenvolvimento Científico e Tecnológico (CNPq) pela concessão da bolsa e por suporte financeiro do projeto de mestrado intitulado "Estudo das atividades antitumorais de peptídeos presentes no veneno do escorpião amarelo *Tityus serrulatus*", processo número 131408/2019-4 e à Fundação de Amparo à Pesquisa do Estado de São Paulo (FAPESP), processos 2013/07467-1, 2016/04000-3 e 2017/17943-6.

Agradecimento à agência de fomento

O presente trabalho foi realizado com apoio do CNPq, Conselho Nacional de Desenvolvimento Científico e Tecnológico – Brasil, processo número 131408/2019-4 e da Fundação de Amparo à Pesquisa do Estado de São Paulo (FAPESP), processos 2013/07467-1, 2016/04000-3 e 2017/17943-6.

"*Seize the day, or die regretting all time you lost, it's empty and cold without you here, too many people to ache over*."

A7X

Stephanie Arcos

Resumo

ARCOS, S. S. S. **Estudo das atividades antitumorais de peptídeos presentes no veneno do escorpião amarelo *Tityus serrulatus*.** 2022. 154 f. Dissertação (Mestrado em Biotecnologia) - Instituto de Ciências Biomédicas, Universidade de São Paulo, São Paulo, 2022.

Peçonhas e venenos de animais como escorpiões, rãs, serpentes e aranhas são pesquisados por apresentarem potencial terapêutico e têm sido utilizados no desenvolvimento de novas drogas de atividade antimicrobiana e para o tratamento de diversos tipos de doenças, como os múltiplos tipos de câncer. A partir de toxinas da peçonha de escorpião já foi isolado e desenvolvido um agente com potencial de marcação de gliomas, além de existirem atualmente diversos trabalhos na literatura descrevendo o potencial anticancerígeno destas toxinas. Apesar de existirem inúmeras abordagens envolvendo a caracterização bioquímica e fisiológica da ação de peçonhas sobre linhagens celulares ou tecidos, ainda não foi descrito nenhum trabalho que aborda a análise das propriedades citotóxicas e do potencial anti-tumorigênico de peptídeos derivados da peçonha dos escorpiões *Tityus serrulatus*. Desta forma, cerca de 700 peptídeos da peçonha de *T. serrulatus* foram analisados *in silico* para identificar potencial atividade anticâncer e citolítica. Dez peptídeos selecionados foram sintetizados e serão testados em diferentes linhagens celulares tumorais e comparados com linhagens celulares normais. O resultado desta análise poderá revelar a ação a nível molecular da peçonha de *T. serrulatus* que pode ser específica em diferentes células tumorais ou específica nas células normais. A descoberta de peptídeos antitumorais pode ajudar no avanço da pesquisa relacionada à terapia anticâncer.

Palavras-chave: Peptídeo, *Tityus serrulatus*, peçonha de escorpião, câncer, linhagens celulares.

Abstract

ARCOS, S. S. S. **Study of the antitumor activities of peptides present in the venom of the yellow scorpion *Tityus serrulatus*.** 2022. 154 p. Masters dissertation (Biotechnology) - Instituto de Ciências Biomédicas, Universidade de São Paulo, São Paulo, 2022.

Venoms and poisons from animals such as scorpions, frogs, snakes and spiders have been studied for their therapeutic potential. Several molecules derived from these biological materials have been used for the development of new drugs with antimicrobial activities and for the treatment of several types of diseases such as some types of cancer. From the scorpion venom, a specific toxin has already been isolated and developed as a potential agent of targeting primary brain tumors. In addition, there are currently several studies described in the literature about the anticancer potential of isolated and/or modified components of these scorpion venoms. Although there are numerous approaches involving the biochemical and physiological characterization of the action of scorpion venom on cell lines or tissues, no work has yet been described addressing the analysis of cytotoxic properties and the anti-tumorigenic potential of peptides derived from the *Tityus serrulatus* scorpion. In this way, about 700 peptide sequences present in the *T. serrulatus* venom were analyzed *in silico* to identify potential anti-cancer and cytolytic activity. *In silico* selected peptides were synthesized, Peptides will be tested in different tumor cell lines and compared to normal cell lines. The results of these analyses may reveal the action at the molecular level of the *T. serrulatus* venom-derived peptides, which can be specific in different tumor cells or specific in normal cells. The discovery of anti-tumor peptides may help advance research related to anti-cancer therapy from natural sources.

Keywords: Peptides, *Tityus serrulatus*, scorpion venom, cancer, cell lines.

LISTA DE FIGURAS

LISTA DE TABELAS

LISTA DE ABREVIATURAS

A204 - Linhagem celular de rabdomiossarcoma

BCA – Ensaio com ácido bicinconínico (do inglês *Bicinchoninic acid assay*)

BcL-2 - Proteína intra-citoplasmática que inibe apoptose

BLZ-100 - Agente marcador de gliomas (*tumor paint*)

BSA - Albumina bovina (do inglês *Bovine Serum Albumin*)

CC50 - Concentração citotóxica 50%

COVID-19 – Doença causada por coronavírus descrita em 2019 (do inglês *Coronavirus disease 2019*)

CRISPR-9 - Repetições palindrômicas curtas agrupadas e regularmente interespaçadas (do inglês *Clustered Regularly Interspaced Short Palindromic Repeats*)

DMEM - Meio essencial mínimo de Dulbecco (do inglês *Dulbecco's Modified Eagle's Medium*)

DU145 - Linhagem celular de câncer de próstata

FasL - Fas Ligante, proteína de membrana que se liga ao Fas

FDR – Proporção esperada de descobertas falsas (do inglês *False Discovery Rate*)

HaCaT - Linhagem celular de células queratinócitos

HEK293 - Linhagem celular de células de rim

HeLa - Linhagem celular de células de adenocarcinoma

HEPES - Solução de tampão (*4-(2-hydroxyethyl)-1-piperazineethanesulfonic acid*)

HPLC - Cromatografia líquida de alta eficiência (do inglês *High Performance Liquid Chromatography*)

HUVEC - Linhagem celular de células de cordão umbilical e endotélio vascular

LC-MS/MS - Cromatografia Líquida acoplada à Espectrometria de Massas (do inglês *Liquid Chromatography coupled to Mass Spectrometry*)

MCF10A - Linha celular epitelial não tumorigênica

MCF7 - Linhagem celular de câncer de mama (do acrônimo *Michigan Cancer Foundation-7*)

MDA-MB231 - Linhagem celular de câncer de mama triplo negativo

MS/MS ou MS2- Espectrometria de massa em tandem

PBS - Solução salina tamponada com fosfato (do inglês *Phosphate Buffer Saline*)

Ras - Proteína oncogênica de vírus tumoral

RPMI - Meio de crescimento para cultura de células (do acrônimo *Roswell Park Memorial Institute*)

SARS-COV-2 – Síndrome Aguda Respiratória de Coronavírus 2 (do inglês *Severe Acute Respiratory Syndrome Coronavirus 2*)

SFB - Soro fetal bovino

SK-MEL-28 - Linhagem celular de células de melanoma

TsAP-1 - Peptídeo proveniente da peçonha de *Tityus serrulatus*

TsAP-2 - Peptídeo proveniente da peçonha de *Tityus serrulatus*

VEGF – Fator de crescimento endotelial vascular (do inglês *Vascular Endothelial Growth Factor*)

Y1 - Linhagem celular de células adrenocorticais

Y1-RasKO - Linhagem celular de células com Ras nocauteado de células Y1

LISTA DE SÍMBOLOS

4-[3-(4-Iodophenyl)-2-(4-nitrophenyl)-2H-5-tetrazolio]-1,3-benzene disulfonate	WST
Ácido aspártico	Asp ou D
Ácido glutâmico	Glu ou E
Alanina	Ala ou A
Arginina	Arg ou R
Asparagina	Asn ou N
Cianoborohidreto de sódio NaBH3CN	$NaBH_3CN$
Cisteína	Cys ou C
Dióxido de carbono	CO_2
Fenilalanina	Phe ou F
Formaldeído deuterado-D_2	CD_2O
Glicina	Gly ou G
Glutamina	Gln ou Q
Hidróxido de Sódio	NaOH
Histidina	His ou H
Isoleucina	Ile ou I
Leucina	Leu ou L
Lisina	Lis ou K
Metanal	CH_2O
Íon potássio	K^+
Prolina	Pro ou P
Serina	Ser ou S
Íon Sódio	Na^+
Tirosina	Tyr ou Y
Treonina	Thr ou T
Triptofano	Trp ou W
Valina	Val ou V

LISTA DE GRÁFICOS

LISTA DE SIGLAS

CENTD - "Centro de Excelência para Descobertas de Novos Alvos Moleculares"

DDI-CPI - "Drug-Drug Interactions – Chemical-Protein Interactome"

LECC - "Laboratório de Ciclo Celular"

LETA - "Laboratório de Toxinologia Aplicada"

SUMÁRIO

1 INTRODUÇÃO

O filo dos artrópodes é um dos mais antigos e com maior número de espécies dentre os filos existentes, ainda que haja uma diversidade enorme de espécies já extintas. Acredita-se que a origem do filo dos artrópodes ocorre há 600 milhões de anos, desde os tempos do Cambriano ou até mesmo do Pré-cambriano (Weygoldt, 1998). Dentro de Arthropoda, existem quatro grupos não extintos, atualmente conhecidos como Euarthropoda, que são os Myriapoda, Chelicerata, Insecta e Crustacea, sendo que possivelmente compartilham de características morfológicas provenientes de um único ancestral comum (Budd & Telford, 2009). Dentro do grupo dos Chelicerata encontra-se a ordem Scorpiones, representada pelos escorpiões. A morfologia dos escorpiões atuais é parecida com a dos fósseis encontrados no período Siluriano (Figura 1) (cerca de 450 milhões de anos atrás), o que mostra a capacidade adaptativa destes animais a diferentes condições ambientais desde o seu surgimento (Brazil & Porto, 2010). Os escorpiões estão amplamente distribuídos geograficamente, por todos os continentes, com exceção da Antártida (Bortoluzzi *et al.*, 2007). No Brasil, estão presentes as famílias Liochelidae, Euscorpiidae, Chactidae, Bothriuridae e Buthidae (Bortoluzzi *et al.*, 2007).

Figura 1 – Exemplares de escorpiões fósseis e atuais

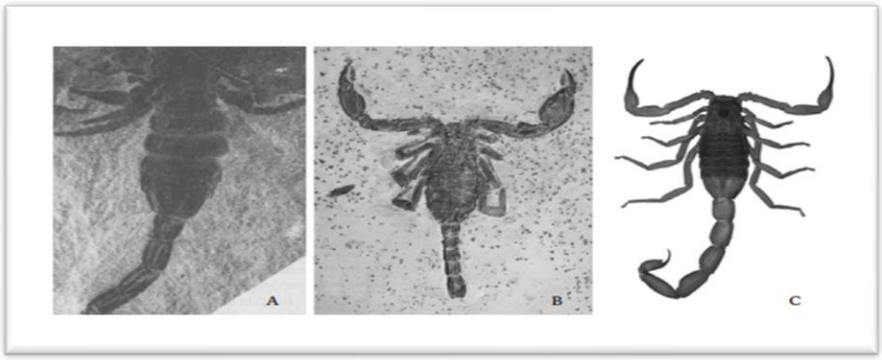

A) *Proscorpius oshorni*, New York, EUA (Siluriano); B) *Protoischnurus axelrodorum*, Ceará, Brasil (Cretáceo); C) *Tityus serrulatus*, Bahia, Brasil (atual). Fonte: Brazil & Porto, 2010.

Os escorpiões são um dos animais peçonhentos mais importantes para a saúde pública, pois podem causar acidentes através da inoculação da peçonha pela ferroada, como mecanismo de defesa. De acordo com o Ministério da Saúde, acidentes escorpiônicos possuem os maiores números de notificações no Brasil. Por exemplo, no estado de Pernambuco foram notificados

cerca de 57 mil acidentes por picadas de escorpiões entre 2012 e 2016, sendo que 74,7% das ocorrências foram causadas por escorpiões. Em São Paulo, entre 2007 e julho de 2017, foram notificados mais de 208 mil acidentes, sendo que 52,91% foram causados por escorpiões. As manifestações clínicas em humanos do envenenamento podem ser classificadas em três níveis, sendo: leve quando só há dor local; moderado quando o indivíduo também apresenta náuseas, vômitos, alterações de batimentos cardíacos, agitação e hipertensão; e grave quando os vômitos são frequentes e profusos, quando há tremores, espasmos musculares, sudorese intensa, palidez, hipotermia, podendo haver evolução de insuficiência cardíaca, edema agudo pulmonar e choque cardiocirculatório, o que pode levar à morte (Brazil & Porto, 2010).

Espécies de escorpiões como *Tityus serrulatus*¸*T. bahiensis* e *T. stigmurus* se adaptaram muito bem ao ambiente urbano, em partes por causa da estratégia reprodutiva de partenogênese onde os óvulos da fêmea se dividem sem fecundação com o espermatozóide, uma vez que não existem escorpiões amarelos machos; sendo elas as três espécies principais responsáveis por acidentes envolvendo escorpiões no Brasil (Brazil & Porto, 2010). Dentre estas, a espécie *Tityus serrulatus*, que faz parte da família Buthidae, é considerada a mais perigosa da América do Sul, sendo então de grande importância para a epidemiologia e saúde pública brasileira (Bortoluzzi *et al.*, 2007; Cajado-Carvalho *et al.*, 2016). Esta espécie foi descrita em 1922 por Adolpho Lutz e Oswaldo Mello de Campos, que destacaram a alta toxicidade de sua peçonha. Estes escorpiões caracterizam-se também por terem cerca de 7 cm, possuírem tronco escuro, metassoma amarelado e serrilhado na parte dorsal (Marcussi *et al*., 2011) (Figura 2), sendo que a origem do nome científico se deve a esta última característica. É no telson que se encontra o par de glândulas da peçonha. A função primária evolutiva da peçonha é a captura e digestão da presa. Todavia, secundariamente pode ser usado como mecanismo de defesa (Brazil & Porto, 2010).

Figura 2 – *Tityus serrulatus* com escala e suas partes

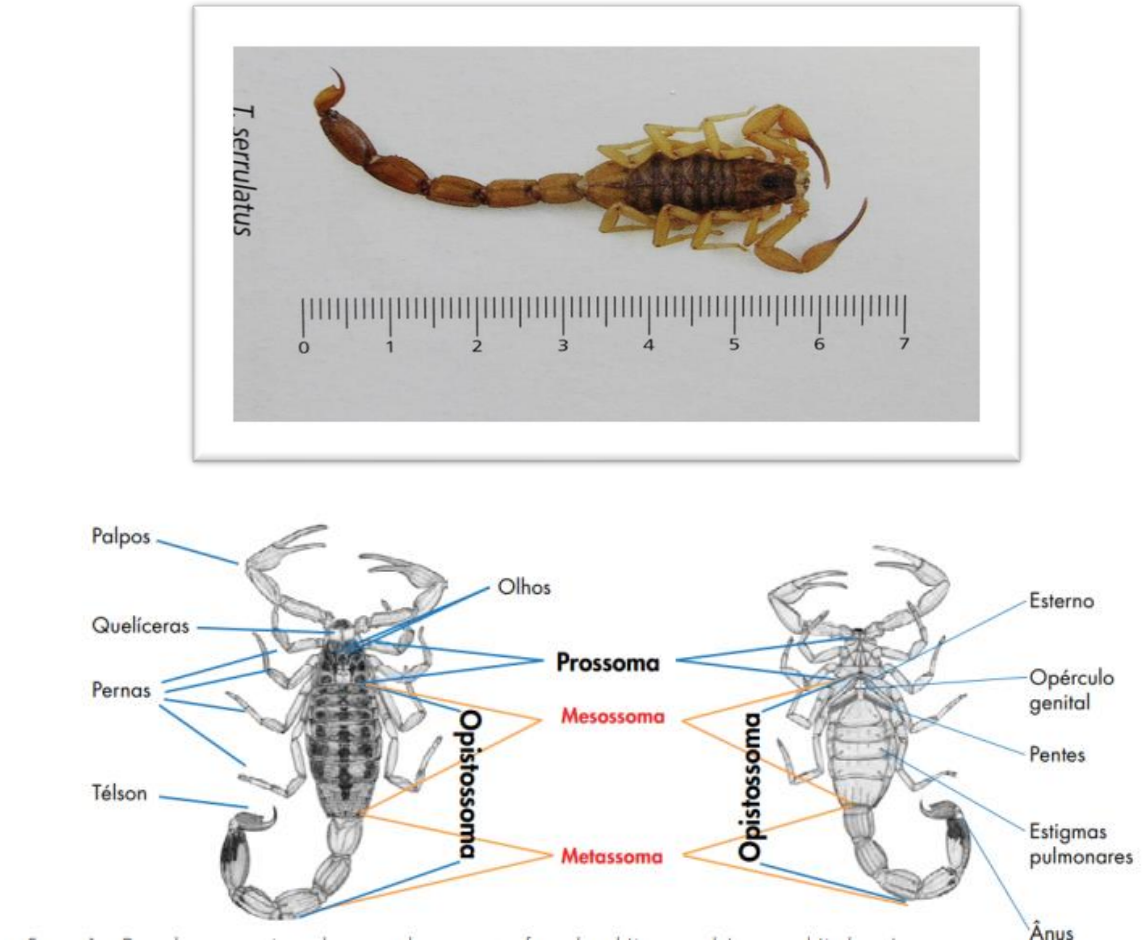

Fonte: Cristine Rochol / PMPA/Divulgação e website: https://www.pragaseeventos.com.br/como-reconhecer-escorpiao-veja-o-guia-do-instituto-butantan/

A nomenclatura que define proteínas e peptídeos da peçonha do *T. serrulatus* é confusa em diversos artigos da literatura. A mesma toxina pode aparecer em estudos diferentes com nomes diversos, gerando uma confusão que pode interferir em estudos futuros e referências bibliográficas. Desta maneira, neste estudo vamos adotar como padrão de nomenclatura aquele proposto por Cologna e colaboradores (*Tityus serrulatus* scorpion venom and toxins: an overview, 2009).

A peçonha de *T. serrulatus* é neurotóxica e é composta por uma mistura rica em proteínas de baixo massa molecular, peptídeos, aminoácidos, sais, açúcares e inibidores de protease (Brazil & Porto, 2010; Marcussi *et al*., 2011; Cologna *et al.*, 2009). A atuação se dá em canais de sódio e potássio, dependendo da neurotoxina. Toxinas com cadeias relativamente longas (60-70 a.a.), interligadas por quatro ligações de ponte dissulfeto, são mais ativas em canais de Na^+, enquanto que toxinas de cadeias mais curtas (30-42 a.a.), interligadas por três

ligações de ponte dissulfeto, são mais ativas em canais de K^+ (Cologna *et al.*, 2009). Quando as neurotoxinas interagem com os canais, ocorre a despolarização de membranas de células excitáveis, liberando neurotransmissores como catecolaminas, acetilcolina e outros, estimulando o sistema nervoso autônomo (Cologna *et al.*, 2009). Estudos recentes revelam que grande parte dos peptídeos de baixo peso molecular encontrados em peçonhas de escorpiões não possuem pontes dissulfeto (Guo *et al*., 2013). Peptídeos sem essas pontes podem atuar em alvos diferentes dos canais de íons (Cologna *et al.*, 2009).

Toxinas relacionadas à peçonha de escorpiões são conhecidas pelos efeitos negativos e deletérios em células, tecidos e organismos. Entretanto, antagonicamente, alguns componentes de peçonhas têm mostrado atividades antimicrobianas, anticâncer e imunossupressoras com potencial para desenvolvimento de drogas farmacêuticas (Ortiz *et al*., 2015). Estudos que permeiam as atividades anticâncer demonstraram que moléculas da peçonha de alguns escorpiões foram capazes de inibir o crescimento de glioma humano (Wang *et al*., 2005), de impedir proliferação, ser citotóxico e induzir apoptose em células leucêmicas (Gupta *et al*., 2010, 2007), inibir o crescimento e induzir apoptose em células de câncer de próstata humanas (DU145) (Zhang *et al*., 2009) e de possuir toxicidade diferencial e seletiva contra células de câncer epiteliais (Díaz-García *et al*., 2013). Além disso, Soroceanu *et al*. (1998) afirma que o uso de clorotoxina, um peptídeo de 36 aminoácidos derivado do escorpião *Leiurus quinquestriatus*, é eficiente na marcação de tumores cerebrais primários (gliomas). Uma aplicação direta dessa toxina está sendo desenvolvida como um agente chamado *Tumor Paint* BLZ-100, para uso em neurocirurgias com intuito de promover ressecção quase completa de gliomas (Butte *et al*., 2014). Além disso, um estudo envolvendo a ação de dois componentes peptídicos da peçonha de um escorpião do gênero *Tityus*, neopladine 1 e neopladine 2, revelou que estas moléculas induzem apoptose em células de carcinoma de mama humanas (SKBR3), induzindo a expressão de FasL e BcL-2 (D'Suze *et al*., 2010).

Apesar de existirem inúmeras abordagens envolvendo a caracterização bioquímica, fisiológica e imunológica da ação da peçonha ou derivados isolados de peçonhas sobre linhagens celulares ou tecidos (Díaz-García *et al*., 2013; D'Suze *et al*. 2010; Guo *et al*., 2013; Gupta *et al*., 2010, 2007; Ortiz *et al*., 2015; Soroceanu *et al*., 1998; Wang *et al*., 2005; Zhang *et al*., 2009), ainda não existem trabalhos que abordam a análise de peptídeos provenientes da toxina dos escorpiões *T. serrulatus* e a correlação com o câncer.

Diante disto, este trabalho teve como objetivo caracterizar o efeito de peptídeos da peçonha de *T. serrulatus* sobre linhagens celulares normais e linhagens celulares de câncer, através das análises computacionais *in silico* para verificar a ação citolítica e anti-tumorigênica. Peptídeos

selecionados foram sintetizados para poderem ser testados funcionalmente em diferentes linhagens celulares oncogênicas e normais e análise por citometria de fluxo utilizando marcadores para apoptose, senescência e diferentes citocinas. Além das análises de peptídeos sintéticos, foram desenhados experimentos para fracionamento de peptídeos da peçonha para analisar frações que tenham maior potencial de aplicação com relação às linhagens de células de câncer devido ao potencial biotecnológico que os peptídeos da peçonha apresentam de acordo com a tese do Bruno Duzzi (dados não publicados, 2018) e dos resultados de atividade anticâncer encontrados por Guo *et al*. (2013) de dois peptídeos da peçonha do escorpião amarelo (TsAP-1 e TsAP-2).

2 OBJETIVOS DO PROJETO I

2.1 Objetivos gerais do projeto

Analisar e caracterizar os perfis proteômicos comparativos das frações da peçonha (menor e maior que 10 kDa) e da peçonha total de *T. serrulatus* sobre diferentes linhagens celulares de câncer (Y1, HeLa, MCF7, MDA-MB231, SK-MEL-28 e A204) comparando com as linhagens celulares normais (Y1-RasKO, HEK293, HUVEC e HaCaT).

2.2 Objetivos específicos desta primeira etapa do projeto

- Extração da peçonha de *T. serrulatus*.
- Quantificar as proteínas totais da peçonha extraída de *T. serrulatus*.
- Cultivar células das linhagens Y1, HeLa, MCF7, MDA-MB231, SK-MEL-28, A204, Y1-RasKO, HEK293, HUVEC e HaCaT.
- Fazer o ensaio de citotoxicidade da peçonha de *T. serrulatus* das células Y1, HeLa, MCF7, MDA-MB231, SK-MEL-28, A204, Y1-RasKO, HEK293, HUVEC e HaCaT usando diferentes concentrações da peçonha para determinação da CC50.
- Comparar a ação citotóxica da peçonha extraída bruta com a ação da peçonha liofilizada.
- Verificar a atividade enzimática das peçonhas disponíveis de *T. serrulatus*.
- Quantificar as proteínas das frações maiores que 10 kDa e os peptídeos das frações menores que 10 kDa da peçonha de *T. serrulatus*.
- Fazer ensaio de citotoxicidade das frações da peçonha de *T. serrulatus* nas linhagens celulares de uso do projeto.
- Analisar as frações de interesse obtidas por espectrometria de massas de baixa resolução.

3 OBJETIVOS DO PROJETO II

3.1 Objetivos Gerais

Identificar e caracterizar peptídeos da peçonha de *T. serrulatus* com potenciais propriedades citolíticas e anti-tumorigênicas.

3.2 Objetivos Específicos

- Fracionar a peçonha total de *T. serrulatus* para obtenção de frações peptídicas (menor que 14 kDa).
- Análise *in silico* de cerca de 700 sequências peptídicas da peçonha de *T. serrulatus* para seleção de até 10 sequências.
- Síntese dos peptídeos selecionados.
- Análise de proliferação celular de diferentes linhagens celulares tumorais e normais frente aos peptídeos sintéticos e frações da peçonha.
- Fazer o ensaio de citotoxicidade da fração peptídica da peçonha de *T. serrulatus* e dos peptídeos sintéticos utilizando as células Y1, HeLa, MCF7, MDA-MB231, SK-MEL-28, A204, Y1-RasKO, HEK293, HUVEC e HaCaT.
- Análise por citometria de fluxo para verificar ação citolítica e tóxico seletiva (anti-tumorigênica), utilizando marcadores de apoptose, senescência e citocinas.

4 MATERIAL E MÉTODOS – PROJETO I

4.1 Extração da peçonha de *T. serrulatus*

Foi extraída peçonha de um total de 27 escorpiões da espécie *Tityus serrulatus* mantidos no biotério do Laboratório de Toxinologia Aplicada do Instituto Butantan em condições adequadas com controle de temperatura e a alimentação constituída por insetos periodicamente. Esses escorpiões foram coletados no estado de São Paulo sob as licenças, SISBIO 11024-3 e CGen Nº 001/2008 e 010345/2014-0. A extração foi realizada utilizando um estimulador elétrico modelo Neurodyn Portable (Ibramed, Amparo, SP, Brasil), com voltagem de 35 V, frequência de 10 Hz e duração de 0,5 ms. Os cabos foram colocados um de cada lado do último segmento da cauda antes do telson para que pudesse estimular a saída da peçonha (Figura 3). As pontas dos cabos foram molhadas em água para melhorar a condução da eletricidade.

Figura 3 – Estímulo elétrico no telson de *T. serrulatus*

Estímulo elétrico no último segmento da cauda antes do telson do escorpião amarelo *T. serrulatus* durante a extração da peçonha. Fonte: Elaborada pela autora.

A coleta foi feita em microtubos eppendorf (Figura 4), tomando o cuidado em manter o produto extraído em gelo, a fim de evitar o deterioramento dos componentes da peçonha. Um

total de quatro microtubos eppendorfs foram utilizados para armazenamento da peçonha extraída. Inicialmente, os tubos foram armazenados a -80°C e posteriormente foram colocados no freezer a -20°C. A quantidade extraída por tubo foi de aproximadamente 20 µL.

Figura 4 – Extração da peçonha em microtubo eppendorf

Microtubo eppendorf utilizado para extrair a peçonha do escorpião amarelo *T. serrulatus*. A abertura do tubo foi coberta com fita plástica flexível para que pudesse segurar as pequenas gotas extraídas da peçonha. Fonte: Elaborada pela autora.

4.2 *Quantificação de proteínas e peptídeos*

As proteínas foram quantificadas pelo método BCA (*Bicinchoninic acid assay, Thermo Pierce*, Estados Unidos) em placas de 96 poços. Neste ensaio, íons de cobre formam complexos com ligações peptídicas produzindo um produto de cor púrpura que é lido em espectrofotômetro a 562 nm. Diluições seriadas do sobrenadante foram plaqueadas em placa de 96 poços de fundo chato, onde foi adicionada uma mistura 50:1 de soluções A (bicinconinato de sódio 10 g/L, carbonato de sódio 20 g/L, tartrato de sódio 1.6 g/L, NaOH 4 g/L e bicarbonato de sódio 9.5 g/L): solução B (sulfato de cobre pentahidratado 40 g/L). A placa foi incubada a 37ºC por 30 minutos e a leitura realizada a 562 nm em espectrofotômetro (leitor de microplacas, modelo

425-301, Hidex). A curva padrão foi feita fazendo-se uma diluição seriada com BSA (albumina bovina) inicialmente a 2 mg/mL.

No caso da quantificação da peçonha extraída de *T. serrulatus*, foi necessário centrifugar as amostras a 14000 G a 4°C por 10 minutos antes de quantificar, a fim de utilizar apenas o sobrenadante para tal, já que no precipitado iria ter todo o acúmulo de hialuronidase, que é um grupo de enzimas que catalisam a degradação do ácido hialurônico, um polissacarídeo bastante encontrado na matriz extracelular de tecidos conjuntivos (Kreil, 1995).

Para a quantificação da fração da peçonha de *T. serrulatus* menor que 10 kDa, foi utilizado o kit *Pierce Quantitative Colorimetric Peptide Assay ((*Thermo Fisher Scientific, Illinois, EUA). Neste ensaio, o cobre é reduzido primeiro pela reação do biureto. Depois, o agente quelante se liga ao cobre reduzido para formar um complexo vermelho com absorbância de 480 nm. O sinal produzido por esta reação é de 3 a 4 vezes mais sensível do que o ensaio de proteína *Micro-BCA Protein Assay* para análise de peptídeo. Diluições seriadas do sobrenadante foram plaqueadas em placa de 96 poços de fundo chato, onde foi adicionada uma mistura de 50 partes do reagente A, mais 48 partes do reagente B e 2 partes do reagente C. A placa foi incubada a 37ºC por 15 minutos e a leitura realizada a 480 nm em espectrofotômetro (*Flex Station* 3, Molecular Devices, Califórnia, EUA) utilizando o software SoftMax Pro (vs 3.0.22). A curva padrão foi feita fazendo-se uma diluição seriada com um padrão de referência de peptídeos oriundos da digestão de BSA de alta qualidade, inicialmente a 1 µg/mL.

4.3 *Linhagens celulares*

Este projeto tem como foco a análise do efeito da peçonha de *T. serrulatus* sobre diferentes linhagens de câncer. Para esta etapa do projeto, de outubro de 2018 a março de 2019, cultivamos as seguintes linhagens celulares tumorais: Y1, HeLa, MCF7, MDA-MB231, e diferentes linhagens de células normais: Y1-RasKO e HEK293. Todas as células foram cultivadas a 37ºC em 5% CO2 em meio de cultura DMEM suplementadas com 10% de soro fetal bovino inativado e os antibióticos ampicilina a 25 mg/L e estreptomicina a 100 mg/L. As células foram repicadas quando a confluência atingiu 80%.

Em nosso laboratório, o Dr. Matheus Dias conseguiu gerar células Y1 depletadas de Ras por CRISPR-9 (Dias *et al*., 2019) aqui denominadas de Y1-RasKO. A célula da linhagem Y1 caracteriza-se por apresentar superexpressão de Ras. Acredita-se que Ras possa ser responsável

pela tumorigenicidade da célula. No presente momento, a análise funcional da célula Y1-RasKO está sendo avaliada em camundongos.

4.4 *Curva de crescimento*

A quantidade de células a serem plaqueadas em placa de 96 poços foi determinada com base em cinco quantidades iniciais de plaqueamento: $5x10^3$, $1x10^4$, $1,5x10^4$, $2x10^4$ e $2,5x10^4$. A quantidade de células plaqueadas por poço variou de acordo com a linhagem celular e a passagem das células, pois a velocidade de replicação diferiu entre elas. Após 48h do plaqueamento, foi visto em microscópio qual a melhor quantidade de células iniciais que atingiram confluência entre 70% a 80% desejada.

4.5 *Peçonha de T. serrulatus*

Foi utilizada peçonha de *T. serrulatus* extraída por mim e por membros do laboratório do Dr. Pedro Ismael da Silva Junior do Laboratório de Toxinologia Aplicada (LETA) do Instituto Butantan como descrito no item 4.1. Como a quantidade de peçonha extraída não foi suficiente para a realização de todos os experimentos iniciais, também foi utilizada a peçonha liofilizada proveniente do Núcleo Estratégico de Venenos e Antivenenos do Instituto Butantan (20 mg - Ts/V170001 e Ts/V170002).

4.6 *Fracionamento da peçonha de T. serrulatus*

A separação de 20 mg de peçonha total em frações peptídicas de *T. serrulatus* foi realizada utilizando a cromatografia de filtração em gel do laboratório do Dr. Pedro Ismael da Silva Junior do LETA. A coluna usada foi a *Superdex peptides (GE) Life Science*, HR 10/30. Antes do fracionamento cromatográfico, foi feita uma limpeza com água ultrapura (MilliQ) *overnight* a um fluxo de 0,05 mL/min. Depois, a água foi retirada com o uso de uma seringa para a saída da válvula das bombas. Então, o sistema foi preenchido com acetato de amônio 50 mM pH 5,5, com fluxo de 0,5 mL/min durante 2 horas.

A coleta da primeira cromatografia foi feita manualmente, por pico. No entanto, nessa mesma corrida ocorreram 3 interrupções por conta do limite da pressão da bomba, que passou de 1,5 MPa. Por conta disso, a corrida teve que ser normalizada somando-se 15 minutos ao

tempo mostrado no perfil cromatográfico (corrida VTS001 - volume de injeção de 300 µL). Foi feita também uma cromatografia de gel separação onde os picos foram coletados pelo tempo. Cada fração foi coletada a cada 1 minuto e 30 segundos, até completar 60 minutos de corrida (corrida VTS002 - volume e 100 µL de injeção). Foram utilizados os mesmos padrões e método da cromatografia anterior. O padrão utilizado para as cromatografias foi composto de lisozima (15 kDa), DODa (1,787 kDa) e Cheliferina (0,748 kDa).

4.7 Ensaio de citotoxicidade

O ensaio de citotoxicidade foi realizado fazendo-se o tratamento das células com diferentes concentrações da peçonha na faixa de 0,1 nM a 100 mM de proteína total. O teste de citotoxicidade foi realizado utilizando o método colorimétrico de análise de viabilidade celular com o reagente WST (*Clontech, Takara Bio*, Japão). Foram plaqueadas células em cada poço de uma placa de 96 poços de fundo chato. O número de células para plaqueamento variou de acordo com o crescimento das células das diferentes linhagens. Um dia depois de plaquear as células (70-80% de confluência), o meio de cultura foi trocado e foram adicionados 100 µL de meio sem soro para que as células passassem a ser sincronizadas e para que a replicação parasse. Após 24 h, 100 µL de meio sem soro com peçonha em diferentes concentrações foi adicionado em cada poço. Após 24 h, foram adicionados 10 µL do reagente WST em cada poço, no escuro. A placa foi mantida a 37°C durante 4 h. Neste ensaio, o sal *tetrazolium* WST-1 é clivado pela ação da enzima *succinato-tetrazolium reductase mitocondrial*, formando um produto (*formazan*) de cor vermelho escuro. Quanto maior o número de células viáveis, maior a quantidade da enzima reductase, resultando no aumento concomitante da conversão de WST-1, formando o corante *formazan*. A quantidade de corante *formazan* é diretamente proporcional ao número de células metabolicamente ativas no meio de cultura. A quantificação das células viáveis foi realizada através da leitura em espectrofotômetro (leitor de microplacas, modelo 425-301, Hidex, Turku, Finlândia e leitor de microplacas, modelo *Flex Station* 3, Molecular Devices, Califórnia, EUA) a 450 nm utilizando o software SoftMax Pro (versão 3.0.22).

4.8 Tratamento das células com peçonha de T. serrulatus, lise celular e extração de proteínas

As células foram cultivadas em garrafas T25 e, após atingirem uma confluência de 70-80% após plaqueamento, as células foram previamente carenciadas com meio DMEM sem soro fetal bovino por 24 h. No dia seguinte, foram adicionadas ao meio de cultura sem soro uma certa quantidade de peçonha para que a concentração final fosse de 10 µg/mL. Este valor foi determinado com base nos ensaios de citotoxicidade, porém não encontramos um valor de CC50. Então, essa concentração foi determinada por conta da baixa quantidade de peçonha disponível e para procurar mudanças proteômicas nas células não visíveis a olho nu. Este grupo de pesquisa achou razoável utilizar esta concentração para posteriores análises proteômicas.

Os tratamentos com a peçonha foram de 6 h, 12 h, 24 h e 48 h. As células foram lavadas com PBS gelado e lisadas com 300 µL de ureia 8 M gelada após cada duração de tratamento. O lisado foi coletado em *eppendorfs* e vortexado por 15 segundos a cada 5 minutos por 30 minutos. Depois, as amostras foram centrifugadas a 4 ºC a 14000 G por 10 min. Por fim, o sobrenadante foi mantido e o precipitado foi descartado. As amostras foram armazenadas no congelador. Para a quantificação protéica por BCA, 10 µL dos lisados foram separados.

4.9 Teste de atividade enzimática das peçonhas de T. serrulatus utilizando substratos fluorescentes

O ensaio de atividade enzimática utilizou como medidor das absorbâncias um espectrofotômetro (Hidex, Turku, Finlândia), onde a leitura de excitação e emissão foi feita em 320 e 420 nm, respectivamente. O substrato utilizado foi Abz-FLRRV-EDDnp (5µM) em tampão Tris 20 mM, NaCl 20 mM, pH 8,2, específico para metaloproteinases presentes na peçonha do escorpião. Foram realizadas 15 leituras com intervalo de 30 segundos. A quantidade de peçonha de *T. serrulatus* utilizada para o ensaio foi de 10 µg da peçonha liofilizada e 81,25 µg da peçonha extraída (1 µL do estoque original colocado na reação de cada microtubo eppendorf). Neste ensaio, o substrato emite fluorescência quando é quebrado pela ação de alguma enzima ou protease. Desta maneira, quanto maior a fluorescência emitida, maior será a atividade enzimática presente nas amostras testadas. O ensaio foi analisado em *software* GraFit Data Analysis (versão 5.0, Erithacus, West Sussex, Inglaterra) onde as atividades específicas das amostras foram determinadas (UF/µg de peçonha/min, sendo UF = unidades de fluorescência).

4.10 Ensaio de atividade antimicrobiana das frações peptídicas da peçonha de T. serrulatus

As atividades das frações peptídicas separadas pelo método de cromatografia de gel separação foram determinadas fazendo-se ensaios iniciais para determinar se havia atividade antimicrobiana nos picos coletados. Esses ensaios foram feitos inicialmente para determinar se havia atividade antimicrobiana em alguma das frações. Em caso positivo, a ideia seria testar se essas moléculas bioativas contra micróbios teriam também potencial ação anti-tumoral (Guo, X., *et al*., 2013).

As frações obtidas da cromatografia VTS001 foram inicialmente liofilizadas e ressuspendidas em água ultrapura (MilliQ) (mesmo volume de 300µL). Algumas frações tiveram que ser juntadas por conta de fazerem parte do mesmo pico majoritário. De 15 frações coletadas, sobraram 11.

Cada fração foi testada utilizando-se o microorganismo *Micrococcus luteus*. Os microrganismos foram plaqueados em uma placa de fundo chato de 96 poços e as frações foram colocadas de acordo com o esquema da figura 5.

Figura 5 - Esquema do ensaio antimicrobiano das frações peptídicas

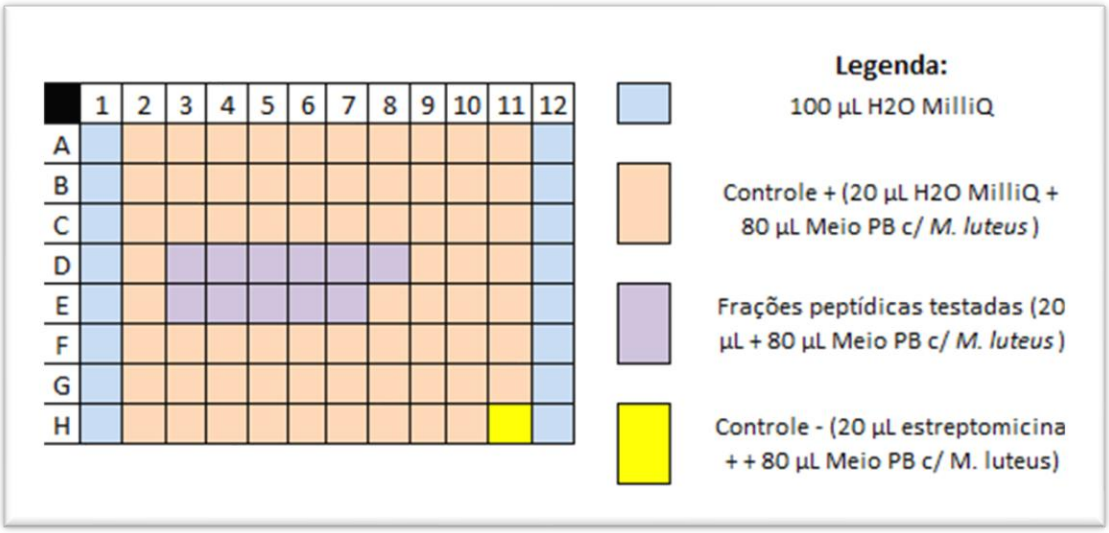

Esquema com legenda de cores do ensaio antimicrobiano feito em placa de 96 poços de fundo chato para testar a atividade das frações peptídicas da peçonha de *T. serrulatus* em bactérias *M. luteus*. Fonte: Elaborada pela autora

Após plaqueamento de acordo com a figura 5, a placa foi mantida *overnight* na estufa em um agitador a 30ºC. A leitura foi feita no espectrofotômetro Victor3 (PerkinElmer Life and

Analytical Sciences, Connecticut, EUA) a 595 nm após 20 h de incubação. Posteriormente, foi feito mais um ensaio antimicrobiano, onde o plaqueamento ocorreu da mesma maneira que na figura 5. Foram feitas duas leituras no espectrofotômetro a 595 nm após 14 h e após 33 h.

4.11 Preparação da amostra para análise proteômica: digestão e dessalinização por Stage Tip

Para cada 100 μg de amostra lisada com ureia 8 M gelada, foram adicionados 7 μL de ditiotreitol (DTT) 10mM, com intuito de reduzir as pontes dissulfeto. Em seguida, as amostras foram incubadas a 37 ºC por 1 h. Após a incubação com DTT, 70 μL de iodoacetamida 55 mM foi adicionada para a alquilação das cisteínas por 1 h no escuro, à temperatura ambiente. Depois da incubação, foram adicionados 2,5 mL de tampão HEPES pH 7,4 a 0,1 M e, em seguida, 20 μL de tripsina (Sigma-Aldrich, Missouri, EUA), quantidade suficiente para se obter uma razão enzima:proteína de 1:50. As amostras foram então incubadas a 37 ºC *overnight*. No dia seguinte, a reação foi interrompida adicionando-se 10% de ácido acético glacial do volume total da reação de digestão.

Depois da digestão, as amostras foram submetidas ao processo de dessalinização em *Stop-and-go extraction tip* (*StageTip*) C18, montados em ponteiras *Tip* p-200 (Axygen, Corning, California, EUA) com uma membrana SDB-XC (*styrene-divinylbenzene*, *Empore*, 3M, Pensilvânia, EUA) para remoção de sal, de acordo com o método descrito por Rappsilber (2007) (Figura 6) (Rappsilber *et al*., 2007). As ponteiras foram acopladas nas tampas de tubos eppendorf de 2 mL e submetidas à centrifugação em todos os passos do protocolo.

Figura 6 - Representação esquemática da produção de StageTip C18

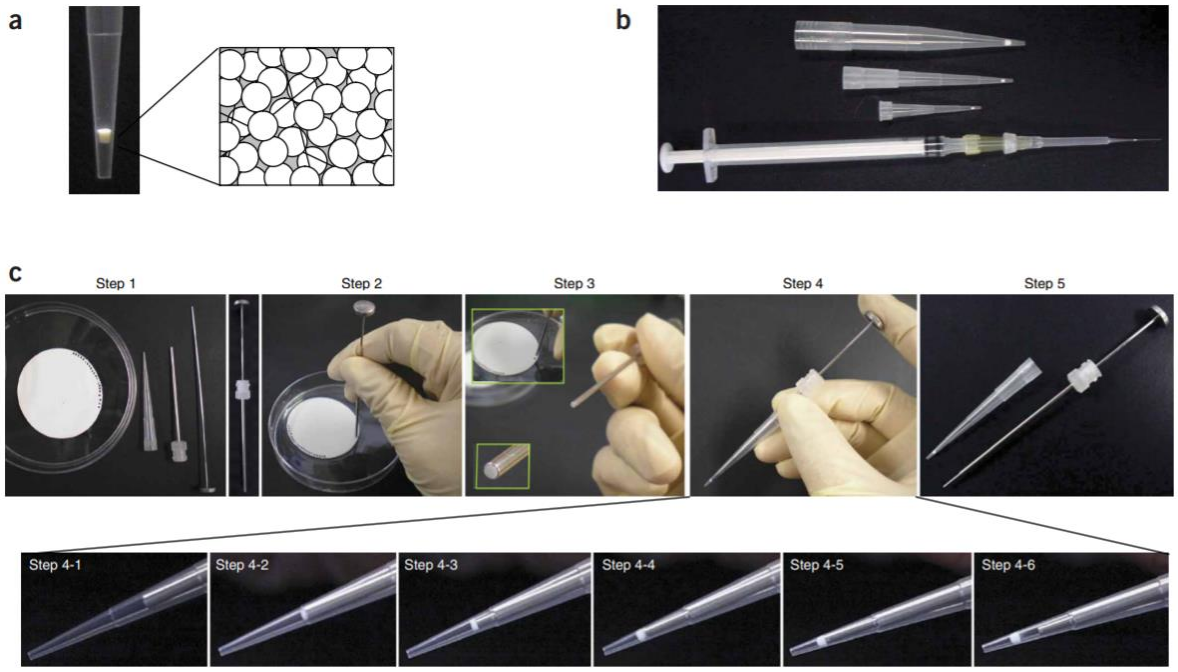

Stop-and-go extraction tip (*StageTip*) C18. A: Produto final do *StageTip* e disposição dos *beads* na malha Teflon. B: *StageTip* feito em diferentes tamanhos de ponteiras. C: Fabricação dos *StageTips*, passo a passo. Fonte: Rappsilber et al. (2007).

As membranas foram inicialmente condicionadas com 20 µL de solução B (80% ACN e 0,5% TFA) e solução A (5% ACN e 0,5% TFA), respectivamente, na centrífuga a 1000 G por 3 minutos. A amostra foi aplicada ao *StageTip* e centrifugada a 800 G por 5 minutos, lavada com 20 µL de solução A e centrifugada a 1000 G por 3 minutos. Os peptídeos ligados à coluna foram eluídos com solução B, centrifugando-os a 1000 G por 5 minutos. O eluato foi liofilizado e dissolvido em ácido fórmico 0,1% para posterior análise por cromatografia líquida acoplada ao espectrômetro de massas (LC-MS/MS).

4.12 Marcação por dimetilação de peptídeos trípticos

A marcação foi realizada incubando-se o extrato de peptídeos por 2 horas com 20 µL da mistura de marcador leve para a condição de controle (500 µL de TEAB 50 mM, 2,8 µL de CH_2O 37% e 25 µL de $NaBH_3CN$ 0,6 M) e 20 µL de mistura de marcador pesado para as amostras tratadas com a peçonha (500 µL de TEAB 50 mM, 5 µL de $^{13}CD_2O$ 20%, 25 µL de

$NaBD_3CN$ 0,6 M) durante 2 horas à temperatura ambiente. A reação foi parada com 5 µL de amônia 1% e incubada por 30 min a 35 ºC. Os extratos tratados com peçonha e PBS (grupos controles) foram combinados na proporção de 1:1 para análise posterior por espectrometria de massas. Todos os reagentes químicos foram adquiridos da *Sigma-Aldrich* (*Saint Louis*, Missouri, EUA).

4.13 Fabricação das colunas analíticas e preparativas para o espectrômetro de massas

As colunas analíticas foram preparadas cortando-se aproximadamente 25 cm de capilar de dimensões: 75 µm ID x 360 µm OD (*NST Nano Separation Technologies,* São Carlos, SP). A coluna analítica foi preparada queimando-se uma janela de aproximadamente 3 cm a partir de uma das extremidades. O capilar foi então fixado no *laser puller* (P-2000, *Sutter Instrument Company*, California, Estados Unidos), de modo que a distância do fechamento do lado esquerdo e o início da parte queimada da coluna fosse de 0,5 cm. O capilar alinhado e fixado foi bombardeado com laser utilizando os parâmetros: *HEAT*: 245, *VEL*: 15, *DEL*: 128, para a formação da ponta na coluna. O controle de qualidade da ponta da coluna foi feito observando-se à lupa (Nikon, Japão), a fim de observar se a ponta não ficou muito fina, ou muito grossa, ou quebrada.

O empacotamento da coluna foi realizado com polímeros (*beads*) C18 de 3 µm (Dr. Maish GmbH HPLC, Alemanha). Em um *vial*, foi adicionado 1 mL da solução com 80% acetonitrila e 20% isopropanol, onde foi adicionada uma ponta de espátula de *beads* de 3 µm e uma mini barra magnética. A coluna foi colocada no reator de nitrogênio a uma pressão de 100 psi e empacotada até que os beads atingirem uma altura de cerca de 15 cm. Esse reator foi colocado em cima de um agitador magnético de modo que a solução com os beads estivesse constantemente sob agitação.

A pré-coluna ou coluna *trap* foram fabricadas utilizando o capilar de dimensões ID 100 µm OD 360 µm que foi cortado com aproximadamente 15 cm de extensão. O *frit* (polímero que serve como filtro) foi feito a partir de uma solução feita com a mistura de 88 µL de Kasil (*PQ Corporation*, Estados Unidos) e 17,6 µL de formamida (*LS Chemicals*, Ribeirão Preto, SP), vortexada por 30 segundos e centrifugada por 1 minuto a 13500 rpm. Uma das extremidades do capilar foi colocada na solução e retirada quando o Kasil atingiu aproximadamente 1 cm. O capilar foi então aquecido em um termo bloco a 100 ºC por 30 minutos até a solidificação do polímero.

A coluna analítica foi empacotada utilizando polímeros (*beads*) de 5 µm (*Phenomenex-Jupiter*, Estados Unidos) em solução com 80% acetonitrila e 20% isopropanol. Os *beads* foram carregados com pressão de 200 a 500 psi, e a pressão liberada quando os *beads* atingiram 7 cm da coluna.

4.14 Análise proteômica por espectrometria de massas

Foram analisadas as amostras decorrentes do ensaio de envenenamento com duração de 6 h, 12 h, 24 h e 48 h das células Y1 e Y1-RasKO. As amostras foram submetidas à análise por LC-MS/MS, utilizando o espectrômetro de massas LTQ-*Orbitrap Velos* (*Thermo Fisher Scientific*, Bremen, Alemanha) acoplado a um cromatógrafo líquido nLC *Easy* II (*Thermo Fisher Scientific*, Bremen, Alemanha). O espectrômetro foi equipado com uma fonte *nanospray* (*Proxeon, Thermo Fisher Scientific*), acoplado a uma coluna analítica C18 e à pré-coluna C18 preparada *in house*, como descrito anteriormente.

A análise foi realizada injetando-se 5 µg a 10 µg de peptídeos tripsínicos em um gradiente de 5 % a 50 % de solvente B (acetonitrila 90%, 0,1% TFA) durante 120 minutos a um fluxo de 200 nL/min. A fonte de *eletrospray* foi operada a 2.2 kV e o espectrômetro de massas foi operado no método de aquisição dependente de dados (DDA), no qual o MS 1 (*full* MS *scan*) foi adquirido utilizando a faixa de m/z 300 – 2000 para varredura com resolução de 30000 no modo FTMS. A fragmentação dos dez íons mais intensos de cada MS1 foi realizada por CID (*collision induced dissociation*) e os fragmentos analisados no *ion trap*.

A configuração da janela de isolamento, tempo de ativação e energia normalizada de colisão foram, respectivamente, 3 m/z, 30 ms e 35%. A energia de colisão usada para a obtenção dos fragmentos (espectros de MS/MS) foi de 35 eV e o tempo de exclusão dinâmica foi ajustado com uma lista contendo 500 íons, no tempo de 90 s, para diminuir a aquisição repetida de um mesmo íon.

4.15 Identificação de Proteínas e busca em banco de dados

A identificação de proteínas dos dados de espectrometria de massa foi realizada usando *Peaks Studio* versão X (*Bioinformatics Solutions Inc.*, Waterloo, ON, Canadá) usando ferramentas de sequenciamento *de novo* para identificação de peptídeos e *Search* DB para a

busca clássica de sequências contra o banco de dados *Mus musculus*, baixado do UniProtKB/Swiss-Prot em agosto de 2019. Também utilizamos os programas *Mascot* (*Matrix Science*, versão 2.4.0) e *MaxQuant* (versão 1.4.1.2) para identificação e quantificação de proteínas, respectivamente, com base no mesmo banco de dados *M. musculus* e *H. sapiens* baixados do Uniprot. Para evitar a presença de contaminantes, o banco de cRap da GPM (*The Global Proteome Machine*) foi usado como banco de dados de contaminantes nas análises por Peaks. O Maxquant já apresenta um banco de dados de contaminantes do próprio programa. Os parâmetros utilizados em todos os diferentes *softwares* para realizar buscas por modificações foram: carbamidometilação da cisteína como modificação fixa e a oxidação da metionina como modificação variável. A tolerância a erros de massa para MS e MS/MS foi ajustada para 10 ppm e 0,02 Da, respectivamente.

A tripsina foi selecionada como a enzima proteolítica usada na digestão de proteínas e foram permitidas até três falhas de clivagem. Terminada a busca no DB, o FDR (determinado pelo método *Benjamini-Hochberg*) foi ajustado para 0,1% e no Peaks, o ALC (confiança local média) foi ajustada para 80%.

Uma das caracterizações funcionais feitas para analisar o perfil proteômico das amostras foi o enriquecimento de termos obtido a partir de análises feitas pelo *WebGestalt* utilizando a busca pelo *Gene Ontology* em processos biológicos e funções moleculares.

5 MATERIAL E MÉTODOS – PROJETO II

5.1 *Seleção de peptídeos*

Um conjunto de 702 fragmentos peptídicos derivados de diferentes proteínas da peçonha de *T. serrulatus* foram pré-selecionados com potencial atividade anti-câncer. Esses fragmentos peptídicos foram determinados a partir do trabalho de tese de doutorado do Dr. Bruno Duzzi sob orientação da Dra Fernanda Calheta Portaro e que estão disponíveis na tese e podem ser baixadas através do link: https://www.teses.usp.br/teses/disponiveis/87/87131/tde-20052019-085022/en.php. As sequências primárias dos 702 peptídeos foram obtidas através do *software Peaks Studio* (versão X, Bioinformatics Solutions, Toronto, Canadá) e foram utilizadas para a análise *in silico* do presente trabalho.

5.2 *Análise in silico*

Um conjunto de *softwares* foi utilizado para testar a ferramenta ideal para as análises *in silico* dos peptídeos selecionados:

- iACP (identifying AntiCancer Peptides) (Chen et al., 2016)
  (http://lin-group.cn/server/iACP)
- AntiCP (Institute of Microbial Technology, Chandigarh India)
  (https://webs.iiitd.edu.in/raghava/anticp/index.html)
- AntiCP 2.0 (Agrawal et al. 2020)
  (https://webs.iiitd.edu.in/raghava/anticp2/index.html)
- ACPred-FL (Wei et al., 2018)
  (http://server.malab.cn/ACPred-FL/).

Como controle positivo, seis peptídeos foram utilizados, com base em dados da literatura que apresentam atividade anti-câncer:

Peptídeo 1: LLGDFFRKSKEKIGKEFKRIVQRIKDFLRNLVPRTES (LL37)
Peptídeo 2: IDWKKLLDAAKQIL (Polybia-MP1)
Peptídeo 3: GIGAVLKVLTTGLPALISWIKRKRQQ (Melittin)
Peptídeo 4: INLKALAALAKKIL (Mastoparan)
Peptídeo 5: DSLSEDNWKFVVSSSCETILEILDIGGCAKGVAEYT (Hemilipin)
Peptídeo 6: MCMPCFTTDHQMARKCDDCCGGKGRGKCYGPQCLCR (Chlorotoxin)

5.3 *Síntese de peptídeos*

Os peptídeos foram sintetizados pela empresa AminoTech (Diadema, SP) com grau de pureza > 95% e sua qualidade foi checada por HPLC e espectrometria de massas.

5.4 Linhagens celulares

As linhagens celulares tumorais Y1, MCF7 e MDA-MB231, bem como a linhagem celular normal Y1-RasKO, foram cultivadas a 37ºC em 5% CO_2 em meio de cultura RPMI ou DMEM suplementadas com 10% de soro fetal bovino inativado e os antibióticos ampicilina a 25 mg/L e estreptomicina a 100 mg/L (algumas linhagens requerem mais cuidados e mais reagentes no cultivo, como a MCF10A). As células foram repicadas quando a confluência atingiu 80%.

Em nosso laboratório, o Dr. Matheus H. Dias conseguiu gerar células Y1 deletadas de Ras por CRISPR-9 (Sanjana et al., 2014) (Dias MH et al, 2018) aqui denominadas de Y1-RasKO. A célula da linhagem Y1 caracteriza-se por apresentar superexpressão de Ras. Acredita-se que Ras possa ser responsável pela tumorigenicidade da célula. A análise funcional da célula Y1-RasKO está sendo avaliada em camundongos no Laboratório de Ciclo Celular (LECC) pela Dra. Rosangela Wailemann, Dra. Luciana Gomes e pelo doutorando Thompson Torres sob supervisão do Prof. Dr. Hugo Aguirre Armelin.

5.5 Análise de proliferação celular

A análise de proliferação celular das diferentes linhagens celulares tumorais e normais frente aos peptídeos selecionados foram cultivadas em placas de 48 ou 96 poços, onde os peptídeos selecionados em diferentes concentrações seriam analisados. Após 24h de incubação, as amostras de cada poço seriam submetidas à análise com o reagente WST para verificar a viabilidade celular de cada linhagem celular. Porém, devido às dificuldades causadas pela pandemia por COVID-19, as etapas experimentais do projeto, incluindo as análises de proliferação celular, citotoxicidade dos peptídeos selecionados, análise por citometria de fluxo com marcadores de morte celular e análise de atividades antimicrobianas e anticâncer não foram realizadas a tempo até a confecção e submissão desta dissertação.

6 RESULTADOS E DISCUSSÃO – PROJETO I

6.1 Cultivo das células e curvas de crescimento

As linhagens celulares cultivadas consistiram em Y1, HeLa, MCF7, MDA-MB231, Y1-RasKO e HEK293. Foram feitas curvas de crescimento em placas de 96 poços para as linhagens celulares HeLa e Y1. As células HeLa testadas eram de passagens diferentes, mas apresentaram confluência similar após 48h do plaqueamento. Com base nestes resultados, foi possível estabelecer que a quantidade de células adequada a serem plaqueadas em poços de 96 foram de: $1{,}5x10^4$ células para HeLa e $2{,}5x10^4$ células para Y1.

O plaqueamento das células MDA-MB231 foi realizado utilizando 10^4 células/cm² para cada poço de uma placa de 96 poços. Desta forma, a quantidade plaqueada por poço foi de $3{,}3x10^3$ células.

6.2 Quantificação de proteínas

A quantificação pelo método de BCA inicial foi realizada para determinar a quantidade de proteínas na peçonha extraída. O experimento foi feito em triplicata, tanto do BSA quanto

da peçonha testada. As diluições foram feitas com valores previamente estipulados para a peçonha, pois era pressuposto que a concentração do estoque principal fosse alta. Desta maneira, a diluições testadas foram de 1:1000, 1:2000 e 1:10000 (Gráfico 1 e Tabela 1). Este teste foi feito utilizando apenas um dos tubos contendo a peçonha extraída, a fim de evitar desperdícios, já que o estoque de peçonha extraída não era abundante. Para o teste, foi escolhido aleatoriamente o tubo enumerado como 4. Os resultados mostraram que a diluição foi exagerada, pois os valores obtidos de concentração das amostras diluídas foram muito destoantes, tendo até um valor de concentração negativo, além de os valores médios de absorbância apresentados encontrarem-se na extremidade menor da curva-padrão, onde não há tanta precisão de quantificação quando comparado ao meio da curva.

Tabela 1 – Valores de concentração da peçonha extraída (microtubo eppendorf 4) em mg/mL obtidos através do gráfico da curva-padrão do método de quantificação por BCA. Diluições feitas de 1:1000, 1:2000 e 1:10000.

	Média		
	Diluído 1:_100		
	1:_10000	1:_2000	1:_1000
Absorbância	0,107	0,127	0,175
	Concentrações mg/mL		
	-0,031	0,014	0,122
Final	_ - _	28,909	122,268

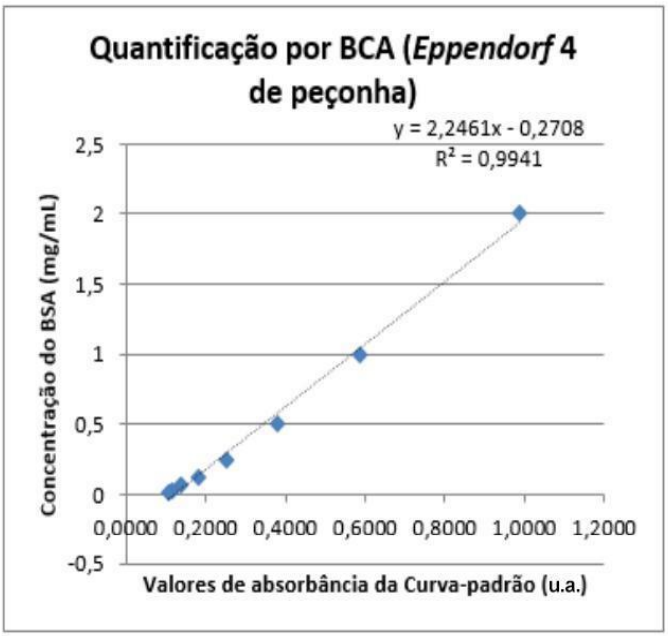

Gráfico 1 – Gráfico da curva-padrão gerada através de concentrações conhecidas de BSA utilizando o método de quantificação por BCA. Equação da reta para determinação da concentração desconhecida de outras amostras (y = 2,2461x – 0,2708). Fonte: Elaborada pela autora.

O mesmo teste foi repetido, agora com uma diluição menor do estoque original do tubo 4. As diluições escolhidas foram de 1:100, 1:200 e 1:1000 (Gráfico 2 e Tabela 2). Os valores de concentrações adquiridos tiveram menos flutuações e os valores de absorbância já não correspondiam a nenhuma extremidade da curva-padrão. Desta maneira, estas diluições foram utilizadas para quantificar o restante dos tubos com a peçonha extraída (1, 2 e 3) (Gráfico 3 e Tabela 3).

Tabela 2 – Valores de concentração da peçonha extraída (microtubo eppendorf 4) em mg/mL obtidos através do gráfico da curva-padrão do método de quantificação por BCA. Diluições feitas de 1:100, 1:200 e 1:1000.

	Média			
	Diluído 1:_100			
	1:_1000	**1:_200**	**1:_100**	
Absorbância	0,137	0,300	0,435	
Concentrações mg/mL				**Média**
Valores das diluições	0,0760	0,4436	0,7453	
Final (valor ajustado)	76,04	88,72	74,53	**79,77**

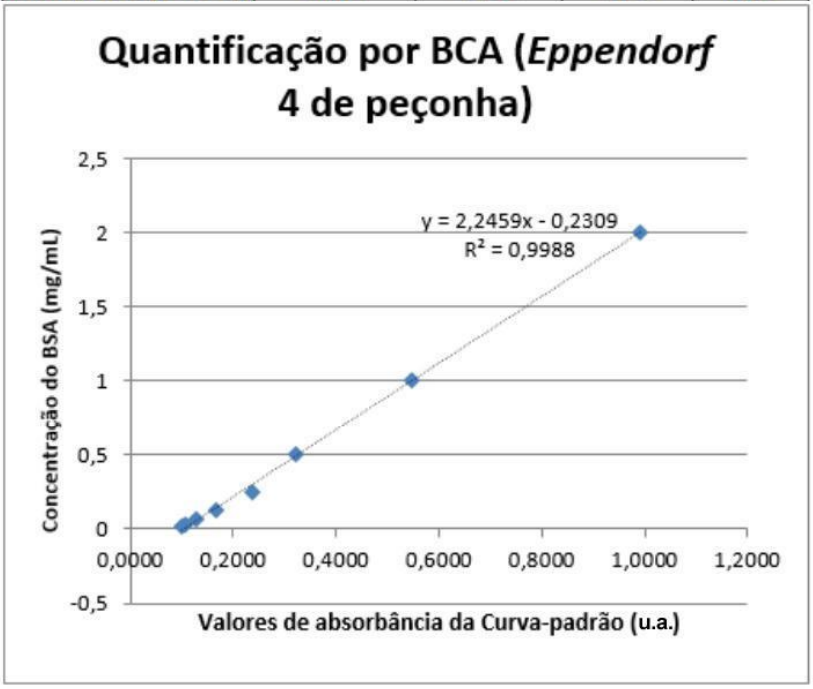

Gráfico 2 – Gráfico da curva-padrão gerada através de concentrações conhecidas de BSA utilizando o método de quantificação por BCA. Equação da reta para determinação da concentração desconhecida de outras amostras (y = 2,2459x – 0,2309). Fonte: Elaborada pela autora.

Tabela 3 – Valores de concentração de cada tubo da peçonha extraída em mg/mL obtidos através do gráfico da curva-padrão do método de quantificação por BCA. Diluições feitas de 1:100, 1:200 e 1:1000.

	Média							
Absorbância	Diluído 1:_100							
(Eppendorfs)	1:_1000	1:_200	1:_100					
1	0,117	0,299	0,463					
2	0,138	0,301	0,452					
3	0,129	0,253	0,371					
4	0,144	0,318	0,484					
Concentrações mg/mL				Final			Média	N° de escorpiões usados na extração
1	0,0161	0,4201	0,7848	16,13	84,01	78,48	81,25	9
2	0,0635	0,4245	0,7604	63,48	84,90	76,04	74,80	12
3	0,0435	0,3187	0,5806	43,50	63,74	58,06	55,10	7
4	0,0761	0,4630	0,8321	76,05	92,59	83,21	83,95	9

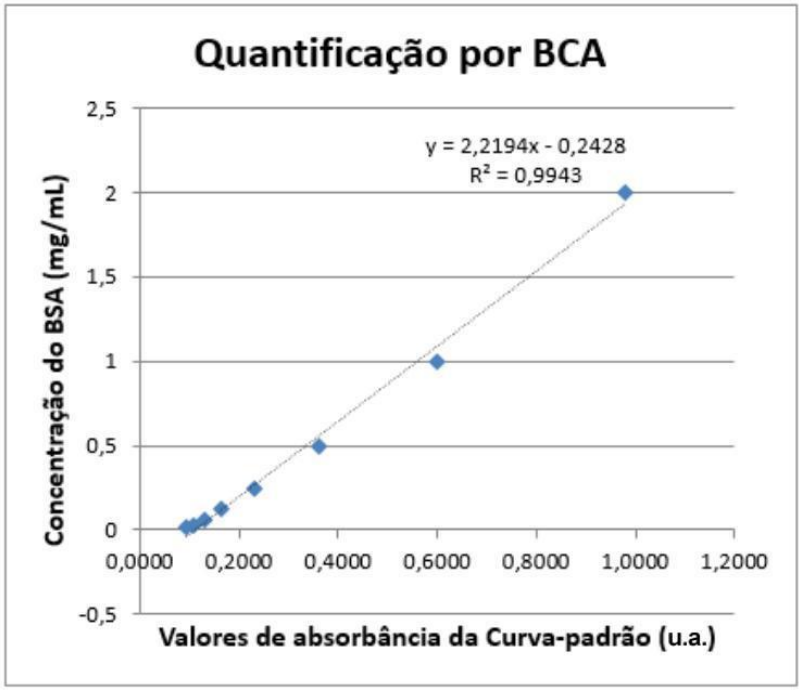

Gráfico 3 – Gráfico da curva-padrão gerada através de concentrações conhecidas de BSA utilizando o método de quantificação por BCA. Equação da reta para determinação da concentração desconhecida de outras amostras (y = 2,2194x – 0,2428). Fonte: elaborada pela autora.

6.3 Ensaio de citotoxicidade: Peçonha total de *T. serrulatus*

Um ensaio inicial foi feito em células HeLa para determinar a CC50. As concentrações da peçonha extraída utilizadas foram de 0,1; 0,3; 0,5; 0,7; 1; 2,5; 5; 10; 20 e 50 µg/mL. O experimento foi feito em triplicata, com controle negativo composto de acetato de amônio pH 5,5 (50mM) e outro controle somente com as células e o meio, com intuito de detectar

contaminações no meio, caso houvesse. Este controle foi necessário pois tivemos alguns casos de contaminação na cultura de células. O acetato de amônio foi a solução utilizada para diluir o estoque original da peçonha de acordo com protocolo já estabelecido no laboratório do Prof Pedro Ismael da Silva Júnior.

O resultado não mostrou grande diferença entre as células tratadas e os controles, uma vez que não observamos morte celular, mesmo as células sendo tratadas com alta concentração da peçonha (50 µg/mL) (Gráfico 4 e Tabela 4). Pode ser que isso tenha acontecido pela peçonha ser neurotóxica e não atuar diretamente nesse tipo de linhagem celular, além de não possuir atividade citotóxica a esta concentração como observado com a peçonha da *Bothrops jararaca*.

Tabela 4 – Valores de absorbância de acordo com as concentrações de peçonha colocadas nos poços da placa multiwell-96 e controles

		Peçonha Extraída *T. serrulatus*										
	Concentração [µg/mL]	0	0,1	0,3	0,5	0,7	1	2,5	5	10	20	50
Médias (nm)	HeLa	3,509	3,509	3,493	3,487	3,517	3,496	3,496	3,508	3,497	3,506	3,540
	Controle -	3,495										
	Controle +	3,515										

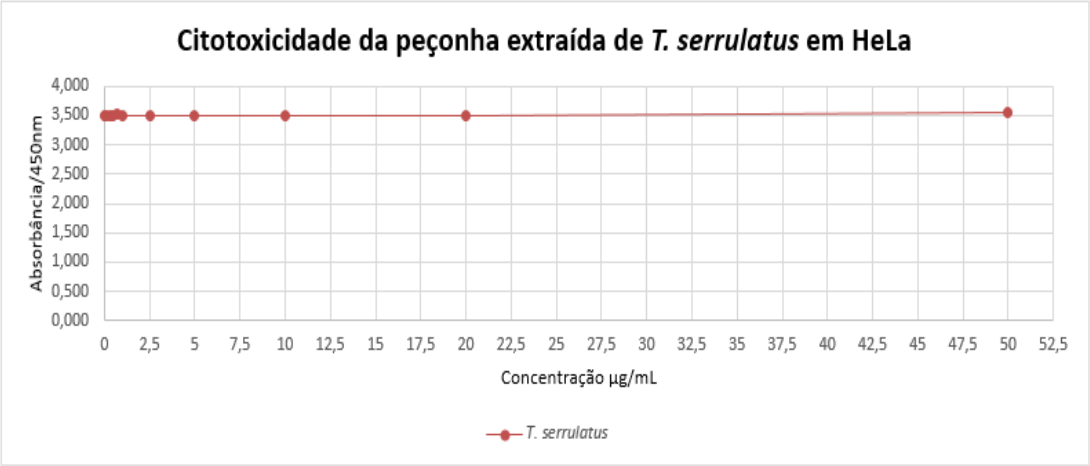

Gráfico 4 – Gráfico de citotoxicidade da peçonha extraída de *T. serrulatus* em células de HeLa. Fonte: elaborada pela autora.

Após testar a atividade das peçonhas (extraída e liofilizada), deu-se continuidade aos ensaios de citotoxicidade (Gráfico 5). Entretanto, todos os experimentos para determinação da CC50 não resultaram em morte celular pronunciada em nenhuma das concentrações da peçonha utilizadas.

Em uma tentativa de visualizar a morte celular como fenótipo resultante do tratamento das células com a peçonha liofilizada de *T. serrulatus*, foi feito um teste onde utilizamos uma concentração alta da peçonha (50 µg/mL). As linhagens celulares utilizadas foram HEK293,

Y1, HeLa e MCF7. Não foi visto morte celular e nenhuma diferença pronunciada entre o antes e depois, sendo que os controles e os poços tratados estavam bastante similares.

As células foram plaqueadas para atingir confluência de cerca de 80% após 48 h. Depois, o meio com soro 10% (S.F.B.) foi trocado por meio sem soro, após uma etapa de lavagem por PBS em cada poço. Após 24 h, com as células sincronizadas, a peçonha foi adicionada ao poço tratado.

As células de HEK293 morreram após 24 horas de tratamento. No entanto, os controles também acabaram morrendo. Desta forma, considera-se que a morte provavelmente decorreu do uso de PBS na etapa de lavagem das células, que eram células mais frágeis à manipulação.

6.4 Ensaio de atividade enzimática da peçonha de *T. serrulatus*

O teste para determinar se a peçonha possuía atividade enzimática foi realizado para dar prosseguimento aos experimentos de citotoxicidade celular para determinação da CC50. Desta forma, foram testadas tanto a peçonha extraída dos escorpiões no LETA quanto a obtida através do Núcleo Estratégico de Venenos e Antivenenos do Instituto Butantan foram testadas. O resultado mostrado no Gráfico 5 mostra a atividade enzimática da peçonha. Portanto, a falta de mudanças tanto na morte quanto no fenótipo das células ao aplicar a peçonha não ocorreu por causa de inatividade ou má qualidade das peçonhas. Pode ser que isso tenha acontecido devido ao tipo de atividade desempenhada pela peçonha, que é neurotóxica, sendo ineficaz na citotoxicidade de células não-neuronais.

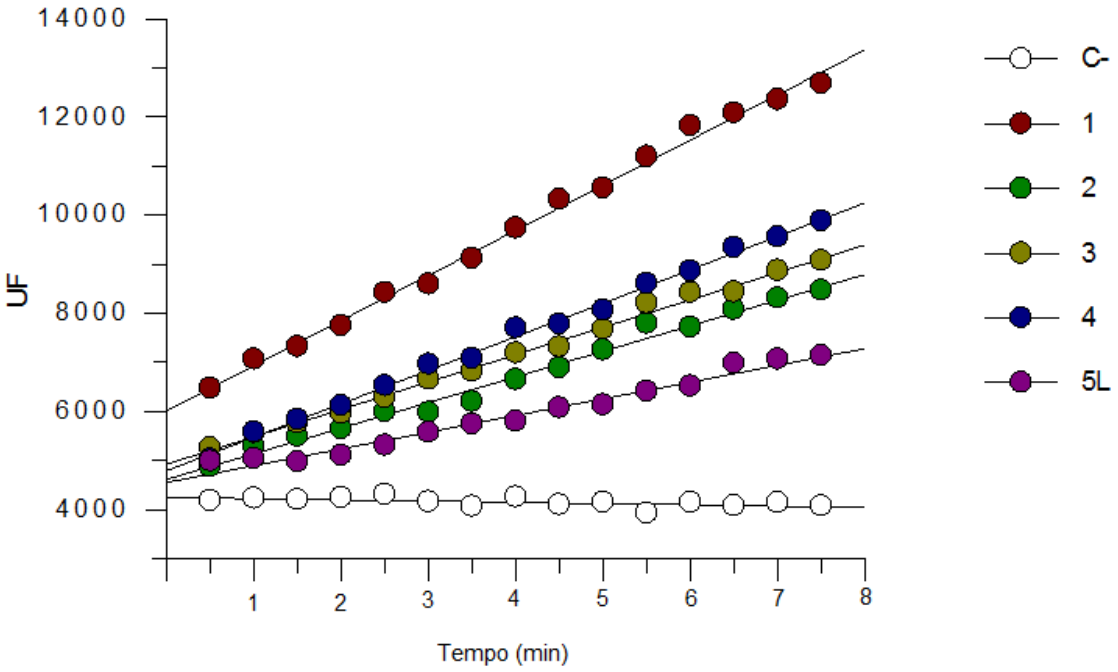

Gráfico 5 – Gráfico do ensaio de atividade enzimática das peçonhas extraída e liofilizada de *T. serrulatus*, onde quanto maior a unidade de fluorescência (UF) maior a atividade enzimática da amostra. 1 – Amostra do microtubo eppendorf 1 da peçonha extraída [81,25 mg/mL]. 2 – Amostra do microtubo eppendorf 2 da peçonha extraída [74,8 mg/mL]. 3 – Amostra do microtubo eppendorf 3 da peçonha extraída [55,1 mg/mL]. 4 – Amostra do microtubo eppendorf 4 da peçonha extraída [83,95 mg/mL]. 5L – Amostra do microtubo eppendorf 1 da peçonha liofilizada [10 mg/mL]. O substrato e tampão (Abz-FLRRV-EDDnp e Tris 20 mM, NaCl 20 mM, respectivamente) foram utilizados como controle negativo (C-). Fonte: elaborada pela autora.

6.5 Cromatografia de gel separação da peçonha total de *T. serrulatus*

As frações peptídicas menores que 14 kDa da peçonha total de *T. serrulatus* foram feitas utilizando cromatografia em de gel separação com coluna *Superdex peptide* HR 10/30 no laboratório do Dr. Pedro Ismael da Silva Junior. Foram feitas duas cromatografias, sendo que a primeira foi coletada por pico (Figura 7), e a segunda por tempo (de 1 em 1 minuto) (Figura 8).

Figura 7 – Cromatografia VTS001 de gel-separação com coleta por pico

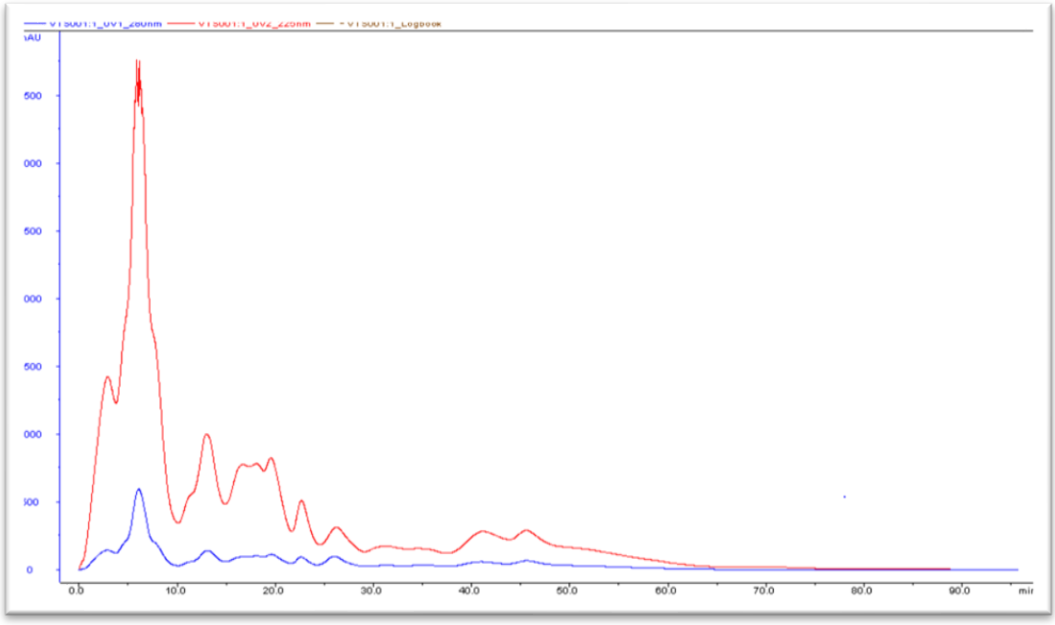

Em azul = leitura a 280 nm. Em vermelho= leitura a 220 nm. Fonte: Elaborada pela autora.

Figura 8 - Cromatografia VTS002 de gel-separação com coleta por pico

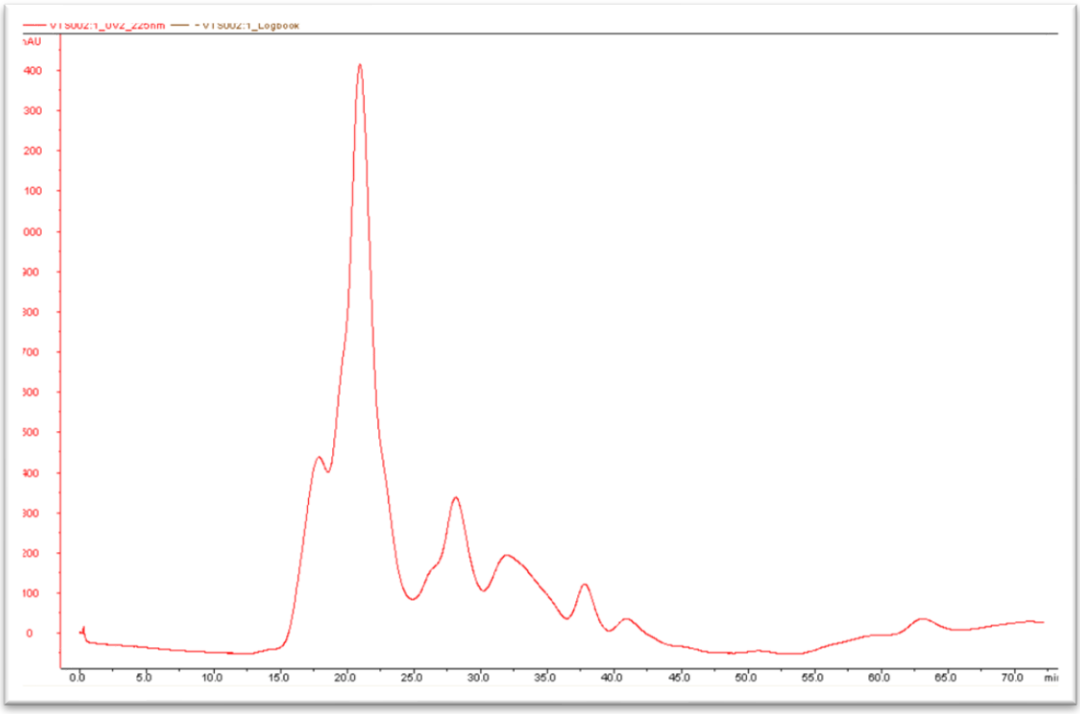

Cromatografia VTS002 resultante da cromatografia feita por gel-separação, com coleta por tempo (de minuto em minuto). Leitura a 220 nm. Fonte: Elaborada pela autora.

Como padrão para as cromatografias das figuras 8 e 9, foram utilizadas lisozima (15 kDa), DODa (1,787 kDa) e Cheliferina (0,748 kDa), onde os cromatogramas resultantes estão representados nas figuras 9, 10 e 11, respectivamente.

Figura 9 - Cromatografia com padrão de Lisozima (15 kDa)

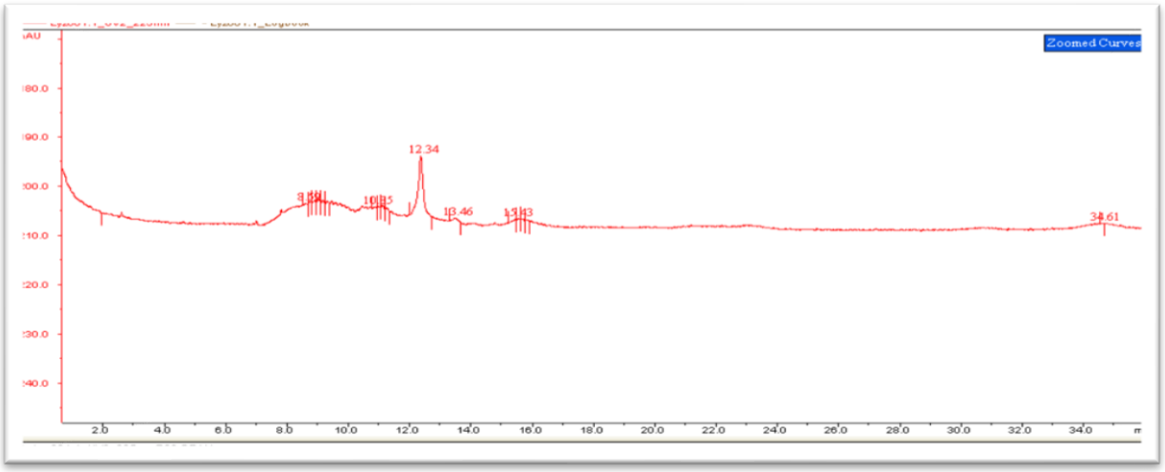

Cromatografia por gel-separação. Fonte: elaborada pela autora.

Figura 10 - Cromatografia com padrão de DODa (1,787 kDa)

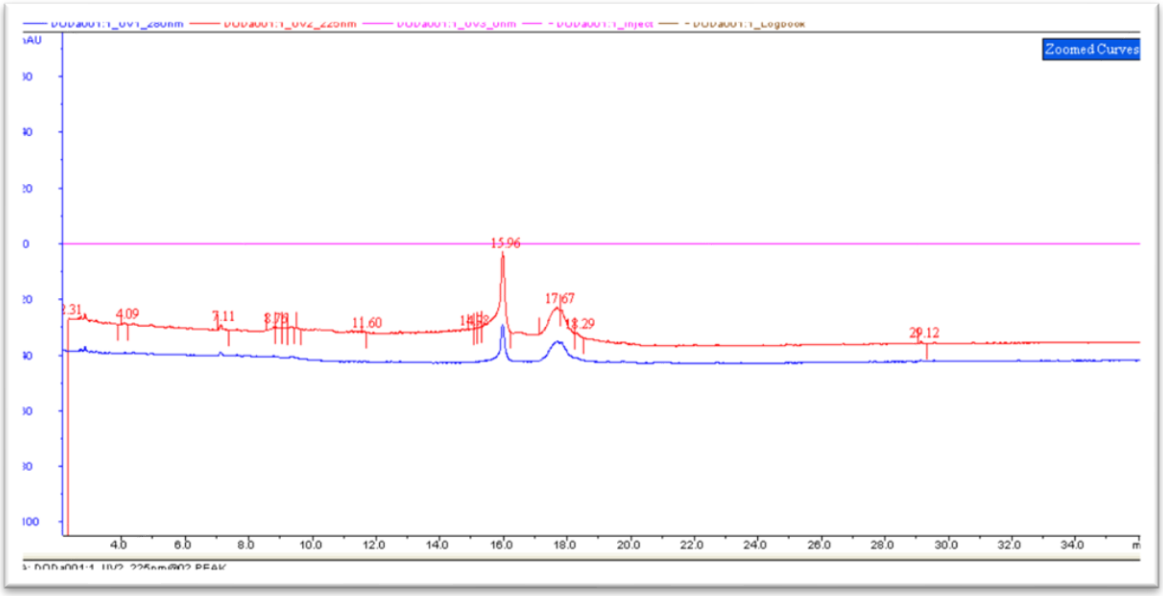

Cromatografia feita por gel-separação. Linha azul = leitura a 280 nm, Linha vermelha = leitura a 220 nm. Fonte: elaborada pela autora.

Figura 11 - Cromatografia com padrão de Cheliferina (0,748 kDa)

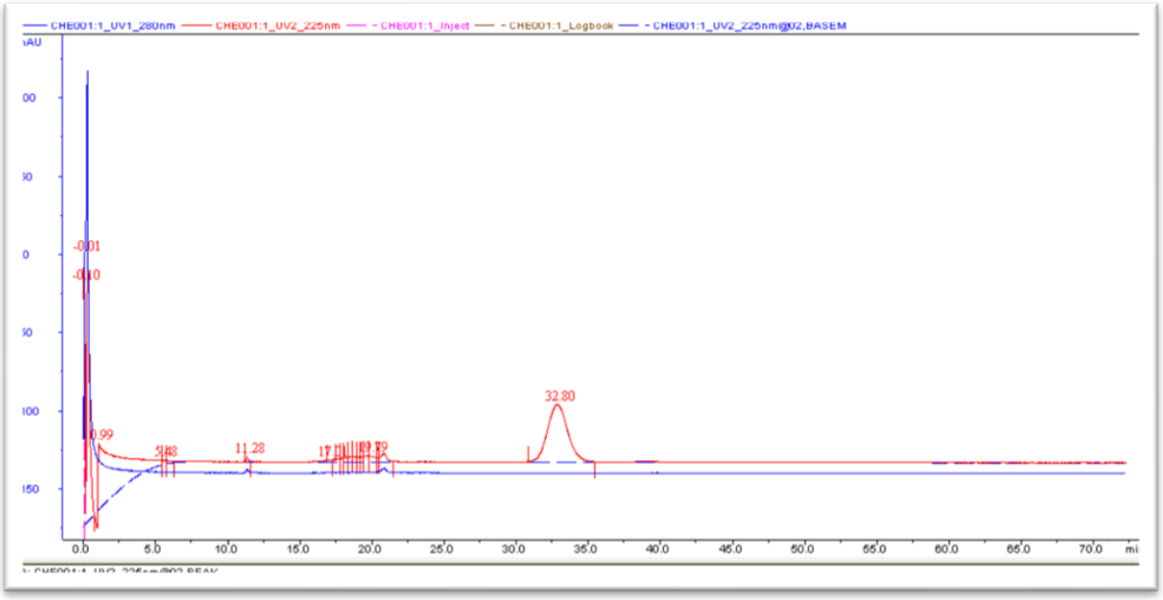

Cromatografia feita por gel-separação. Linha azul = leitura a 280 nm, Linha vermelha = leitura a 220 nm. Fonte: elaborada pela autora.

Na cromatografia VTS001 (figura 7), foram coletados 15 picos, onde posteriormente foram juntados após interpretação do cromatógrafo de cada pico. Desta forma, as frações foram unidas ou não da seguinte maneira: “1 + 2”, “3 + 4”, “5”, “6”, “7”, “8 + 9”, “10”, “11”, “12”, “13” e “14+15”. As frações foram renomeadas respectivamente de números de 1 a 11 para testes posteriores de citotoxicidade.

A cromatografia VTS002 não foi juntada em picos da mesma maneira que a VTS001. Também não foram realizados testes com as frações resultantes desta cromatografia. As frações decorrentes da VTS001 foram priorizadas para utilização por conta de ter sido injetado uma quantidade inicial 3 vezes maior que a VTS002 no cromatógrafo para separação por tamanho de peptídeos. Desta maneira, as frações resultantes de VTS001 a princípio estavam mais concentradas. A concentração das frações foi definida somente após o teste de citotoxicidade feito em células MDA-MB231.

6.6 Ensaio de atividade antimicrobiana

Os ensaios de atividade antimicrobiana foram feitos com objetivo de verificar se havia atividade contra o microorganismo *M. luteus*, uma bactéria gram-positiva, já que estudos

mostram que moléculas bioativas também têm potencial ação anti-tumoral (Guo, X., *et al*., 2013). Os dois ensaios, feitos como descritos em materiais e métodos, mostraram que as bactérias cresceram muito pouco após cerca de 20 horas nos controles de água ultrapura (MilliQ) com meio PB + bactérias, exceto dois poços específicos (B2 e H5) (Figura 12). Já no ensaio que teve leitura em espectrofotômetro Hidex feita após 14 h e 33 h, pode-se notar que as bactérias começaram a crescer nos controles, mas que na maioria dos poços com as frações houve um aumento muito maior no crescimento bacteriano comparado com os controles (Figuras 13 e 14, respectivamente).

Figura 12 - Ensaio antimicrobiano contra o microorganismo *M. luteus. Ensaio 1*.

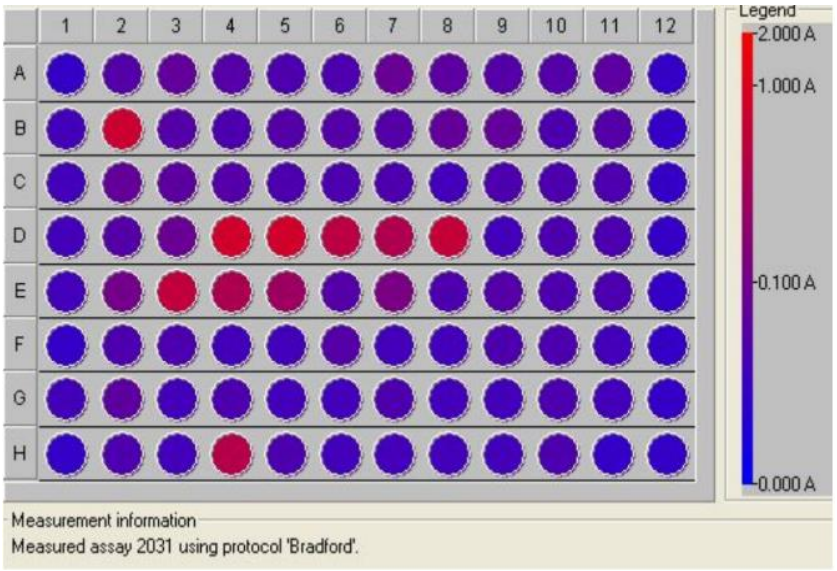

Primeiro ensaio antimicrobiano contra o microorganismo *M. luteus* utilizando as frações juntadas correspondentes à cromatografia VTS001. Espectro foi mensurado após 20h de incubação a 30ºC sob agitação. Fonte: elaborada pela autora.

Figura 13 - Ensaio antimicrobiano contra o microorganismo *M. luteus. Ensaio 2.*

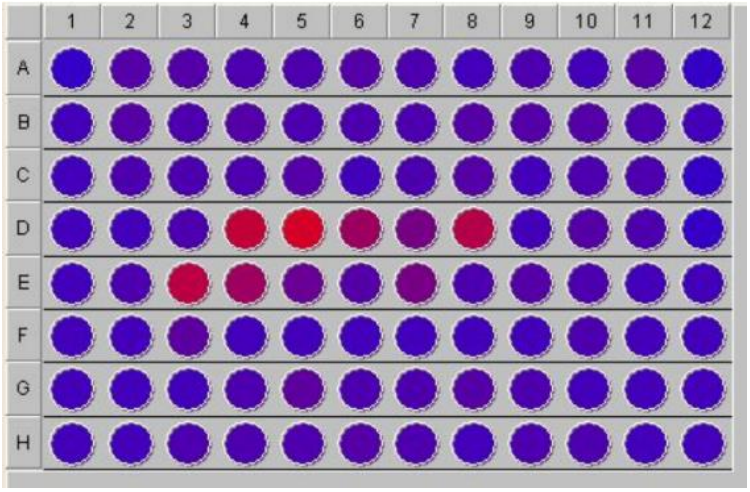

Segundo ensaio antimicrobiano contra o microorganismo *M. luteus* utilizando as frações juntadas correspondentes à cromatografia VTS001. Espectro foi mensurado após 14h de incubação a 30ºC sob agitação. Fonte: elaborada pela autora.

Figura 14 - Ensaio antimicrobiano contra o microorganismo *M. luteus. Ensaio 3.*

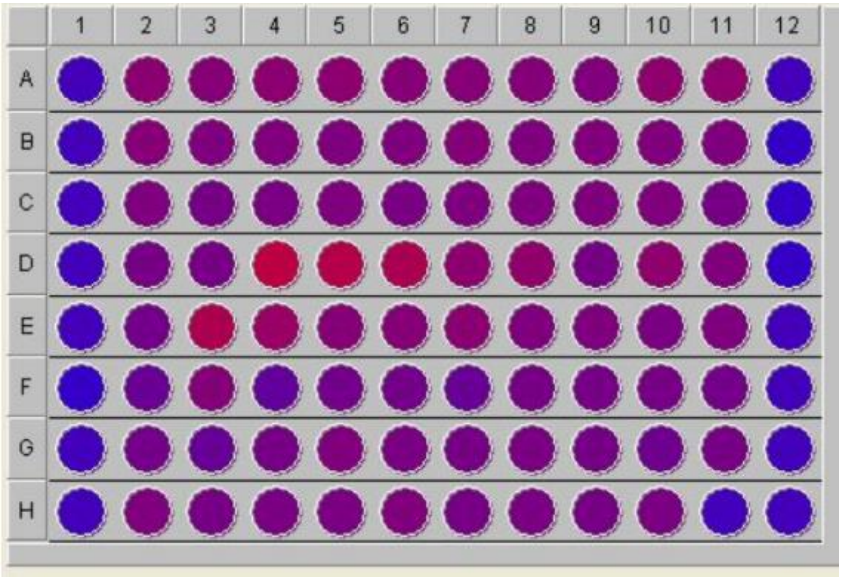

Terceiro ensaio antimicrobiano contra o microorganismo *M. luteus* utilizando as frações juntadas correspondentes à cromatografia VTS001. Espectro foi mensurado após 33h de incubação a 30ºC sob agitação. Fonte: elaborada pela autora.

6.7 Peçonha fracionada de *T. serrulatus*

As frações peptídicas da peçonha de *T. serrulatus* separadas por cromatografia de gel separação foram utilizadas em teste citotóxico nas células MDA-MB231. Inicialmente, o teste

foi feito para verificar se existia alguma atividade das frações peptídicas contra as células tumorais de mama. Porém, a determinação da citotoxicidade CC50 não foi realizada a tempo para a confecção desta tese.

As frações de 1 a 11 foram testadas em dois tempos e duas quantidades diferentes. Os tempos testados foram de 24h e 48h após a adição de cada tratamento. Já a quantidade foi determinada com base nos testes antimicrobianos, já que ainda não sabíamos a concentração de cada fração. A concentração foi obtida posteriormente pela quantificação por BCA de peptídeos das frações 2 a 11 (a fração 1 contém todos os componentes maiores que 14 kDa da peçonha total). Portanto, as duas quantidades utilizadas para testar as frações foram de 20 µL mais 80 µL de meio RPMI sem soro e de 50 µL mais 50 µL de meio RPMI sem soro. Os controles utilizados neste experimento foram de poços com 100 µL de meio RPMI sem soro e poços com 20 µL de água ultrapura mais 80 µL de meio RPMI sem soro e 50 µL de água Ultrapura (MilliQ) mais 50 µL de meio RPMI sem soro. A água Ultrapura (MilliQ) foi utilizada como controle por ser o veículo das frações peptídicas testadas. Foram feitos testes de 24 e 48 h para as duas quantidades aplicadas nas células (20 µL e 50 µL de fração peptídica) (Gráficos 6, 7, 8 e 9).

Para o experimento onde foram aplicados 20 µL de cada fração pode-se notar que algumas frações têm potencial atividade antitumoral (2, 6 e 10) quando comparadas com os controles após 48 h de tratamento (12 e 13) (Gráfico 7). Não houveram tantas mudanças após 24 h de tratamento (Gráfico 6). No entanto, quando são aplicados 50 µL, podemos notar que o controle com 50 µL de água Ultrapura (MilliQ) (12) (Gráfico 8) possui menos atividade mitocondrial medida através do uso de WST. Entretanto, mesmo o controle estando com baixa quantidade de células que apresentam atividade mitocondrial, pode-se notar que após 48 h de tratamento algumas frações (3 e 11) diminuem ainda mais a quantidade de atividade mitocondrial quando comparado com os controles (12 e 13) (Gráfico 9). No tratamento após 24 h é difícil dizer se as frações tiveram alguma atividade, já que o controle 12 apresentou baixa atividade mitocondrial, sem que nenhuma fração causasse atividade menor (Gráfico 9).

Pode ser que a baixa atividade mitocondrial encontrada também nos controles seja reflexo do uso parcial de água Ultrapura (MilliQ) dos poços, pois isso pode ter causado estresse oxidativo nas células pela presença de Ultrapura (MilliQ).

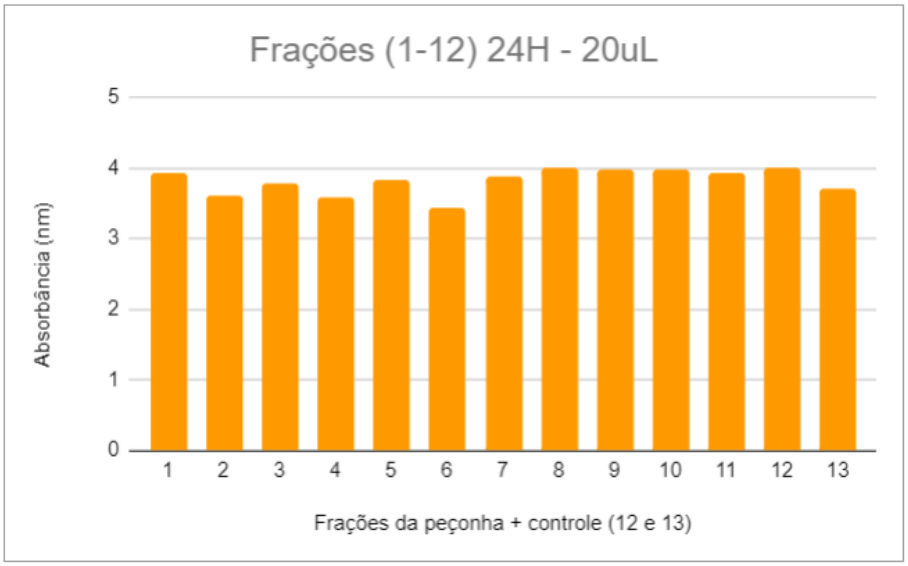

Gráfico 6 – Teste de atividade citotóxica das frações peptídicas de 1 a 11 em células MDA-MB231 em *multiwell* de 96 poços de fundo chato após 24 h. Foram adicionados a cada poço 20 µL de cada fração mais 80 µL de meio RPMI sem soro. Os controles 12 e 13 são, respectivamente, 20 µL de água Ultrapura (MilliQ) mais 80 µL de meio RPMI sem soro e 100 µL de meio RPMI sem soro em células. Os valores de absorbância foram obtidos por leitura dos poços a 450 nm em espectrofotômetro após 4 h de tratamento com 10 µL de WST. Fonte: elaborada pela autora.

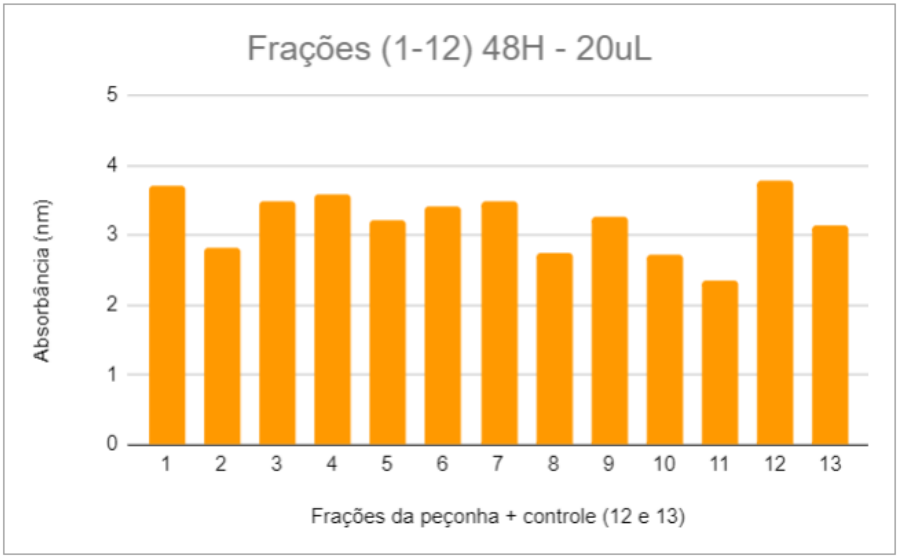

Gráfico 7 – Teste de atividade citotóxica das frações peptídicas de 1 a 11 em células MDA-MB231 em *multiwell* de 96 poços de fundo chato após 48 h. Foram adicionados a cada poço 20 µL de cada fração mais 80 µL de meio RPMI sem soro. Os controles 12 e 13 são, respectivamente, 20 µL de água Ultrapura (MilliQ) mais 80 µL de meio RPMI sem soro e 100 µL de meio RPMI sem soro em células. Os valores de absorbância foram obtidos por leitura dos poços a 450 nm em espectrofotômetro após 4h de tratamento com 10 µL de WST. Fonte: elaborada pela autora.

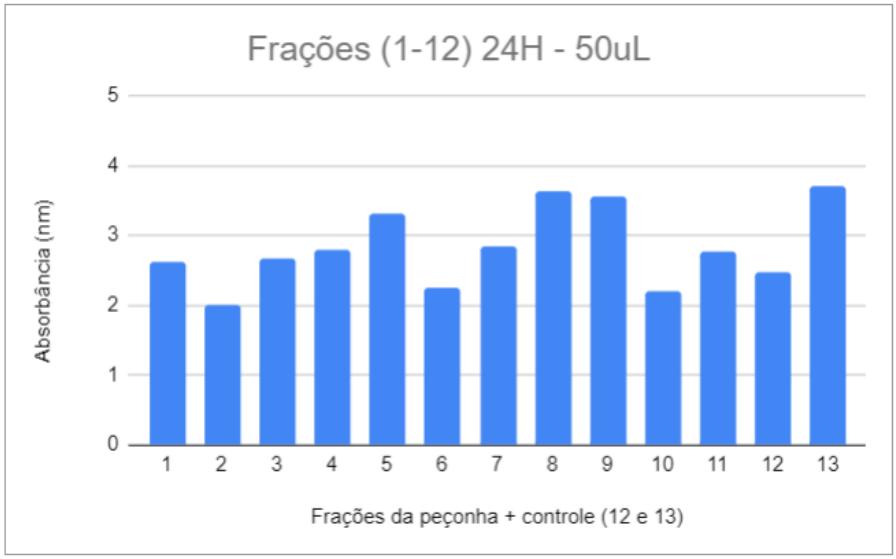

Gráfico 8 – Teste de atividade citotóxica das frações peptídicas de 1 a 11 em células MDA-MB231 em *multiwell* de 96 poços de fundo chato após 24 h. Foram adicionados a cada poço 50 µL de cada fração mais 50 µL de meio RPMI sem soro. Os controles 12 e 13 são, respectivamente, 50 µL de água Ultrapura (MilliQ) mais 50 µL de meio RPMI sem soro e 100 µL de meio RPMI sem soro em células. Os valores de absorbância foram obtidos por leitura dos poços a 450 nm em espectrofotômetro após 4h de tratamento com 10 µL de WST. Fonte: elaborada pela autora.

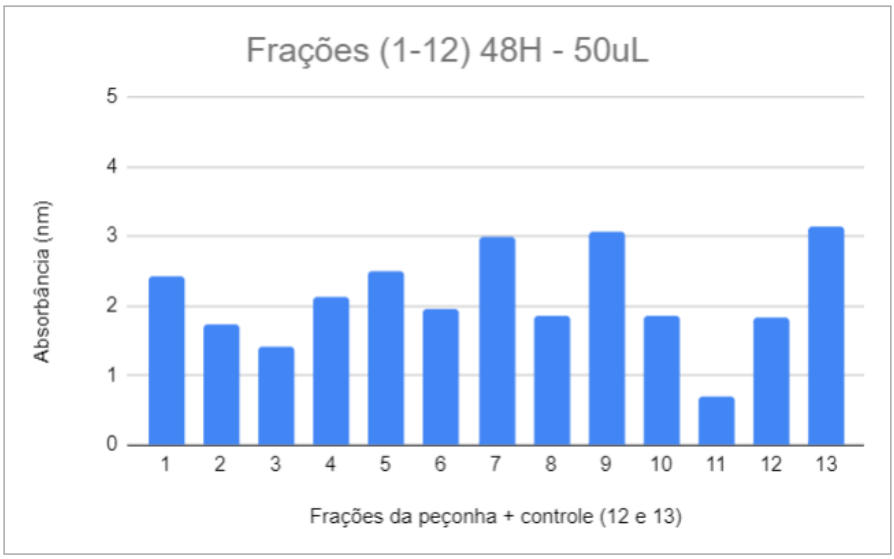

Gráfico 9 – Teste de atividade citotóxica das frações peptídicas de 1 a 11 em células MDA-MB231 em *multiwell* de 96 poços de fundo chato após 48 h. Foram adicionados a cada poço 50 µL de cada fração mais 50 µL de meio RPMI sem soro. Os controles 12 e 13 são, respectivamente, 50 µL de água Ultrapura (MilliQ) mais 50 µL de meio RPMI sem soro e 100 µL de meio RPMI sem soro em células. Os valores de absorbância foram obtidos por leitura dos poços a 450 nm em espectrofotômetro após 4 h de tratamento com 10 µL de WST. Fonte: elaborada pela autora.

6.8 Quantificação de peptídeos

A quantificação de peptídeos das frações obtidas a partir da cromatografia de gel separação da peçonha total de *T. serrulatus* foi feita utilizando o kit *Pierce ™ Quantitative Colorimetric Peptide Assay (500 assays)* da *Thermofisher*. A curva-padrão foi feita em 8 diluições a partir de 1 mg/mL.

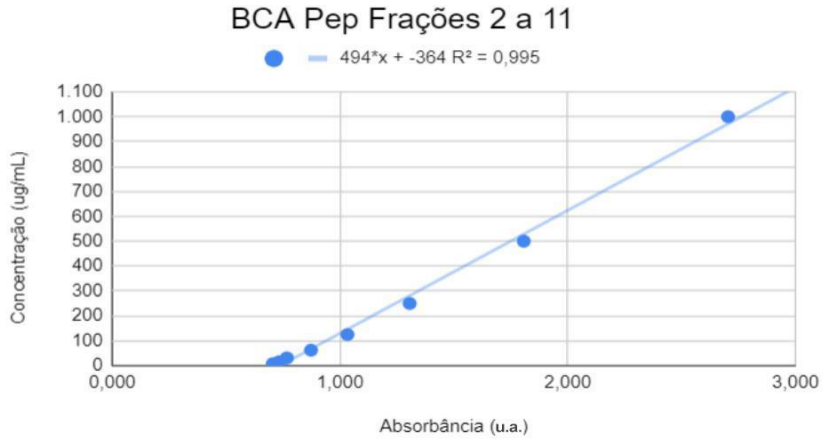

Gráfico 10 - Gráfico da curva-padrão gerada através de concentrações conhecidas de padrão de referência de peptídeos digeridos de alta qualidade utilizando o método de quantificação por BCA para peptídeos. Equação da reta para determinação da concentração desconhecida de outras amostras (y = 494x - 364). Fonte: elaborada pela autora.

Com base na equação da reta proveniente do gráfico 10, foi possível determinar as concentrações de cada fração (de 2 a 11), como mostra a tabela 5. A fração 1 não foi quantificada por conter proteínas maiores que 14 kDa, já que foi o primeiro pico a sair da cromatografia de gel separação, que separa das proteínas maiores para menores de acordo com a coluna utilizada. Desta forma, este kit não seria adequado para quantificação desta fração protéica.

Tabela 5 – Valores de concentração de cada fração peptídica da peçonha (2 a 11) em µg/mL obtidos através do gráfico da curva-padrão do método de quantificação BCA de peptídeos.

Frações	Abs das frações (u.a.)	Concentração (ug/mL)
2	1,647	449,618
3	3,791	1508,754
4	2,770	1004,38
5	1,971	609,674
6	2,348	795,912
7	1,578	415,532
8	1,075	167,05
9	0,981	120,614
10	0,998	129,012
11	1,369	312,286

A partir dos valores de concentração obtidos das frações de 2 a 11, foi possível determinar as concentrações aplicadas nos testes de atividade de citotoxicidade nas células MDA-MB231 (Tabela 6).

Tabela 6 – Valores de concentração de cada fração peptídica da peçonha (2 a 11) em µg/mL aplicada nos testes de citotoxicidade em *multiwell* 96 poços de fundo chato descrito anteriormente.

Frações	Concentração em ug/mL nos poços com 20 uL	Concentração em ug/mL nos poços com 50 uL
2	89,92	224,8
3	301,75	754,37
4	200,87	502,19
5	121,93	304,83
6	159,18	397,95
7	83,1	207,76
8	33,41	83,52
9	24,12	60,3
10	25,8	64,5
11	62,45	156,14

6.9 Análise proteômica por Espectrometria de Massas

As proteínas das amostras das células Y1 e Y1RasKO tratadas com a peçonha por 6 h, 12 h, 24 h e 48 h foram modificadas quimicamente (reduzidas com DTT e alquiladas com IAA), digeridas com tripsina na razão 1:50 de enzima: substrato, dessalinizadas em colunas de extração de fase sólida confeccionadas *in house* (Stage-Tip) e marcadas por dimetilação leve (células Y1RasKO tratadas com a peçonha de *T. serrulatus*) e pesada (células Y1 tratadas com a peçonha de *T. serrulatus*) o que permitiu a redução do número de amostras para 50%, reduzindo também o tempo de utilização do espectrômetro de massas.

Uma vez que o equipamento LTQ-Orbitrap Velos de nosso laboratório LETA e o espectrômetro Q-Exactive Plus do laboratório de espectrometria de massas do CENTD, Instituto Butantan, estavam com problemas técnicos, iniciamos um trabalho colaborativo com o Dr. Valdemir Carvalho do Grupo Fleury. As amostras pareadas entre controle e tratado com peçonha e a aquisição dos dados foram realizadas no espectrômetro de massas Q-Exactive HF onde foram injetadas 1 µg/µl de amostra.

6.10 Identificação das proteínas e Caracterização Funcional

Os dados brutos do espectrômetro de massas (*raw files*) foram analisados no software PEAKS Studio X plus, conforme os parâmetros apresentados no item Material e Métodos – projeto I.

Identificamos um total de 601 proteínas em todas as condições, das amostras das células Y1 e Y1RasKO tratadas com a peçonha de *T. serrulatus*.

A análise por Ontogenia Gênica (do inglês *Gene Ontology*, GO) permitiu-nos traçar um perfil de enriquecimento de algumas categorias como mostrado na figura abaixo.

A.

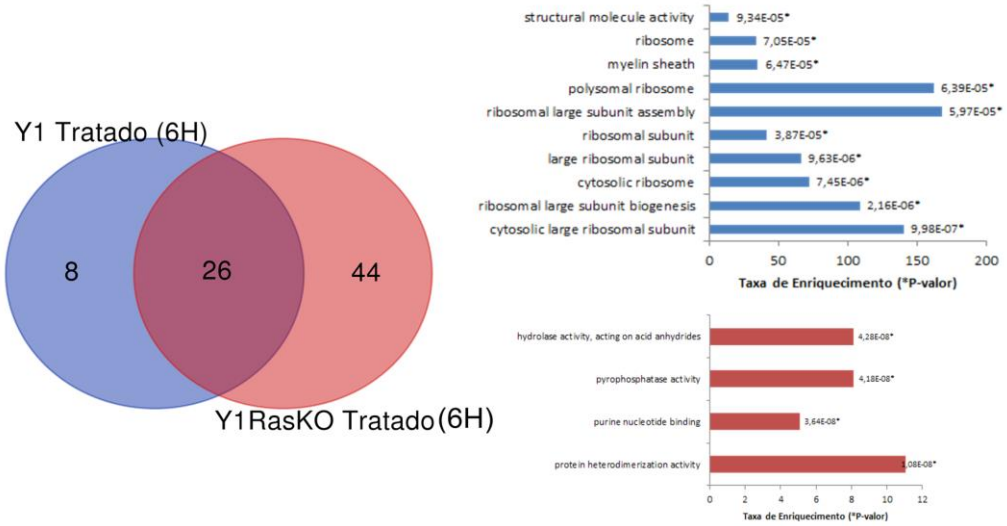

B.

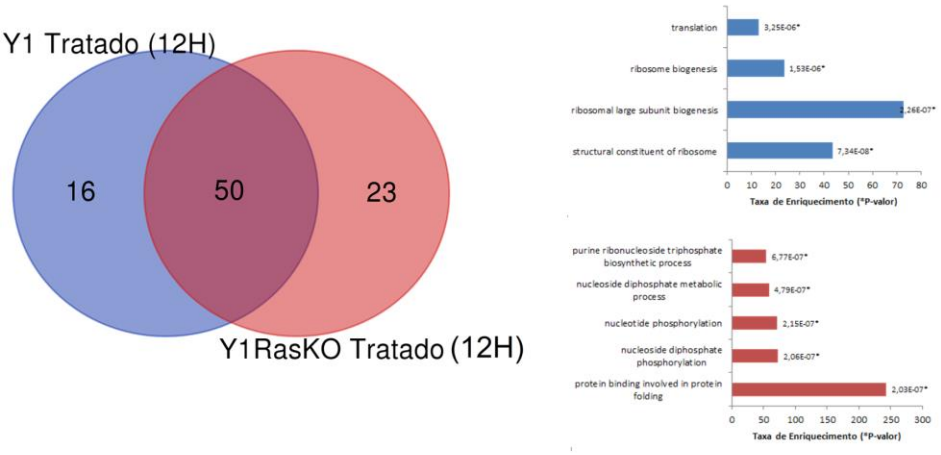

C.

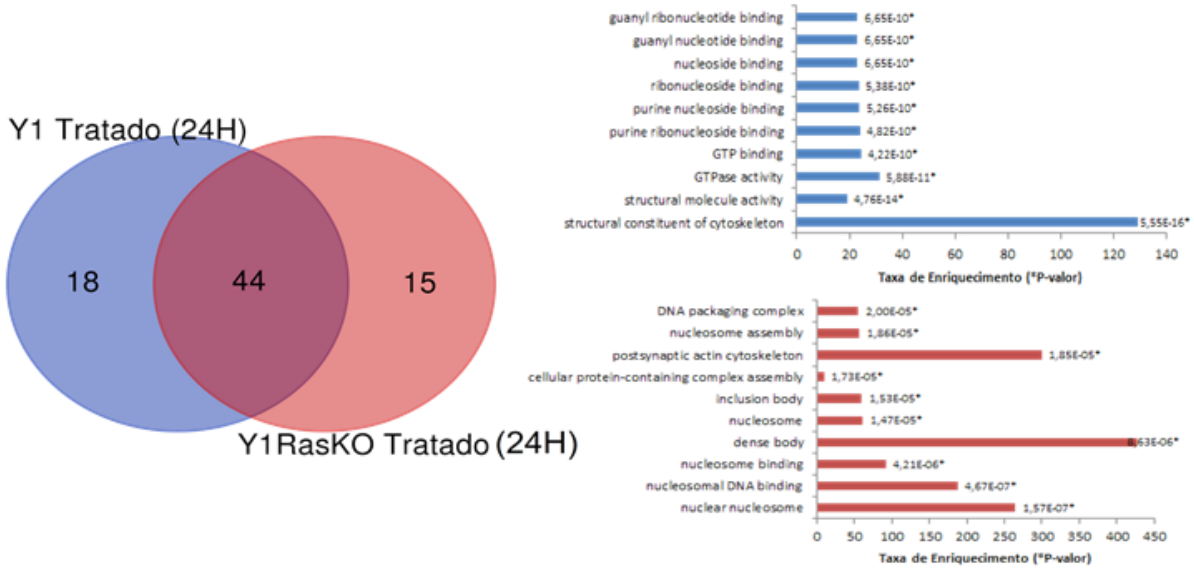

D.

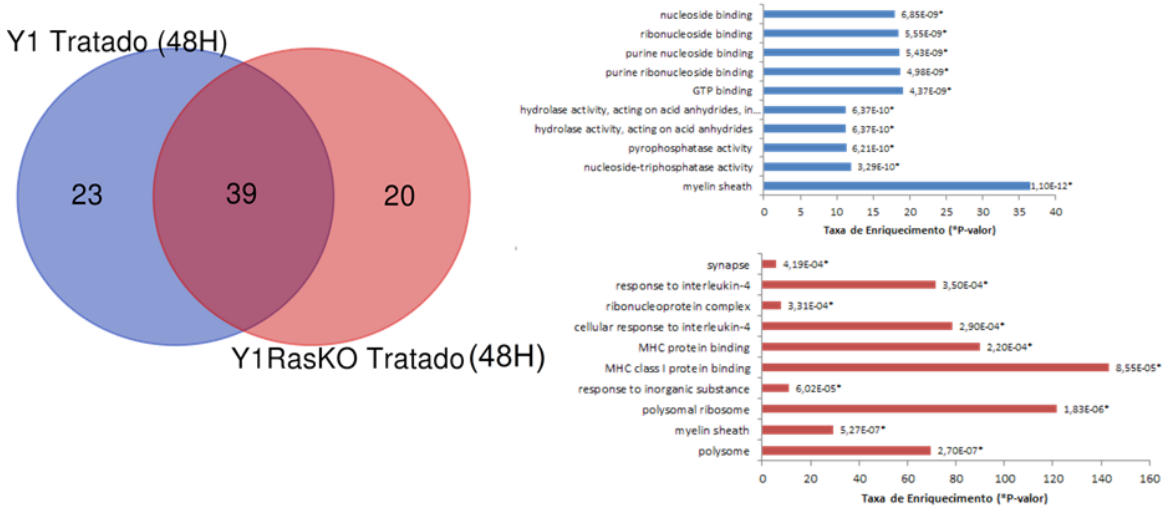

Gráfico 11: Diagramas de Venn das proteínas detectadas por espectrometria de massas na linhagem celular cancerígena Y1 e na linhagem celular normal Y1RasKO nas amostras tratadas com a peçonha de *T. serrulatus* [10 µg/mL] e caracterização funcional das proteínas exclusivas detectadas. *Taxa de Enriquecimento = número observado dividido pelo número esperado de genes da categoria GO ou KEGG na lista de genes de acordo com o WebGestalt. A. tratamento por 6 h, B. tratamento por 12 h, C. tratamento por 24 h, D. tratamento por 48 h com a peçonha de *T. serrulatus.*
Fonte: elaborada pela autora.

A quantificação das proteínas permitiu identificar 106 proteínas em todas as condições. Porém, verificamos que as 2 das 3 réplicas analisadas não estavam boas em todas as condições testadas. Uma análise geral dos dados mostrou que algumas proteínas apresentaram abundância

maior que 2x (marcadas em rosa) sendo que algumas apresentaram abundância maior que 8x (marcadas em vermelho) em comparação com as células tratadas com PBS. Outras proteínas apresentaram uma mudança na abundância menor que 0.5x (mostradas em verde) (Gráfico 12).

	6 h		12 h		24 h		48 h	
Protein	Y1rasKO	Y1	Y1rasKO	Y1	Y1rasKO	Y1	Y1rasKO	Y1
Kpnb1								43.1
Pgd			5.1	3.2	2.4	3.7	3.7	3.1
Mdh2	12.2		11.6	8.7	5.4	6.1		2.5
Arhgdia	1.1			24.1		1.9		2.4
Hnrnpk	2.1		2.3	2.5		1.9		2.2
Ctsa	2.4		1.5	2.1			2.4	2.0
Tuba1c	1.6			15.9		2.7		1.8
Msn	1.1			3.2		2.2		1.7
Myl6	1.7			2.0		1.8	2.3	1.5
Rps19			2.8	2.4		2.4	2.2	1.5
Cct8	1.7		1.9	2.1				1.5
Sod1	20.4			1.8		1.6		1.4
Hnrnpa2b1	0.8		2.1	0.9	1.7	1.4	1.8	1.3
Anxa2	1.2		1.1	1.1		3.4	1.4	1.1
Rap1b			1.4	2.0		0.8		1.1
Hnrnpa3	0.7		3.4	0.9				1.0
Eno1	8.1					1.0		0.9
Tubb4b	3.3		8.6	13.9			0.5	0.6
Inppl1								0.5
Calm2	0.8		2.0	0.9		1.0		0.5
Rab8a								0.5
Rpa3	0.2		0.5	0.5			0.4	0.4
Hsd17b4								0.4
Trim28	0.7					0.9		0.4
Gsn								0.3
Eif3a							7.5	
Guf1				0.4		0.7	0.3	
Rab7				2.6		2.0		
Sod2						0.4		
Rps8					6.4			
Sepinh1	10.0			9.8				
Cct4				5.1				
Lrrc59	7.8			4.0				
Usp14				3.5				
Cast	5.0		2.4	3.1				
Acot7				0.5				
Hspa9				0.3				
Hdlbp	7.0		4.3					
Hspb1	3.4		3.3					
Anxa5	220.6							
Nsun2	12.9							
Q922F6	10.8							
Psat1	4.3							
Cyc1	2.1							
Ybx1	2.0							
Akr1b3	2.0							
Rps6	0.5							
Gdi2	0.5							
Tnni3	0.1							

Gráfico 12. Análise quantitativa proteômica das células Y1 e Y1RasKO tratadas com peçonha de *T. serrulatus* por 6 h, 12 h, 24 h, e 48 h.

Os ensaios de citotoxicidade da peçonha total de *T. serrulatus* não resultaram no esperado: a morte celular. Apesar disso, após tratamento com 10 µg/mL de peçonha total em células Y1 e Y1-RasKO, foi possível perceber que ocorreram modificações a nível proteômico após análise inicial por espectrometria de massas de baixa resolução. As análises das amostras marcadas por dimetilação foram analisadas no espectrômetro de massas, porém, observamos que as amostras estavam com algum problema o que necessitaria sua repetição.

Diante desses resultados e devido à pandemia por SARS-COV-2, em agosto de 2020 entrei com pedido para mudança de tema do meu projeto, pois não estava contente com o antigo tema do projeto I, que era totalmente centrado em análise por espectrometria de massas. Não prossegui, portanto, com a análise dos dados gerados pelas poucas corridas feitas em colaboração com o grupo Fleury. Objetivando buscar algo mais específico que pudesse gerar resultados menos abrangentes e mais focados, meu projeto mudou para “Estudo das atividades antitumorais de peptídeos presentes no veneno do escorpião amarelo *T. serrulatus*”.

7 RESULTADOS E DISCUSSÃO– PROJETO II

Nesse período de pandemia, na impossibilidade de realizar experimentos no laboratório foquei meu trabalho nas análises computacionais de predição *in silico* de 702 fragmentos peptídicos derivados de diferentes proteínas da peçonha de *Tityus serrulatus*, de modo a selecionar peptídeos com potencial atividade anti-câncer. Os mais de 700 fragmentos peptídicos foram determinados a partir do trabalho de doutorado do Dr. Bruno Duzzi (https://www.teses.usp.br/teses/disponiveis/87/87131/tde-20052019-085022/en.php). Neste trabalho foram selecionadas frações de interesse decorrentes da peçonha de *T. serrulatus*, das quais onze amostras foram sequenciadas empregando técnicas de sequenciamento de novo. A estrutura primária de 700 peptídeos foi obtida através do *software Peaks Studio* 7.0 e foram utilizadas para a análise *in silico* do presente trabalho.

Para a análise *in silico*, foram utilizadas diferentes ferramentas disponíveis online. Seis peptídeos foram utilizados como controle positivo que, baseados em dados da literatura, apresentam atividade anti-câncer:

Peptídeo 1: LLGDFFRKSKEKIGKEFKRIVQRIKDFLRNLVPRTES (LL37)
Peptídeo 2: IDWKKLLDAAKQIL (Polybia-MP1)
Peptídeo 3: GIGAVLKVLTTGLPALISWIKRKRQQ (Melittin)
Peptídeo 4: INLKALAALAKKIL (Mastoparan)
Peptídeo 5: DSLSEDNWKFVVSSSCETILEILDIGGCAKGVAEYT (Hemilipin)
Peptídeo 6: MCMPCFTTDHQMARKCDDCCGGKGRGKCYGPQCLCR (Chlorotoxin)

O peptídeo LL37 (peptídeo 1) caracteriza-se por ser anti-inflamatório, anticâncer e antimicrobiano de acordo com a plataforma de análise de peptídeos anticâncer previamente testada por Chen e colaboradores (Chen *et al.*, 2016). O valor resultante da análise deste peptídeo nesta plataforma foi de 0,995, sendo 1 o valor máximo de associação a peptídeos anticâncer. É um polipeptídeo antimicrobial derivado da família das catelicidinas (Chuang et al. 2008), além de ter a habilidade de suprimir o desenvolvimento do câncer de cólon (Niemirowicz et al. 2015). O peptídeo 2 (Polybia-MP1) inibe seletivamente a proliferação de células de câncer de bexiga, próstata, células leucêmicas resistentes a múltiplas drogas e linfócitos T leucêmicos, sem ser hemolítico e citotóxico (Wang et al. 2008; Wang et al. 2009; dos Santos Cabrera et al. 2012). O peptídeo 3 (Melitina) mostrou apresentar atividade

anticâncer em câncer renal, de pulmão, de fígado, de próstata, da bexiga, de mama e leucemia (Ma et al. 2017). O peptídeo 4 (Mastoparan) exibe efeito citotóxico contra células de câncer de pâncreas (de Azevedo et al. 2015). O peptídeo 5 (Hemilipina) tem a habilidade de inibir migração celular, e isso levou à hipótese desse peptídeo exibir efeitos anti-angiogênicos através da redução de fatores de crescimento como as isoformas VEGF e seus receptores (Ma et al. 2017). O peptídeo 6 (Clorotoxina) levou ao desenvolvimento da droga BLZ100 específica para gliomas, conhecida como "tumor paint" (Patil et al. 2019).

As análises *in silico* foram realizadas utilizando quatro diferentes ferramentas:

- iACP (identifying AntiCancer Peptides) (Chen et al., 2016) (http://lin-group.cn/server/iACP)
- AntiCP (Institute of Microbial Technology, Chandigarh India) (https://webs.iiitd.edu.in/raghava/anticp/index.html)
- AntiCP 2.0 (Agrawal et al. 2020) (https://webs.iiitd.edu.in/raghava/anticp2/index.html)
- ACPred-FL (Wei et al., 2018) (http://server.malab.cn/ACPred-FL/).

Dentre as quatro ferramentas, a iACP entregou resultados mais confiáveis quando comparamos os valores de score para peptídeo anticâncer entre os 6 controles utilizados, como mostra a Tabela 7. Cada ferramenta tem uma maneira diferente de medir o score para obter um resultado final, onde o peptídeo previsto é ou não é anti-câncer. No caso dos Anti-CP e Anti-CP 2.0 do grupo da Índia, não ficou claro como o valor do score influencia no peptídeo ser anticâncer, assim como no caso do ACPred-FL. Na análise empregando Anti-CP 2.0, os peptídeos 5 e 6 retornaram como não sendo anticâncer, e somente o peptídeo 5 retornou como não sendo anticâncer quando analisados utilizando a ferramenta ACPred-FL. O iACP se mostrou mais coerente em seus valores, sendo que o score vai de 0 a 1, onde <0,5 não é um peptídeo com potencial anticâncer e >0,5 é previsto com potencial propriedade anticâncer. Apesar de termos focado nos resultados da ferramenta iACP, todos os peptídeos foram testados em todas as ferramentas online disponíveis.

	Sequências Peptídicas	Score				ACP			
		Anti-CP (India)	Anti-CP 2.0 (India)	iACP (China)	ACPred-FL (China)	Anti-CP (India)	Anti-CP 2.0 (India)	iACP (China)	ACPred-FL (China)
(1) Controle +	LLGDFFRKSKEKIGKEFKRIVQRIKDFLRNLVPRTES	0.75	1.0	0.995802	92.55%	Sim	Sim	Sim	Sim
(2) Controle + (Polybia-MP1)	IDWKKLLDAAKQIL	0.91	0.48	0.997646	99.22%	Sim	Sim	Sim	Sim
(3) Controle + (Melittin)	GIGAVLKVLTTGLPALISWIKRKRQQ	0.79	1.0	0.996736	98.11%	Sim	Sim	Sim	Sim
(4) Controle + (Mastoparan)	INLKALAALAKKIL	0.85	0.48	0.710708	99.22%	Sim	Sim	Sim	Sim
(5) Controle + (Hemilipin)	DSLSEDNWKFVVSSSCETILEILDIGGCAKGVAEYT	0.74	0.34	0.949433	79.97%	Sim	Não	Sim	Não
(6) Controle + (Chlorotoxin)	MCMPCFTTDHQMARKCDDCCGGKGRGKCYGPQCLCR	0.74	0.16	0.989752	92.55%	Sim	Não	Sim	Sim

Tabela 7. Score das quatro ferramentas utilizadas na análise *in silico* dos 6 peptídeos anticâncer.

Baseados nas análises *in silico*, as sequências apresentando os maiores valores associados à atividade anti-câncer dentre os seis peptídeos controles foram os peptídeos 2, 3 e 1, seguidos dos peptídeos 6, 5 e 4.

Dos 702 peptídeos analisados, 106 peptídeos apresentaram score iACP acima de 0,5, sendo assim, previstos com potencial anticâncer. Dentre estes 106 peptídeos, 75 eram estáveis de acordo com a ferramenta Protparam (https://web.expasy.org/protparam/). O Protparam é uma ferramenta que analisa diversos parâmetros químicos e físicos para uma dada sequência proteica para determinar sua estabilidade. Os parâmetros incluem o peso molecular, pI teórico, composição de aminoácidos, composição atômica, coeficiente de extinção, meia vida estimada, índice de instabilidade, índice alifático e média de hidropaticidade.

Levando em consideração o score iACP, o número de aminoácidos, o número total de resíduos carregados negativamente (Asp + Glu), o número total de resíduos carregados positivamente (Asp + Lys), o tempo de vida estimado (in vitro em mamíferos), o índice de instabilidade (obtidos pelo Protparam tool) e o score hemolítico (mensurado pela ferramenta HemoPI: *Hemolytic Peptide identification*, http://crdd.osdd.net/raghava/hemopi/batch.php), selecionamos um total de 11 peptídeos para síntese (Tabela 8).

Esses 11 peptídeos apresentaram o maior índice de potencial anti-câncer e são os previstos por apresentarem maior estabilidade.

PEPTÍDEOS PARA SÍNTESE	BLAST - Uniprot (Arthropoda)	Score - iACP (China)	N° de Aminoácidos	Peso Molecular	PI Teórico	N° total de resíduos carregados - (Asp + Glu	N° total de resíduos carregados + (Asp + Lys	Tempo de vida estimado (in vitro mamíferos	Score Hemolítico (0 a 1)	Índice de Instabilidade
CGALKHKALVKQLN	-	0.999790	14	1522.87	9.79	0	3	1.2h	0.42	Estável
KLFKLPTH	-	0.998466	8	983.22	10.00	0	2	1.3h	0.48	Estável
KIIEAKDRCKAGSVER	Ts19 (P86822 (KBX2_TITSE))	0.997666	16	1803.11	9.19	3	5	1.3h	0.46	Estável
HLVYWDYLPMYGK	-	0.997462	13	1684.97	6.74	1	1	3.5h	0.49	Estável
NNGGGLGSKWR	-	0.995528	11	1145.24	11.00	0	2	1.4h	0.49	Estável
GKGKEILGKLFAL	Ts19 (P86822 (KBX2_TITSE))	0.994763	13	1373.70	9.70	1	3	30h	0.55	Estável
GKTALVK	-	0.987986	7	715.89	10.00	0	2	30h	0.37	Estável
KIKKTGKKLSAHH	-	0.983997	13	1475.80	10.60	0	5	1.3h	0.48	Estável
EAGKGKEILGKIKE	Ts19 (P86822 (KBX2_TITSE))	0.983728	14	1499.77	8.53	3	4	1h	0.49	Estável
VADLGLLKCCSGSKAAKH	-	0.980601	18	1801.15	8.86	1	3	100h	0.45	Estável

Tabela 8. Peptídeos anticâncer selecionados para síntese.

Os peptídeos selecionados foram sintetizados pela empresa AminoTech com pureza > 95% e estão armazenados no freezer -20º C e prontos para posterior testes e experimentação.

Devido à pandemia por COVID-19 e restrições ao acesso presencial ao laboratório, os experimentos subsequentes não puderam ser continuados.

Tentamos analisar os peptídeos identificados utilizando a ferramenta Drug-Drug Interactions – Chemical-Protein Interactome (DDI-CPI) (http://cpi-bio-x.cn) de Luo e colaboradores (Luo *et al*, 2014). Esta ferramenta permite a predição em tempo real de DDI

baseados apenas na estrutura molecular fazendo o *docking* das moléculas (peptídeos) submetidos a um conjunto de 611 proteínas humanas gerando um perfil CPI que pode ser usado como um vetor de recursos para modelos de predição. Porém, infelizmente esta ferramenta permaneceu *off-line* até a confecção desta tese impedindo a sua análise a tempo.

Durante o período de pandemia e elaboração da dissertação, trabalhei na elaboração de um mini-review "*Scorpion venom as a potential source for cancer drug*" que foi submetido para a Toxicon: X recentemente (Artigo submetido disponível no Apêndice III ao final desta tese).

Além disso, durante meu mestrado, ajudei na análise e confecção do artigo "Bothrops jararaca *snake venom modulates key cancer-related proteins on breast tumor cell lines*" publicado na revista Toxicon (Kisaki et al, 2021), do artigo "*The impact of rattlesnake on mice cerebellum proteomics points to synaptic inhibition and tissue damage*" publicado no Journal of Proteomics (Montoni et al, 2020), e no artigo "*Proteomic analysis reveals rattlesnake venom modulation of proteins associated with cardiac tissue damage in mouse Hearts*" publicado recentemente na revista *Journal of Proteomics* (Santos et al, 2022). Além disso, ajudei na análise de dados do trabalho da aluna Fernanda Midori Abukawa orientada pelo Dr Milton Yutaka Nishiyama-Jr cujo trabalho intitulado "*A hybrid approach for identification and classification of arachnids venom components*" está em preparação para ser submetido na revista Frontiers in Pharmacology.

8 CONCLUSÕES

A análise *in silico* de mais de 700 fragmentos peptídeos derivados de proteínas da peçonha de *T. serrulatus* permitiu a identificação de 11 peptídeos com os maiores potenciais anti-câncer. Esses peptídeos foram selecionados baseados no número de aminoácidos, o número total de resíduos carregados negativamente (Asp e Glu), o número total de resíduos carregados positivamente (Arg, His e Lys), o tempo de vida estimado *in vitro* em mamíferos, o índice de instabilidade e o score hemolítico. Esses peptídeos foram sintetizados e estão prontos para análises experimentais. Porém, devido à pandemia por SARS-CoV-2 e restrições impostas pelo governo do Estado de São Paulo e pela diretoria do Instituto Butantan, não consegui finalizar as análises experimentais que deveriam ter sido realizadas no laboratório.

A perspectiva futura destes resultados é determinar se estes 11 peptídeos possuem ou não atividade antitumoral, a princípio trabalhando com teste em cultura celular e, se os resultados se mostrarem promissores, este projeto pode contribuir para descobertas de novos agentes antitumorais, derivados da peçonha de *T. serrulatus*.

REFERÊNCIAS*

AGRAWAL P, BHAGAT D, MAHALWAL M, SHARMA N, RAGHAVA GPS. AntiCP 2.0: an updated model for predicting anticancer peptides. Brief Bioinform. 2021 May 20;22(3): bbaa153.

BORTOLUZZI, LR, QUEROL MVM, QUEROL E. Notes on the occurrence of *Tityus serrulatus* Lutz & Mello, 1922 (*Scorpiones, Buthidae*) in the Western areas of Rio Grande do Sul, Brazil. Biota Neotropica 2007, 7(3), 357-359.

BRAZIL, TK, & PORTO TJ. Os escorpiões. Editora Universidade Federal da Bahia EDUFBA. Salvador, Bahia, 1a Edição. 83p. 2010.

BUDD GE, & TELFORD MJ. The origin and evolution of arthropods. Nature 2009, 457(7231), 812.

BUTTE PV, MAMELAK A, PARRISH-NOVAK J, DRAZIN D, SHWEIKEH F, GANGALUM PR, CHESNOKOVA A, LJUBIMOVA JY, BLACK K. Near-infrared imaging of brain tumors using the Tumor Paint BLZ-100 to achieve near-complete resection of brain tumors. Neurosurg Focus. 2014 Feb;36(2):E1.

CAJADO-CARVALHO D, KUNIYOSHI AK, DUZZI B, IWAI LK, OLIVEIRA ÚC, JUNQUEIRA DE AZEVEDO IL, KODAMA RT, PORTARO FV. Insights into the hypertensive effects of *Tityus serrulatus* scorpion venom: Purification of an angiotensin-converting enzyme-like peptidase. Toxins 2016, 8(12), 348.

CHEN W, DING H, FENG P, LIN H, CHOU KC. iACP: a sequence-based tool for identifying anticancer peptides. Oncotarget 2016, 7(13), 16895.

CHUANG C-M, MONIE A, WU A, MAO CP, HUNG CF. Treatment with LL-37 peptide enhances antitumor effects induced by CpG oligodeoxynucleotides against ovarian cancer. Hum Gene Ther. 2009 Apr;20(4):303-13.

COLOGNA CT, MARCUSSI S, GIGLIO JR, SOARES AM, ARANTES EC. *Tityus serrulatus* scorpion venom and toxins: an overview. Protein Pept Lett. 2009;16(8):920-32.

D'SUZE G, ROSALES A, SALAZAR V, SEVCIK C. Apoptogenic peptides from Tityus discrepans scorpion venom acting against the SKBR3 breast cancer cell line. Toxicon 2010, 56(8), 1497-1505.

DE AZEVEDO RA, FIGUEIREDO CR, FERREIRA AK, MATSUO AL, MASSAOKA MH, GIROLA N, AUADA AV, FARIAS CF, PASQUALOTO KF, RODRIGUES CP, BARBUTO JA, LEVY D, BYDLOWSKI SP, DE SÁ-JUNIOR PL, TRAVASSOS LR, LEBRUN I. Mastoparan induces apoptosis in B16F10-Nex2 melanoma cells via the intrinsic mitochondrial pathway and displays antitumor activity in vivo. Peptides 2015, 68, 113-119.

---

* De acordo com: ASSOCIAÇÃO BRASILEIRA DE NORMAS TÉCNICAS. NBR 6023: informação e documentação: referências: elaboração. Rio de Janeiro, 2022.

DIAS MH, FONSECA CS, ZEIDLER JD, ALBUQUERQUE LL, DA SILVA MS, CARARO-LOPES E, REIS MS, NOËL V, DOS SANTOS EO, PRIOR IA, ARMELIN HA. Fibroblast Growth Factor 2 lethally sensitizes cancer cells to stress-targeted therapeutic inhibitors. Mol Oncol. 2019 Feb;13(2):290-306.

DÍAZ-GARCÍA A, MORIER-DÍAZ L, FRIÓN-HERRERA Y, RODRÍGUEZ-SÁNCHEZ H, CABALLERO-LORENZO Y, MENDOZA-LLANES D, RIQUENES-GARLOBO Y, FRAGA-CASTRO JA. In vitro anticancer effect of venom from Cuban scorpion *Rhopalurus junceus* against a panel of human cancer cell lines. J Venom Res. 2013 Jun 12;4:5-12

DOS SANTOS CABRERA MP, ARCISIO-MIRANDA M, GORJÃO R, LEITE NB, DE SOUZA BM, CURI R, PROCOPIO J, RUGGIERO NETO J, PALMA MS. Influence of the bilayer composition on the binding and membrane disrupting effect of Polybia-MP1, an antimicrobial mastoparan peptide with leukemic T-lymphocyte cell selectivity. Biochemistry 2012, 51(24), 4898-4908.

GUO X, MA C, DU Q, WEI R, WANG L, ZHOU M, CHEN T, SHAW C. Two peptides, TsAP-1 and TsAP-2, from the venom of the Brazilian yellow scorpion, *Tityus serrulatus*: evaluation of their antimicrobial and anticancer activities. Biochimie 2013, 95(9), 1784-1794.

GUPTA SD, DEBNATH A, SAHA A, GIRI B, TRIPATHI G, VEDASIROMONI JR, GOMES A. Indian black scorpion (*Heterometrus bengalensis* Koch) venom induced antiproliferative and apoptogenic activity against human leukemic cell lines U937 and K562. Leuk Res 2007, 31(6), 817-825.

GUPTA SD, GOMES A, DEBNATH A, SAHA A, GOMES A. Apoptosis induction in human leukemic cells by a novel protein Bengalin, isolated from Indian black scorpion venom: through mitochondrial pathway and inhibition of heat shock proteins. Chem Biol Interact 2010, 183(2), 293-303.

KISAKI CY, ARCOS SSS, MONTONI F, DA SILVA SANTOS W, CALACINA HM, LIMA IF, CAJADO-CARVALHO D, FERRO ES, NISHIYAMA-JR MY, IWAI LK. *Bothrops Jararaca* Snake Venom Modulates Key Cancer-Related Proteins in Breast Tumor Cell Lines. Toxins (Basel). 2021 Jul 25;13(8):519.

KREIL, G. Hyaluronidases - a group of neglected enzymes. Protein Sci., v. 4(9), p. 1666-1669. 1995

LUO H, ZHANG P, HUANG H, HUANG J, KAO E, SHI L, HE L, YANG L. DDI-CPI, a server that predicts drug-drug interactions through implementing the chemical-protein interactome. Nucleic Acids Res. 2014 Jul;42: W46-52.

LUTZ A, & DE MELLO O. Cinco novos escorpiões brasileiros dos gêneros *Tityus* e *Rhopalurus*. Folha Médica Anales 1922, 3(4), 25-26.

MA R, MAHADEVAPPA R, KWOK HF. Venom-based peptide therapy: Insights into anti-cancer mechanism. Oncotarget 2017, 8(59), 100908-100930.

MARCUSSI S, ARANTES EC, SOARES AM, GIGLIO JR, MAZZI MV. Escorpiões: biologia, envenenamento e mecanismos de ação de suas toxinas. Ribeirão Preto: Fundação de Pesquisas Científicas (FUNPEC). 2011

MONTONI F, ANDREOTTI DZ, EICHLER RADS, SANTOS WDS, KISAKI CY, ARCOS SSS, LIMA IF, SOARES MAM, NISHIYAMA-JR MY, NAVA-RODRIGUES D, FERRO ES, CARVALHO VM, IWAI LK. The impact of rattlesnake venom on mice cerebellum proteomics points to synaptic inhibition and tissue damage. J Proteomics. 2020 Jun 15;221:103779.

NIEMIROWICZ K, PROKOP I, WILCZEWSKA AZ, WNOROWSKA U, PIKTEL E, WĄTEK M, SAVAGE PB, BUCKI R. Magnetic nanoparticles enhance the anticancer activity of cathelicidin LL-37 peptide against colon cancer cells. Int J Nanomedicine. 2015 Jun 4;10:3843-53.

ORTIZ E, GURROLA GB, SCHWARTZ EF, POSSANI LD. Scorpion venom components as potential candidates for drug development. Toxicon. 2015, 93, 125-135.

PATIL CG, WALKER DG, MILLER DM, BUTTE P, MORRISON B, KITTLE DS, HANSEN SJ, NUFER KL, BYRNES-BLAKE KA, YAMADA M, LIN LL, PHAM K, PERRY J, PARRISH-NOVAK J, ISHAK L, PROW T, BLACK K, MAMELAK AN. Phase 1 Safety, Pharmacokinetics, and Fluorescence Imaging Study of Tozuleristide (BLZ-100) in Adults With Newly Diagnosed or Recurrent Gliomas. Neurosurgery. 2019 Oct 1;85(4):E641-E649.

RAPPSILBER J, MANN M., ISHIHAMA Y. Protocol for micro-purification, enrichment, pre-fractionation and storage of peptides for proteomics using StageTips. Nat Protoc 2007, 2(8), 1896-1906.

Seminário sobre Vigilância de Acidentes por Animais Peçonhentos (2017: Niterói, RJ) Livro de resumos do Seminário sobre Vigilância de Acidentes por Animais Peçonhentos, 23 a 25 de agosto de 2017 [recurso eletrônico]. – Niterói: Instituto Vital Brazil, 2018. 172p.

SOROCEANU L, GILLESPIE Y, KHAZAELI MB, SONTHEIMER H. Use of chlorotoxin for targeting of primary brain tumors. Cancer Res 1998, 58(21), 4871-4879.

WANG KR, ZHANG BZ, ZHANG W, YAN JX, LI J, WANG R. Antitumor effects, cell selectivity and structure–activity relationship of a novel antimicrobial peptide polybia-MPI. Peptides. 2008 Jun;29(6):963-8.

WANG KR, YAN JX, ZHANG BZ, SONG JJ, JIA PF, WANG R. Novel mode of action of polybia-MPI, a novel antimicrobial peptide, in multi-drug resistant leukemic cells. Cancer Lett. 2009 Jun 8;278(1):65-72.

WANG WX, JI YH JJ, JIA PF, WANG R. Scorpion venom induces glioma cell apoptosis in vivo and inhibits glioma tumor growth in vitro. J Neurooncol. 2005 May;73(1):1-7.

WEI L, ZHOU C, CHEN H, SONG J, SU R. ACPred-FL: a sequence-based predictor using effective feature representation to improve the prediction of anti-cancer peptides. Bioinformatics. 2018 Dec 1;34(23):4007-4016.

WEYGOLDT, P. REVIEW Evolution and systematics of the Chelicerata. Experimental & Applied Acarology 1998, 22(2), 63-79.

ZHANG YY, WU LC, WANG ZP, WANG ZX, JIA Q, JIANG GS, ZHANG WD. Anti-proliferation effect of polypeptide extracted from scorpion venom on human prostate cancer cells in vitro. J Clin Med Res. 2009 Apr;1(1):24-31.

ANEXO A – PUBLICAÇÕES

Santos WS, Montoni F, Eichler RAS, **Arcos SSS**, Andreotti DZ, Kisaki CY, Evangelista KB, Calacina HM, Lima IF, Soares MAM, Gren ECK, Carvalho VM, Ferro ES, Nishiyama-Jr MY, Chen Z, Iwai LK. Proteomic analysis reveals rattlesnake venom modulation of proteins associated with cardiac tissue damage in mouse hearts. J Proteomics. 2022 Apr 30;258:104530. doi: 10.1016/j.jprot.2022.104530.

Montoni F, Andreotti DZ, Eichler RADS, Santos WDS, Kisaki CY, **Arcos SSS**, Lima IF, Soares MAM, Nishiyama-Jr MY, Nava-Rodrigues D, Ferro ES, Carvalho VM, Iwai LK. The impact of rattlesnake venom on mice cerebellum proteomics points to synaptic inhibition and tissue damage. J Proteomics. 2020 Jun 15;221:103779. doi: 10.1016/j.jprot.2020.103779.

Kisaki CY, **Arcos SSS**, Montoni F, da Silva Santos W, Calacina HM, Lima IF, Cajado-Carvalho D, Ferro ES, Nishiyama-Jr MY, Iwai LK. *Bothrops Jararaca* Snake Venom Modulates Key Cancer-Related Proteins in Breast Tumor Cell Lines. Toxins (Basel). 2021 Jul 25;13(8):519. doi: 10.3390/toxins13080519.

Journal of Proteomics 258 (2022) 104530

Contents lists available at ScienceDirect

Journal of Proteomics

journal homepage: www.elsevier.com/locate/jprot

Proteomic analysis reveals rattlesnake venom modulation of proteins associated with cardiac tissue damage in mouse hearts

W.S. Santos [a], Fabio Montoni [a], R.A.S. Eichler [b], Stephanie Santos Suehiro Arcos [a], Diana Zukas Andreotti [b], Carolina Yukiko Kisaki [a], Kimberly Borges Evangelista [a], Hamida Macêdo Calacina [a], Ismael Feitosa Lima [a], Magna Aparecida Maltauro Soares [c], Eric Conrad Kyle Gren [d], Valdemir Melechco Carvalho [e], Emer Suavinho Ferro [b], Milton Yutaka Nishiyama-Jr [a], Zhibin Chen [f], Leo Kei Iwai [a,*]

[a] Laboratory of Applied Toxinology (LETA) and Center of Toxins, Immune-Response and Cell Signaling (CeTICS), Butantan Institute, São Paulo 05503-900, Brazil
[b] Department of Pharmacology, Biomedical Sciences Institute (ICB), University of São Paulo (USP), São Paulo 05508-000, Brazil
[c] Laboratory of Pathophysiology, Butantan Institute, São Paulo 05503-900, SP, Brazil
[d] Bitterroot College, University of Montana, Hamilton, MT 59840, USA
[e] Grupo Fleury, São Paulo 04355-000, SP, Brazil
[f] Department of Microbiology and Immunology, University of Miami Miller School of Medicine, Miami, FL 33136, USA

ARTICLE INFO

Keywords:
Crotalus durissus terrificus
Snake venom
Mass spectrometry-based proteomics
Mouse heart
Cardiotoxicity
Envenomation

ABSTRACT

Snake envenomation is a common but neglected disease that affects millions of people around the world annually. Among venomous snake species in Brazil, the tropical rattlesnake (*Crotalus durissus terrificus*) accounts for the highest number of fatal envenomations and is responsible for the second highest number of bites. Snake venoms are complex secretions which, upon injection, trigger diverse physiological effects that can cause significant injury or death. The components of *C. d. terrificus* venom exhibit neurotoxic, myotoxic, hemotoxic, nephrotoxic, and cardiotoxic properties which present clinically as alteration of central nervous system function, motor paralysis, seizures, eyelid ptosis, ophthalmoplesia, blurred vision, coagulation disorders, rhabdomyolysis, myoglobinuria, and cardiorespiratory arrest. In this study, we focused on proteomic characterization of the cardiotoxic effects of *C. d. terrificus* venom in mouse models. We injected venom at half the lethal dose (LD50) into the gastrocnemius muscle. Mouse hearts were removed at set time points after venom injection (1 h, 6 h, 12 h, or 24 h) and subjected to trypsin digestion prior to high-resolution mass spectrometry. We analyzed the proteomic profiles of >1300 proteins and observed that several proteins showed noteworthy changes in their quantitative profiles, likely reflecting the toxic activity of venom components. Among the affected proteins were several associated with cellular deregulation and tissue damage. Changes in heart protein abundance offer insights into how they may work synergistically upon envenomation.

Significance: Venom of the tropical rattlesnake (*Crotalus durissus terrificus*) is known to be neurotoxic, myotoxic, nephrotoxic and cardiotoxic. Although there are several studies describing the biochemical effects of this venom, no work has yet described its proteomic effects in the cardiac tissue of mice. In this work, we describe the changes in several mouse cardiac proteins upon venom treatment. Our data shed new light on the clinical outcome of the envenomation by *C. d. terrificus*, as well as candidate proteins that could be investigated in efforts to improve current treatment approaches or in the development of novel therapeutic interventions in order to reduce mortality and morbidity resulting from envenomation.

1. Introduction

Snakebite is a serious but understudied global health concern, classified by the World Health Organization as a neglected tropical disease. The impacts on public health are especially pronounced in developing countries. About 2.7 million snake envenomations occur

* Corresponding author at: Av. Vital Brasil, 1500, São Paulo, SP 05503-900, Brazil.
E-mail address: leo.iwai@butantan.gov.br (L.K. Iwai).

https://doi.org/10.1016/j.jprot.2022.104530
Received 16 August 2021; Received in revised form 19 January 2022; Accepted 13 February 2022
Available online 17 February 2022

around the world annually, resulting in up to 138,000 fatalities and 414,000 permanent disabilities [1,2].

Brazil is home to four genera of medically significant venomous snakes: *Bothrops*, *Lachesis*, *Crotalus* (Viperidae family) and the *Micrurus* (Elapidae family) [3]. *Crotalus* species are distributed from southern Canada to central Argentina. Available epidemiological data, however, are largely limited to bites occurring in Brazil and the United States. According to the Notifiable Diseases Information System (SINAN) of the Health Surveillance Secretariat of the Brazilian Ministry of Health, 11,825 *Crotalus* envenomations occurred in Brazil, resulting in 108 deaths from 2015 to 2020. *Crotalus* accounted for the highest number of fatal bites [4] and the second highest number of bites by venomous snakes in the country [5]. The American Association of Poison Control Center's National Poison Data System (NPDS) indicates that 4674 venomous snakebites occurred in the United States, of which 426 resulted in major outcomes and six bites led to patient death from 2014 to 2018 (https://aapcc.org/annual-reports).

Advancing our understanding of animal toxins' physiological activities is critical for improving clinical care, developing more effective antivenoms, and identifying candidate molecules for potential therapeutic applications [6].

Crotalus venom is composed of five major proteins: crotoxin, crotapotin, crotamine, gyroxin, and convulxin. Crotoxin is a neurotoxin that makes up about 65% of the dry weight of the venom [7,8], and is responsible for observed neurotoxicity [9,10]. Crotapotin is the acidic subunit of crotoxin and functions as a chaperone to potentiate the action of the basic phospholipase A2 (PLA2) subunit [11,12]. Crotamine is a myotoxin, which, together with crotoxin, can cause systemic lesions in skeletal muscle tissue [13,14]. Gyroxin is a neurotoxin that causes aberrant muscle behavior often manifested by severe characteristic barrel rotation of the body [15,16]. Convulxin is a hemotoxin in the C-type lectin family that can contribute to seizures and respiratory disturbance [17]. Investigations of whole-venom toxicity have also documented coagulation disorders, hemolytic action, nephrotoxicity [18,19] and cardiotoxicity [20–23].

Proteomic, transcriptomic, immunological, and biochemical analyses have been used to describe whole venom composition, and to study the effects of individual toxins in the venoms of numerous snake species [24–27]. However, few studies have described the proteomic effects of envenomation within cells [28,29], tissues, or isolated organs [30].

The mammal heart has been the target of countless studies investigating the development of cardiovascular diseases [31,32]. Numerous substances including industrial chemicals, heavy metals, pharmaceuticals, and biotoxins [33] exhibit cardiotoxicity but snake venom cardiotoxins are often especially remarkable for their specificity and potency [20–22,34–37]. Molecular analysis of cardiac tissue is an efficient strategy to search for candidate molecules to be targeted in the treatment of heart disease [38]. Mass spectrometry-based technologies can be used to probe the pathology of heart conditions, as well as the effects of drugs and toxins, at the protein level [39].

In this study, we use a proteomic approach to assess the effect of *C. d. terrificus* venom on cardiac tissue in Swiss mice and explore the mechanisms of action and specific molecular targets of the venom.

2. Experimental section

2.1. C. durissus terrificus venom

C. durissus terrificus venom was extracted and lyophilized at the Butantan Institute Herpetology Department and supplied to our lab through the Strategic Core of Venom and Anti-Venom (NEVAS). The sample used in this study was a pool of venom from 256 individual snakes collected in the states of São Paulo, Goiás, Minas Gerais, Mato Grosso do Sul, and Paraná. The LD50 of this lot of venom (01/14–2) was determined to be 0.71 μg/animal (Karen de Morais Zani and Anita Mitico Tanaka Azevedo of the Butantan Institute Herpetology Department). The venom was diluted with 0.9% NaCl to a concentration of 1.0 mg/ mL, aliquoted, and stored at −80 °C until use.

2.2. Animals

We used 64 adult Swiss male mice weighing between 18 and 22 g. These animals were provided by the Central Animal Facility of the Butantan Institute and were approved for experimental use by the Animal Use Ethics Committee of the Butantan Institute under the certification CEUAIB: 2283181019 (2019).

The animals to be used for proteomic analysis ($n = 40$) were placed in polycarbonate boxes coated with a Millipore filter, containing five mice in each box. For histological analysis ($n = 24$), three animals were placed in each box. Mice were kept at room temperature (22 °C) and constant humidity (45 to 60%), positive pressure, 12-h light/dark cycle, and had free access to water and food. The methodology applied in this study followed the standards established by the National Council for the Control of Animal Experimentation (CONCEA) and all applicable legislation.

2.3. Treatment of mice with C. d. terrificus venom

Mice were treated with 0.5 LD50 of the venom (0.355 μg/ animal). Venom was diluted in 50 μL of saline solution (0.9% NaCl) and injected into the gastrocnemius muscle. After 1 h, 6 h, 12 h, or 24 h of the treatment, mice were euthanized and the heart was removed for mass spectrometry analysis and histology analysis. Experiments were performed in quintuplicate for mass spectrometry analysis and in triplicate for histological analysis. Control mice were injected with the vehicle (saline) only and euthanized at the same time periods as mice injected with venom.

2.4. Sample processing for histology analysis

After treatment, animals were anesthetized with isoflurane and hearts were immediately placed in a solution of cadmium chloride (100 mM) for 30 s, then fixed in 4% PFA (pH 6.9) for 24 h and stored in 70% ethanol. Paraffin blocks were assembled and cut at 30 μm thickness and stained with hematoxylin-eosin (H-E) for microscopy analysis. Cardiac tissue slides were stained with H-E according to the protocol by Fischer et al. (2008) [40] and analyzed using objectives of 4×, 10×, 25×, and 40× magnification in a upright Olympus microscope (Shinjuku City, Tokyo, Japan).

2.5. Sample processing for mass spectrometry analysis

We could not predict which portions of the mouse heart would show effects of exposure to venom treatment. So, we prepared whole heart samples for mass spectrometric analysis in order to avoid missing any proteomic alterations that may have occurred only in localized regions of the organs. Similarly, a separate sample group of whole heart samples (which had been subjected to identical venom treatment) were used to prepare formalin-fixed paraffin-embedded (FFPE) tissue sections for histological analysis to allow observation of even very localized tissue damage in the organs.Heart tissue was dissected and washed with saline solution to remove excess blood, samples were weighed and immediately frozen in liquid nitrogen until further processing for mass spectrometry analysis. The hearts were lysed with phase-transfer surfactant (PTS) lysis buffer as previously described [41], supplemented with protease and phosphatase inhibitors (Halt, Thermo Fisher Scientific, IL, USA). Lysis was performed on ice using a rate of 6 x heart volume-to-weight ratio as previously described [30]. Immediately after lysis, heart tissue was homogenized using a tissue homogenizer (Precellys 24, Bertin Instruments, Montigny-le-Bretonneux, France) at 6800 g for 30 s. Samples were then heated at 95 °C for 5 min, sonicated on ice for 20 min, then centrifuged at 14,000 g at 4 °C for 30 min. The supernatant was

collected and stored at −80 °C until use. Protein concentration was determined using a BCA Protein Assay Kit (Thermo Fisher Scientific, IL, USA) following the manufacturer's protocol. A 10 μg aliquot from each sample was run on a 10% SDS-PAGE to evaluate total extract.

Protein digestion was performed with trypsin (Sigma-Aldrich, MO, USA) at a 1:50 ratio using a modified FASP protocol, originally described by Wiśniewski and colleagues [42]. Briefly, 200 μg of proteins from the total extract were reduced with 0.02 mM dithiothreitol (DTT) at room temperature, then alkylated with 0.05 mM iodoacetamide on a Microcon YM-10 MWCO 10 KDa filter (Merck Millipore Ltd., County Cork, Ireland) at room temperature while protected from light. The pH of each sample was checked and, if necessary, adjusted to pH 8.0 with 0.1 M HCl or 0.1 M NaOH. Further incubation was done at 37 °C for 18 h and digestion was terminated with the addition of 2 μL of 10% TFA. Tryptic peptides were labeled through dimethylation, performed by incubating the peptide extract with 20 μL of the light label mixture for the control condition (500 μL of 50 mM TEAB, 2.8 μL of 37% CH_2O and 25 μL of 0.6 $NaBH_3CN$) and 20 μL of the heavy marker mixture for samples treated with venom (500 μL of 50 mM TEAB, 5 μL of 20% $^{13}CD_2O$, 25 μL of 0.6 M $NaBD_3CN$) for 2 h at room temperature. The reaction was stopped with 5 μL of 1% ammonia and incubated for 30 min at 35 °C. The extracts treated with saline and venom were combined in a 1:1 ratio. Desalting was carried out following the method described by Rappsilber et al. 2007 [43] with some modifications. Briefly, 30 μg of tryptic peptides were desalted on Stage-Tips on 200 μL pipettor tips with three layers of SDB-XC membrane (styrene-divinylbenzene, Empore, 3 M, Royersford, PA, USA). The membranes were initially conditioned with 100% methanol, washed with solution A (5% acetonitrile, 0.1% TFA), loaded with samples, and subsequently washed with solution A. The peptides retained on the membranes were eluted three times with 20 μL of solution B composed of 80% acetonitrile, 0.1% TFA and combined. Before proceeding to mass spectrometry analysis, all tryptic peptides were analyzed on an SDS-PAGE stained with silver nitrate in order to verify the digestion quality.

2.6. Mass spectrometry-based proteomic analysis

Light and heavy dimethylated tryptic peptide samples were analyzed on the Q-Exactive HF quadrupole hybrid mass spectrometer (Thermo Scientific, Bremen, Germany) coupled to a nano LC UltiMate 3000 system (Thermo Scientific) using the shotgun/bottom-up approach in positive ion mode. One microgram of peptides from each sample was injected at a gradient of 5 to 50% solvent B (90% acetonitrile, 0.1% TFA) in 60 min at a flow rate of 200 nL/ min. The electrospray source was operated at 2.2 kV, and the peptide mixture was analyzed by acquiring full scan mode spectra with a resolution of 120,000 for the determination of MS1 with a maximum injection time of 60 ms in the range of 375 to 1500 m/z. The dependent data acquisition (DDA) was carried out by automatically selecting the 20 most intense peaks for the subsequent acquisition of product ion spectra with MS/MS (MS2) with a resolution of 15,000 with a maximum injection time of 40 ms over a range of 200 to 2000 m/z with a dynamic exclusion of 15 s.

2.7. Data processing and statistical methods

Raw data files were analyzed using PEAKS Studio version X plus software (Bioinformatics Solutions Inc., Toronto, Canada) using de novo sequencing tools and Search DB for the classic search of sequences against the *Mus musculus* databank, downloaded from UniProtKB/Swiss-Prot in July 2020. The parameters used were: carbamidomethylation of cysteine as fixed modification; methionine oxidation and deamination of asparagine and glutamine as variable modifications with mass error tolerance ±10 ppm for MS and ± 0.02 Da for MS/ MS. Trypsin was selected as the enzyme used in protein digestion and two lost cleavages per peptide and up to three post-translational modifications were allowed. Protein decoy was enabled and false discovery rate (FDR) using the Benjamini-Hochberg method was set to 0.1% and the ALC (average local confidence) was set to 80%. The maximum allowable retention time window was three minutes. Protein quantification was performed by dimethylation labeled as light (+28 Da) for control and heavy (+36 Da) for venom treated samples [44]. The identification of protein groups, normalization of the ion spectra areas, and determination of the significance of the protein groups were performed using the algorithm included in the PEAKS X plus software. Protein identification comparison was analyzed using an online Venn diagram generator (http://bioinformatics.psb.ugent.be/webtools/Venn/). Unique proteins identified in the venom-treated mice for each time point were obtained through a screening analysis, in which only proteins present in each of the venom treated-condition (exclusive proteins) were analyzed. Data from all time points were analyzed through the functional enrichment analysis available in the Webgestalt tool (http://www.webgestalt.org/) as described by Wang et al. [45]. Overrepresentation Enrichment Analysis (ORA) was created for the Gene Ontology (GO) of biological process, cellular component, and molecular function. The FDR was set to 0.05 using the Benjamini Rochberg method, which was used in the statistical tests to determine the enrichment when comparing among all tested time points.

Semi-quantitative analysis values from the raw data table generated by the PEAKS X plus software were filtered according to the minimum occurrence of at least three of the five valid values of the normalized ratio in each experimental condition. Afterward, the data were transformed using log2 and z-scored using Perseus software version 1.6.5.0 [46] and submitted to a hierarchical grouping based on Euclidean distance. Clusters were analyzed performing an ORA analysis for Mammalian phenotype ontology in order to verify the behavior of the proteins grouped in each cluster. Also, the same protein set was analyzed using STRING [47], keeping only proteins that were involved in cardiomyopathy and formed a protein-protein interaction (PPI) network. The network was uploaded to Cytoscape [48,49] to generate a pathway overview. Principal component analysis (PCA) used the normalized protein quantification values to find which linear combinations would explain most of the variability of the differentially expressed proteins for the different assays. The PCA studies were performed using the R-statistics FactoMineR [50] and Factoextra (http://www.sthda.com/english/rpkgs/factoextra) for graphical visualization.

All of the raw data were uploaded and stored at the Center for Computational Mass Spectrometry of the University of California, San Diego, MassIVE website and can be downloaded from: ftp://massive.ucsd.edu/MSV000087836/

3. Results

3.1. Unique proteins identified in venom-treated mice

Hearts were dissected, lysed and total protein was quantified using the BCA protein assay kit. Cardiac tissue yield ranged from 5.72 to 8.18 mg (Supplemental Table 1). Each sample was lysed using PTS buffer, reduced with DTT, alkylated with IAA, and digested with trypsin. Among all treatment and control samples, mass spectrometry analysis of trypsin-digested tissue samples identified a total of 20,146 spectra corresponding to 9767 peptides and 1341 distinct proteins (Supplemental Table 2). We identified 1047 unique proteins at the 1 h time point, 747 at 6 h, 860 at 12 h, and 1027 at 24 h (Supplemental Fig. 1A and Supplemental Table 3). To identify proteins unique to the venom treatment groups, we compared control (saline) groups against the venom-treated samples from each time point. In the venom treatment samples, we identified 73 unique proteins at the 1 h time point, 5 at 6 h, 11 at 12 h, and 40 at 24 h (Supplemental Fig. 1A and Supplemental Table 3). Functional enrichment analysis of differentially abundant proteins at each time point revealed that after 1 h of venom treatment, proteins involved in "cell adhesion mediator activity" and "mitochondrial gene expression" showed the highest and the lowest enrichment rates, respectively (Supplemental Fig. 1B). In the 6 h post-treatment group,

"deaminase activity" and "foam cell differentiation" showing the highest enrichment rates and "platelet-derived growth factor receptor signaling pathway" showed the lowest enrichment rate (Supplemental Fig. 1C). At the 12 h venom-treatment time, the GO category "peroxisome organization" showed an FDR ≤ 0.05 with the highest enrichment rate, while "somatic diversification of immune receptors" showed the lowest enrichment rate (Supplemental Fig. 1D). At 24 h venom treatment, the "retromer complex" GO function presented the highest enrichment rate, while "signal transduction in response to DNA damage" showed the lowest enrichment rate (Supplemental Fig. 1E).

Among the 676 proteins identified only in venom-treated samples, 62 were exclusively present in the 1 h group, 8 in the 6 h group, 10 in the 12 h group, and 29 in the 24 h group (Fig. 1A and Supplemental Table 4). We used the Webgestalt tool to perform functional enrichment and classify these exclusive proteins based on their biological process (Fig. 1B), cellular components (Fig. 1C), and molecular function (Fig. 1D) at each time point.

A total of 36 GO categories were identified and enriched in order to classify identified proteins according to which biological processes they are involved in. Many of the GO categories were only represented at certain time points. However, "spindle localization" was enriched in both the 6 h and 24 h sample groups. "Peroxisome organization," present in the 12 h group, exhibited the highest enrichment rate (FDR ≤ 0.05) of any GO category (Fig. 1B).

Cellular component analysis showed 26 enriched GO categories. "Endoplasmic reticulum-Golgi intermediate compartment", "Sm-like protein family complex", and "extracellular organelle" showed enrichment with FDR ≤ 0.05 in the 1 h venom treatment group. In the 6 h treatment group, "neuromuscular junction" and "cell division site" showed enrichment with FDR ≤ 0.05. In the 24 h venom treatment group, "retromeric complex" showed the highest enrichment rate with FDR ≤ 0.05. The "polysome" GO category showed significant enrichment rates after 6 h, 12 h and 24 h venom treatment while "NADH dehydrogenase complex" and "COP9 signalosome" were enriched at 1 h and 6 h after venom treatment (Fig. 1C).

Among the 28 GO categories enriched and identified in the molecular function analysis, "AU-rich element binding" were enriched at 1 h and 24 h after venom treatment. "ADP binding" was the only category to show an enrichment rate with FDR ≤ 0.05 at 6 h venom treatment. "Hijacked molecular function" was observed at 12 h after venom treatment and showed the highest enrichment rate of any of the GO categories (Fig. 1D).

3.2. Semi-quantitative analysis

Quantitative mass spectrometry analysis was performed on a total of 1108 proteins identified in either control and venom-treated samples (Supplemental Table 5). Quantitative enrichment analysis was performed using gene set enrichment analysis (GSEA) supported by the Webgestalt tool. At the 1 h time point, the venom-treated group showed enrichment of several GO categories including "abnormal cholesterol homeostasis", "abnormal cholesterol level", "abnormal nervous system

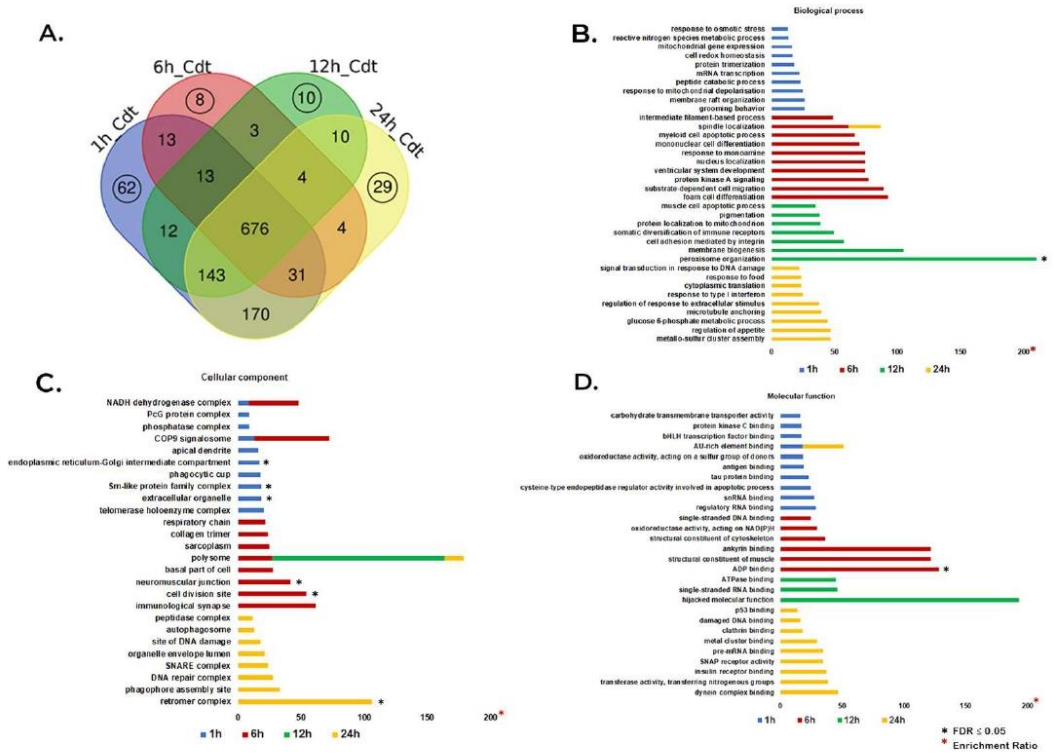

Fig. 1. Identification of proteins in the venom treatment groups. A. Venn diagram comparing proteins exclusively found in the venom treatment group at each time point is represented by black circles. These were submitted to subsequent functional analysis. B. Enrichment for GO biological process. C. Enrichment for GO cellular component. D. Enrichment for GO molecular function.

physiology", and "abnormal cell differentiation" and a decrease in "abnormal motor neuron morphology" and "abnormal heart ventricle pressure" categories (Fig. 2A). At 6 h, the venom-treated group showed increased enrichment for "abnormal sensitivity to induced morbidity/mortality", "abnormal induced morbidity/mortality", "abnormal heart left ventricle morphology", "abnormal muscle morphology", and "abnormal leukocyte cell number" and decreased enrichment was observed for "abnormal artery morphology", "decrease total body fat amount" and "abnormal circulating protein level" (Fig. 2B). At 12 h, the venom treatment group showed an increase in enrichment for "abnormal fibroblast physiology", "abnormal developmental patterning", "decreased fibroblast proliferation", and "digestive/alimentary phenotype" and decreased enrichment for "irregular heartbeat", "decrease circulating cholesterol level", "abnormal mitochondrial ATP synthesis coupled electron transport", "abnormal heart right ventricle size", and "increase heart right ventricle size" (Fig. 2C). At 24 h, the venom treatment group showed increased enrichment for "abnormal heart development", "dilated heart", "abnormal heart left ventricle morphology", "abnormal cardiac muscle tissue morphology", "increased heart rate", "small heart", "abnormal heart layer morphology", and "abnormal myocardium layer morphology" and decreased enrichment for "abnormal white adipose tissue amount", "abnormal circulating free fatty acids level", "increase total tissue mass", "increase body weight", "abnormal circulating enzyme level", and "abnormal food intake" (Fig. 2D).

Analysis of changes in relative abundance identified 191 unique proteins among all time points in both the control and venom-treated samples (Supplemental Table 6). Hierarchical clustering analysis clustered venom treatment proteins into six clusters (Fig. 3A). Based on these results, we performed an Overrepresentation Enrichment Analysis (ORA) for phenotype (Mammalian Phenotype Ontology) using the Webgestalt tool for each cluster (Fig. 3C).

The expression plot in cluster 1 shows an increase in the relative abundance of proteins at 6 h and 24 h and a decrease in abundance at 1 h and 12 h after venom treatment (Fig. 3B). Enrichment analysis for phenotype of this set of proteins showed an increase of four GO categories: "abnormal vitamin or vitamin cofactor metabolism", "abnormal vitamin metabolism", "disorganized mitochondrial cristae" and "abnormal vitamin A metabolism" (Fig. 3C, shown in light blue). Cluster 2 showed a decrease in the relative abundance of proteins at 6 h and an increase at 1 h, 12 h and 24 h (Fig. 3B). The total number of GO categories identified with the highest enrichment rate were: "decreased circulating lactate level", "metabolic acidosis" and "abnormal coronary circulation" (Fig. 3C, shown in orange). Cluster 3 showed a decrease in the relative abundance of proteins at 12 h and an increase in relative abundance at 1 h, 6 h, and 24 h after venom treatment (Fig. 3B). The enrichment analysis for the phenotype of these proteins were related to phenomena that occur in the heart. Among them, we highlight "common ventricle" and "increased ventricle muscle contractility" with the highest enrichment rate (Fig. 3C, shown in red). Cluster 4 showed an increase in relative abundance of proteins at 6 h and a decrease in abundance at 1 h, 12 h and 24 h after venom treatment (Fig. 3B). Phenotype enrichment analysis revealed several GO categories, of which "abnormal cardiac muscle relaxation" and "acidosis" showed the highest enrichment rates (Fig. 3C, shown in dark blue). Relative expression analysis of proteins in cluster 5 grouped proteins that increased in the relative abundance at 12 h and a decrease in this abundance at 1 h, 6 h, and 24 h after envenomation (Fig. 3B). Phenotype enrichment analysis of proteins in this cluster yielded four GO categories, including "decreased response of heart to induced stress". (Fig. 3C, shown in pink). Cluster 6 showed decreased protein abundance from 6 h to 24 h (Fig. 3B). Functional enrichment for phenotype showed 10 GO categories with potential relevance to pathology in the heart, including "dilated heart left ventricle", "cardiomyopathy", "decreased ventricle muscle contractility", "increased heart left ventricle size", "abnormal heart ventricle pressure", "abnormal muscle relaxation", "cardiac interstitial fibrosis", "abnormal heart left ventricle pressure", "abnormal cardiac muscle relaxation", and "decreased left ventricle systolic pressure" (Fig. 3C,

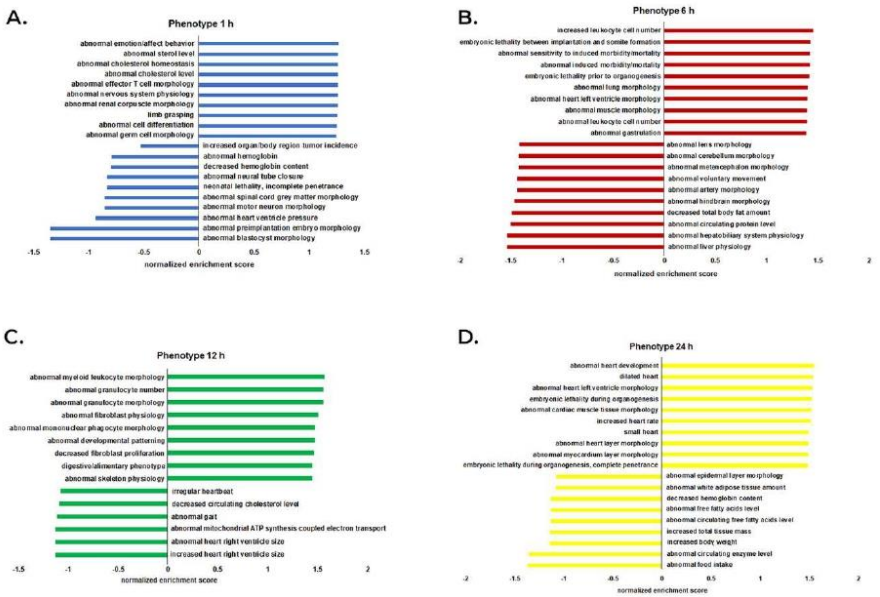

Fig. 2. Semi-quantitative functional analysis for mammalian phenotype enrichment. All protein intensity values identified by mass spectrometry quantification analysis were averaged and submitted to functional analysis. A-D denote 1 h to 24 h time points, respectively.

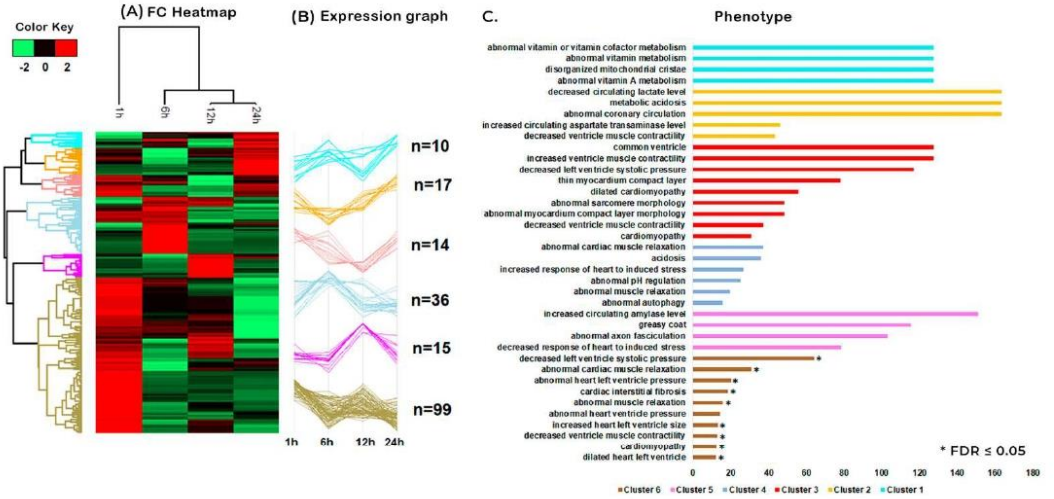

Fig. 3. Hierarchical clustering of protein quantification at 1 h, 6 h, 12 h, and 24 h post venom treatment. A. Hierarchical cluster of the most significant proteins for each treatment showing changes in protein abundance over time. The fold change (FC) in protein abundance of venom treated samples over the control samples is represented on a log2 scale. (B) Expression graphs of each cluster and the numbers of proteins composing each cluster. The protein quantification values were normalized by *Z*-score in rows. (C) The GO mammalian phenotype enrichment for all clusters.

shown in brown).

3.3. PCA analysis

For all treatment groups, proteins present in at least three replicates were subjected to Principal Component Analysis (PCA) and time points were projected into new component space to visualize differences at each time point. The orthogonal projection between the vectors for the 1 h and 6 h time points highlight key proteins at each time point potentially involved in physiological activity in heart tissue resulting from venom injection. The first two components (PC1 and PC2) explain 63% of the total variability in protein expression (Fig. 4).

At 6 h after envenomation, an intermediary time point for the systemic response, there was a negative correlation based on PC2 to the other time points, corroborating the clustering analysis. This is especially evident in Cluster 4, where many proteins increased in abundance. Notably included in this increase are MYOZ2 and NDUS6, which are related to "increased response of heart to induced stress" and "abnormal cardiac muscle relaxation", respectively (Fig. 3C). A strong positive correlation between PC1 and PC2 presented at the 12 h and 24 h time points, again corroborating the clustering analysis (Fig. 3C). This is evident in Cluster 2, where many proteins decreased in abundance. Notably, though, some proteins increased in abundance, including SODM and MYG, which are both related to "decreased ventricle muscle contractility". At the 1 h time point, a strong positive correlation presented in the PC2, significantly diverging from the other time points. This is due to a set of exclusive recruited proteins associated with the early response to the venom treatment, as evidenced by the clustering analysis (Fig. 3C). Cluster 6, for example, includes PDLI5 and MYH6 related to "dilated heart left ventricle", "cardiomyopathy" and "abnormal heart left ventricle pressure".

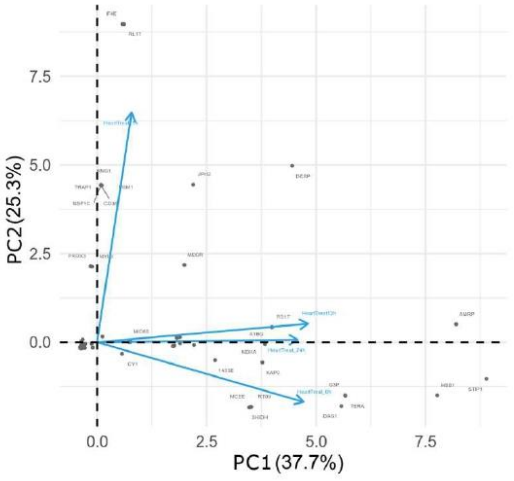

Fig. 4. Comparison of protein log2 fold change (FC) profiles across different time points upon venom treatment. The first two components, PC1 and PC2, explain 63% of the protein variability observed among all time points, as shown in the 2D graph. Note that 12 h and 24 h data graph closer to each other, representing higher correlation between their respective protein profiles. The 1 h and 6 h venom treatment vectors are orthogonal in terms of the observed proteome and indicate that those proteins, and their respective profiles, are very divergent.

3.4. Network analysis

Network analysis (Fig. 5) found nine proteins with important roles in cardiac tissue that fell into two clusters. The first cluster contained Murc, Myh6, Mb, Tnnt2, Myoz2, Pdim5, and Myl2, and the second cluster contained Opa1 and Sod2 (Fig. 5A). All of these proteins are involved in heart structure development, and Myh6, Tnnt2 and Myl2 are also involved in Hypertrophic cardiomyopathy (HCM) and Dilated cardiomyopathy (DCM) (Fig. 5A). All of these proteins showed increased

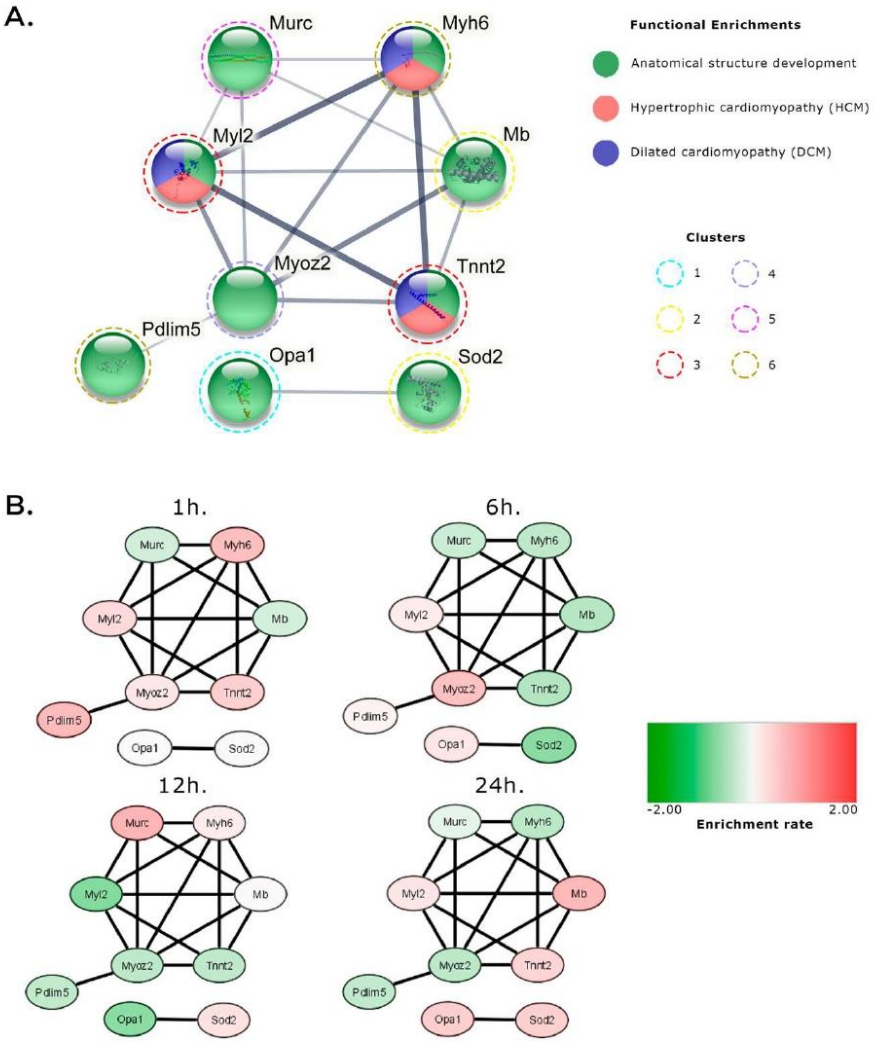

Fig. 5. Network visualization of semi-quantitative highlighted proteins. A. STRING PPI analysis. The edge width represents the confidence found for the given interaction. The color of each node is represented by its functional assignment or related disease. The dashed colored line around nodes represents the cluster of origin. B. Network analysis combining quantitative results using Cytoscape. This result shows individual patterns of up- or down-regulation (represented as red and green, respectively) of these proteins. Minimum required interaction score: medium confidence (0.400). (For interpretation of the references to color in this figure legend, the reader is referred to the web version of this article.)

abundance at 1 h. Only Myl2 was upregulated at the 6 h time point, only Myh6 was upregulated at 12 h, and at 24 h both Myl2 and Tnnt2 were upregulated (Fig. 5B).

3.5. Histology analysis

Examination by microscopy of H-E stained heart tissue sections did not show major changes in gross histopathology during the acute phase of venom challenge. The heart tissues collected at 1 h, 6 h, 12 h and 24 h after venom treatment did not show apparent increase of necrosis or inflammatory infiltration when compared to the control groups. There were signs of blood vasculature leakage in some of animals 12 h or 24 h after venom treatment, but the alteration was subtle and could be detected in only half of the venom treated animals at the 12 h to 24 h time points (Supplemental Fig. 2). No such changes were observed at the 1 h or 6 h time points (Chi Square $p = 0.045$, considering the observation

of both 12 h and 24 h).

4. Discussion

Crotalus d. terrificus venom is known to have myotoxic, nephrotoxic, neurotoxic, and cardiotoxic activities which result in a variety of clinical symptoms including alteration of central nervous system function, motor paralysis, eyelid ptosis, ophthalmoplesia, blurred vision, rhabdomyolysis, myoglobinuria and cardiorespiratory arrest, and in the most severe cases, death. Clinical effects of *C. d. terrificus* venom on patients' have been previously described, as have the physiological effects of both whole venom and isolated venom components in animal models. Siqueira and colleagues (1990) observed extensive and severe myocardial injury in a patient bitten by *C. d. terrificus*. Electrocardiogram alterations included low QRS voltage, diffuse changes in ventricular repolarization, and increased serum enzymes such as total CK, CK-MB, HDL cholesterol, aspartate (AST), and alanine aminotransferases (ALT) which peaked 48 h after hospitalization [22]. In a clinical review of 21 cases of children envenomated by *C. d. terrificus*, Cupo and colleagues (1993) describe tachycardia, serum CK, lactate dehydrogenase (LD), isoenzymes, CK-MB, and LD1–5 levels similar to those observed in acute myocardial infarction [20]. Santos and colleagues (1990) analyzed the effect of crotoxin, isolated from *C. d. terrificus* venom, perfused into guinea pig hearts for 90 min. They noted decreased contraction force and negative inotropic effect without changes in heart rate. They also reported increased CK activity related to the reduced force of contraction [21]. In an earlier study, Breithaupt (1976) perfused phospholipase A2, crotaponin, or a combination of the two into rat and rabbit hearts. They observed no alterations on heart rate, contractility, or coronary flow with any of these conditions [51].

More recently, Simoes and colleagues described the effect of *C. d. cascavella* venom in the heart of Wistar rats. They observed that 30 μg/mL venom induced significant negative inotropic effects due to reduced contractile force with no changes in rhythmicity. This suggested the absence venom action on the sinoatrial node and participation of the NO/cGMP/PKG pathway. The venom induced hypotension followed by bradycardia. Neither total-CK or CK-MB levels showed any change, suggesting that the venom is not myotoxic in cardiac tissue. Interestingly, electron microscopy analysis of cardiac tissue showed that the negative inotropic effect is not related to cardiac tissue damage or cell death but may be associated with focal injury to the cell ultrastructure by inducing mitochondrial dysfunction [34].

Our characterization of heart tissue after exposure to *C. d. terrificus* venom found changes in abundance of several noteworthy proteins at various time periods following after treatment. Functional analysis of the identified proteins based on the GO phenotype analysis found affects on several proteins associated with mitochondria at different time points after venom injection, corroborating the electron micrograph analysis performed by Simoes and colleagues [34].

At 1 h (Fig. 2A) after venom treatment, we observed upregulation of proteins related to abnormalities of the renal corpuscle. Kidney disorders following Crotalid envenomation have been previously reported. Acute kidney injury (AKI) and renal failure was the most severe complication reported; proteinuria, and hematuria, which are the most common manifestations of Crotalid snakebites [37,52–55].

Crotoxin exhibits strong neurotoxic action, impacting both the nervous system and the conduction pathways of cardiac tissue [56]. Interestingly, we detected enrichment of several GO protein categories related to lipid disorders associated with abnormal levels of sterols and cholesterols. Our data support Marinovic and coworkers, who found that crotamine reduces the level of low-density cholesterol and triglycerides, and increases levels of high-density cholesterol [57]. Our observation of downregulation of proteins related to tumorigenicity also supports previous reports of antitumoral activity by crotamine [58].

The 6 h post-venom time point approximately corresponds to the average time from envenomation before patients receive medical assistance (personal communication with doctors at Hospital Vital Brazil (HVB), Butantan Institute São Paulo, specialized in the care of patients bitten by venomous animals). This is the time point when we observed a pronounced increase in GO categories related to processes contributing to ultimate mortality, suggesting that the venom causing critical disturbances in the heart and in the organism as a whole. Protein GO categories related to ventricular abnormalities were observed as at other time points but at 6 h, we also observed an increase in left ventricle pressure. This may signal a change in the scenario observed at 1 h post-venom time point, although we cannot explain the exact mechanism for this occurrence. We also observed changes in proteins belonging to GO categories related to embryonic development and lung abnormalities. Proteins downregulated at the 6 h time point mostly belong to GO categories related to impaired liver function, abnormal voluntary movement, and altered brain morphology. Interestingly, we previously reported changes in several proteins, including proteins related to brain morphology, in the cerebellum of mice treated with *C. d. terrificus* venom [30].

At the 12 h time point (Fig. 2C), we observed an increase in a protein GO category related to the abnormal number of granulocytes, which may indicate an activation of local immune activity against the venom. An increase in proteins belonging to GO categories related to myeloid leukocyte morphology and abnormal morphology of mononuclear phagocytes and granulocytes also indicate implications for these immune cell types. Cruz et al. (2005) have previously observed that *C. d. terrificus* venom contributed to morphological, functional, and biochemical alterations of macrophages in BALB/c mice [59]. We observed an increased enrichment for the GO categories and function related to abnormal fibroblast physiology and decreased fibroblast proliferation. In contrast to earlier time points, we observed a reduction of GO categories related to arrhythmia, abnormal right ventricle size, and increased right ventricle size at 12 h. We also saw a reduction of proteins in the GO category involved in decreased circulating cholesterol, in stark contrast to the 1 h time point. Winkler and colleagues (1993) noted a decrease in circulating cholesterol in patients and rabbits after *Vipera palaestinae* envenomation which negatively correlated with overall case severity [60]. The authors suggested that this phenomenon was likely due to transcapillary lipoprotein leakage as well as changes in lipoprotein transport and metabolism caused by venom components such as PLA2.

At the 24 h time point (Fig. 2D), we observed an increase in several GO categories and function involved in cardiac cell damage and altered heart morphology, suggesting possible damage to the cardiac tissue in mice. These data corroborate previous reports of similar phenotypes, such as bilateral ventricle damage and infiltration of immune defense cells [23]. Protein GO categories associated with white adipose tissue were reduced at the 24 h time point, as was body mass. This supports similar observations presented by Morinovic et al. [57].

Hierarchical clustering analysis allowed us to observe changes in protein abundance among post venom treatment time points (Fig. 3 and Supplemental Table 6). Among the identified proteins, we highlight OPA1 (dynamin-like 120 kDa protein) in cluster 1, SODM (superoxide dismutase) and MYG (myoglobin) in cluster 2, MLRV (Myosin Regulatory Light Chain) and TNNT2 (Troponin T2) proteins in cluster 3, MYOZ2 (myozenin 2) in cluster 4, CAVN4 (caveolae-associated protein 4) in cluster 5, and PDLI5 (PDZ and LIM domain protein 5) from cluster 6 (Table 1). All these proteins are related to dysfunctions and damage in the heart and in other organs. SODM is an antioxidant enzyme, which is associated with oxidative stress. Interestingly, one of the enzyme families present in *C. d. terrificus* venom is the L-amino acid oxidases (LAAOs). The LAAOs are flavoenzymes that catalyze the stereospecific oxidative deamination of L-amino acid substrates to yield an alpha-keto acid, ammonia, and hydrogen peroxide (H_2O_2). Although LAAO's physiological role in venom is still unknown, it is speculated that they may be related to venom conservation and stabilization of the venom glands due to their antibacterial properties. L-amino acid oxidases also

Table 1
Description of proteins identified and highlighted from each cluster 1–6 shown in Fig. 3.

Accession #	Protein	Protein name	Cluster	Related GO category	Description	Fold change				Reference
						1 h	6 h	12 h	24 h	
P58281	OPA1	Dynamin-like 120 kDa protein	1	disorganized mitochondrial cristae	Maintain the normal structure and function of mitochondrial crests, and preserves the structure of the inner membrane to protect cells from apoptosis. The reduction of OPA1 may lead to cell death and contribute to the progression of heart failure.	0.03	0.43	-1,39	0.93	[74,75]
P09671	SODM	Superoxide dismutase	2	decreased ventricle muscle contractility	Play an important role in inducing the mitochondrial pathway of apoptosis in the heart, arising mainly through the mitochondrial permeability transition.	−0.04	−1.39	0.53	0.89	[76–80]
P04247	MYG	Myoglobin	2	decreased ventricle muscle contractility	Present in the cytoplasm of skeletal and cardiac muscles, and can be detected in high plasma concentrations as one of the first biomarkers in the first hours after an acute myocardial infarction	−0.54	−0.89	0.04	1.39	[81–83]
P51667	MRLV	Myosin regulatory light chain	3	cardiomyopathy, decreased ventricle muscle contractility, abnormal sarcomere morphology and dilated cardiomyopathy	Play an important role in the structure and function of the cardiac muscle, Mutations found in the gene encoding MLRV have been reported to be associated with left ventricular middle chamber hypertrophic cardiomyopathy (HCM) and a role in the development and progression of chronic heart failure	0.68	0.34	−1.48	0.46	[66–69]
P50752	TNNT2	Troponin T2	3	cardiomyopathy, decreased ventricle muscle contractility, abnormal sarcomere morphology and dilated cardiomyopathy	Present a physiological activity in calcium regulation of the actin thin filament function, which ultimately becomes essential for the cardiac muscles contraction. It has also been reported that mutations in the gene encoding TNNT2 could result in dilated cardiomyopathy	0.91	−0.95	−0.78	0.81	[70,72,84]
Q9JJW5	MYOZ2	Myozenin 2	4	Increased response of heart to induced stress	Related to hypertrophic cardiomyopathy (HCM) due to mutations in its encoding gene	0.43	1.21	−0.81	−0.83	[85,86]
P52503	NDUS6	NADH:Ubiquinone Oxidoreductase Subunit S protein	4	abnormal cardiac muscle relaxation	Relate to possible specific cardiomyopathy due to mitochondrial complex I deficiency, which may increase the risk of heart failure and death	−0.34	1.49	−0.61	−0.54	[87–89]
A2AMM0	CAVN4	Caveolae-associated protein 4	5	decreased response of heart to induced stress	Mutations in the MURC/Cavin-4 gene of the CAVN4 protein can be observed in individuals with dilated heart disease and a possible gene deletion could reduce ischemic-reperfusion injury in mice	−0.56	−0.65	1.48	−0.28	[90]
Q8CI51	PDLI5	PDZ and LIM domain protein 5	6	dilated heart left ventricle, cardiomyopathy, abnormal heart left ventricle pressure	Responsible for maintaining cellular homeostasis when the heart is subjected to biomechanical stress and thus regulates the activity of the cardiac calcium channel, preserving cardiac contractility	1.35	0.17	−0.75	−0.77	[91,92]
Q02566	MYH6	Myosin-6	6	dilated heart left ventricle, cardiomyopathy, abnormal heart left ventricle pressure	Mutations in the gene encoding MYH6 may be related to diseases such as hypertrophic cardiomyopathy CMH and dilated CMD	1.26	−0.78	0.34	−0.83	[71–73]

cause plasma clotting and platelet aggregation. Some authors suggest that these hemolytic activities may be related to the H_2O_2 produced during the chemical reaction catalyzed by LAAOs, which may cause oxidative stress to the targeted cells and tissues. Although no references are found relating the oxidative stress and free radical pathways to snake venom activity in heart tissue, oxidative stress following *Crotalus* envenomation has been noted in other mammalian organs, such as liver and kidney [61–65].

Some of the proteins noted above were also subjected to PCA analysis. Network and PPI analysis of the highlighted proteins revealed that all of these proteins play distinct roles in heart function: Myh6 is involved in muscle contraction, Tnnt2 serves as the tropomyosin-binding subunit of troponin, and Myl2 plays key roles in heart development and function (Fig. 5A). These proteins have been reported to be involved in cardiomyopathies [66–73]. In the present study, these proteins showed upregulation at 1 h, which might suggest that they are involved in an early response to venom damage (Fig. 5B), although we were not able to observe a consistent pattern through the entire post venom treatment process.

Histological analysis showed no significant sign of morphological alterations after *C. d. terrificus* venom treatment when compared to control. This is in line with recent observations by Simoes and colleagues (2021) who injected *C. d. cascavellas* venom in Wistar rats [34]. However, when De Paola and Rossi (1993) injected high dose of *C. d. terrificus* venom (80 μg in 0.2 mL of saline) intraperitoneally in Wistar rats, they observed swollen muscle fibers, contraction bands, and myocytolytic necrosis with a large number of mast cells corresponding to a mild to moderate edema in the interstitial space and infiltration of mononuclear cells 4 days after treatment [23]. In our experiments, we also observed signs of blood vasculature leakage in some of the animals at 12 h and 24 h after venom injection. Although not significant, these data corroborate the molecular changes observed in the mass spectrometry-based proteomic analysis.

Our observations shed new light on the clinical outcome of *C. d. terrificus* snakebite. At each time point after venom treatment, we noted altered profiles of proteins involved in classic Crotalid envenomation symptoms such as impaired kidney function, nervous system disruption, and damaged cardiac tissue. Furthermore, the modulations we observed may indicate proteins that could be incorporated into the production of improved antivenoms, facilitate improvements in clinical treatment strategies, or be candidates for novel therapeutic interventions to reduce the debilitating effects of Crotalid snakebite.

5. Conclusion

In this study, we analyzed the proteomic profile of >1300 proteins present in mouse cardiac tissue 1 h, 6 h, 12 h, and 24 h after injection of 0.5 LD *C. durissus terrificus* venom into the gastrocnemius muscle. We found substantial alterations of proteins related to heart tissue damage at both early and later time points following venom treatment. Venom induced changes in several cardiac tissue proteins that work synergistically through distinct functions in the heart tissue, and thus trigger a variety of immunological and biochemical effects leading to cellular damage in the early time points and, later, to structural damage.

Funding

This work was supported by grants 2013/07467-1, 2016/04000-3, and 2017/17943-6 from the São Paulo Research Foundation (FAPESP), Brazil. ESF was supported by an Erna and Jakob Michael "Visiting Professorship", Department of Biological Regulation, Weizmann Institute of Science, Rehovot, Israel and grant 302809/2016-3 from the Brazilian National Council for Scientific and Technological Development, CNPq, Brazil. WSS was supported by the Coordination for the Improvement of Higher Education Personnel (CAPES), Brazil institutional fellowship #88882.442313/2019-01 (Butantan Institute, Brazil), and SSSA was supported by CNPq institutional fellowship #131408/2019-4 (University of São Paulo, Brazil). CYK was supported by FAPESP master's degree program fellowship 2017/06496-9. ZC was supported in part by a grant from the National Cancer Institute (NCI) of National Institutes of Health (NIH) R01CA245673.

Declaration of Competing Interest

The authors declare that there is no conflict of interest.

Data availability

No

Acknowledgements

We thank Dr. Solange M.T. Serrano, Prof Hugo A. Armelin, Prof Graziella E. Ronsein, and Dr. Eduardo S. Kitano for insightful discussion.

Appendix A. Supplementary data

Supplementary data to this article can be found online at https://doi.org/10.1016/j.jprot.2022.104530.

References

[1] World Health Organization, Snakebite Envenoming, Available online: https://www.who.int/news-room/fact-sheets/detail/snakebite-envenoming, 2021 (accessed on 8 January, 2022).
[2] R.S. Jadon, R. Sood, N.K. Bauddh, A. Ray, M. Soneja, P. Agarwal, N. Wig, Ambispective study of clinical picture, management practices and outcome of snake bite patients at tertiary care Centre in Northern India, J. Family Med. Prim. Care 10 (2) (2021) 933–940.
[3] M.M. Azevedo-Marques, P. Cupo, S.E. Hering, Accidents by venomous animals: venomous snakes (Portuguese), Medicina (Ribeirao Preto. Online) 36 (2/4) (2003) 480–489.
[4] Brazilian Ministry of Health, Accidents by Venomous Animals: What to do and How to Avoid Them (Portuguese). Available online: https://antigo.saude.gov.br/saude-de-a-z/acidentes-por-animais-peconhentos, 2019 (accessed 12 August, 2021).
[5] SINAN - Notifiable Diseases Information System (Sistema de Informação de Agravos de Notificação), Notification of Health and Diseases, – present: accident by poisonous animals (2020) (Portuguese). Available online: http://tabnet.datasus.gov.br/cgi/deftohtm.exe?sinannet/cnv/animaisbr.def, 2007 (accessed 12 August, 2021).
[6] J.W. Fox, S.M.T. Serrano, Approaching the golden age of natural product pharmaceuticals from venom libraries: an overview of toxins and toxin-derivatives currently involved in therapeutic or diagnostic applications, Curr. Pharm. Des. 13 (28) (2007) 2927–2934.
[7] K.H. Slotta, H. Fraenkel-Conrat, Two active proteins from rattlesnake venom, Nature 142 (3587) (1938) 213.
[8] J.M. Gonçalves, Purification and properties of crotamine, in: E.E. Buckley, N. Porges (Eds.), American Association for the Advancemet of Science, Washington, DC, 1956, pp. 261–273.
[9] O.V. Brazil, Pharmacology of crystalline crotoxin. II. Neuromuscular blocking action, Mem. Inst. Butantan 33 (3) (1966) 981–992.
[10] R.D.S. Lomeo, A.P.D.F. Gonçalves, C.N. da Silva, A.T. de Paula, D.O. Costa Santos, C.L. Fortes-Dias, D.A. Gomes, M.E. de Lima, Crotoxin from *Crotalus durissus terrificus* snake venom induces the release of glutamate from cerebrocortical synaptosomes via N and P/Q calcium channels, Toxicon: Off. J. Int. Soc. Toxinol. 85 (2014) 5–16.
[11] C.L. Fortes-Dias, Y. Lin, J. Ewell, C.R. Diniz, T.Y. Liu, A phospholipase A2 inhibitor from the plasma of the south American rattlesnake (*Crotalus durissus terrificus*). Protein structure, genomic structure, and mechanism of action, J. Biolo. Chem. 269 (22) (1994) 15646–15651.
[12] C.A.H. Fernandes, W.M. Pazin, T.R. Dreyer, R.N. Bicev, W.L.G. Cavalcante, C. L. Fortes-Dias, A.S. Ito, C.L.P. Oliveira, R.M. Fernandez, M.R.M. Fontes, Biophysical studies suggest a new structural arrangement of crotoxin and provide insights into its toxic mechanism, Sci. Rep. 7 (1) (2017) 1–15.
[13] A.L. Bieber, D. Nedelkov, Structural, biological and biochemical studies of myotoxin a and homologous myotoxins, J. Toxicol.Toxin Rev. 16 (1–2) (1997) 33–52.
[14] N. Oguiura, M. Boni-Mitake, G. Rádis-Baptista, New view on crotamine, a small basic polypeptide myotoxin from South American rattlesnake venom, Toxicon 46 (4) (2005) 363–370.
[15] H. Barrabin, J.L. Martiarena, J.C. Vidal, A. Barrio, in: P. Rosemberg (Ed.), Isolation and characterization of gyroxin from *Crotalus durissus terrificus* venom, Pergamon Press, New York, 1978, pp. 113–133.

[16] A. Barrio, Gyroxin, a new neurotoxin of *Crotalus durissus terrificus* venom, Assn Latinoamer Cienc Fisiol, Serrano 665, 1414 Buenos Aires, Argentina (1961) 224–232.

[17] J. Prado-Franceschi, O., Vital Brazil, Convulxin, a new toxin from the venom of the south American rattlesnake *Crotalus durissus terrificus*, Toxicon 19 (6) (1981) 875–887.

[18] W.A. Hadler, O.V. Brazil, Pharmacology of crystalline crotoxin. IV. Nephrotoxicity, Mem. Inst. Butantan 33 (3) (1966) 1001–1008.

[19] C.H. Tokarnia, M.F. Brito, J.D. Barbosa, J. Döbereiner, Clinicopathological features of snakebite envenomation by *Crotalus durissus terrificus* and *Bothrops spp.* in production animals (Portuguese), Pesqui. Vet. Bras. 34 (4) (2014) 301–312.

[20] P. Cupo, M.M. Azevedo-Marques, S.E. Hering, Acute myocardial infarction-like enzyme profile in human victims of *Crotalus durissus terrificus* envenoming, Trans. R. Soc. Trop. Med. Hyg. 84 (3) (1990) 447–451.

[21] P.E.B. Santos, S.D. Souza, L. Freire-Maia, A.P. Almeida, Effects of crotoxin on the isolated guinea pig heart, Toxicon 28 (2) (1990) 215–224.

[22] J.E. de Siqueira, M.D.L. Higuchi, N. Nabut, A. Lose, J.K. Souza, M. Nakashima, Myocardial lesions after snake bites by the *Crotalus durissus terrificus* species (rattlesnake). A case report, Arq. Bras. Cardiol. 54 (5) (1990) 323–325.

[23] F. de Paola, M.A. Rossi, Myocardial damage induced by tropical rattlesnake (*Crotalus durissus terrificus*) venom in rats, Cardiovasc. Pathol. 2 (1) (1993) 77–81.

[24] L. Gonçalves-Machado, D. Pla, L. Sanz, R.J.B. Jorge, M. Leitão-De-Araújo, M.L. M. Alves, D.J. Alvares, J. De Miranda, J. Nowatzki, K. de Morais-Zani, W. Fernandes, A.M. Tanaka-Azevedo, J. Fernández, R.B. Zingali, J.M. Gutiérrez, C. Corrêa-Netto, J.J. Calvete, Combined venomics, venom gland transcriptomics, bioactivities, and antivenomics of two *Bothrops jararaca* populations from geographic isolated regions within the Brazilian Atlantic rainforest, J. Proteome 135 (2016) 73–89.

[25] C.A. Nicolau, P.C. Carvalho, I.L.M. Junqueira-de-Azevedo, A. Teixeira-Ferreira, M. Junqueira, J. Perales, A.G.C. Neves-Ferreira, R.H. Valente, An in-depth snake venom proteopeptidome characterization: benchmarking *Bothrops jararaca*, J. Proteome 151 (2017) 214–231.

[26] T. Reeks, V. Lavergne, K. Sunagar, A. Jones, E. Undheim, N. Dunstan, B. Fry, P. F. Alewood, Deep venomics of the Pseudonaja genus reveals inter- and intra-specific variation, J. Proteome 133 (2016) 20–32.

[27] I.S.D. Oliveira, I.A. Cardoso, K.D.C.F. Bordon, S.E.I. Carone, J. Boldrini-França, M. B. Pucca, K.F. Zoccal, L.H. Faccioli, S.V. Sampaio, J.C. Rosa, E.C. Arantes, Global proteomic and functional analysis of *Crotalus durissus collilineatus* individual venom variation and its impact on envenoming, J. Proteome 191 (2019) 153–165.

[28] M.C. Menezes, E.S. Kitano, V.C. Bauer, A.K. Oliveira, E. Cararo-Lopes, M. Y. Nishiyama, A. Zelanis, S.M.T. Serrano, Early response of C2C12 myotubes to a sub-cytotoxic dose of hemorrhagic metalloproteinase HF3 from Bothrops jararaca venom, J. Proteome 198 (2019) 163–176.

[29] C.Y. Kisaki, S.S.S. Arcos, F. Montoni, W. da Silva Santos, H.M. Calacina, I.F. Lima, D. Cajado-Carvalho, E.S. Ferro, M.Y. Nishiyama-Jr, L.K. Iwai, *Bothrops Jararaca* snake venom modulates key cancer-related proteins in breast tumor cell lines, Toxins 13 (8) (2021) 1–28, 519.

[30] F. Montoni, D.Z. Andreotti, R.A.D.S. Eichler, W.D.S. Santos, C.Y. Kisaki, S.S. S. Arcos, I.F. Lima, M.A.M. Soares, M.Y. Nishiyama-Jr, D. Nava-Rodrigues, E. S. Ferro, V.M. Carvalho, L.K. Iwai, The impact of rattlesnake venom on mice cerebellum proteomics points to synaptic inhibition and tissue damage, J. Proteomics 221 (2020) 1–12.

[31] E.F. Teston, H.P.M. Cecilio, A.L. Santos, G.O.D. Arruda, C.A.T. Radovanovic, S. S. Marcon, Factors associated with cardiovascular diseases in adults, Medicina (Ribeirao Preto. Online) 49 (2) (2016) 95–102.

[32] C.A.T. Radovanovic, L.A.D. Santos, M.D.D.B. Carvalho, S.S. Marcon, Arterial hypertension and other risk factors associated with cardiovascular diseases among adults, Rev. Latino-Am. Enfermagem 22 (4) (2014) 547–553.

[33] L.A. Bharadwaj, in: B. Ballantyne, T.C. Marrs, T. Syversen, D.A. Casciano, S.C. Sahu (Eds.), Cardiac Toxicology, John Wiley & Sons, Ltd, Chichester, UK, 2009, pp. 1–22.

[34] L.O. Simoes, Q.L. Alves, S.B. Camargo, F.A. Araujo, V.R.S. Hora, R.L.C. Jesus, B. C. Barreto, S.G. Macambira, M.B.P. Soares, C.S. Meira, M.C. Aguiar, R.D. Couto, B. Lomonte, J.E. Menezes-Filho, J.S. Cruz, M.A. Vannier-Santos, E.S.L.L. Casais, D. F. Silva, Cardiac effect induced by *Crotalus durissus cascavella* venom: Morphofunctional evidence and mechanism of action, Toxicol. Lett. 337 (2021) 121–133.

[35] Z. Wollberg, R. Shabo-Shina, N. Intrator, A. Bdolah, E. Kochva, G. Shavit, Y. Oron, B.A. Vidne, S. Gitter, A novel cardiotoxic polypeptide from the venom of *Atractaspis engaddensis* (burrowing asp): cardiac effects in mice and isolated rat and human heart preparations, Toxicon: Off. J. Int. Soc. Toxinol. 26 (6) (1988) 525–534.

[36] P. Cupo, M.M. Azevedo-Marques, S.E. Hering, Clinical and laboratory features of south American rattlesnake (*Crotalus durissus terrificus*) envenomation in children, Trans. R. Soc. Trop. Med. Hyg. 82 (6) (1988) 924–929.

[37] M.M. Azevedo-Marques, P. Cupo, T.M. Coimbra, S.E. Hering, M.A. Rossi, C. J. Laure, Myonecrosis, myoglobinuria and acute renal failure induced by south American rattlesnake (*Crotalus durissus terrificus*) envenomation in Brazil, Toxicon: Off. J. Int. Soc. Toxinol. 23 (4) (1985) 631–636.

[38] D.S. Celermajer, C.K. Chow, E. Marijon, N.M. Anstey, K.S. Woo, Cardiovascular disease in the developing world: prevalences, patterns, and the potential of early disease detection, J. Am. Coll. Cardiol. 60 (14) (2012) 1207–1216.

[39] B.A. Stanley, R.L. Gundry, R.J. Cotter, J.E. Van Eyk, Heart disease, clinical proteomics and mass spectrometry, Dis. Markers 20 (3) (2004) 167–178.

[40] A.H. Fischer, K.A. Jacobson, J. Rose, R. Zeller, Hematoxylin and eosin staining of tissue and cell sections, CSH Protocols 3 (5) (2008) pdb.prot4986-pdb.prot4986.

[41] T. Masuda, M. Tomita, Y. Ishihama, Phase transfer surfactant-aided trypsin digestion for membrane proteome analysis, J. Proteome Res. 7 (2) (2008) 731–740.

[42] J.R. Wiśniewski, A. Zougman, N. Nagaraj, M. Mann, Universal sample preparation method for proteome analysis, Nat. Methods 6 (5) (2009) 359–362.

[43] J. Rappsilber, M. Mann, Y. Ishihama, Protocol for micro-purification, enrichment, pre-fractionation and storage of peptides for proteomics using StageTips, Nat. Protoc. 2 (8) (2007) 1896–1906.

[44] P.J. Boersema, R. Raijmakers, S. Lemeer, S. Mohammed, A.J.R. Heck, Multiplex peptide stable isotope dimethyl labeling for quantitative proteomics, Nat. Protoc. 4 (4) (2009) 484–494.

[45] J. Wang, S. Vasaikar, Z. Shi, M. Greer, B. Zhang, WebGestalt 2017: a more comprehensive, powerful, flexible and interactive gene set enrichment analysis toolkit, Nucleic Acids Res. 45 (W1) (2017) W130–W137.

[46] S. Tyanova, T. Temu, P. Sinitcyn, A. Carlson, M.Y. Hein, T. Geiger, M. Mann, J. Cox, The Perseus computational platform for comprehensive analysis of (prote) omics data, Nat. Methods 13 (9) (2016) 731–740.

[47] D. Szklarczyk, A. Franceschini, S. Wyder, K. Forslund, D. Heller, J. Huerta-Cepas, M. Simonovic, A. Roth, A. Santos, K.P. Tsafou, M. Kuhn, P. Bork, L.J. Jensen, C. von Mering, STRING v10: protein-protein interaction networks, integrated over the tree of life, Nucleic Acids Res. 43 (Database issue) (2015) D447–D452.

[48] P. Shannon, A. Markiel, O. Ozier, N.S. Baliga, J.T. Wang, D. Ramage, N. Amin, B. Schwikowski, T. Ideker, Cytoscape: a software environment for integrated models of biomolecular interaction networks, Genome Res. 13 (11) (2003) 2498–2504.

[49] N.T. Doncheva, J.H. Morris, J. Gorodkin, L.J. Jensen, Cytoscape StringApp: network analysis and visualization of proteomics data, J. Proteome Res. 18 (2) (2019) 623–632.

[50] S. Lê, J. Josse, F. Husson, FactoMineR: an R package for multivariate analysis, J. Stat. Softw. 25 (1) (2008) 1–18.

[51] H. Breithaupt, Neurotoxic and myotoxic effects of crotalus phospholipase a and its complex with crotapotin, Naunyn Schmiedeberg's Arch. Pharmacol. 292 (3) (1976) 271–278.

[52] K.S. Chugh, V. Sakhuja, in: A.T. Tu (Ed.), Renal Disease Caused by Snake Venom, Routledge, Abingdon, England, United Kingdom, 2017, pp. 471–493.

[53] A.M.C. Martins, M.H. Toyama, A. Havt, J.C. Novello, S. Marangoni, M.C. Fonteles, H.S.A. Monteiro, Determination of *Crotalus durissus cascavella* venom components that induce renal toxicity in isolated rat kidneys, Toxicon 40 (8) (2002) 1165–1171.

[54] L.E. Danzig, Hemodialysis of acute renal failure following rattlesnake bite, with recovery, JAMA 175 (2) (1961) 136–137.

[55] P.L.M.M. Albuquerque, C.N. Jacinto, G.B. Silva Junior, J.B. Lima, M.D.S.B. Veras, E.F. Daher, Acute kidney injury caused by Crotalus and Bothrops snake venom: a review of epidemiology, clinical manifestations and treatment, Rev. Inst. Med. Trop. Sao Paulo 55 (5) (2013) 295–301.

[56] M. Hernández, H. Scannone, H.J. Finol, M.E. Pineda, I. Fernández, A.M. Vargas, M. E. Girón, I. Aguilar, A. Rodríguez-Acosta, Alterations in the ultrastructure of cardiac autonomic nervous system triggered by crotoxin from rattlesnake (*Crotalus durissus cumanensis*) venom, Exp. Tox. Pathol. 59 (2) (2007) 129–137.

[57] M.P. Marinovic, J.D. Campeiro, S.C. Lima, A.L. Rocha, M.B. Nering, E.B. Oliveira, M.A. Mori, M.A.F. Hayashi, Crotamine induces browning of adipose tissue and increases energy expenditure in mice, Sci. Rep. 8 (1) (2018) 1–12.

[58] I.G.C. dos Santos, C.L. Fortes-Dias, M.C. dos Santos, Pharmacological applications of Brazilian snake venoms with emphasis in *Crotalus durissus terrificus* and *Crotalus durissus ruruima*, Sci. Amaz. 6 (1) (2017) 42–53.

[59] A.H. Cruz, R.Z. Mendonca, V.L. Petricevich, *Crotalus durissus terrificus* venom interferes with morphological, functional, and biochemical changes in murine macrophage, Mediat. Inflamm. 2005 (6) (2005) 349–359.

[60] E. Winkler, M. Chovers, S. Almog, S. Pri-Chen, M. Rotenberg, M. Tirosh, D. Ezra, H. Halkin, Decreased serum cholesterol level after snake bite (*Vipera palaestinae*) as a marker of severity of envenomation, J. Lab. Clin. Med. 121 (6) (1993) 774–778.

[61] J.G.D. Silva, B.D.S. Soley, V. Gris, A.D.R.A. Pires, S.M.S.C. Caderia, G.J. Eler, A.P. M. Hermoso, A. Bracht, P.R. Dalsenter, A. Acco, Effects of the *Crotalus durissus terrificus* snake venom on hepatic metabolism and oxidative stress, J. Biochem. Mol. Toxicol. 25 (3) (2011) 195–203.

[62] S.C. Yamasaki, J.S. Villarroel, J.M. Barone, L. Zambotti-Villela, P.F. Silveira, Aminopeptidase activities, oxidative stress and renal function in *Crotalus durissus terrificus* envenomation in mice, Toxicon 52 (3) (2008) 445–454.

[63] R. Frezzatti, P.F. Silveira, Allopurinol reduces the lethality associated with acute renal failure induced by *Crotalus durissus terrificus* snake venom: comparison with probenecid, PLoS Negl. Trop. Dis. 5 (9) (2011), e1312.

[64] C.R.C. Costa, M.N. Belchor, C.F.B. Rodrigues, D.O. Toyama, M.A. de Oliveira, D. P. Novaes, M.H. Toyama, Edema induced by a *Crotalus durissus terrificus* venom serine protease (Cdtsp 2) involves the PAR pathway and PKC and PLC activation, Int. J. Mol. Sci. 19 (8) (2018).

[65] D. Melendez-Martinez, J.M. Munoz, G. Barraza-Garza, M.S. Cruz-Perez, A. Gatica-Colima, E. Alvarez-Parrilla, L.F. Plenge-Tellechea, Rattlesnake *Crotalus molossus nigrescens* venom induces oxidative stress on human erythrocytes, J. Venom Anim. Toxins. Incl. Trop. Dis. 23 (2017) 24.

[66] F. Sheikh, R.C. Lyon, J. Chen, Functions of myosin light chain-2 (MYL2) in cardiac muscle and disease, Gene 569 (1) (2015) 14–20.

[67] Y. Li, G. Wu, Q. Tang, C. Huang, H. Jiang, L. Shi, X. Tu, J. Huang, X. Zhu, H. Wang, Slow cardiac myosin regulatory light chain 2 (MYL2) was down-expressed in chronic heart failure patients, Clin. Cardiol. 34 (1) (2011) 30–34.

[68] J. Flavigny, P. Richard, R. Isnard, L. Carrier, P. Charron, G. Bonne, J.F. Forissier Le, M. Desnos, O. Dubourg, M. Komajda, K. Schwartz, B. Hainque, Identification of two novel mutations in the ventricular regulatory myosin light chain gene (MYL2)

associated with familial and classical forms of hypertrophic cardiomyopathy, J. Mol. Med. (Berlin, Germany) 76 (34) (1998) 208–214.
[69] Z.T. Kabaeva, A. Perrot, B. Wolter, R. Dietz, N. Cardim, J.M. Correia, H.D. Schulte, A.A. Aldashev, M.M. Mirrakhimov, K.J. Osterziel, Systematic analysis of the regulatory and essential myosin light chain genes: genetic variants and mutations in hypertrophic cardiomyopathy, Eur. J. Human Gene. 10 (11) (2002) 741–748.
[70] R.E. Hershberger, J.R. Pinto, S.B. Parks, J.D. Kushner, D. Li, S. Ludwigsen, J. Cowan, A. Morales, M.S. Parvatiyar, J.D. Potter, Clinical and functional characterization of TNNT2 mutations identified in patients with dilated cardiomyopathy, Circ. Cardiovasc. Genet. 2 (4) (2009) 306–313.
[71] E. Carniel, M.R.G. Taylor, G. Sinagra, A. Di Lenarda, L. Ku, P.R. Fain, M.M. Boucek, J. Cavanaugh, S. Miocic, D. Slavov, S.L. Graw, J. Feiger, X.Z. Zhu, D. Dao, D. A. Ferguson, M.R. Bristow, L. Mestroni, Alpha-myosin heavy chain: a sarcomeric gene associated with dilated and hypertrophic phenotypes of cardiomyopathy, Circulation 112 (1) (2005) 54–59.
[72] R.E. Hershberger, N. Norton, A. Morales, D. Li, J.D. Siegfried, J. Gonzalez-Quintana, Coding sequence rare variants identified in MYBPC3, MYH6, TPM1, TNNC1, and TNNI3 from 312 patients with familial or idiopathic dilated cardiomyopathy, Circ. Cardiovasc. Genet. 3 (2) (2010) 155–161.
[73] H. Niimura, K.K. Patton, W.J. McKenna, J. Soults, B.J. Maron, J.G. Seidman, C. E. Seidman, Sarcomere protein gene mutations in hypertrophic cardiomyopathy of the elderly, Circulation 105 (4) (2002) 446–451.
[74] A. Olichon, L. Baricault, N. Gas, E. Guillou, A. Valette, P. Belenguer, G. Lenaers, Loss of OPA1 perturbates the mitochondrial inner membrane structure and integrity, leading to cytochrome c release and apoptosis, J. Biol. Chem. 278 (10) (2003) 7743–7746, https://doi.org/10.1074/jbc.C200677200, 74.
[75] L. Chen, Q. Gong, J.P. Stice, A.A. Knowlton, Mitochondrial OPA1, apoptosis, and heart failure, Cardiovasc. Res. 84 (1) (2009) 91–99, https://doi.org/10.1093/cvr/cvp181.
[76] H. Van Remmen, M.D. Williams, Z. Guo, L. Estlack, H. Yang, E.J. Carlson, C. J. Epstein, T.T. Huang, A. Richardson, Knockout mice heterozygous for Sod2 show alterations in cardiac mitochondrial function and apoptosis, Am. J. Physiol. Heart Circ. Physiol. 281 (3) (2001) H1422–H1432, https://doi.org/10.1152/ajpheart.2001.281.3.H1422.
[77] T. Fukai, R.J. Folz, U. Landmesser, D.G. Harrison, Extracellular superoxide dismutase and cardiovascular disease, Cardiovasc. Res. 55 (2) (2002) 239–249, https://doi.org/10.1016/s0008-6363(02)00328-0.
[78] X. Li, Y. Lin, S. Wang, S. Zhou, J. Ju, X. Wang, Y. Chen, M. Xia, Extracellular Superoxide Dismutase Is Associated With Left Ventricular Geometry and Heart Failure in Patients With Cardiovascular Disease, J. Am. Heart Assoc. 9 (15) (2020) 1–19, https://doi.org/10.1161/JAHA.120.016862, e016862.
[79] E. Romuk, W. Jacheć, E. Kozielska-Nowalany, E. Birkner, A. Zemła-Woszek, C. Wojciechowska, **Superoxidedismutase activity** as a **predictor of adverse outcomes in patients** with **nonischemic dilated cardiomyopathy**, Cell Stress Chaperones 24 (3) (2019) 661–673, https://doi.org/10.1007/s12192-019-00991-3.
[80] S. Winnik, J. Auwerx, D.A. Sinclair, C.M. Matter, Protective effects of sirtuins in cardiovascular diseases: from bench to bedside, Eur. Heart J. 36 (48) (2015) 3404–3412, https://doi.org/10.1093/eurheartj/ehv290.
[81] E.M. Ohman, C. Casey, J.R. Bengtson, D. Pryor, W. Tormey, J.H. Horgan, Early detection of acute myocardial infarction: additional diagnostic information from serum concentrations of myoglobin in patients without ST elevation, Br. Heart J. 63 (6) (1990) 335–338, https://doi.org/10.1136/hrt.63.6.335.
[82] S.V. Parikh, J.A. de Lemos, Biomarkers in cardiovascular disease: integrating pathophysiology into clinical practice, Am. J. Med. Sci. 332 (4) (2006) 186–197.
[83] T.V. Störk, A.H. Wu, M. Müller-Bardorff, R. Gareis, R. Müller, V. Hombach, H. Katus, M. Möckel, North-Wurttemberg Infarction Study (NOWIS) Group, Diagnostic and prognostic role of myoglobin in patients with suspected acute coronary syndrome. North-Württemberg Infarction Study (NOWIS) Group, Am. J. Cardiol. 86 (12) (2000) 1371–1374, https://doi.org/10.1016/s0002-9149(00)01246-7.
[84] B. Wei, J.P. Jin, TNNT1, TNNT2, and TNNT3: Isoform genes, regulation, and structure-function relationships, Gene 581 (1) (2016) 1–13, https://doi.org/10.1016/j.gene.2016.01.006.
[85] A. Osio, L. Tan, S.N. Chen, R. Lombardi, S.F. Nagueh, S. Shete, R. Roberts, J. T. Willerson, A.J. Marian, Myozenin 2 is a novel gene for human hypertrophic cardiomyopathy, Circ. Res. 100 (6) (2007) 766–768, https://doi.org/10.1161/01.RES.0000263008.66799.aa.
[86] A.J. Marian, Genetic determinants of cardiac hypertrophy, Curr. Opin. Cardiol. 23 (3) (2008) 199–205, https://doi.org/10.1097/HCO.0b013e3282fc27d9.
[87] B.X. Ke, S. Pepe, D.R. Grubb, J.C. Komen, A. Laskowski, F.A. Rodda, B. M. Hardman, J.J. Pitt, M.T. Tyan, M. Lazarou, J. Koleff, M.M.H. Cheung, J. J. Smolich, D.R. Thorburn, Tissue-specific splicing of an Ndufs6 gene-trap insertion generates a mitochondrial complex I deficiency-specific cardiomyopathy, Proc. Natl. Acad. Sci. USA 109 (16) (2012) 6165–6170, https://doi.org/10.1073/pnas.1113987109.
[88] J.L. Loeffen, J.A. Smeitink, J.M. Trijbels, A.J. Janssen, R.H. Triepels, R.C. Sengers, L.P. van den Heuvel, Isolated complex I deficiency in children: clinical, biochemical and genetic aspects, Hum. Mutat. 15 (2) (2000) 123–134, https://doi.org/10.1002/(SICI)1098-1004(20000215:2<123::AID-HUMU1>3.0.CO;2-P.
[89] R. Spiegel, A. Shaag, H. Mandel, D. Reich, M. Penyakov, Y. Hujeirat, A. Saada, O. Elpeleg, S.A. Shalev, Mutated NDUFS6 is the cause of fatal neonatal lactic acidemia in Caucasus Jews, Eur. J. Hum. Genet. 17 (9) (2009) 1200–1203, https://doi.org/10.1038/ejhg.2009.24.
[90] M. Nishi, T. Ogata, C.V. Cannistraci, S. Ciucci, N. Nakanishi, Y. Higuchi, A. Sakamoto, Y. Tsuji, K. Mizushima, S. Matoba, Systems Network Genomic Analysis Reveals Cardioprotective Effect of MURC/Cavin-4 Deletion Against Ischemia/Reperfusion Injury, J. Am. Heart Assoc. 8 (15) (2019) 1–106, https://doi.org/10.1161/JAHA.119.012047.
[91] H. Cheng, K. Kimura, A.K. Peter, Li Cui, K. Ouyang, T. Shen, Y. Liu, Y. Gu, N. D. Dalton, S.M. Evans, K.U. Knowlton, K.L. Peterson, J. Chen, Loss of enigma homolog protein results in dilated cardiomyopathy, Circ. Res. 107 (3) (2010) 348–356, https://doi.org/10.1161/CIRCRESAHA.110.218735.
[92] A. Li, F. Ponten, C.G. dos Remedios, The interactome of LIM domain proteins: the contributions of LIM domain proteins to heart failure and heart development, Proteomics 12 (2) (2012) 203–225.

Montoni F, Andreotti DZ, Eichler RADS, Santos WDS, Kisaki CY, **Arcos SSS**, Lima IF, Soares MAM, Nishiyama-Jr MY, Nava-Rodrigues D, Ferro ES, Carvalho VM, Iwai LK. The impact of rattlesnake venom on mice cerebellum proteomics points to synaptic inhibition and tissue damage. J Proteomics. 2020 Jun 15;221:103779. doi: 10.1016/j.jprot.2020.103779

Journal of Proteomics 221 (2020) 103779

Contents lists available at ScienceDirect

Journal of Proteomics

journal homepage: www.elsevier.com/locate/jprot

The impact of rattlesnake venom on mice cerebellum proteomics points to synaptic inhibition and tissue damage

Fabio Montoni[a], Diana Zukas Andreotti[b], Rosangela Aparecida dos Santos Eichler[b], Wellington da Silva Santos[a], Carolina Yukiko Kisaki[a], Stephanie Santos Suehiro Arcos[a], Ismael Feitosa Lima[a], Magna Aparecida Maltauro Soares[c], Milton Yutaka Nishiyama-Jr[a], Daniel Nava-Rodrigues[e], Emer Suavinho Ferro[b], Valdemir Melechco Carvalho[d], Leo Kei Iwai[a,*]

[a] Laboratory of Applied Toxinology and Center of Toxins, Immune-Response and Cell Signaling, LETA/CeTICS, Butantan Institute, Av. Vital Brazil, 1500, São Paulo 05503-900, SP, Brazil
[b] Department of Pharmacology, Biomedical Sciences Institute (ICB), University of São Paulo (USP), Av. Prof. Lineu Prestes, 1524, sala 317, São Paulo 05508-000, SP, Brazil
[c] Laboratory of Pathophysiology, Butantan Institute, Av. Vital Brazil, 1500, São Paulo 05503-900, SP, Brazil
[d] Grupo Fleury, Av. João Pedro Cardoso, 158, São Paulo 04355-000, SP, Brazil
[e] The Institute of Cancer Research, The Royal Marsden NHS Foundation Trust, 15 Cotswold Road, Sutton, SM2 5NG London, United Kingdom

ARTICLE INFO

Keywords:
Mass spectrometry
Proteome analysis
Crotalus durissus terrificus
Snake envenomation
Mus musculus
Cerebellum

ABSTRACT

Snake envenomation is responsible for more than 130,000 deaths worldwide. In Brazil, the Crotalus rattlesnake is responsible for the second largest number of accidental snake bites in the country. Although there are many descriptions of the clinical and biochemical effects of *Crotalus* envenoming, there are few works describing the molecular events in the central nervous system of an organism due to envenomation. In this study, we analyzed the proteomic effect of *Crotalus durissus terrificus* snake venom on mice cerebellums. To monitor the envenomation over time, changes in the protein abundance were evaluated at 1 h, 6 h, 12 h and 24 h after venom injection by mass spectrometry. The analysis of the variation of over 4600 identified proteins over time showed a reduction in components of inhibitory synapse signaling, oxidative stress, and maintenance of neuronal cells, which paralleled increasing tissue damage and apoptosis factors. These analyses revealed the potential protein targets of the *C. d. terrificus* venom on the murine cerebellum, showing new aspects of the snake envenomation effect. These data may contribute to new therapeutic approaches (i.e., approaches directed at protein targets affected by the envenomation) on the treatment of envenomation by the neurotoxic *C. d. terrificus* snake venom.

Significance: Snakebites are a neglected global health problem that affects mostly rural and tropical areas of developing countries. It is estimated that over 5.4 million people are bitten by snakes each year, from which 2.7 million people are bitten by venomous snakes, resulting in disabilities such as amputations and in some cases leading to death.

The *C. d. terrificus* snake is the most lethal snake in Brazil. Studying the molecular changes upon envenomation in a specific tissue may lead to a better understanding of the envenomation process by *C. d. terrificus* snakebites.

1. Introduction

According to the World Health Organization, snakebites are a neglected health problem that affects mostly tropical and subtropical countries. Every year, ~2.7 million venomous snakes accidents occur worldwide, resulting in 130,000 deaths, 490,000 amputations, and other severe health problems [1]. In Brazil, according to the Brazilian Ministry of Health, 22,000 accidents occur with venomous snakes every year [2]. These accidents are mainly caused by four genera of venomous snakes found in the Brazilian territory: *Bothrops*, responsible for 90.5% of the accidents; *Micrurus*, responsible for 0.4% of the accidents; *Lachesis*, responsible for 1.4% of the accidents; and *Crotalus*, known as rattlesnakes, responsible for 7.7% of the accidents. Although *Crotalus* accidents are the second largest cause of snakebite accidents in the country, their lethality is the highest, reaching 1.87% [3].

Crotalus durissus snake venom is mainly composed of a mixture of

* Corresponding author.
E-mail address: leo.iwai@butantan.gov.br (L.K. Iwai).

https://doi.org/10.1016/j.jprot.2020.103779
Received 2 October 2019; Received in revised form 30 March 2020; Accepted 2 April 2020
Available online 07 April 2020

peptides and other minor chemical compounds. Among these compounds are presynaptic neurotoxins that act on nerve terminals, inhibiting acetylcholine and causing motor paralysis [4,5]. Within the first six hours of accidental venom inoculation, patients typically report several eye-related problems, such as palpebral, uni- or bilateral ptosis, ophthalmoplegia, blurred vision, and diplopia, which is a consequence of the paralysis of the extrinsic and intrinsic musculature of the eyeball after impairment of the third pair of cranial nerves [6]. In addition to its neurotoxic activity, myotoxic and abnormal coagulant activities of the venom have been observed. The myotoxic activity can be observed in the most serious cases, where various painful systemic lesions occur against the muscular fibers, leading to a release of enzymes and myoglobin to the blood, which are excreted by the urine and turn it a reddish-brown color. The abnormal coagulant activity comes from a fraction containing a thrombin-like enzyme, which causes disturbances in blood coagulation in approximately 40% of patients [7]. In addition, *C. durissus* venom has also been described to be neurotoxic [8], nephrotoxic [9], and cardiotoxic [10,11].

A composition analysis of *C. durissus* venom revealed four major components. Crotoxin is the most abundant toxin in the venom (65% of dry weight) and has neurotoxic activity and a secondary hemolytic activity [12]. Crotamine is related to myotoxic effects [13]. Gyroxin causes strong involuntary contractions of the muscles and a severe loss of balance, making mice spin on their own axis after subjecting the animals to toxin injection [14]; additionally, gyroxin has also been described to transpose the blood-brain barrier [15]. Convulxin has been described to present the same effects of gyroxin in tests performed in mice, in addition to an abrupt and transient fall of arterial blood pressure and late hypotension in dogs [16].

These descriptions show the severity of the venom action in crotalic accidents and the need to rapidly neutralize these toxins in an injured individual. Currently, the antivenom antiophidic sera, first described by Albert Calmette in 1859 [17], is still used to treat snakebites. These sera are developed by injecting small amounts of snake venom in horses and then purifying the antibodies against the venom. However, many countries that present high incidences of snakebite accidents, especially in Asia and Africa, have few companies that produce the antiophidic sera, making obtaining the sera an aggravating problem for the treatment of this type of medical emergency [1].

Several studies have described the clinical features of *C. durissus* snakebites and many others have studied the venom composition of these snakes at the genomic, transcriptomic, and proteomic levels. Previous studies also evaluated the biological and therapeutic effects of specific molecules isolated from Crotalus snake venom. However, even though *C. d. terrificus* is responsible for the second largest number of envenomation accidents and the highest lethality in Brazil, no previous studies evaluated the effect of its venom on the central nervous system.

To obtain a comprehensive proteomic characterization of the effects of the *C. d. terrificus* venom in mice cerebellums, which is responsible for equilibrium, coordination, balance, motor learning, motor memory, and motor consolidation, we used high-resolution mass spectrometry-based proteomics to analyze mice cerebellums injected with the venom at different time points over the period when patients seek the hospital after a snakebite [18]. The results indicated effects not previously described in the literature, such as the perturbation of proteins involved in the blood brain barrier, synaptic transmission, and tissue damage. These data add a greater understanding of the mechanism of action for venom in the context of the ophidian accidents, thus yielding new approaches to the study of ophidian accidents.

2. Experimental section

2.1. C. d. terrificus venom

Venom was extracted at the herpetology department of the Butantan Institute, and the supplied venom was lyophilized by the Venom and Antivenom Strategic Nuclei of Butantan Institute. The department pooled venom extracted from 256 snakes collected at various Brazilian locations (the states of São Paulo, Goiás, Minas Gerais, Mato Grosso do Sul, and Paraná). The venom pool was quantified according to the curve protocol described by Markwell [19] and analyzed by SDS-PAGE, and its median lethal dose (LD50) was determined according to the protocol described by Villarroel [20]. For this lot, the LD50 was established as 0.71 μg per adult mouse weighing between 18 and 22 g.

2.2. Mice

Male mice of the SWR/J Swiss strain weighing between 18 and 22 g were bred in polycarbonate boxes at room temperature of 22 °C, constant humidity, positive pressure, a light/dark cycle of 12 h, and free access to food and water. All mice used in this project were approved by the Ethics Committee on Animal Use of the Butantan Institute under certification CEUAIB #4959200217. The methodology applied in this study followed the norms of the National Council for the Control of Animal Experimentation (CONCEA) and all associated legislation.

2.3. Treatment of mice with C. d. terrificus snake venom

The mice were treated with venom by injecting 0.5 LD50 (0.36 μg/animal) of the rattlesnake venom solubilized in 0.9% NaCl into the gastrocnemius muscle in a volume of 50 μL with an Ultrafine-II BD micro syringe. As a control for the experiment, the vehicle alone (0.9% NaCl) was injected at the same time points, in the same volume and to the same number of animals as the treated mice.

2.4. Tissue acquisition

Tissues were removed after 1 h, 6 h, 12 h, or 24 h of venom gastrocnemius intramuscular administration from anesthetized mice following the inhalation of isoflurane in a small glass chamber. Upon losing consciousness, the animal was removed and immediately euthanized.

For the mass spectrometry analysis ($n = 5$ for each condition), individual cerebellums were carefully removed with the aid of appropriate tweezers and scalpels, immediately washed in ice-cold PBS, and flash frozen in liquid nitrogen. After each extraction, the samples were stored in a −80 °C freezer until use.

For the histological microscopy analysis using the hematoxylin-eosin (HE)-staining assay ($n = 3$ for each condition), the brains were removed and fixed in 4% PFA (pH 6.9, Merck, São Paulo, Brazil) for 24 h and then stored in 70% ethanol until the paraffin blocks were assembled and cut into 15-μm-thick slices for further histological analyses.

2.5. Cerebellar tissue protein extraction for mass spectrometry analysis

After tissue dissection, the cerebellums were weighed and lysed with a phase-transfer surfactant (PTS) lysis buffer composed of 100 mM Tris-HCl pH 9.0, 12 mM SDC (sodium dodecyl sulfate), and 12 mM SLS (sodium lauryl sulfate), supplemented with protease and phosphatase inhibitors (Halt, Thermo Fisher Scientific, IL, USA) [21]. The lysis buffer was added at an 8:1 volume:weight ratio. The cerebellums were homogenized immediately afterward using the Precellys 24 tissue homogenizer (Bertin Instruments, France) at 6800 g for 30 s. Samples were then heated at 95° C for 5 min and sonicated on ice for 20 min, followed by centrifugation at 14,000*g* at 4 °C for 30 min. The supernatant was collected and samples underwent protein precipitation.

Protein precipitation was performed by methanol/chloroform precipitation, which also delipidated the sample. A 4:3:1 (v:v:v) mixture of methanol:water:chloroform was added at a 1:1 volume ratio to the protein, followed by centrifugation at 10,000*g* for 5 min. The aqueous methanol phase was carefully removed, and three volumes of methanol

were added. Then, the sample was vortexed for 10 s and centrifuged at 10,000*g* for 15 min. The supernatant was carefully removed, and the samples were resuspended in 1 mL of 0.1 M NaOH. The samples were quantified using the BCA Protein Assay Kit (Thermo Fisher Scientific, IL, USA), following the manufacturer's recommendations. In addition, 15 μg of the total extract after precipitation was analyzed using 12% SDS PAGE and stained with colloidal coomassie to verify the consistency of the extracts obtained (Supplemental Fig. 1).

2.6. Sample preparation for mass spectrometry analysis

The proteins were digested with trypsin using a modified FASP protocol described by Wiśniewski [22]. Briefly, 100 μg of the total extract were reduced with 0.02 mM DTT and 0.05 mM cystein alkylated with iodoacetamide in the Microcon filter YM-10 MWCO 10KDa (Millipore, Ireland) and digested with trypsin (Sigma-Aldrich, MO, USA) in a 1:50 ratio of enzyme: substrate. The pH of each sample was tested and, if necessary, adjusted to pH 8.0 with 0.1 M HCl or 0.1 M NaOH. Digestion was carried out by incubation at 37 °C for 18 h. As a quality control for digestion, 3 μg of each digested sample was analyzed using 12% SDS PAGE, stained with silver nitrate and compared to the non-digested sample (Supplemental Fig. 2).

2.7. Stage tip desalting

Desalting was performed following the method described by Rappsilber [23] with modifications. Briefly, 30 μg of tryptic peptides were desalted in stage tips made in house and mounted in 200-μL pipette tips with three layers of SDB-XC membranes (Empore styrene divinylbenzene extraction disk cartridge, 3 M, PA, USA). The membranes were first equilibrated with 100% methanol and washed with Solution A (5% acetonitrile, 0.1% TFA); then, the samples were loaded and subsequently washed with Solution A. The samples were eluted with 100 μL of Solution B (80% acetonitrile, 0.1% TFA). Washing and elution were performed by centrifuging the tips mounted on Eppendorf tubes at 1000*g* for 5 min. After elution, the samples were dried in a speedvac and resuspended with 0.1% TFA. The samples were quantified using the Pierce BCA Peptide Assay Kit (Thermo Fisher Scientific, IL, USA) following the manufacturer's recommendations using the standard protocol.

2.8. Dimethyl labeling of tryptic peptides

Labeling was performed by incubating the protein extract for 2 h with 20 μL of the light label mix (500 μL of 50 mM TEAB, 2.8 μL of 37% CH_2O and 25 μL of 0.6 M $NaBH_3CN$) for the control condition and 20 μL of the heavy label mix (500 μL of 50 mM TEAB, 5 μL of 20% CD_2O, and 25 μL of 0.6 M $NaBD_3CN$) for the venom-treated samples for 2 h at room temperature. The reaction was stopped with 5 μL of 1% ammonia and incubated for 30 min at 35 °C. The control and venom-treated extracts were combined at a 1:1 proportion for further mass spectrometry analysis. All of the chemicals were purchased from Sigma-Aldrich.

2.9. Mass spectrometry-based proteomics

Mass spectrometry analyses were performed on a hybrid quadrupole orbitrap Q-Exactive HF mass spectrometer (Thermo Scientific, Bremen, Germany) coupled to an UltiMate 3000 capillary nano LC system (Thermo Scientific) using the shotgun/bottom up approach in positive ion mode. One microgram of the peptides was injected with a gradient of 5 to 50% solvent B (acetonitrile 90%, 0.1% TFA) over 120 min at a flow of 200 nL/min. The electrospray source was operated at 2.2 kV. The peptide mixture was analyzed by the acquisition of the spectra in full scan mode at a resolution of 120,000 for the determination of MS1, with a maximum injection time of 60 ms in the range of 375 to 1500 *m/z*. The 20 most intense peaks were automatically selected via data-dependent acquisition for the subsequent acquisition of the spectra of the product ions with the MS/MS at a resolution of 15,000, a maximum injection time of 40 ms, a range of 200 to 2000 m/z, and a dynamic exclusion of 15 s.

2.10. Protein identification

Proteins were identified from the mass spectrometry data using Peaks Studio version X (Bioinformatics Solutions Inc., Waterloo, ON, Canada) with de novo sequencing tools for peptide identification and Search DB for the classical search of sequences against the *Mus musculus* database, downloaded from UniProtKB/Swiss-Prot in March of 2019. To avoid the presence of contaminants, the Global Proteome Machine (GPM) cRap bank [24] was used as a contaminant database. The parameters used were carbamidomethylation of cysteine as a fixed modification and oxidation of methionine and N-terminal acetylation as variable modifications. The mass error tolerance for MS and MS/MS were set to 10 ppm and 0.02 Da, respectively. Trypsin was selected as the proteolytic enzyme used in the digestion of proteins and up to three miscleavages were allowed. Once the DB search was finished, the FDR (Benjamini - Hochberg) was adjusted to 0.1%, and the average local confidence (ALC) was adjusted to 80%.

2.11. Dimethyl quantification

The quantification of the proteins in the samples was performed by the dimethylation method that compares the difference in the relative abundance of the ions generated in the MS spectrum between the light- and heavy-labeled samples [25]. Maxquant software algorithms were used to identify the groups of proteins, normalize the ion spectra intensities, and determine the significance of the protein groups [26]. The global parameters for the search were light labeling for the control samples (Dimethyl Lys0, +28 Da) and heavy labeling for the venom-treated samples (Dimethyl Lys8, +36 Da). The proteolytic enzyme of choice was set to trypsin with three allowed miscleavages. The carbamidomethylation of cysteine was chosen as a fixed modification, and the oxidation of methionine and acetylation of the N-terminal was set as a variable modification, with a maximum of 5 modifications per peptide allowed. Regarding the instrument parameters, the default settings for Orbitrap were used: a tolerance of 20 ppm for the first peptide search and 4.5 ppm for the second. The database used in this search was the Swissprot *M. musculus* database described in Section 3.10 above.

2.12. Hematoxylin eosin (HE) assays

The tissue was stained with HE following standard procedures [27]. The tissue slides were analyzed using objectives of 5×, 10×, and 40× magnification with a pixel image of 1.12 μm and 0.28 μm. The images were obtained with the TCS SP5 microscope (Leica, Wetzlar, Germany) using ×10/1.25 oil. All of the slides images were sorted randomly.

2.13. Bioinformatic analysis

2.13.1. Non-ranked enrichment analysis

Proteins identified exclusively in venom-treated mice over the controls were analyzed using WebGestalt [28] (WEB-based Gene SeT AnaLysis Toolkit) for a functional enrichment analysis (webgestalt.org). The Overrepresentation Enrichment Analysis (ORA) was created for the GO of the biological process, cellular components, and molecular function. The FDR was adjusted to 0.05 using the Benjamini-Rochberg procedure, which was used in the statistical test to determine the enrichment when comparing all time points.

2.13.2. Quantitative proteomics analysis

Heatmaps were developed to comprise the protein abundance changes during envenomation. The data were plotted using R studio,

and replicates were normalized using log2 and *Z*-scores to provide a visualization of the total protein change profile. For individual protein heatmap plots, the samples were normalized using log2 and each replicate was submitted to the Welch *t*-test. Significant proteins were plotted using Perseus software tools.

The fold change and the protein-protein interactions provided by information from the String database [29] were uploaded into the open source platform Cytoscape [30] to create a network and visualize the change profiles of protein quantities during the envenomation time points. The auto annotate tool [31] was used to cluster the protein network into GO [32] molecular functions.

2.13.3. Principal component analysis

Based on the normalized observations we used principal component analysis (PCA) to find which linear combinations of protein quantification values would explain most of the variability of the differentially expressed proteins for the different assays. The PCA studies were performed using the R-statistics built in functions of princomp (https://www.rdocumentation.org/packages/stats/versions/3.6.2/topics/princomp) and ggbiplot (https://www.rdocumentation.org/packages/ggbiplot) for graphical visualization.

3. Results

To obtain a comprehensive proteomic molecular characterization of the effects of the *C. d. terrificus* venom in the mice cerebellums, we used high-resolution mass spectrometry-based proteomics to analyze mice cerebellums at different time points after injection with the *C. d. terrificus* venom. Thirty-two mice were injected with *C. d. terrificus* venom in the gastrocnemius muscle and 32 animals were injected with the saline control. Five mice from each group were sacrificed at 1 h, 6 h, 12 h and 24 h post-venom or saline injection for mass spectrometry–based proteomics analyses.

3.1. Total extract of cerebellum protein acquisition

The cerebellum tissue preparation for the mass spectrometry analysis yielded 340 to 520 μg of sample (Table 1, Supplemental Table 1). Each sample was lysed with PTS buffer, reduced with DTT, alkylated with IAA and digested with trypsin. The digested samples were isotopically labeled with light and heavy formaldehyde and desalted using an in-house prepared stage tip. The samples were analyzed using a Q Exactive HF hybrid quadrupole-Orbitrap mass spectrometer, and the generated data were analyzed using the Peaks X, Maxquant, and Perseus software to identify and quantify the proteins. The obtained data sets were further analyzed according to their biological functions and displayed in the form of comparative charts, graphs, heatmaps, and network views. All of the raw data were uploaded and stored at the Center for Computational Mass Spectrometry of the University of California, San Diego, MassIVE website and can be downloaded from: ftp://massive.ucsd.edu/MSV000084135/

Table 1
Quantity of total protein extract obtained from each mouse/mg.

	Replicate #					
Sample	1	2	3	4	5	Mean
1 h CTRL	0.45	0.52	0.52	0.45	0.51	0.49
1 h CDTv	0.44	0.39	0.45	0.49	0.61	0.48
6 h CTRL	0.47	0.51	0.48	0.57	0.45	0.50
6 h CDTv	0.47	0.48	0.45	0.47	0.23	0.42
12 h CTRL	0.45	0.38	0.34	0.38	0.36	0.38
12 h CDTv	0.42	0.33	0.35	0.46	0.38	0.39
24 h CTRL	0.39	0.42	0.34	0.38	0.42	0.39
24 h CDTv	0.39	0.42	0.41	0.41	0.40	0.41

CTRL = control.
CDTv = *Crotalus durissus terrificus* venom treatment.

3.2. Overview of identified proteins

A total of 4614 protein groups were identified with an FDR score of 0.1% for peptides and 11.3% for proteins (Supplemental Table 1). The analysis of the 5 replicates of each condition showed a high overlap of > 80% of the identified proteins (Supplemental Fig. 3).

Of the 4614 proteins identified, 1938 proteins were identified at all time points in both the control and venom-treated samples (Supplemental Fig. 3A). The global profiles of all of the identified proteins were listed and compared (Fig. 1). Fig. 1A shows proteins that were identified exclusively in the control group or the venom-treated cerebellum at 1 h, 6 h, 12 h, and 24 h. When the proteins from all of the venom-treated groups from each time point were compared (Fig. 1B), we were able to identify 40 proteins that are exclusively expressed at 1 h, 54 proteins that are exclusively expressed at 6 h, 43 proteins that are exclusively expressed at 12 h, and 36 proteins that are exclusively expressed at 24 h post venom treatment (Supplemental Table 2). Proteins from each of these exclusively identified groups from each of the venom treatment time points were analyzed based on the Gene Ontology (GO) terms for biological processes, cellular components, and molecular function to identify the enrichment of specific terms (Fig. 1C). Biological processes showed no particular enrichment for any of the specific terms. Although a few cellular components were exclusively identified for ribosomes (at 1 h and 6 h), microbodies (at 1 h and 12 h) and liquid droplets (at 6 h and 24 h), the data revealed no significant enrichment of any specific category. For the molecular function analyses, molecular adaptor and transducer activity were exclusively observed at 1 h, and chromatin and carbohydrate binding were exclusively observed at 6 h and 24 h.

3.3. Non-ranked enrichment

To distinguish proteins that were up- and downregulated in both the control and venom-treated conditions, we focused on the over-represented enrichment analyses that highlighted distinct biological processes, molecular functions, and cellular components (Fig. 2). At 1 h post-venom injection, we observed the downregulation of proteins involved with symmetric synapses formation (inhibitory synapses), the positive regulation and modulation of proteins involved on inhibitory post-synaptic potential, and the upregulation of proteins involved with oxidoreductase activities acting on the CH-CH group of donors, the cellular response to increased oxygen levels and membrane hyper-polarization. At 6 h, we observed the downregulation of proteins from the MAPK3 signaling pathway and the mitotic G2 DNA damage checkpoint, and an upregulation of neuropilin binding proteins. At 12 h, proteins involved on cellular and structure development were downregulated, such as those related to forebrain neuroblast division, intercellular canaliculus, lateral ventricle involvement, and neuroblast division (Fig. 2). In addition, proteins involved on the regulation of intestinal absorption were also downregulated, and proteins involved with the establishment of the blood-brain barrier were in both up- and downregulated biological processes. At 24 h, we observed a different pattern of enrichment of terms compared to the other time points. We observed a downregulation of proteins from the myosin filament, the microfilament motor activity, the myosin complex and the motor activity, and an increased abundance of proteins related to the response to endogen compounds such as metal ions and nitrogen compounds (Fig. 2).

3.4. Hierarchical clustering analysis

3.4.1. Protein profile change over envenomation

The log2-fold change data at all time points were plotted in a heatmap to compare the changes among clustered proteins during the envenomation process (Fig. 3A). The Euclidean clustering analysis

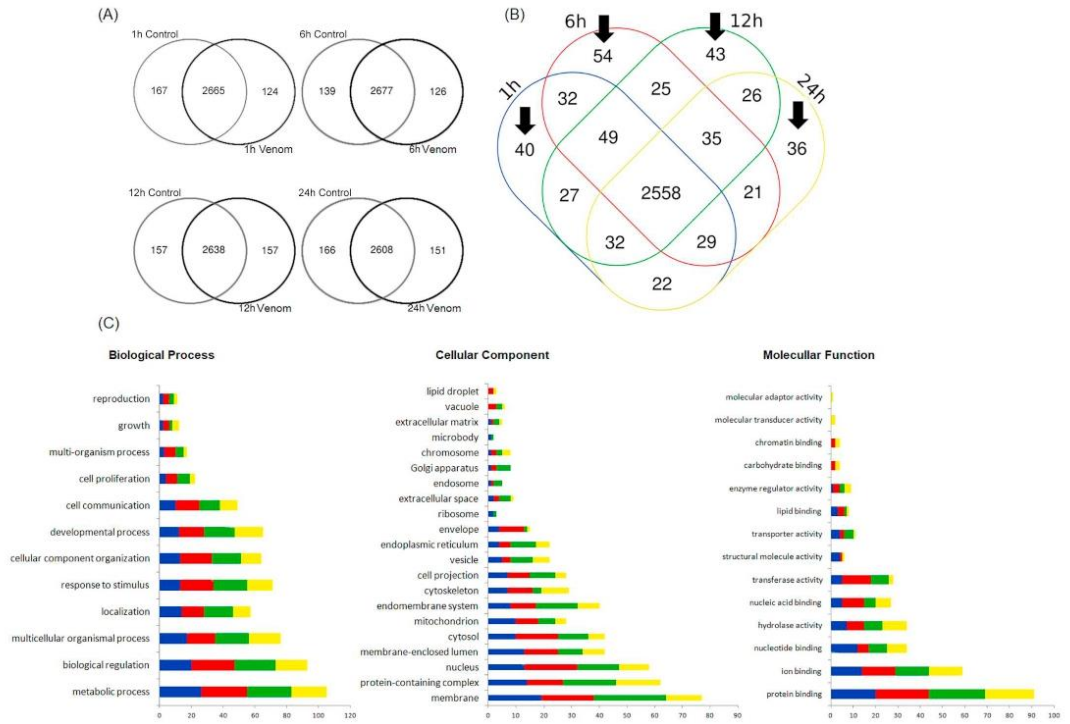

Fig. 1. Comparison of identified proteins in control and venom-treated mice among (A) all proteins identified in the control vs. mice treated with 0.5 LD *C. d. terrificus* venom injection after 1 h, 6 h, 12 h and 24 h and (B) all identified proteins at all time points for mice treated with the rattlesnake venom. The arrows show proteins identified exclusively at each of the time points. These proteins are listed in Supplementary Table 2A. (C) GO terms for biological processes, cellular components and molecular function that are exclusively expressed in mice cerebellum treated with rattlesnake venom (shown in Supplementary Table 2). N = 5 for each condition.

grouped the entire data in 6 clusters (Fig. 3B), and their GO cellular component is displayed in a graphical format (Fig. 3C). In the first cluster (marked in gray), 49 proteins were upregulated after 1 h, 12 h, and 24 h of *C. d. terrificus* venom injection, but decreased at 6 h. In the second cluster (marked in light blue), the highlighted 43 proteins increased in abundance from 1 h to 24 h. The third cluster (marked in dark red) represents 11 proteins, which deceased in abundance at 12 h and showed a little growth at 24 h. This cluster shows proteins related with protein location and apoptosis. The fourth cluster (marked in dark yellow) contains 12 proteins and showed the opposite behavior compared to the second cluster, where the protein abundances decrease from 1 h to 24 h. The enriched proteins in this cluster were associated with mitochondrion organization, chaperone-mediated protein complex assembly and the response to aluminum ions. The fifth cluster (marked in blue) contained 131 elements representing proteins that increase in abundance until 12 h and decrease at 24 h. The enriched proteins in this cluster were related to the mitochondria and its matrix, and the myelin sheath. The sixth cluster (marked in purple) contains 95 proteins and showed a constant decrease of abundance over time but an abrupt decrease at 24 h. This cluster had enriched proteins related to the mitochondria, respiratory chain complex and mitochondrial respiratory chain.

3.4.2. Principal component analysis

PCA projects a multidimensional space into a derived space spanned by new variables called principal components ordered in decreasing amount of explained variability, where the first components will retain the maximal amount of correlated information (i.e. coordinated activity of proteins). The PCA was applied to the proteins quantification data, and the time points projected into the component space showing a wide distribution of proteins and their relation to each specific time point (Supplemental Fig. 4). In addition, orthogonal vectors showed poor correlation between these time points. We have chosen the first two components (PC1 and PC2) solution as a bona fide signal, explaining 75.4% of the total proteomics variability carried by the protein expression. At the 12 h and 24 h after the envenomation there are higher and positive correlation in the PC1, and present an opposite and negative correlation to the 1 h and 6 h time points. The PC1 explains more than 40.9% of total variance for these two time points, and corroborate to the clustering analysis (Fig. 3A and B) of multiple proteins that decreased at 6 h, mainly related to the oxidoreductase, mitochondria and cellular respiration processes. Furthermore, a cluster with 131 highly increased proteins at 12 h, which decreased at 24 h, was related to mitochondrial part and matrix, and myelin sheath. The PC1 explains more than 34.5% of total variance, with positive correlation to the 1 h time point after the envenomation in which proteins related to transport, hydrolase processes and mitochondrion, respiratory chain complex and mitochondrial respiratory chain are enriched. Interestingly enough, PC1 correlates well with changes between the 12 h and 24 h time points after venom treatment, which can be similarly seen for the 1 h and 6 h time points as the projection of the tips of the arrows on PC1 axis indicate. Moreover, PCA results corroborate to the organism

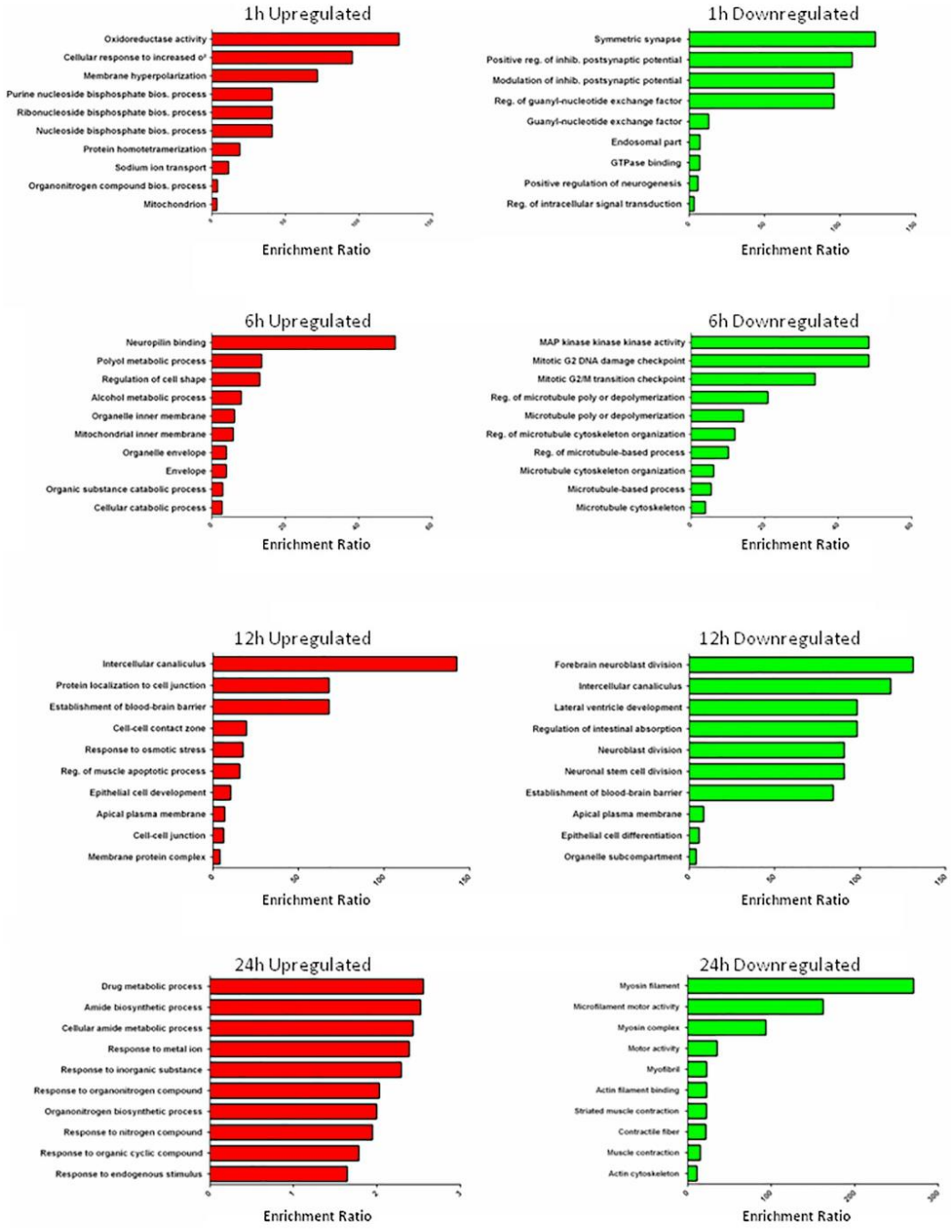

Fig. 2. Over-representation enrichment analysis using the WebGestalt tool. Protein enrichment analysis was performed using the proteins exclusively identified at each time point. The graph summarizes the GO terms for biological process, cellular components and molecular function.

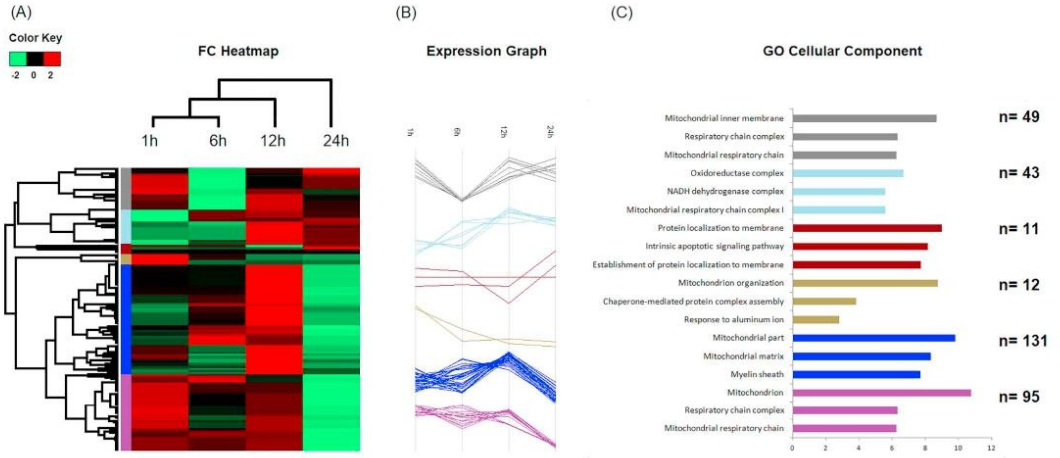

Fig. 3. Hierarchical clustering of protein quantification levels in the cerebellum at 1 h, 6 h, 12 h, and 24 h after *C. d. terrificus* venom injection in mice. (A) A heatmap presentation of a hierarchical cluster of the most significant proteins detected with quantification in at least two replicates for each treatment time showing the changes in protein behavior over time. The protein fold change is represented on a log2 scale. Each color at the left side of the heatmap represents protein hierarchies represented in the expression graphs and their GO component for cellular enrichment. (B) Expression graphs of each cluster. The protein quantification values were normalized by *Z*-score by rows. (C) The GO cellular component enrichment for all clusters and the numbers of proteins composing each cluster.

response after 24 h in the envenomation process.

3.4.3. Network analysis

The clustering data and the protein abundance changes over time were further compiled with a network analysis that showed the top five enriched GO terms: the vascular xenobiotic process (24 proteins), the membrane potential process (21 proteins), calcium ion homeostasis (4 proteins), the development and polymerization of the microtubule (4 proteins), and the tRNA aminoacetylation process (4 proteins) (Fig. 4). Moreover, we were able to highlight the specific protein abundance variation along with the time from 1 h to 24 h in each network clustered group.

In general, it is possible to observe a variable variation in the abundance of several proteins from 1 h to 6 h in each of the five highlighted GO terms. However, at 12 h, most of the proteins were upregulated, and at 24 h, most of these proteins were downregulated. We will resolve these results in the discussion section below.

4. Discussion

The proteomic analysis of the mouse cerebellum after the inoculation of 0.5 LD50 *C. d. terrificus* venom pointed to proteomic variations from 1 h to 24 h, in which several proteins were exclusively expressed in the control group or in the venom-injected mice (Fig. 1A). From the enrichment analysis, all of the biological functional terms of each protein group that pointed to the enhancement or diminishment of the terms at each time point were analyzed in non-ranked and quantitative mass spectrometry approaches, giving us an insight into how *C. d. terrificus* venom injection modulates biological functions from 1 h to 24 h.

In the non-ranked enrichment analysis at 1 h (Fig. 2), we observed an enrichment of oxidoreductases that act on the CH—CH_2 group of donors that uses oxygen as a receptor. Such a response to increase the oxygen levels might indicate oxidative stress events that may have occurred in the cerebellar tissue. Oxidative stress events have been reported mainly due to the nephrotoxicity that is the result of rhabdomyolysis and acute renal failures induced by the rattlesnake venom [33]. Yamasaki and colleagues [34] have already described the oxidative stress caused by *C. d. terrificus* venom in mice, in which concentrations of 80% of the crude venom were able to cause oxidative stress on the cortical and medullar tissue. In the same context, Melendez-Martinez and colleagues [35] have also recently described how rattlesnake venom from *Crotalus molossus nigrescens* induces oxidative stress on human erythrocytes after 24 h of venom treatment. Additionally, at 1 h, it was possible to observe that the venom might be directly or indirectly affecting the neuronal transmission in the cerebellum. As an example, the enrichment of proteins involved in membrane hyperpolarization alongside the downregulation of proteins involved with the symmetric synapse, the positive regulation of proteins involved in the inhibitory potential, and the modulation of the proteins related to inhibitory post-synaptic potentials, shows that the venom might be acting preferentially on proteins involved on neuronal synaptic signaling. At 6 h, we observed an enrichment of the highly conserved neuropillin neural receptors, which are single-pass transmembrane proteins specific to vertebrates that were originally identified as adhesion molecules in the nervous system [36]. The main protein class that binds to neuropillins is the semaphorins [37]. Semaphorins are proteins that guide and prevent neurons from moving to inappropriate areas in the neural tissue; thus, they have an important role in neural development [37]. Since these proteins are strongly related to the maintenance of neural health, we speculate that their upregulation in the neural tissue might be an indicative of a response to venom-related damage to the brain tissue. In fact, previous reports have shown the neurotoxicity effects of the *C. d. terrificus* venom or some of its components on the synapses and the central nervous system [38]. The downregulation of proteins that involve the MAPK3 signaling pathway, checkpoint on G2/M and mitosis on the G2 phase indicates possible damage to DNA. The downregulation of protein kinases related to the cell cycle might indicate an impairment of the entire DNA repair mechanism. In fact, the cytotoxic effect of crotoxin, the major component of *C. d. terrificus* venom, on DNA damage has already been reported by Muller and colleagues when exploring the cytotoxic potential of crotoxin in different tumor cell lines [39]. At 12 h, we observed the enrichment of proteins related to the blood-brain barrier establishment, which means that while some molecules are disturbing the homeostasis of the barrier, the organism is trying to repair the damage. It has been previously reported that gyroxin, another important constituent of the

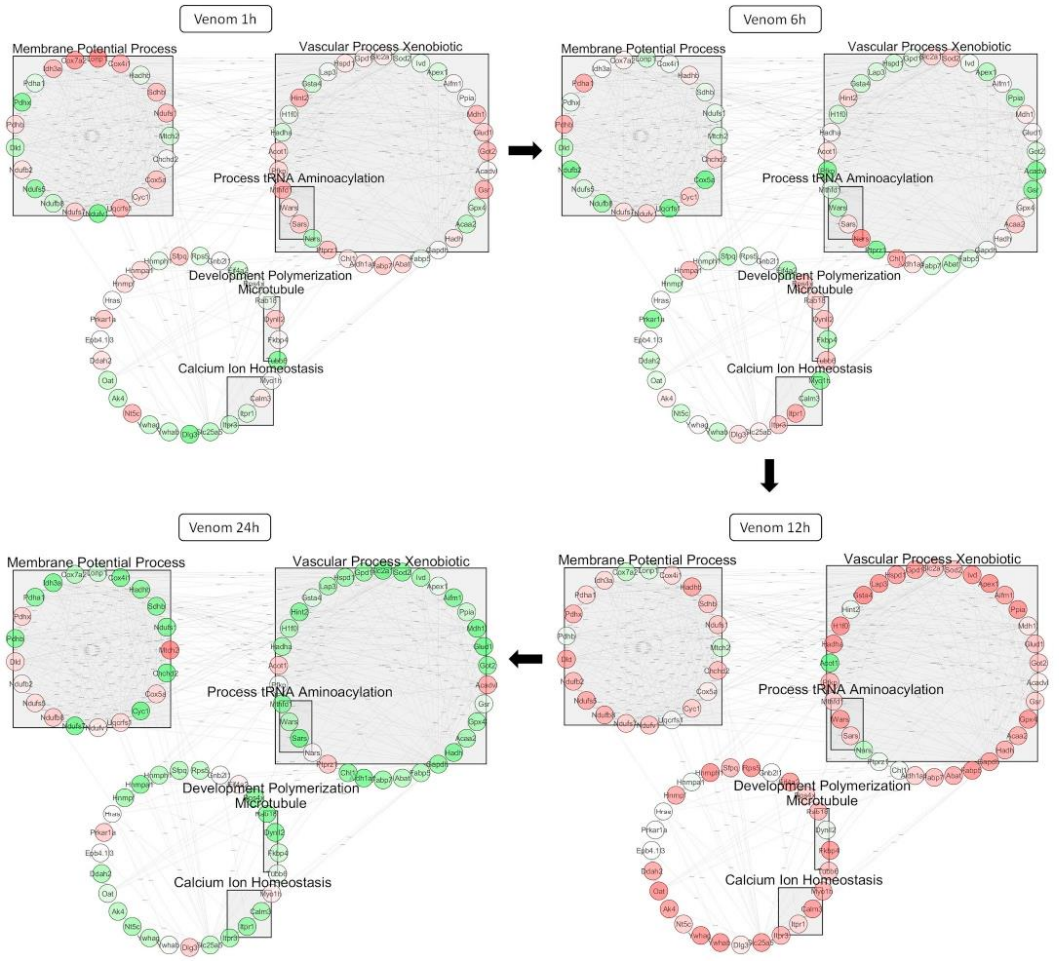

Fig. 4. Network views of the total profile of the protein fold changes from 1 h to 24 h. The PPI analysis was performed using the String-db tool with its own *Mus musculus* database. The PPI information was added to the Cytoscape software, and network views were created by clustering proteins from the top 5 GO enriched biological processes. The rectangle shows the GO biological process-enriched proteins.

C. d. terrificus venom, is able to transpose the blood-brain barrier [15]. Therefore, gyroxin or some other venom constituent might be playing a role in this process by transposing the brain barrier and causing direct damage in the cerebellum. Proteins shown here to be altered at 24 h seem to be related to muscle maintenance. In fact, rhabdomyolysis has been reported in patients upon *C. d. terrificus* snake bite [40]. This disease is a serious syndrome due to a direct or indirect muscle injury resulting from the death of muscle fibers and release of their contents into the bloodstream.

In the first cluster of our initial quantitative approach (Fig. 3) where 49 proteins were upregulated after 1 h, 12 h, and 24 h of *C. d. terrificus* venom injection and decreased at 6 h, we can find proteins that are mainly related to mitochondria and cellular respiration processes. Their decrease at 6 h suggests that the organism was suffering major disturbances in respiration-related processes, and the upregulation of such proteins at the later time points were due to the organism reacting to the stress caused by this perturbation. In the second cluster, the highlighted 43 proteins increased in abundance from 1 h to 24 h. This particular cluster is in line with the occurrence of oxidative stress in the cerebellar tissue. NADH dehydrogenase protein complex represented in this cluster, is important for oxidative phosphorylation processes, playing a fundamental role in brain function and, in the case of dysfunction, in neuronal diseases [41]. The third cluster is represented by 11 proteins, which decreased in abundance at 12 h and showed a little growth at 24 h. This cluster shows proteins that are related to apoptosis, indicating that the cerebellar tissue survival ability was affected by the envenomation process. The fourth cluster contains 12 proteins, which abundances decreases from 1 h to 24 h. Proteins present in this cluster were enriched for mitochondrial organization, chaperone-mediated protein complex assembly and response to the aluminum ion. The fifth cluster, which contained 131 proteins, presented proteins that increase in abundance until 12 h and decrease at 24 h. The enriched proteins in

this cluster were related to the mitochondria and its matrix and the myelin sheath, which corroborates the data shown in Fig. 2 that shows the disturbances in proteins that play a role in the blood-brain barrier. The cerebellar tissue might be prone to be directly affected by proteins that increasingly affect the myelin sheath in 24 h. Last, the sixth cluster, containing 95 proteins, showed their constant decrease of abundance with time and an abrupt decrease at 24 h. This cluster was enriched of mitochondrial proteins from the respiratory chain complex. It is already known that there is a relationship between the venom and the mitochondrial respiratory chain that is reduced after the envenomation of a diverse group of animals [42,43].

A quantitative approach to the network analysis showed that some proteins have stood out at all time points on certain clustered functions (Fig. 4), such as members of the cyclooxygenase (Cox) c family, Cox7a2 and Cox4i1. Under normal conditions, these proteins contribute to the maintenance of synaptic activity, memory consolidation and hyperemia [44]. In addition, these proteins also play important roles in neuroinflammation [45]. The envenomation process is normally characterized by a generalized inflammatory state, where the normal reaction prompts a protective response to the venom. Although in some cases, the response to envenomation may lead to sepsis [46], the organism is usually able to counterbalance the immune response due to the envenomation. Several works have described the effect of the inflammatory response modulation and hyperalgesia by *Bothrops* and *Crotalus* snake venoms [47,48]. The use of corticosteroid medication has been proposed to increase the efficacy of antivenom therapies in combination with Dexamethasone in experimental *Bothrops atrox* envenomation [49]. In this same cluster, which contains the Cox family of proteins, we can find the ubiquinone oxidoreductases subunit family of proteins (Ndufs) that upregulates at 12 h and abruptly downregulates at 24 h. Mutations affecting the NDUFS gene result in a mitochondrial complex I deficiency that is responsible for a wide range of clinical manifestations, from lethal neonatal disease to adult-onset neurodegenerative disorders such as Liegh syndrome [50], which causes several neurological disorders such as psychomotor and mental regression [50–52], Leber's hereditary optic neuropathy [53], and some forms of Parkinson's disease [54]. Although the observation of this protein family's modulation has not yet been described in the process of snake envenomation and more specifically in the case of *Crotalus* family envenomation, further investigations linking the neurotoxic effect of the *C. d. terrificus* venom to the modulation of these proteins may reveal a different role of venom action in the brain.

From the calcium ion homeostasis cluster, we highlight Itpr1 and Itpr3, which downregulate at 1 h and 24 h and upregulate between 6 h and 12 h. These proteins are known to play a role in apoptosis mediated by ER stress that releases calcium ions into the cytoplasm [55–57]. It is also known that Itpr1 downregulation is related with ataxia, a condition where the individual develops severe cerebellum disturbances and consequently impairs their voluntary movements and body balance. Several studies have shown that venoms in general, such as from the scorpion *Tityus serrulatus*, induces ataxia in individuals alongside other symptoms observed in individuals bitten by *C. d. terrificus*, such as rhabdomyolysis and acute kidney injury [58]. Works related to the same issue has also pointed that ataxia may be associated with crotalic accidents, and the disturbances observed in the Itpr proteins may be a clue for the molecular pathway for this severe damage caused by the *C. d. terrificus* envenomation process [59,60]. In the same cluster, Calmodulin 3 (Calm3) has also shown similar abundance modulation to Itpr proteins, with a peak of upregulation at 12 h after venom inoculation. Calmodulin is a protein that participates in the signaling pathways of a wide variety of biological processes, such as proliferation and growth, and is a primary Ca^{2+} sensor in eukaryotic cells [61]. Additionally, Calmodulin has been described to play a role in the neurotoxicity process by being the receptor for the internalization of neurotoxins such as PLA2 [62] and inhibiting neurotransmission by associating snake venom PLA2 in the nerve terminal [63,64]. Therefore, the observed increase of Calm3 in the cerebellum may be linked to its possible binding to the *C. d. terrificus* venom PLA2 subunit of crotoxin, resulting in blockage of synapses in the brain.

From the tRNA aminoacylation proteins group, we highlight Wars, Sars and Nars proteins, which are the tryptophan, serine, and asparagine t-RNA synthetases, respectively. The Wars protein has a role in cytoskeleton organization and the stress response. Its mutation leads to severe neuropathy [65–68]. The major role of Sars protein is in binding to the VEGFA growth factor that inhibits MYC proto-oncogene binding and, therefore, its transcriptional factor activity. Nars protein has been described to play an important role in the catalytic activity and the mutation of the NARS gene, and has been linked to severe neuropathies such as combined oxidative phosphorylation deficiency, which affects gray matter and causes severe disorders, Alpers syndrome, and Leigh syndrome [69–71]. The network analysis of these proteins suggested no synergy among Wars, Sars and Nars with time. Although all of these proteins are related to neurological disorders, their exact role in the cerebellum upon *C. d. terrificus* envenomation still needs to be elucidated.

Regarding the development and polymerization of the microtubule group, two proteins in this group, Rab18 and Tubb6, showed downregulation at 1 h and at 24 h. Tubb6, which is a microtubule constituent protein [72,73], was observed at a reduced abundance early after envenomation at 1 h and in late envenomation at 24 h. This profile shows a possible result of the response to tissue damage caused by the envenomation during the intermediate points. The downregulation at these time points may characterize a possible tissue damage response, corroborating the observation of microtubule polymerization downregulation observed in Fig. 2. These data may indicate that snake envenomation can directly damage the cerebellum tissue, but it may be possible that toxins are reaching the blood-brain barrier and acting in a direct form on certain brain tissues, such as the cerebellum. In addition, Rab 18 protein showed the same pattern. This protein is highly expressed in the brain and plays a role in synaptic vesicles function. Its downregulation may disrupt the neuronal cytoskeleton, and its absence has been related to abnormal ER structures. It has also been shown that Rab18 downregulation is related to several neural deficiencies and the accumulation of microtubule filaments in synaptic terminals [74,75].

In the xenobiotic vascular process cluster, several proteins were altered in a complex form during the early envenomation time points from 1 h to 6 h. Although almost all of the proteins in this cluster were upregulated at 12 h, the ACOT1 protein, which is related to fatty acid and amino acid metabolism and regulation pathways [76], is the only protein that was downregulated. This opposite behavior of ACOT1 to most of the proteins inside a cluster can again be observed at 24 h, alongside the behaviors of ACADVL and Ptprz1 proteins, and its overexpression in the brain is suggested to have a role in the remyelination of oligodendrocytes [77], strengthening the argument that the brain might be responding to the damaged brain tissue during the envenoming process in the gastrocnemius muscle.

Light microscopy histological analysis showed no remarkable differences between mice brains following the intramuscular injection of either venom or saline (Supplemental Table 5). Sangiorgio and colleagues [78] injected *C. d. terrificus* venom at 1 mg/kg in seven young adult female and male dogs weighting 4 to 7 kg and collected macro- and microscopic data at different sites and organs. Despite the alterations observed in the spleen, liver, kidney and stomach, no alterations were observed in the brain. Additionally, Venkatesan et al. [79] injected *Naja naja naja* snake venom in Swiss albino mice at 2 LD50, and found no significant changes in the brain tissue of the envenomed mice cells, except for some marked infiltration of leukocytes after 48 h of envenomation. Although different researchers have used different ratios of venom to animal weight, the sub-lethal dose used in this study might have not been enough to induce tissue damage that could be observed at the light microscope level. The ELISA test using anti-*C. d. terrificus* venom serum against the whole cerebellum lysate showed no

antibody recognition at any of the time points tested from 1 h to 24 h (data not shown). Additional analysis by Western blot using antibodies against specific components of the venom should be able to validate some of effects of the venom components on proteins altered in cerebellum of mice inject with *C. d. terrificus* venom shown here by mass spectrometry-based proteomics analysis.

5. Conclusion

The proteomic modulation events in the mice cerebellum after the *C. d. terrificus* venom injection in mice gastrocnemius muscle highlight the complex temporal dynamic of the envenomation process in one of the brain regions. The neurotoxicity of this snake venom and its effects on different brain regions still need to be elucidated. However, the proteomic data presented in this work have provided insights into the mechanisms of the venom-induced tissue damage, elucidating novel events that can change perspectives and the way that snake envenomation is molecularly described. The protein modulation observed in the cerebellar tissue caused by *C. d. terrificus* suggests synapse inhibition and perturbation of the blood brain-barrier maintenance that points to the possible participation of venom toxins in generating the actions described in this study. These findings shed new light on the complex mechanisms involved in the responses of tissues in snakebite envenomation, and points to potential novel routes for therapeutic interventions to attenuate envenomation mortality and morbidity.

Declaration of Competing Interest

The authors declare that there is no conflict of interest.

Acknowledgments

We thank Dr. Marisa Maria Teixeira da Rocha and Dr. Anita Tanaka from the Herpetology Department, Butantan Institute for the provision of the snake venom; Prof. Graziella Eliza Ronsein, Dr. Eduardo Shigueo Kitano and Dr. Daniel de Carvalho Pimenta for useful discussion; Alyson Matheus de Araújo Ferreira for the design of the graphical abstract. This work was supported by grants 2013/07467-1, 2016/04000-3, 2017/17943-6 and 2015/50040-4 (FAPESP/GSK) from the São Paulo Research Foundation (FAPESP), Brazil. Prof Emer S. Ferro is supported by Erna and Jakob Michael "Visiting Professorship", Department of Biological Regulation, Weizmann Institute of Science, Rehovot, Israel and grant 302809/2016-3 from the Brazilian National Council for Scientific and Technological Development, CNPq, Brazil. FM, WSS, and SSSA were supported by the Coordination for the Improvement of Higher Education Personnel (CAPES, Brazil) and CNPq institutional fellowship #88882.442313/2019-01 (Instituto Butantan, Brazil) for WSS and # 131408/2019-4 for SSSA (University of São Paulo, Brazil) and CYK was supported by the FAPESP master's degree program fellowship 2017/06496-9, Brazil.

Appendix A. Supplementary data

Supplementary data to this article can be found online at https://doi.org/10.1016/j.jprot.2020.103779.

References

[1] World Health Organization (WHO), Snakebite Envenoming, (2017) (https://www.who.int/health-topics/snakebite; https://www.who.int/snakebites/disease/en).
[2] Brazilian National Grievance Notification Information System SINAN, Epidemiological Data of Snakes in Brazil, http://portalsinan.saude.gov.br/acidente-por-animais-peconhentos, (2018).
[3] Brazilian Ministry of Health, Accidents by Venomous Animals: what to Do and How to Avoid Snakebite Accidents (Portuguese), http://www.saude.gov.br/saude-de-a-z/acidentes-por-animais-peconhentos, (2019).
[4] A. Rangel-Santos, E.C. Dos-Santos, M. Lopes-Ferreira, C. Lima, D.F. Cardoso, I. Mota, A comparative study of biological activities of crotoxin and CB fraction of venoms from *Crotalus durissus terrificus*, *Crotalus durissus cascavella* and *Crotalus durissus collilineatus*, Toxicon. 43 (2004) 801–810, https://doi.org/10.1016/j.toxicon.2004.03.011.
[5] F.V. Fonseca, E. Antunes, R.P. Morganti, H.S.A. Monteiro, A.M.C. Martins, D.O. Toyama, S. Marangoni, M.H. Toyama, Characterization of a new platelet aggregating factor from crotoxin *Crotalus durissus cascavella* venom, Protein J. 25 (2006) 183–192, https://doi.org/10.1007/s10930-006-9001-z.
[6] M.M. Azevedo-Marques, S.E. Hering, P. Cupo, Envenomation caused by poisonous animals: poisonous snakes, Med. (RibeiraoPreto. Online) 36 (2/4) (2003) 480–489, https://doi.org/10.11606/issn.2176-7262.v36i2/4p480-489.
[7] M.M. Azevedo Marques, S.E. Hering, P. Cupo, J.L.C. Cardoso, F.O.S. França, F.H. Wen, C.M.S. Málaque, V. Haddad-Jr (Eds.), Acidente Crotálico. In: Animais peçonhentos no Brasil: Biologia, Clínica e Terapêutica dos Acidentes [Crolalic accident: Venomous animals in Brazil: biology, clinical and therapeutic accidents"], 2, Sarvier, São Paulo, 2009, pp. 108–115.
[8] O.V. Brazil, Pharmacology of crystalline crotoxin. II. Neuromuscular blocking action, Mem. Inst. Butantan 33 (1966) 981–992.
[9] W.A. Hadler, O.V. Brazil, Pharmacology of crystalline crotoxin. IV. nephrotoxicity, Mem. Inst. Butantan. 33 (1966) 1001.
[10] F. de Paola, M.A. Rossi, Myocardial damage induced by tropical rattlesnake (Crotalus durissus terrificus) venom in rats, Cardiovasc. Pathol. 2 (1) (1993) 77–81, https://doi.org/10.1016/1054-8807(93)90016-U.
[11] P.E. Santos, S.D. Souza, L. Freire-Maia, A.P. Almeida, Effects of crotoxin on the isolated guinea pig heart, Toxicon 28 (1990) 215–224.
[12] S.C. Sampaio, S. Hyslop, M.R.M. Fontes, J. Prado-Franceschi, V.O. Zambelli, A.J. Magro, P. Brigatte, V.P. Gutierrez, Y. Cury, Crotoxin: novel activities for a classic β-neurotoxin, Toxicon. 55 (2010) 1045–1060, https://doi.org/10.1016/j.toxicon.2010.01.011.
[13] A.L. Bieber, D. Nedelkov, Structural, biological and biochemical studies of myotoxin a and homologous myotoxins, J. Toxicol. Toxin Rev. 16 (1997) 33–52, https://doi.org/10.3109/15569549709064092.
[14] T. Kozako, A. Kawachi, S.-B. Cheng, S. Kuchiiwa, T. Motoya, S. Nakagawa, K. Yamada, Role of the vestibular nuclei in endothelin-1-induced barrel rotation in rats, Eur. J. Pharmacol. 454 (2002) 199–207, https://doi.org/10.1016/S0014-2999(02)02498-6.
[15] J.A.A. da Silva, K.C. Oliveira, M.A.P. Camillo, Gyroxin increases blood-brain barrier permeability to Evans blue dye in mice, Toxicon. 57 (2011) 162–167, https://doi.org/10.1016/j.toxicon.2010.06.027.
[16] J. Prado-Franceschi, O.V. Brazil, Convulxin, a new toxin from the venom of the South American rattlesnake *Crotalus durissus terrificus*, Toxicon. 19 (1981) 875–887, https://doi.org/10.1016/0041-0101(81)90085-4.
[17] A. Calmette, The treatment of animals poisoned with snake venom by the injection of antivenomous serum, Br. Med. J. 2 (1896) 399, https://doi.org/10.1136/bmj.2.1859.399.
[18] M.T. Jorge, L.A. Ribeiro, Epidemiology and clinical features of South American rattlesnakes (*Crotalus durissus*) envenomation, Rev. Inst. Med. Trop. Sao Paulo 34 (1992) 347–354.
[19] M.A.K. Markwell, S.M. Haas, L.L. Bieber, N. Tolbert, A modification of the Lowry procedure to simplify protein determination in membrane and lipoprotein samples, Anal. Biochem. 87 (1978) 206–210, https://doi.org/10.1016/0003-2697(78)90586-9.
[20] R.S. Villarroel, M. Siles, F. Zelante, R. Rolim Rosa, R.S. Furlanetto, Padronização da titulação da atividade tóxica de venenos botrópicos em camundongos [Standardization of the toxic activity titration of botropic venoms in mice], Mem. Inst. Butantan 42/43v (1979) 311–323.
[21] T. Masuda, M. Tomita, Y. Ishihama, Phase transfer surfactant-aided trypsin digestion for membrane proteome analysis, J. Proteome Res. 7 (2008) 731–740, https://doi.org/10.1021/pr700658q.
[22] J.R. Wiśniewski, A. Zougman, N. Nagaraj, M. Mann, Universal sample preparation method for proteome analysis, Nat. Methods 6 (2009) 359, https://doi.org/10.1038/nmeth.1322.
[23] J. Rappsilber, M. Mann, Y. Ishihama, Protocol for micro-purification, enrichment, pre-fractionation and storage of peptides for proteomics using StageTips, Nat. Protoc. 2 (2007) 1896–1906, https://doi.org/10.1038/nprot.2007.261.
[24] R.C. Beavis, Using the global proteome machine for protein identification, New Emerg. Proteomic Tech, Springer, 2006, pp. 217–228, , https://doi.org/10.1385/1-59745-026-X:217.
[25] P.J. Boersema, R. Raijmakers, S. Lemeer, S. Mohammed, A.J.R. Heck, Multiplex peptide stable isotope dimethyl labeling for quantitative proteomics, Nat. Protoc. 4 (2009) 484, https://doi.org/10.1038/nprot.2009.21.
[26] J. Cox, M. Mann, MaxQuant enables high peptide identification rates, individualized p.p.b.-range mass accuracies and proteome-wide protein quantification, Nat. Biotechnol. 26 (2008) 1367–1372, https://doi.org/10.1038/nbt.1511.
[27] A.H. Fischer, K.A. Jacobson, J. Rose, R. Zeller, Hematoxylin and eosin staining of tissue and cell sections, CSH Protocol. (2008) 1–3, https://doi.org/10.1101/pdb.prot4986.
[28] J. Wang, S. Vasaikar, Z. Shi, M. Greer, B. Zhang, WebGestalt 2017: a more comprehensive, powerful, flexible and interactive gene set enrichment analysis toolkit, Nucleic Acids Res. 45 (2017) W130–W137, https://doi.org/10.1093/nar/gkx356.
[29] D. Szklarczyk, A. Franceschini, S. Wyder, K. Forslund, D. Heller, J. Huerta-Cepas, M. Simonovic, A. Roth, A. Santos, K.P. Tsafou, M. Kuhn, P. Bork, L.J. Jensen, C. von Mering, STRING v10: protein-protein interaction networks, integrated over the tree of life, Nucleic Acids Res. 43 (2015) D447–D452, https://doi.org/10.1093/nar/gku1003.

[30] P. Shannon, A. Markiel, O. Ozier, N.S. Baliga, J.T. Wang, D. Ramage, N. Amin, B. Schwikowski, T. Ideker, Cytoscape: a software environment for integrated models of biomolecular interaction networks, Genome Res. 13 (2003) 2498–2504, https://doi.org/10.1101/gr.1239303.

[31] M. Kucera, R. Isserlin, A. Arkhangorodsky, G.D. Bader, AutoAnnotate: A Cytoscape app for summarizing networks with semantic annotations, F1000Res. 5 (2016), https://doi.org/10.12688/f1000research.9090.1.

[32] G.O. Consortium, Gene ontology consortium: going forward, Nucleic Acids Res. 43 (2014) D1049–D1056, https://doi.org/10.1093/nar/gku1179.

[33] F.M.O. Pinho, D.M.T. Zanetta, E.A. Burdmann, Acute renal failure after *Crotalus durissus* snakebite: a prospective survey on 100 patients, Kidney Int. 67 (2005) 659–667, https://doi.org/10.1111/j.1523-1755.2005.67122.x.

[34] S.C. Yamasaki, J.S. Villarroel, J.M. Barone, L. Zambotti-Villela, P.F. Silveira, Aminopeptidase activities, oxidative stress and renal function in *Crotalus durissus terrificus* envenomation in mice, Toxicon. 52 (2008) 445–454, https://doi.org/10.1016/j.toxicon.2008.06.015.

[35] D. Meléndez-Martínez, J.M. Muñoz, G. Barraza-Garza, M.S. Cruz-Peréz, A. Gatica-Colima, E. Alvarez-Parrilla, L.F. Plenge-Tellechea, Rattlesnake *Crotalus molossus nigrescens* venom induces oxidative stress on human erythrocytes, J. Venom. Anim. Toxins Incl. Trop. Dis. 23 (2017) 24, https://doi.org/10.1186/s40409-017-0114-y.

[36] M. Tata, M. Tillo, C. Ruhrberg, Neuropilins in development and disease of the nervous system, Neural Surface Antigens, from Basic Biology Towards Biomedical Applications, Academic Press/ ScienceDirect, 2015, pp. 65–75, , https://doi.org/10.1016/B978-0-12-800781-5.00006-2.

[37] M. Tata, C. Ruhrberg, A. Fantin, Vascularisation of the central nervous system, Mech. Dev. 138 (2015) 26–36, https://doi.org/10.1016/j.mod.2015.07.001.

[38] R. da Silva Lomeo, A.P. de Faria Gonçalves, C.N. da Silva, A.T. de Paula, D.O.C. Santos, C.L. Fortes-Dias, D.A. Gomes, M.E. de Lima, Crotoxin from *Crotalus durissus terrificus* snake venom induces the release of glutamate from cerebrocortical synaptosomes via N and P/Q calcium channels, Toxicon. 85 (2014) 5–16, https://doi.org/10.1016/j.toxicon.2014.04.008.

[39] S.P. Muller, V.A.O. Silva, A.V.P. Silvestrini, L.H. de Macedo, G.F. Caetano, R.M. Reis, M.V. Mazzi, Crotoxin from *Crotalus durissus terrificus* venom: in vitro cytotoxic activity of a heterodimeric phospholipase A2 on human cancer-derived cell lines, Toxicon. 156 (2018) 13–22, https://doi.org/10.1016/j.toxicon.2018.10.306.

[40] S.P. Bush, P.W. Jansen, Severe rattlesnake envenomation with anaphylaxis and rhabdomyolysis, Ann. Emerg. Med. 25 (1995) 845–848, https://doi.org/10.1016/S0196-0644(95)70218-0.

[41] W. Ying, NAD+ and NADH in brain functions, brain diseases and brain aging, Front. Biosci. 12 (2007) 1863–1888.

[42] S. Al-Saleh, H. Ghneim, S. Khan, The effect of crude and purified *Cerastes vipera* venom protein fractions on respiratory chain function in cultured human fibroblasts, Cell. Physiol. Biochem. 13 (2003) 315–320, https://doi.org/10.1159/000074547.

[43] H.K. Ghneim, The effect of *Echis coloratus* venom on biochemical and molecular markers of the antioxidant capacity in human fibroblasts, Libyan J. Med. 12 (2017), https://doi.org/10.1080/19932820.2017.1304515.

[44] K. Yamagata, K.I. Andreasson, W.E. Kaufmann, C.A. Barnes, P.F. Worley, Expression of a mitogen-inducible cyclooxygenase in brain neurons: regulation by synaptic activity and glucocorticoids, Neuron. 11 (1993) 371–386, https://doi.org/10.1016/0896-6273(93)90192-T.

[45] L. Minghetti, Cyclooxygenase-2 (COX-2) in inflammatory and degenerative brain diseases, J. Neuropathol. Exp. Neurol. 63 (2004) 901–910, https://doi.org/10.1093/jnen/63.9.901.

[46] M. Gonzalez, R. Sanchez, E.H. Carrillo, Septic shock syndrome resulting from snakebite, J. Trauma Acute Care Surg. 68 (2010) 1015, https://doi.org/10.1097/TA.0b013e31815edf21.

[47] F.P.B. Nunes, S.C. Sampaio, M.L. Santoro, M.C.C. Sousa-e-Silva, Long-lasting anti-inflammatory properties of *Crotalus durissus terrificus* snake venom in mice, Toxicon. 49 (2007) 1090–1098, https://doi.org/10.1016/j.toxicon.2007.01.017.

[48] R.A. do Olivo, C.F.P. Teixeira, J.L. Wallace, J.M. Gutierrez, S.R. Zamuner, Role of cyclooxygenases in oedema-forming activity of bothropic venoms, Toxicon 49 (2007) 670–677, https://doi.org/10.1016/j.toxicon.2006.11.006.

[49] F.C. Patrão-Neto, M.A. Tomaz, M.A. Strauch, M. Monteiro-Machado, J.R.D.S. Rocha-Junior, P.A. Borges, S. Calil-Elias, P.A. Melo, Dexamethasone antagonizes the in vivo myotoxic and inflammatory effects of *Bothrops* venoms, Toxicon. 69 (2013) 55–64, https://doi.org/10.1016/j.toxicon.2013.01.023.

[50] R.H. Triepels, L.P. den Heuvel, J. Loeffen, C.A.F. Buskens, R.J.P. Smeets, M.E. Rubio Gozalbo, S.M.S. Budde, E.C. Mariman, F.A. Wijburg, P.G. Barth, Leigh syndrome associated with a mutation in the NDUFS7 (PSST) nuclear encoded subunit of complex I, Ann. Neurol. 45 (1999) 787–790 (doi:10.1002/1531-8249(199906)45:6787::AID-ANA13 > 3.0.CO;2-6).

[51] J. Finsterer, Leigh and Leigh-like syndrome in children and adults, Pediatr. Neurol. 39 (2008) 223–235, https://doi.org/10.1016/j.pediatrneurol.2008.07.013.

[52] S. Lebon, D. Rodriguez, D. Bridoux, A. Zerrad, A. Rötig, A. Munnich, A. Legrand, A. Slama, A novel mutation in the human complex I NDUFS7 subunit associated with Leigh syndrome, Mol. Genet. Metab. 90 (2007) 379–382, https://doi.org/10.1016/j.ymgme.2006.12.007.

[53] K.T. Fahnehjelm, M. Olsson, K. Naess, M. Wiberg, J. Ygge, L. Martin, U. von Döbeln, Visual function, ocular motility and ocular characteristics in patients with mitochondrial complex I deficiency, Acta Ophthalmol. 90 (2012) 32–43, https://doi.org/10.1111/j.1755-3768.2010.01865.x.

[54] A.H.V. Schapira, J.M. Cooper, D. Dexter, J.B. Clark, P. Jenner, C.D. Marsden, Mitochondrial complex I deficiency in Parkinson's disease, J. Neurochem. 54 (1990) 823–827.

[55] S. Park, N. Shcheynikov, J.H. Hong, C. Zheng, S.H. Suh, K. Kawaai, H. Ando, A. Mizutani, T. Abe, H. Kiyonari, Irbit mediates synergy between Ca2+ and cAMP signaling pathways during epithelial transport in mice, Gastroenterology. 145 (2013) 232–241, https://doi.org/10.1053/j.gastro.2013.03.047.

[56] H. Yamazaki, J. Chan, M. Ikura, T. Michikawa, K. Mikoshiba, Tyr-167/Trp-168 in type 1/3 inositol 1, 4, 5-trisphosphate receptor mediates functional coupling between ligand binding and channel opening, J. Biol. Chem. 285 (2010) 36081–36091, https://doi.org/10.1074/jbc.M110.140129.

[57] G. Li, M. Mongillo, K.-T. Chin, H. Harding, D. Ron, A.R. Marks, I. Tabas, Role of ERO1-α–mediated stimulation of inositol 1, 4, 5-triphosphate receptor activity in endoplasmic reticulum stress–induced apoptosis, J. Cell Biol. 186 (2009) 783–792 https://10.1074/jbc.M110.140129.

[58] P.P.Q. Torrez, M.M.M. Quiroga, P.A.M. Abati, M. Mascheretti, W.S. Costa, L.P. Campos, F.O.S. França, Acute cerebellar dysfunction with neuromuscular manifestations after scorpionism presumably caused by *Tityus obscurus* in Santarém, Pará/Brazil, Toxicon. 96 (2015) 68–73, https://doi.org/10.1016/j.toxicon.2014.12.012.

[59] T.M. Julius, M.K. Kaelble, E.B. Leech, K.L. Boyle, E.J. Strandberg, M.C. Clare, Retrospective evaluation of neurotoxic rattlesnake envenomation in dogs and cats: 34 cases (2005–2010), J. Vet. Emerg. Crit. Care 22 (2012) 460–469, https://doi.org/10.1111/j.1476-4431.2012.00775.x.

[60] C.L. Singleton, J.E. Oosterhuis, K. Seibold, N. Lamberski, Successful treatment of a southern pacific rattlesnake (*Crotalus viridis helleri*) bite in a caracal (*Caracal caracal*), J. Zoo Wildl. Med. 40 (2009) 378–381, https://doi.org/10.1638/2008-0113.1.

[61] W.Y. Tsang, A. Spektor, D.J. Luciano, V.B. Indjeian, Z. Chen, J.L. Salisbury, I. Sánchez, B.D. Dynlacht, CP110 cooperates with two calcium-binding proteins to regulate cytokinesis and genome stability, Mol. Biol. Cell 17 (2006) 3423–3434, https://doi.org/10.1091/mbc.e06-04-0371.

[62] P. Prijatelj, J. Šribar, G. Ivanovski, I. Križaj, F. Gubenšek, J. Pungerčar, Identification of a novel binding site for calmodulin in ammodytoxin A, a neurotoxic group IIA phospholipase A2, Eur. J. Biochem. 270 (2003) 3018–3025, https://doi.org/10.1046/j.1432-1033.2003.03679.x.

[63] J. Šribar, A. Copic, A. Pariš, N.E. Sherman, F. Gubenšek, J.W. Fox, I. Krizaj, A high affinity acceptor for phospholipase A2 with neurotoxic activity is a calmodulin, J. Biol. Chem. 276 (2001) 12493–12496, https://doi.org/10.1074/jbc.C100048200.

[64] I. Križaj, F. Gubenšek, Neuronal receptors for phospholipases A2 and β-neurotoxicity, Biochimie. 82 (2000) 807–814, https://doi.org/10.1016/S0300-9084(00)01172-X.

[65] K. Wakasugi, B.M. Slike, J. Hood, A. Otani, K.L. Ewalt, M. Friedlander, D.A. Cheresh, P. Schimmel, A human aminoacyl-tRNA synthetase as a regulator of angiogenesis, Proc. Natl. Acad. Sci. 99 (2002) 173–177, https://doi.org/10.1073/pnas.012602099.

[66] F.-C. Bange, T. Flohr, U. Buwitt, E.C. Böttger, An interferon-induced protein with release factor activity is a tryptophanyl-tRNA synthetase, FEBS Lett. 300 (1992) 162–166, https://doi.org/10.1073/pnas.012602099.

[67] A. Otani, B.M. Slike, M.I. Dorrell, J. Hood, K. Kinder, K.L. Ewalt, D. Cheresh, P. Schimmel, M. Friedlander, A fragment of human TrpRS as a potent antagonist of ocular angiogenesis, Proc. Natl. Acad. Sci. 99 (2002) 178–183, https://doi.org/10.1073/pnas.012601899.

[68] P.-C. Tsai, B.-W. Soong, I. Mademan, Y.-H. Huang, C.-R. Liu, C.-T. Hsiao, H.-T. Wu, T.-T. Liu, Y.-T. Liu, Y.-T. Tseng, A recurrent WARS mutation is a novel cause of autosomal dominant distal hereditary motor neuropathy, Brain. 140 (2017) 1252–1266, https://doi.org/10.1093/brain/awx058.

[69] M. Simon, E.M. Richard, X. Wang, M. Shahzad, V.H. Huang, T.A. Qaiser, P. Potluri, S.E. Mahl, A. Davila, S. Nazli, Mutations of human NARS2, encoding the mitochondrial asparaginyl-tRNA synthetase, cause nonsyndromic deafness and Leigh syndrome, PLoS Genet. 11 (2015) e1005097, , https://doi.org/10.1371/journal.pgen.1005097.

[70] A.V. Vanlander, B. Menten, J. Smet, L. De Meirleir, T. Sante, B. De Paepe, S. Seneca, S.F. Pearce, C.A. Powell, S. Vergult, Two siblings with homozygous pathogenic splice-site variant in mitochondrial asparaginyl–t RNA synthetase (NARS2), Hum. Mutat. 36 (2015) 222–231, https://doi.org/10.1002/humu.22728.

[71] K. Sofou, G. Kollberg, M. Holmström, M. Dávila, N. Darin, C.M. Gustafsson, E. Holme, A. Oldfors, M. Tulinius, J. Asin-Cayuela, Whole exome sequencing reveals mutations in NARS2 and PARS2, encoding the mitochondrial asparaginyl-tRNA synthetase and prolyl-tRNA synthetase, in patients with Alpers syndrome, Mol. Genet. Genomic Med. 3 (2015) 59–68, https://doi.org/10.1002/mgg3.115.

[72] A.L. Risinger, F.J. Giles, S.L. Mooberry, Microtubule dynamics as a target in oncology, Cancer Treat. Rev. 35 (2009) 255–261, https://doi.org/10.1016/j.ctrv.2008.11.001.

[73] L.J. Leandro-García, S. Leskelä, I. Landa, C. Montero-Conde, E. López-Jiménez, R. Letón, A. Cascón, M. Robledo, C. Rodríguez-Antona, Tumoral and tissue-specific expression of the major human β-tubulin isotypes, Cytoskeleton. 67 (2010) 214–223, https://doi.org/10.1002/cm.20436.

[74] S.M. Carpanini, L. McKie, D. Thomson, A.K. Wright, S.L. Gordon, S.L. Roche, M.T. Handley, H. Morrison, D. Brownstein, T.M. Wishart, A novel mouse model of Warburg micro syndrome reveals roles for RAB18 in eye development and organization of the neuronal cytoskeleton, Dis. Model. Mech. 7 (2014) 711–722, https://doi.org/10.1242/dmm.015222.

[75] M.L. Mignogna, P. D'Adamo, Critical importance of RAB proteins for synaptic function, Small GTPases. 9 (2018) 145–157, https://doi.org/10.1080/21541248.2016.1277001.

[76] M.C. Hunt, A. Rautanen, M.A.K. Westin, L.T. Svensson, S.E.H. Alexson, Analysis of the mouse and human acyl-CoA thioesterase (ACOT) gene clusters shows that convergent, functional evolution results in a reduced number of human peroxisomal

ACOTs, FASEB J. 20 (2006) 1855–1864, https://doi.org/10.1096/fj.06-6042com.
[77] S. Harroch, G.C. Furtado, W. Brueck, J. Rosenbluth, J. Lafaille, M. Chao, J.D. Buxbaum, J. Schlessinger, A critical role for the protein tyrosine phosphatase receptor type Z in functional recovery from demyelinating lesions, Nat. Genet. 32 (2002) 411, https://doi.org/10.1038/ng1004.
[78] F. Sangiorgio, M. Sakate, R.M.B. Nogueira, R.A. Tostes, Histopathological evaluation in experimental envenomation of dogs with *Crotalus durissus terrificus* venom, J. Venom. Anim. Toxins Incl. Trop. Dis. 14 (2008) 82–99, https://doi.org/10.1590/S1678-91992008000100007.
[79] C. Venkatesan, M. Sarathi, G. Balasubramanian, J. Thomas, V. Balachander, V.S. Babu, S.M.Y. Bilal, S.A. Majeed, N. Madan, N.S. Raj, Antivenom activity of triterpenoid ($C_{34}H_{68}O_2$) from *Leucas aspera* Linn. against *Naja naja naja* venom induced toxicity: Antioxidant and histological study in mice, Hum. Exp. Toxicol. 33 (2014) 336–359, https://doi.org/10.1177/0960327113494901.

Kisaki CY, **Arcos SSS**, Montoni F, da Silva Santos W, Calacina HM, Lima IF, Cajado-Carvalho D, Ferro ES, Nishiyama-Jr MY, Iwai LK. *Bothrops Jararaca* Snake Venom Modulates Key Cancer-Related Proteins in Breast Tumor Cell Lines. Toxins (Basel). 2021 Jul 25;13(8):519. doi: 10.3390/toxins13080519.

toxins

MDPI

Article

Bothrops Jararaca Snake Venom Modulates Key Cancer-Related Proteins in Breast Tumor Cell Lines

Carolina Yukiko Kisaki [1], Stephanie Santos Suehiro Arcos [1], Fabio Montoni [1], Wellington da Silva Santos [1], Hamida Macêdo Calacina [1], Ismael Feitosa Lima [1], Daniela Cajado-Carvalho [1], Emer Suavinho Ferro [2], Milton Yutaka Nishiyama-Jr [1,*] and Leo Kei Iwai [1,*]

[1] Laboratory of Applied Toxinology (LETA) and Center of Toxins, Immune-Response and Cell Signaling (CeTICS), Butantan Institute, São Paulo 05503-900, Brazil; carolkisaki@hotmail.com (C.Y.K.); stephanie.arcos@usp.br (S.S.S.A.); fabio.montoni@esib.butantan.gov.br (F.M.); wellington.silva@esib.butantan.gov.br (W.d.S.S.); hamidamacedo33@gmail.com (H.M.C.); ismael.lima@butantan.gov.br (I.F.L.); daniela.carvalho@butantan.gov.br (D.C.-C.)

[2] Department of Pharmacology, Biomedical Sciences Institute (ICB), University of São Paulo (USP), São Paulo 05508-000, Brazil; eferro@usp.br

* Correspondence: milton.nishiyama@butantan.gov.br (M.Y.N.-J.); leo.iwai@butantan.gov.br (L.K.I.)

Abstract: Cancer is characterized by the development of abnormal cells that divide in an uncontrolled way and may spread into other tissues where they may infiltrate and destroy normal body tissue. Several previous reports have described biochemical anti-tumorigenic properties of crude snake venom or its components, including their capability of inhibiting cell proliferation and promoting cell death. However, to the best of our knowledge, there is no work describing cancer cell proteomic changes following treatment with snake venoms. In this work we describe the quantitative changes in proteomics of MCF7 and MDA-MB-231 breast tumor cell lines following treatment with *Bothrops jararaca* snake venom, as well as the functional implications of the proteomic changes. Cell lines were treated with sub-toxic doses at either 0.63 µg/mL (low) or 2.5 µg/mL (high) of *B. jararaca* venom for 24 h, conditions that cause no cell death per se. Proteomics analysis was conducted on a nano-scale liquid chromatography coupled on-line with mass spectrometry (nLC-MS/MS). More than 1000 proteins were identified and evaluated from each cell line treated with either the low or high dose of the snake venom. Protein profiling upon venom treatment showed differential expression of several proteins related to cancer cell metabolism, immune response, and inflammation. Among the identified proteins we highlight histone H3, SNX3, HEL-S-156an, MTCH2, RPS, MCC2, IGF2BP1, and GSTM3. These data suggest that sub-toxic doses of *B. jararaca* venom have potential to modulate cancer-development related protein targets in cancer cells. This work illustrates a novel biochemical strategy to identify therapeutic targets against cancer cell growth and survival.

Keywords: mass spectrometry; proteome; snake venom; *Bothrops jararaca*; breast cancer

Key Contribution: We describe that *B. jararaca* snake venom modulates specific protein pathways related to cancer cell growth and invasion, which could be a useful approach to identify novel therapeutic targets for cancer treatment.

check for updates

Citation: Kisaki, C.Y.; Arcos, S.S.S.; Montoni, F.; da Silva Santos, W.; Calacina, H.M.; Lima, I.F.; Cajado-Carvalho, D.; Ferro, E.S.; Nishiyama-Jr, M.Y.; Iwai, L.K. Bothrops Jararaca Snake Venom Modulates Key Cancer-Related Proteins in Breast Tumor Cell Lines. *Toxins* **2021**, *13*, 519. https://doi.org/10.3390/toxins13080519

Received: 5 July 2021
Accepted: 19 July 2021
Published: 25 July 2021

1. Introduction

Ophidian accidents constitute a serious public health problem in Brazil, with an average of 29,000 cases and 125 deaths reported every year (Brazilian Ministry of Health, 2019) [1]. Approximately 80% of ophidian accidents are caused by snakes of the Viperidae family, more specifically of the *Bothrops* genus [2]. Among them, about 25% lead to death or sequels capable of generating temporary or permanent incapacity for work and customary activities. Venom from the *Bothrops jararaca* (*B. jararaca*) snake is a complex mixture composed of proteins, peptides, amino acids, nucleotides, lipids, and carbohydrates that

present a range of different actions when they are isolated or together [3–7], leading to hemotoxic, cardiotoxic, cytotoxic, or neurotoxic effects [8,9]. Several previous reports have defined the proteomics composition of *Bothrops* venoms [5,10–16]. These studies have shown that *Bothrops* venoms are composed of various classes of toxin, including metalloproteinases, serine proteinases, phospholipases A2, and C-type lectins, the most abundant components participating in the local and systemic envenomation effects.

The venom of *B. jararaca* engenders three main activities: proteolytic, coagulant, and hemolytic. The proteolytic activity causes degradation of extracellular matrix proteins, plasma, and cell surface [17], which represents an important factor for the clinical characterization of a bothropic accident [2,18]. In addition, venom can cause local tissue lesion, myonecrosis, edema, cardiovascular alterations, hypovolemic shock, coagulation alteration and renal alterations, resulting from the combined action of the enzymatic and toxic activity of the venom [19]. About 90 to 95% of the dry weight of the *B. jararaca* venom is composed of a complex mixture of proteins, mainly metalloproteinases, serine proteinases, phospholipases (PLA2), and L-amino acid oxidases. The metalloproteinases comprise most of the venom composition [20,21]. They are proteolytic enzymes associated with fibrinolysis and coagulation, and they are involved in cell migration and tissue repair, besides being related to pathological effects such as cancer [22,23]. In terms of therapeutic interventions, protease inhibitors have been shown to inhibit homeostasis and thrombosis by acting on the coagulation cascade [24]. The third major component of the venom, PLA2, is an enzyme capable of hydrolyzing the ester bonds at the sn2 position of glycerolphospholipids, releasing arachidonic acid, important for the biosynthesis of many mediators involved in inflammation, such as prostaglandins, thromboxanes, and leukotrienes [25]. Finally, the L-amino acid oxidases (LAAOs), which make up about 1 to 9% of the venom composition [26], are flavoenzymes belonging to the class of oxidoreductases, which produce alpha-keto acid, hydrogen peroxide, and ammonia [27,28]. However, when there is a high production of hydrogen peroxide, it has been found that L-amino acid oxidases can induce apoptosis in mammalian endothelial cells [29].

Snake venom constituents have been isolated and studied for their therapeutic potential in the treatment of various diseases. One example is Eptifibatide, marketed as Integrilin, derived from the *Echis carinatus* snake venom and produced by Millennium Pharmaceuticals and Schering-Plow. It is used as an antiplatelet drug [30]. Another example is the angiotensin I converting enzyme inhibitor Captopril produced by Bristol-Myers Squibb whose active component was derived from *B. jararaca* venom. It is used for the treatment against hypertension and renal insufficiency [31,32]. In addition to the potential use of the derivatives of snake venom toxins in the treatment of non-malignant diseases [33], several studies have described anti-tumorigenic characteristics of snake venom, stating that snake venom may be capable of inhibiting cell proliferation and promoting cell death by different means: inducing apoptosis in cancer cells by increasing the influx of Ca^{2+}, inducing the release of cytochrome C, decreasing or increasing the expression of proteins that control the cell cycle, and causing damage to cell membranes [26,34–36]. With the goal of searching novel therapy against cancer, studies have characterized the proteins, peptides or enzymes derived from snake venom to identify components that are capable of interfering with the transport of substances or signal transduction across the membrane or disrupting the cell membrane [35,37].

With the rapid advances of nano-scale liquid chromatography (nLC) and mass spectrometry (MS) technologies in the last two decades, nLC-MS/MS-based proteomics analysis has been widely applied as a powerful tool for biomarker discovery to improve cancer therapy [38,39]. A number of studies have characterized the biochemical and physiological action of venom or isolated venom derivatives on cell lines or tissues [40–43]. In addition, several works have shown proteomic changes of cancer cell lines upon drug treatment that suggest molecular mechanisms of drug action, including diverse effects on proteasome regulation, metabolic processes, and oxidative stress [44,45].

However, to the best of our knowledge, there has been no report that describes the effects of *B. jararaca* snake venom treatment on breast cancer-related cell proteome. In the present study, nLC-MS/MS was used to characterize the effects of sub-toxic doses of *B. jararaca* snake venom on two different breast cancer cell lines MCF7 and MDA-MB-231. MCF7 and MDA-MB-231 are non-metastatic and metastatic tumor cell lines, respectively. They are characterized by a high degree of glycolytic efficiency that promotes the interaction between the tumor cell and the extracellular matrix [46]. Although both cell lines are from breast origin, they are molecularly distinct. MCF7 are estrogen and progesterone receptors positive and HER2 negative, while MDA-MB-231 are triple negative (estrogen receptor, progesterone receptor, and HER2 negatives) and prone to cytotoxic agents because of their impaired DNA repairing capability which is in part due to mutation in the p53 gene [47,48]. Proteomic changes observed herein upon treatment with *B. jararaca* snake venom in these cell lines highlight proteins and cell pathways that could be targeted in cancer therapy.

2. Results

2.1. The Cytotoxicity of B. jararaca Snake Venom in MCF7 and MDA-MB-231 Cells

The *B. jararaca* venom cytotoxicity assay on MCF7 and MDA-MB-231 cell lines was monitored using the WST-1 reagent. This analysis showed that although cell viability was similar between both MCF7 and MDA-MB-231 cell lines, they had different venom resistance profiles where MDA-MB-231 cells showed to be more resistant to the venom when compared to the MCF7 cells. Although both cell lines started to die at doses higher than 2.5 µg/mL, at the 5.0 µg/mL of venom, only about half of the MDA-MB-231 cells have died while most of the MCF7 have died at this venom concentration (Figure 1). Lethal concentration 50 (LC50) was determined as 4.50 µg/mL for MCF7 and 4.76 µg/mL for MDA-MB-231 cell line. Interestingly, the treatment of cells with the low dose at 0.5 µg/mL of venom also killed more MCF7 cells compared to the MDA-MB-231 cells when compared to the venom doses of 0.63 µg/mL and 1.25 µg/mL (Figure 1).

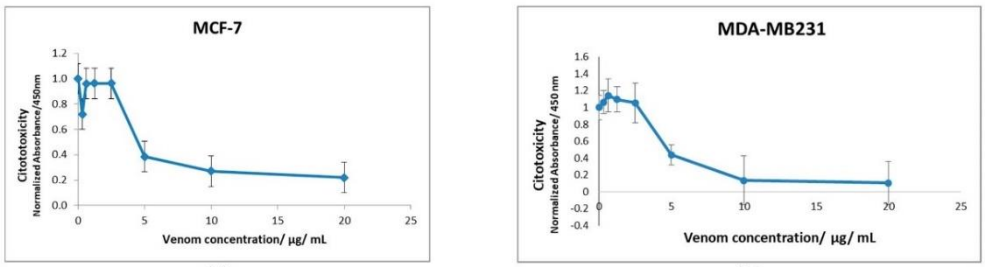

(**a**) (**b**)

Figure 1. Cytotoxicity assay of (**a**) MCF7 and (**b**) MDA-MB-231 cell lines treated with *B. jararaca* snake venom ranging from 0 to 20 µg/mL for 24 h. Experiment was performed using the WST-1 reagent kit.

2.2. Optical Microscopy Analysis of MCF7 and MDA-MB-231 Cells under B. jararaca Venom Treatment

Optical microscopy analysis at 10× magnification of MCF7 and MDA-MB-231 cell lines treated with concentrations higher than 2.5 µg/mL of *B. jararaca* snake venom showed cellular morphological changes such as cell shrinkage and cell birefringence change (Figure S1). At the 20 µg/mL of venom treatment all MCF7 cells detached from the plate, whereas the MDA-MB-231 cell line continued to show morphological death-like changes, but the cells did not detach from the plate (Figure S1).

Based on the cytotoxicity assays and visualization of cell morphology changes through the microscope images, two working concentrations, representing a low dose of 0.63 µg/mL and a high sub-toxic dose of 2.5 µg/mL of venom, were selected for further proteomics analysis.

2.3. Mass Spectrometry-Based Proteomics of MCF7 and MDA-MB-231 Cells Treated with *B. jararaca* Venom

Protein identification was performed analyzing the raw data using the MaxQuant software against the *Homo sapiens* database downloaded from Uniprot. Analysis of the MCF7 cell line treated with different venom concentrations allowed the identification of 789 proteins from which 704 proteins were identified in the control group (non-venom treatment), 725 proteins were identified in cells treated with 0.63 µg/mL of venom, and 713 proteins were identified in the cells treated with 2.5 µg/mL of venom. Comparative analysis of the identified proteins showed that among all of the 789 proteins identified, 637 proteins were in common to all conditions, 657 proteins were in common between the control and the 0.63 µg/mL venom treatment, 656 proteins were in common between control and the 2.5 µg/mL venom treatment, and 677 proteins were in common between the 0.63 µg/mL and 2.5 µg/mL venom treatments (Figure 2a, Table S1a). In addition, we also identified exclusive proteins in each condition: 28 proteins in the control group, 28 proteins in 0.63 µg/mL venom treatment, and 17 proteins exclusive in the 2.5 µg/mL venom treatment (Figure 2a, Table S1a).

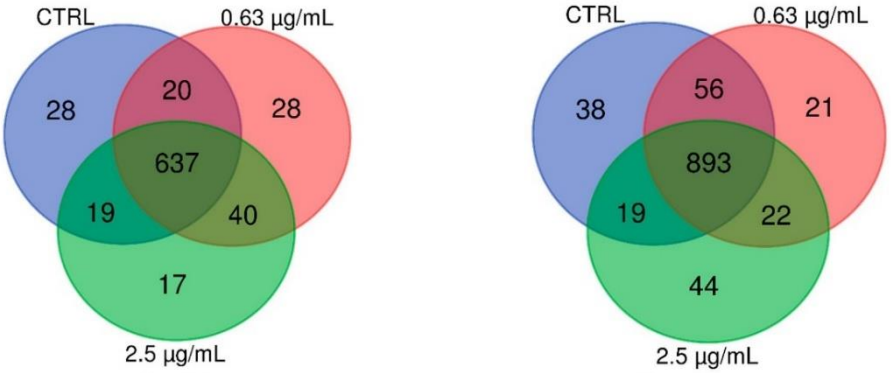

(**a**) MCF7 (**b**) MDA-MB-231

Figure 2. Diagrammatic representation of the comparative analysis of identified proteins under the three conditions: no venom control group, low venom dose at 0.63 µg/mL and high venom sub-toxic dose of 2.5 µg/mL of *B. jararaca* venom. (**a**) MCF7 and (**b**) MDA-MB-231.

In the MDA-MB-231 cell line, mass spectrometry-based proteomics analysis allowed us to identify a total of 1093 proteins from which 1006 proteins in the control group, 992 proteins in the cells treated with 0.63 µg/mL of venom, and 978 proteins in the cells treated with 2.5 µg/mL of venom. Comparative analysis of the identified proteins showed 893 proteins identified in common to all conditions, 949 proteins in common between the control group and 0.63 µg/mL venom treatment, 912 proteins were in common between control group and 2.5 µg/mL venom treatment, and 915 proteins were in common between the 0.63 µg/mL and 2.5 µg/mL venom treatments (Figure 2a, Table S1a). We also observed 38 exclusive proteins in the control group, 21 proteins in 0.63 µg/mL venom treatment, and 44 proteins exclusive in the 2.5 µg/mL venom treatment (Figure 2b, Table S1b).

2.4. Semi-Quantitative Proteomics Analysis: MCF7 and MDA-MB-231 Cell Line Protein Abundance Variation

In general, we observed a higher number of proteins whose abundance had changed more than 1.5× or less than 0.67× in MCF7 cell lines when compared to the MDA-MB-231 cell lines. The semi-quantitative analysis of the MCF7 cell line (Table S2a,) treated with 2.5 µg/mL venom allowed us to identify 137 proteins, whose abundance changed over

1.5× (fold change FC ≥ 1.5, marked in light red) when compared to the control group, from which 55 proteins presented FC ≥ 2.0 (marked in red). We highlight 12 highly abundant proteins with FC ≥ 3.0, marked in dark red: Sorting nexin-3 (SNX3), Purine nucleoside phosphorylase (HEL-S-156an), Peroxisome proliferator activated receptor interacting complex protein (PRIC295), Small nuclear ribonucleoprotein component (SNRP116), Eukaryotic translation initiation factor 4B (EIF4B), Methylcrotonoyl-CoA carboxylase beta chain (MCCC2), 26S proteasome non-ATPase regulatory subunit 5 (PSMD5), Heterogeneous nuclear ribonucleoprotein R (HNRNPR), Full-length cDNA clone CS0DJ015YJ12 of T cells (PSME2), Isoleucyl-tRNA synthetase (IARS), Large proline-rich protein BAG6 (BAG6), and Glutathione S-transferase (GSTM3). In addition, we identified 23 proteins with FC ≤ 0.67 (marked in light green) from which five proteins presented FC ≤ 0.5 (marked in dark green): Histone H4 (HIST1H4J), ATP synthase subunit d, mitochondrial (ATP5PD), Voltage-dependent anion-selective channel protein 2 (VDAC2), 4a-hydroxytetrahydrobiopterin dehydratase (PCBD), and Histone H3 (H3F3B). At the low 0.63 µg/mL venom treatment, we identified 25 proteins with FC ≥ 1.5 (marked in light red) from which only two proteins presented FC ≥ 2.0 (marked in red): Anterior gradient 2 homolog (AGR2) and Leucine-rich PPR-motif containing protein (LRPPRC); and 19 proteins with FC ≤ 0.67 (marked in light green) from which two proteins with FC ≤ 0.5 (marked in dark green): PCBD and 40S ribosomal protein S29 (RPS29). The description of the highlighted proteins is shown in Table 1.

Semi-quantitative proteomic analysis of the MDA-MB-231 cell line (Table S2b) treated with 2.5 µg/mL allowed the identification of 34 proteins whose abundance changed (FC) ≥1.5 over the control (marked in light red), nine proteins with FC ≥ 2 (marked in red) from which we highlight three proteins with FC ≥ 3 (marked in dark red): Histone H3.2 (H3C15/HIST2H3), 14 kDa phosphohistidine phosphatase (HEL-S-132P), and Mitochondrial carrier homolog 2 (MTCH2). Moreover, 41 proteins presented FC ≤ 0.67 (light green) from which we highlight four proteins with FC ≤ 0.5 (marked in dark green): DnaJ homolog subfamily A member 1 (DNAJA1), Insulin-like growth factor 2 mRNA-binding protein 1 (IGF2BP1), Cysteine-rich angiogenic inducer 61 (CYR61), and Thrombospondin-1 (THBS1). At the lower 0.63 µg/mL venom treatment, 16 proteins presented FC ≥ 1.5 (marked in light red) from which we highlight H3C15/HIST2H3 with FC = 3.8 and MTCH2 with FC = 2.3 (marked in red); and 28 proteins with FC ≤ 0.67 (marked in light green) from which 12 proteins with FC ≤ 0.5 (marked in dark green): 60S ribosomal protein L37 (RPL37), D-3-phosphoglycerate dehydrogenase (HEL-S-113), ATPase inhibitor, mitochondrial (ATP5IF1), Non-histone chromosomal protein HMG-14 (HMGN1), RCC2 protein (RCC2), Serine/threonine-protein phosphatase PP1-gamma catalytic subunit (PPP1CC), D-dopachrome decarboxylase (DDT), Ran GTPase-activating protein 1 (RANGAP1), dCTP pyrophosphatase 1 (DCTPP1), IGF2BP1, THBS1, and CYR61 (Table 1).

Table 1. Description of the highlighted proteins and their association with cancer.

Protein	Protein Name	Protein Description Related to Cancer	Cancer Type Association	References
AMOT	Angiomotin	Plays a central role in tight junction maintenance. Appears to regulate endothelial cell migration and tube formation. May also play a role in the assembly of endothelial cell-cell junctions. Plays a critical role in angiogenesis, proliferation and migration and invasion of cancer cells	BL, BR, CE, CL, CR, EN, HN, KD, LE, LI, LA, LS, OV, PR, ST	[49–51]
ATP5PD	ATP synthase peripheral stalk subunit D	Mitochondrial ATP synthase catalyzes ATP synthesis, utilizing an electrochemical gradient of protons across the inner membrane during oxidative phosphorylation. Linked to failure of therapy, disease progression, and poor survival in patients with cancer. High expression of ATP5PD has been observed in several types of cancer	BR, CE, CL, EN, GL, HN, LI, LU, LY, ME, OV, PA, PR, RE, SK, TE, TY	[52]
ATR	Serine/threonine-protein kinase	Plays important roles for cell survival and is considered a major mediator of DNA response in human cells, preventing cells with damaged or incompletely replicated DNA from entering mitosis when cells are damaged by radiotherapy or chemotherapy during cancer treatment	BL, BR, CE, CR, EN, GB, HN, KD, LU, LA, LS, OV, ST, TY	[53,54]
CYR61	Cysteine-rich heparin-binding protein 61	Plays an important role in cell proliferation, survival, chemotaxis, angiogenesis, adhesion, and migration of different types of cells. Participate in key different cellular events during vascular development, angiogenesis, wound healing and the development and progression of various types of cancers	BN, BR, CR, EN, GA, GB, GL, LI, LU, OV, PA, PR, ST, TE, UR	[55,56]
GSTM3	The glutathione S-transferase Mu 3	Part of the GSTs enzymes that have functions such as immunological system evasion and inhibition of apoptosis. Involved in prostaglandin and leukotriene synthesis and metabolization of both endogenous compounds and xenobiotics such as chemotherapeutic drugs, insecticides, carcinogens, and oxidative stress byproducts	BL, BR, CR, EN, LE, LA, LS, OV, PA, ST, TY, UR	[57,58]
H3F3B/H3C15	H3 histone family member 3B	Core component of nucleosome. Histones play a central role in transcription regulation, DNA repair, DNA replication and chromosomal stability and are related to different types of cancer. H3F3B mutation has been described to lead to some human cancers	BL, BN, BR, CE, CH, CR, EN, GB, HN, LU, OV, UR	[59–61]
HEL-S-156an PNP	Purine nucleoside phosphorylase	Catalyze the phosphorolysis of purine nucleosides. Mutations which result in nucleoside phosphorylase deficiency result in defective T-cell (cell-mediated) immunity but can also affect B-cell immunity and antibody responses. High expression of PNP has been observed in several types of cancer	BR, CL, CR, GA, GL, KD, LI, LU, LA, LY, ME, OV, PR, TY	[62–64]

Table 1. *Cont.*

Protein	Protein Name	Protein Description Related to Cancer	Cancer Type Association	References
HIST1H4J	Histone H4	Core component of nucleosome. Histones play a central role in transcription regulation, DNA repair, DNA replication and chromosomal stability. Post-translational alterations of histones have been shown to affect the activation and repression of oncogenes and tumor suppressor genes	BR, CE, CR, GL, HN, LI, LU, ME, OV, PA, PR, SK, ST, TE, TY	[65–68]
IGF2BP1	Insulin like growth factor 2 MRNA binding protein 1	RNA-binding factor that recruits target transcripts to cytoplasmic protein–RNA complexes (mRNPs). IGF2BP1 has an oncogenic role, characterized by changes in actin dynamics, migration, invasion, proliferation, and self-renewal. Play a role in resistance to drugs	BR, CE, CR, EN, GB, HN, LI, LU, LA, LS, ME, OV, PR, ST, TE, UR	[69–71]
KRT1	Keratin	May regulate the activity of kinases such as PKC and SRC via binding to integrin beta-1 (ITB1) and to the receptor of activated protein C kinase 1 (RACK1). High expression of KRT1 protein has been observed in several types of cancer and is correlated with advanced melanoma tumor stage and infiltration of immune cells	BR, CE, CR, EN, GB, HN, KD, LI, LS, LA, OV, SK, ST, UR	[72,73]
LAP3	Leucine aminopeptidase 3	Cytosolic metallopeptidase that catalyzes the removal of unsubstituted N-terminal hydrophobic amino acids from various peptides. Involved in the metabolism of glutathione and in the degradation of glutathione S-conjugates, which may play a role in the control of the cell redox status. Related to protein renewal. Have a potential for determining the prognosis for breast cancer	BL, BR, CR, EN, HN, KD, LI, LA, LS, PA, ST, TY	[74–77]
MCCC2	Methylcrotonoyl-CoA carboxylase beta chain, mitochondrial	Enzyme that catalyzes the conversion of 3-methylcrotonyl-CoA to 3-methylglutaconyl-CoA, a critical step for leucine and isovaleric acid catabolism. Overexpression of MCCC2 is associated with tumor stage, node, metastasis, lymph node metastasis and predicts unfavorable prognosis. Additionally, involved in the development and formation of some tumors, such as breast cancer	BL, BR, CR, EN, HN, KD, LI, LA, OV, PA, PR, ST, TY	[78]
MTCH2	Mitochondrial carrier homolog 2	Member of the SLC25 family of nuclear-encoded transporters that are localized in the inner mitochondrial membrane. Members of this superfamily are involved in many metabolic pathways and cell functions. Associated with metastasis and tumor cell survival. Indirect involvement in the expression of miR-135b mRNA, which is one of the proteins responsible for tumorigenicity	BL, BR, CR, EN, HN, KD, LI, LA, ME, OV, PA, PR, ST, TY	[79–81]

Table 1. *Cont.*

Protein	Protein Name	Protein Description Related to Cancer	Cancer Type Association	References
PCBD	4a-hydroxytetrahydrobiopterin dehydratase	Involved in tetrahydrobiopterin biosynthesis. Regulates various aspects of cell morphogenesis and differentiation as a cofactor for the homeobox transcription factor. Several types of cancer show expression or alteration in the homeobox genes. PCBD degradation increases cell survival and proliferation, and inhibits tumor cell differentiation	BR, CL, CR, EN, LE, LI, LU, OV, PA, PR, RE, SK	[82–84]
PRIC295	Peroxisome proliferator-activated receptor-a (PPARα)-interacting cofactor	Functions as a transcriptional coactivator for nuclear receptors. Enhances the activation of PPARα and PPARγ and plays a key role in lipid metabolism and energy combustion regulating the genes for fatty acid oxidation. Observed to be significantly enhanced in chemotherapy recurrence when compared to chemotherapy treatment in ovarian cancer patients	BL, BR, CR, EN, GB, HN, KD, LE, LA, LS, ME, OV, PA, PR, ST, TY	[85–87]
PSMD5	The 26S proteasome non-ATPase regulatory subunit 5	Acts as a chaperone during the assembly of the 26S proteasome. Expression reduced in several types of cancer including intestinal and colorectal tumors	BL, BR, CR, EN, HN, PR, ST, TY	[88]
PSME2	The proteasome activator complex subunit 2	Implicated in immunoproteasome assembly and required for efficient antigen processing. Member of the PSME family that regulates proteasome function. Elevated expression of PSME have also been associated with several types of cancer	BR, CR, EN, HN, LC, LA, LS, ME, PR, ST	[89–91]
RPS29	Ribosomal protein S29	Belongs to the universal ribosomal protein uS14 family. Related to have tumor suppressor activity for ras-transformed NIH3T3 cells. High expression RPS29 mRNA levels observed in adenomas	BR, CE, CR, EN, HN, KD, LA, OV, ST	[92,93]
SNRP116/EFTUD2	Small nuclear ribonucleoprotein component	Required for pre-mRNA splicing as a component of the spliceosome, including pre-catalytic, catalytic, and post-catalytic spliceosomal complexes. Knockout of EFTUD2 suppressed the development and tumor progression due to impaired activation of NF-kB signaling in macrophages	BL, BR, CR, EN, GB, HN, KD, LA, LS, ME, OV, PR, ST, TE, TY, UR	[94,95]
SNX3	The sorting nexin 3	Phosphoinositide-binding protein required for multivesicular body formation. Plays a role in protein transport between cellular compartments. The knockdown of SNX3 is associated with degradation of the EGF receptor which is related to resistance to chemotherapy and radiotherapy	BR, CR, EN, GL, HN, KD, LU, OV, RE, TY	[96,97]
THBS1	Thrombospondin 1	Adhesive glycoprotein that mediates cell-to-cell and cell-to-matrix interactions. Influences angiogenesis modulation by regulating adhesion, invasion, metastasis, migration, proliferation, and apoptosis and has been implicated in numerous types of cancers	BR, CR, EN, ES, HN, KD, LA, LS, LY, ME, OV, PA, PR, SK, ST, TE, TY	[98–100]

Table 1. *Cont.*

Protein	Protein Name	Protein Description Related to Cancer	Cancer Type Association	References
TUFM	Tu translation elongation factor, mitochondrial	Promotes the GTP-dependent binding of aminoacyl-tRNA to the A-site of ribosomes during protein biosynthesis. Plays important roles in the regulation of autophagy and innate immunity. TUFM is highly expressed in several types of cancers	BR, CR, EN, ES, GA, GS, HN, LI, LU, LA, ME, PA, PR, RE, SK, ST, TE	[101–103]
UQCRC1	The ubiquinol-cytochrome C reductase core protein 1	Component of the ubiquinol-cytochrome c reductase complex, which is part of the mitochondrial respiratory chain. High expression was observed in several types of cancer. Negative expression correlated significantly with clinical and pathological parameters including tumor stage, vascular invasion, and lymph node metastasis, suggesting that the reduction of this protein is associated with tumor progression	BR, CR, EN, GB, GL, HN, LI, LA, LY, ME, OV, PA, PR, RE, ST, TE, TY, UR	[104–106]
VDAC1 and VDAC2	The voltage-dependent anion selective channel 1 and 2	Forms a channel through the mitochondrial outer membrane and plasma membrane allowing diffusion of small hydrophilic molecules. In the plasma membrane it is involved in cell volume regulation and apoptosis. The abnormal expression or mal functioning of VDACs has been reported in multiple tumors and it has been considered as a biomarker capable of predicting treatment failure and breast cancer recurrence	BL, BR, CR, EN, GB, HN, LI, LA, LS, ME, OV, PA, PR, RE, ST, TY, UR	[107–110]

Note: This description may include information from UniProtKB, PhosphoSitePlus (v.6.5.9.3), GeneCards (Human Gene Database), and Human Protein Atlas [111–113]. Bladder: BL, bone (osteosarcoma): BN, breast: BR, cervical: CE, chondroblastoma: CH colon: CL, colorectal: CR, endometrial: EN, esophageal: ES, gastric: GA, gastrointestinal stromal tumor: GS glioblastoma: GB, glioma: GL, head and neck: HN, kidney: KD, laryngeal carcinoma: LC, leukemia: LE, liver: LI, lung: LU, lung adenocarcinoma: LA, lung squamous: LS, lymphoma: LY, melanoma: ME, ovarian: OV, pancreatic: PA, prostate: PR, renal: RE, skin: SK, stomach: ST, testis: TE, thyroid: TY, urothelial: UR.

2.5. Hierarchical Clustering Analysis

Hierarchical clustering analysis of differentially expressed proteins with FC $\geq$ 1.5 identified in both MCF7 and MDA-MB-231 cell lines characterized those proteins in seven major clusters (Figure 3, Table S3). Clusters 1–4 had proteins with fold change (FC) increased at 2.5 µg/mL of venom treatment in MCF7 cells and presented no change in MDA-MB-231 cell lines. Proteins in these clusters include HEL-S-156 and PRIC295 in cluster 1 and PSMD5 and PSME2 in cluster 2. Cluster 5 identified proteins that decreased in FC at 2.5 µg/mL of venom treatment in both cell lines including HIST1H4J, VDAC1, and VDAC2. Cluster 6 identified proteins that increased FC at 2.5 µg/mL of venom treatment in MDA-MB-231 cell line including H3F3B, LAP3, and KRT1, and cluster 7 identified proteins that did not change when cells were treated with low and high venom treatment, but they presented higher FC change in MDA-MB-231 when compared to MCF7 cell line such as RPS29 (Table 1).

2.6. Principal Component Analysis

PCA was applied to the differentially expressed proteins identified from both MCF7 and MDA-MB-231 cell lines based on the log2 FC of cells treated with low and high *B. jararaca* venom compared to the PBS treatment control group (Figure 4). The projection into the component space shows a distinct coordinated activity of proteins between the cell lines conditions. Orthogonal vectors show highly positive correlation between both venom concentrations in MDA-MB-231 cell line which may represent similar cell line responses to the different venom concentrations, but they present a highly negative correlation to both venom concentrations in MCF7 and respective set of expressed proteins. In the MCF7 cell line, however, we observe a negative correlation between the 0.63 µg/mL and 2.5 µg/mL venom treatment, indicating a differential response upon low and high dose venom treatment. PCA also shows differential correlation between both cell lines where the first two components showed 40% variation in the PC1 and 26.7% variation in the PC2 between the MCF7 and MDA-MB-231 cell lines. In addition, we observed clusters of proteins positively correlating with both low and high venom treatment in MDA-MB-231 cell line such as LAP3, H3F3B, and KRT1. On the other hand, we also observed proteins such as H2AC20 and TUFM correlating with low venom treatment, and proteins such as HEL-S-156an correlating with high venom treatment on MCF7 cell line (Table 1).

2.7. Gene Ontology Functional Analysis

The most enriched protein families and functional categories were analyzed based on highly abundant proteins with FC $\geq$ 1.5 for each cell line and treatment at low and high *B. jararaca venom* conditions (Figures S2–S5). The functional ontology classification analysis of these sets of proteins showed that both MCF7 and MDA-MB-231 venom-treated cell lines showed similar enriched categories. In addition, the most prominent enrichment was identified for treated cells with the sub-toxic dose of 2.5 µg/mL of venom. The molecular function enrichment analysis in both the MCF7 and MDA-MB-231 cell lineages showed an enrichment of proteins related to binding, structural molecule activity, and catalytic activity. In addition, the MCF7 cells had enriched, albeit in a lower amount, proteins related to function and transcriptional regulatory activity and carrier activity (Figure S2). The functional classification analysis related to biological processes showed enriched proteins related to the metabolic process and the cellular component organization or biogenesis. Moreover, the analysis of proteins identified in the MCF7 cell line presented proteins related to the cellular process, localization, biological regulation, stimulus response, developmental process, multicellular organismal process, and the immune system process (Figure S3). The analysis of protein distribution by cellular components showed an enrichment related to the "cell", protein complex, and organelle (Figure S4), and the enrichment analysis of protein family classification showed an enrichment of cytoskeleton proteins, ligase, nucleic acid binding, signaling molecule, modulating enzyme, calcium binding protein, and hydrase (Figure S5).

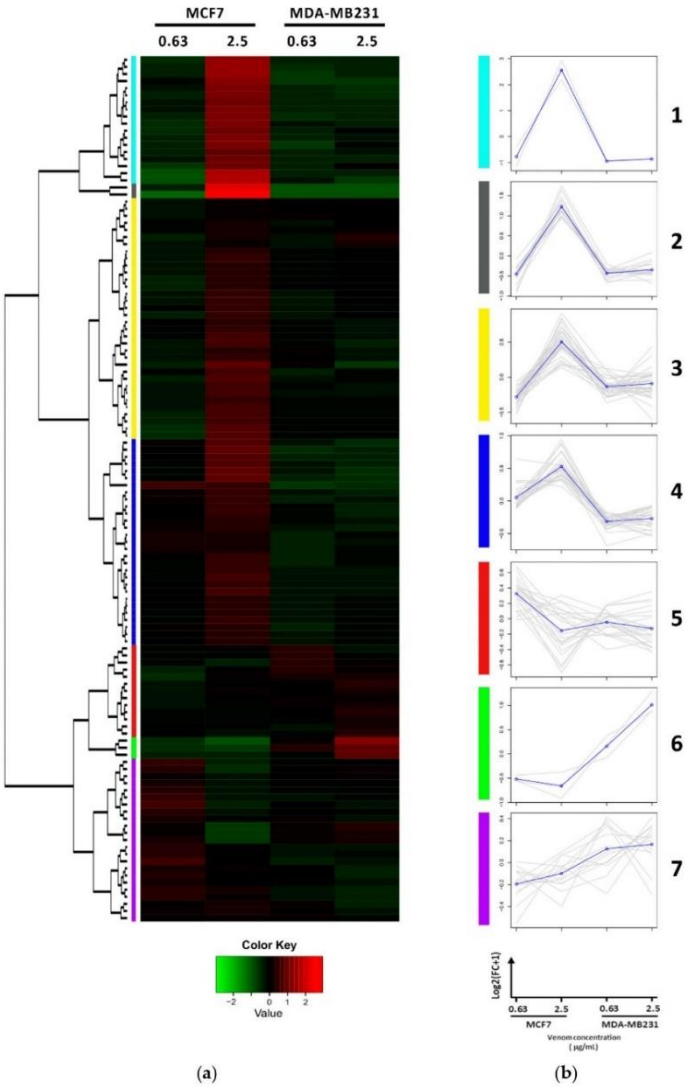

Figure 3. Hierarchical clustering of differentially expressed proteins detected in both MCF7 and MDA-MB-231 cells treated with low (0.63 µg/mL) and high (2.5 µg/mL) *B. jararaca* venom for 24 h. (**a**) Heatmap representation of the hierarchical clustering of proteins detected in both cell lines with quantification in at least two replicates showing the changes in protein abundance. The protein fold change is log2 transformed and normalized with mean-centering scale. (**b**) Protein Clusters extracted from the hierarchical clustering. X axis: Cell types treated with different *B. jararaca* venom concentrations (MCF7 0.63 µg/mL; MCF7 2.5 µg/mL, MDA-MB-231 0.63 µg/mL, MDA-MB-231 2.5 µg/mL); Y axis: mean-centered log2 Fold Change. Grey lines: individual proteins; Black line: average expression values per cluster.

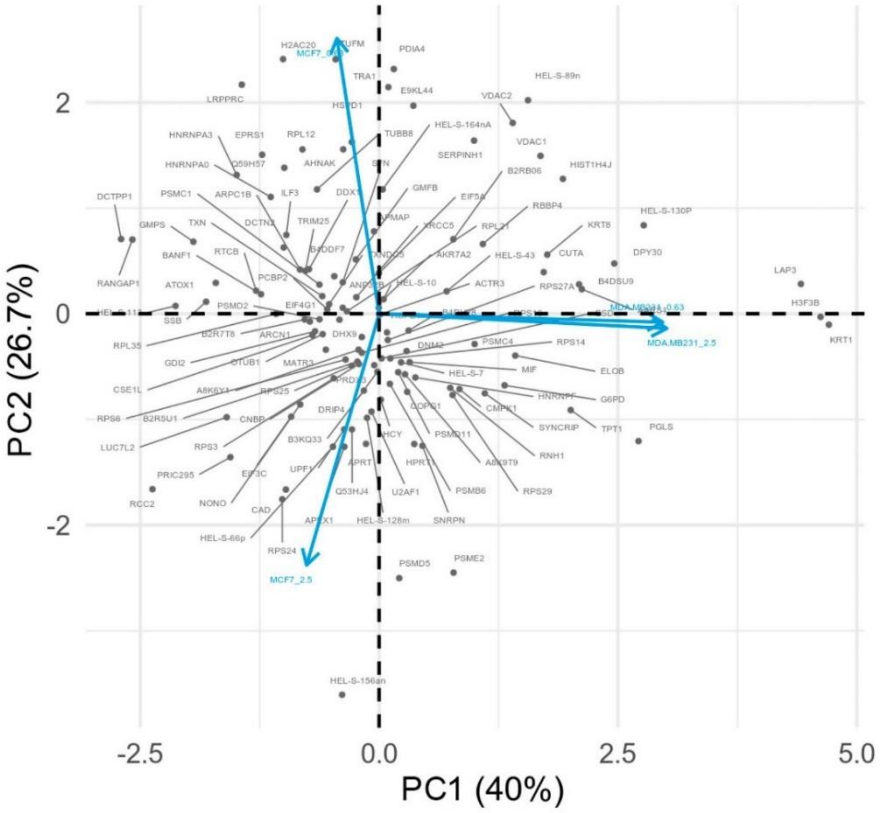

Figure 4. Comparison of protein log2 Fold Change profiles across treated cell lines. Principal component analysis in a 2D graph represented by the first two components PC1 and PC2 explains 67.7% of the protein variability among the different conditions. Vectors that are closer are highly correlated. Vectors representing the conditions which are orthogonal or well-spaced in terms of the observed proteome indicate that those proteins can be closely related to each specific cell line condition.

2.8. Protein–Protein Interaction Analysis

STRING protein–protein interaction network analysis tool was used to evaluate protein–protein interactions identified among proteins with FC $\geq$ 1.5 from each cell line treated with *B. jararaca* venom. According to Doncheva and colleagues [114], STRING indicates interactions according to co-expression analyzes and evolutionary signals in all genomes based on data described in the literature between genes or proteins using functional classification systems such as Gene Ontology, KEGG (Kyoto Encyclopedia of Genes and Genomes), and Reactome.

Analysis of protein–protein interactions (PPIs) of proteins whose abundance increased more than 1.5× in the MCF7 cell line treated with 2.5 µg/mL of venom showed a high interconnection of proteins related to metabolic process (in red) and metabolism pathways (in blue) (Figure 5a). Interestingly, among the proteins identified in the MCF7, we observed clusters of highly connected proteins related to proteasome pathway (in green) and mRNA splicing (in yellow). We highlight the proteins PSMD2 and PSMD11 (26S proteasome non-ATPase regulatory subunit 2 and 11, respectively), PSME1 and PSME2 (Proteasome activator complex subunit 1 and 2, respectively), PSMC1, PSMC4, and PSMC5

(26S proteasome regulatory subunit 4, 6B, and 8, respectively), TXNL (Thioredoxin-like protein 1), and USP14 (Ubiquitin carboxyl-terminal hydrolase 14), which are all members of the proteasome pathway (in green) and proteasome complex, and, together with MST4 (Serine/threonine-protein kinase 26) and PSMD5 (26S proteasome non-ATPase regulatory subunit 5) they are all related to apoptosis (Figure 5a). PPI analysis of proteins identified in the MDA-MB-231 in the same conditions showed less interaction among the proteins identified with FC $\geq$ 1.5 (Figure 5b).

PPI analysis of the MCF7 cell lines with FC $\geq$ 1.5 treated with 0.63 µg/mL and FC $\leq$ 0.67 when cells were treated with 0.63 µg/mL and 2.5 µg/mL of venom are shown in Figure S6. Additionally, PPI analysis of proteins identified in the MDA-MB-231 at 0.63 µg/mL and 2.5 µg/mL venom treatment presenting FC $\leq$ 0.67 and FC $\geq$ 2.5 are shown in Figure S7.

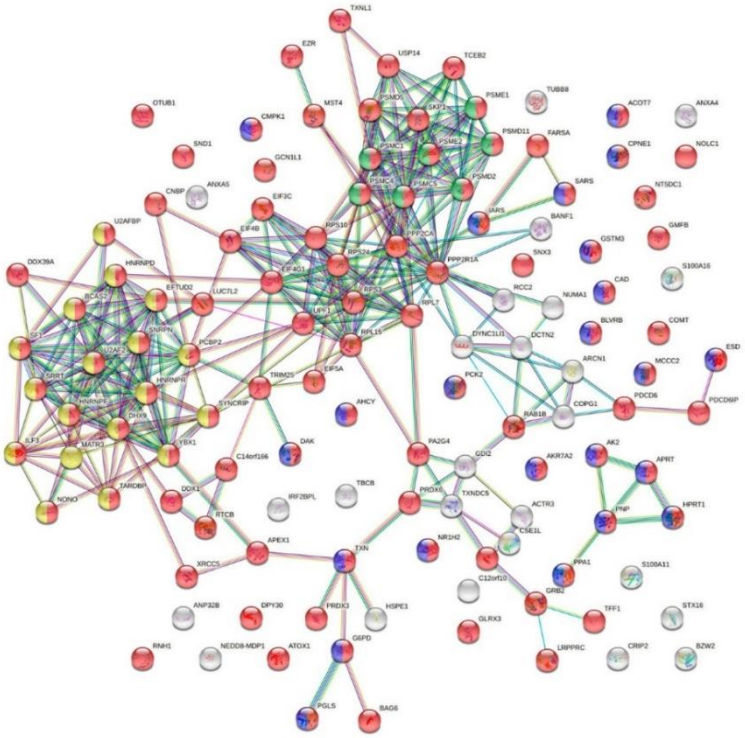

Red: Biological Process of Metabolism. Blue: Metabolism Pathways (Reactome). Yellow: mRNA Splicing local network cluster (STRING). Green: Proteasome pathway (KEGG). Number of nodes: 125, Number of edges: 327, Average node degree: 5.23, Avg. local clustering coefficient: 0.47, Expected number of edges: 120, PPI enrichment *p*-value: $< 1.0 \times 10^{-16}$.

(**a**)

Figure 5. *Cont.*

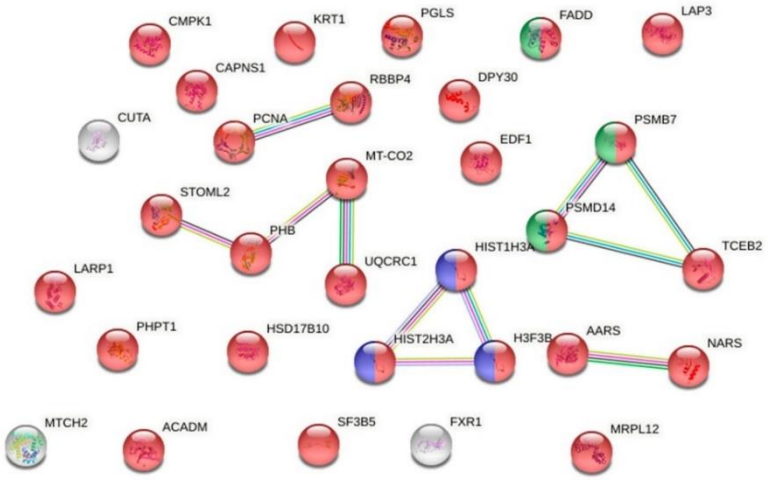

Red: Biological Process of Metabolism. Blue: Histone H3 complex (SMART, Simple Modular Architecture Research Tool). Green: apoptosis (Reactome pathways). Number of nodes: 31, Number of edges: 11, Average node degree: 0.71, Avg. local clustering coefficient: 0.387, Expected number of edges: 5, PPI enrichment *p*-value: 0.0192

(**b**)

Figure 5. Protein–protein interaction of proteins identified in (**a**) MCF7 and (**b**) MDA-MB-231 cell lines presenting FC $\geq$ 1.5 at 2.5 g/mL *B. jararaca* venom treatment.

2.9. Exclusive Proteins

We further analyzed proteins exclusively identified in one or two of the three conditions in both MCF7 cell line (Table S4a, Figure S8) and MDA-MB-231 cell line (Table S4b, Figure S8). Proteins identified only on PBS treated cells (control group), suggesting that the expression of the proteins was inhibited with the addition of venom, allowed us to identify 28 proteins in the MCF7 cell line from which we highlight proteins: eukaryotic peptide chain release factor subunit 1 (ETF1), serine/arginine repetitive matrix protein 2 (SRRM2), PHD finger-like domain containing protein 5A (PHF5A), and lamina-associated polypeptide 2 (TMPO). The analysis of the MDA-MB-231 cell line allowed us to identify 41 proteins exclusively expressed at the control group from which we highlight Plasminogen activator inhibitor 1 (SERPINE1), MHC class I antigen (HLA-C), Transcription factor BTF3 (BTF3L4), Cytochrome c oxidase subunit 6C (COX6C), Myb-binding protein 1A (MYBBP1A), and MYCBP protein (MYCBP) (Figure S8a, Table S4).

Of the proteins identified exclusively when cells were treated with 0.63 µg/mL of venom there were 28 proteins from MCF7 cell line, from which we highlight Cytochrome b-c1 complex subunit 1, mitochondrial (UQCRC1), Latexin (LXN), Vesicle-associated membrane protein-associated protein B/C (VAPB), Cysteine and glycine-rich protein 1 (CSRP1), and DDB1- and CUL4-associated factor 7 (DCAF7). From MDA-MB-231 cell line, 20 proteins were identified from which we highlight Eukaryotic translation initiation factor 2 subunit 2 (EIF2S2), low molecular weight phosphotyrosine protein phosphatase (ACP1), Transcription factor A, mitochondrial (TFAM), and Rae1 protein homolog (RAE1) (Table 1 and Table S4, Figure S8b).

Proteins identified exclusively at the high dose treatment of 2.5 µg/mL of venom included 17 proteins detected in the MCF7 cell line, from which we highlight 26S proteasome non-ATPase regulatory subunit 6 (PSMD6) and 60S ribosomal protein L36 (RPL36).

Similarly, we identified 44 proteins in MDA-MB-231 cell line from which we highlight protein Ubiquitin carboxyl-terminal hydrolase (HEL-117) (Figure S8c, Table S4).

We also identified proteins that were expressed exclusively when cells were treated with low and high doses of *B. jararaca* venom. From the MCF7 cell line, we identified 40 proteins from which we highlight: Serine/threonine-protein kinase ATR (ATR) and Jupiter microtubule-associated homolog 1 (JPT1). From the MDA-MB-231 cell line, we identified 22 proteins from which we highlight Angiomotin (AMOT) and Small nuclear ribonucleoprotein G (SNRPG) (Table 1, Tables S3 and S4, Figure S8d).

Among the proteins that were identified in the control group and at the 2.5 μg/mL venom treatment, we highlight: Small nuclear ribonucleoprotein Sm D1 (SNRPD1) in MCF7, and Epididymis secretory protein Li 71 (Hel-S-71) and Isoform Far upstream element-binding protein 3 (FUBP3) in MDA-MB-231 cell line (Figure S8e, Table S4). Of proteins that were identified in the control group and low 0.63 μg/mL dose of venom, we highlight Serine/arginine-rich splicing factor 10 (SRSF10) in MCF7 cell line, and Histone H2B type 2-E (HIST2H2BE), 60S ribosomal protein L34 and L37a (RPL34, RPL37A) in MDA-MB-231 cell line (Figure S8f, Tables S3 and S4).

3. Discussion

The present study successfully identified cancer-related proteins that undergo significant changes upon *B. jararaca* venom treatment of MCF7 and MDA-MB-231 cells, including SNX3, HEL-S-156an, UQCRC1, RPL36, and ATR identified in MCF7 cell line and H3C15/HIST2H3, HEL-S-132P, MTCH2, TFAM, KCTD12, RPL34, and RPL37A identified in MDA-MB-231 cell line, and histone H3F3B and LAP3 in both cell lines.

With the discovery of rattlesnake venom's antitumor activity in 1931 by Essex and Priestley [115] and later the angiotensin-converting enzyme inhibitor drug Captopril in 1981, developed originally from *B. jararaca* snake venom [116–118], several groups have been focusing on to the therapeutic potentials of bioactive compounds in snake venoms by isolating and characterizing components of the venom and analyzing their pharmacological potential that may lead to the development of more efficacious drugs [119,120].

Snake venoms have a complex mixture of proteins that can account for 95% of the total dried weight. Metalloproteases, serine proteases, LAAOs, and PLA2s are some of the most abundant proteins present in bothropic venoms, and the toxic action of these proteins are responsible for myotoxic effects, disruption in the coagulation cascade through thrombin-like proteins (serine proteases), imbalance in the blood homeostasis by the action of some metalloproteinases, apoptosis induction, and changes in the protein expression in oxidative stress and energy metabolism by the increase of Ca^{2+} influx. Several studies have revealed that these enzymes are critical regulators of cancer pathologies in several types of cancers including breast cancer [121–127]. Moreover, it has been previously shown that *B. jararaca* venom may have an important antitumor effect on Ehrilich ascites tumor cells in vivo and in vitro [36].

Aiming at the drug development, several groups have used proteomics approach to observe up- or down-regulated effects of proteins resulting from disease activity or side effects of the treatments [44,45,128–131]. Moreover, the quest for the identification of biological markers or biomarkers using venom that may help in the early detection of pathologies such as cancer, and the quest for products able to evaluate the metastatic potential and propose new forms of treatment to tumors, remains an important goal of research groups and pharmaceutical companies.

Proteomics studies using tumor cell lines has been performed to systematically characterize protein complexes that may be important in disease or drug development, comparing the protein levels of cells in normal versus pathological situations [132]. Studies have shown that venoms from several snakes such as *Calloselasma rhodostoma*, *Macrovipera lebetina* and *Bothrops mattogrossensis* significantly inhibit cell viability, either with crude or fractionated venoms and in different tumor cell lines such as LS174T (colorectal adenocarci-

noma), HCT116 (colorectal carcinoma), HT29 (colorectal adenocarcinoma), HEL92.1.7 (erythroleukemia), and SK-BR-3 (breast adenocarcinoma) cell lines [133,134].

To evaluate the cytotoxicity of *B. jararaca* venom, we tested two different invasive breast cancer cell lines with different phenotypic and genotypic differences, MCF7 and MDA-MB-231 cell lines. They were treated with different venom concentrations ranging from 0.32 μg/mL to 20 μg/mL. When treated with over 10 μg/mL of venom both MCF7 and MDA-MB-231 cell lines showed rounded and irregular morphologies and the MCF7 cell line detached from the plate. These results are similar to the results observed by Bernardes-Oliveira et al. (2016) when testing 50 μg/mL of venom from *B. jararaca* and *Bothrops erythromelas* for 48 h on SiHa HPV-16 and HeLa cells, both derived from cervical tumors. They observed that the cells became more rounded, with gradual size reduction and detachment from the cell monolayer [135]. In addition to the morphological analyses, we evaluated cell viability through mitochondrial cell activity using WST-1 assay for cell proliferation and viability. We observed that cell death of both MCF7 and MDA-MB-231 cell lines started with 2.5 μg/mL of *B. jararaca* venom treatment. Based on both morphological and cell viability analyses, we selected the concentrations of 0.63 μg/mL (low sub-toxic dose) and 2.5 μg/mL (high sub-toxic dose) for further proteomic analyses.

Semi-quantitative proteomics analysis of the MDA-MB-231 cell line treated with the low 0.63 μg/mL and the sub-lethal dose of 2.5 μg/mL of *B. jararaca* venom presented less proteins with FC $\geq$ 1.5 when compared to the MCF7 cell line. We identified 137 proteins with FC $\geq$ 1.5 at 2.5 μg/mL venom treatment in MCF7 while 34 proteins in MDA-MB-231 at 2.5 μg/mL venom treatment. At the low 0.63 μg/mL venom treatment, 25 proteins in MCF7 presented FC $\geq$ 1.5 and 16 proteins in MDA-MB-231. However, MDA-MB-231 showed more proteins with FC $\leq$ 0.67 compared to MCF7 cell lines. MDA-MB-231 showed 28 proteins presenting FC $\leq$ 0.67 at 0.63 μg/mL venom treatment and 19 proteins in MCF7; and 41 proteins with FC $\leq$ 0.5 at 2.5 μg/mL venom treatment in MDA-MB-231 cell lines compared to 23 proteins in MCF7 cell line. Among these proteins, our data showed that *B. jararaca* venom was able to modulate, up or down, the abundance of several proteins playing essential roles in tumorigenicity. For example, the venom treatment increased the abundance of SNX3, HEL-S-156, MCCC2, and GSTM3 in the MCF7 cell line, and H3C15/HIST2H3 and MTCH2 in the MDA-MB-231 cell line whose overexpression has been related to increase in tumorigenicity (Table 1). Furthermore, among the proteins that decreased the abundance presenting FC $\leq$ 0.67, we highlight PCBD, PSMD5, RPS29, H3F3B, VDAC1 and VDAC2, ATP5PD, and HIST1H4J in MCF7 cell line and IGF2BP1, THBS1, and CYR61 in MDA-MB-231 cell line. These proteins have also been described to be related to several mechanisms and pathways in the onset of different types of cancer (Table 1). Additionally, cytotoxicity analysis performed in our laboratory (data not shown) evaluated the effects of *B. jararaca* venom on non-tumor HEK293 and HUVEC cell lines, which showed relatively less sensitivity to cell-death induction by snake venoms compared to MCF7 and MDA-MB-231 cancer cells. These data suggest that cancer cells could be more sensitive to snake venom components than non-cancer cells in certain situations.

Proteomic analysis also revealed exclusive proteins, i.e., proteins that were only identified in one or two of the three conditions analyzed. Among these proteins, we highlight the UQCRC1, identified in the MCF7 cell line only when these cells were treated with 0.63 μg/mL venom. High expression of this protein was observed in 74% of cases of breast cancer and 34% of ovarian cancer [104] (Table 1). Among proteins identified exclusively in the MCF7 cell line we highlight ATR (serine/threonine-protein kinase ATR) which plays important roles for cell survival and is considered a major mediator of DNA response in human cells, preventing cells with damaged or incompletely replicated DNA from entering mitosis when cells are damaged by radiotherapy or chemotherapy during cancer treatment [53]. In the MDA-MB-231 cell line, we highlight AMOT (angiomotin) protein identified only when cells were treated with either low or high concentration venom treatment and is known to play a critical role in angiogenesis, proliferation, and migration

of cancer cells and is also known to promote proliferation and invasion of several types of tumor cells, including breast, prostate, colon, cervical, and liver cancer (Table 1).

Semi-quantitative proteomics analysis of proteins with FC $\geq$ 1.5 after addition of venom in both MCF7 and MDA-MB-231 cell lines also identified enrichment of proteins related to protein metabolism pathways as well as cellular stress response pathway. The protein metabolism pathway ranges from protein synthesis to post-translational protein modification and degradation [136]. It is likely that the set of modifications undergone in the protein metabolism pathway undermine the tumorigenic activity of the cell line MCF7 and MDA-MB-231. Therefore, the activation of the apoptotic pathways using snake venom may be a potential treatment approach aiming at tumor degradation preferentially over the normal cells. The ribosome pathway enrichment was also observed in both cell lines. The lack of ribosomes in the cell impairs cell growth even under optimal conditions for it to happen [137]. Protein enrichment in ribosome pathway suggests increased protein synthesis, which may be related to damage repair mechanisms and cellular responses to external stimuli. Alterations in ribosomal pathways are related to cellular alterations and susceptibility to cancer. However, there is still no consensus if deregulation of ribosomes alteration is a cancer consequence or cause [138]. In addition, downregulation of cell maintenance-related proteins may also be related to tumorigenicity, thus opening the door for debate on the role of ribosomes in tumor cell lines [139].

The increase of terms involved in cellular stress response pathway, the metabolic pathway, the proteasome pathway, and the spliceosome pathway in MCF7 cell line suggests that the cells activated the metabolic pathways in response to stress, mRNA transcription and spliceosome activation, and ultimately activation of the proteasome. The proteasome is a cell apparatus that has several cellular functions, such as cell cycle regulation, differentiation, signal transduction pathway, antigen processing for immune responses, stress signaling, inflammatory responses and apoptosis, the latter being mediated by ubiquitination [140–142]. Since the inhibition of proteasome is related to cancer onset (i.e., p53 stability), proteolytic activity of the proteasome and its role in both biology and cancer treatment suggest an effective way to treat cancer [143,144].

In the MCF7 cell line treated with *B. jararaca* snake venom, a higher number of proteins changed in abundance when compared to the MDA-MB-231 cell line. Some of our observations showed that *B. jararaca* venom was able to up or down modulate the abundance of proteins that plays essential roles in tumorigenicity, conversely to what has been frequently described in the literature to decrease or increase cell tumorigenicity [113,145]. For example, the venom treatment was able to increase abundance of SNX3, HEL-S-156, MCCC2, and GSTM3 in the MCF7 cell line and H3C15/HIST2H3 and MTCH2 in the MDA-MB-231 cell line whose overexpression is related to increase in tumorigenicity. Although we cannot explain the mechanism on how the increase in abundance of these already overexpressed proteins is contributing to cell death of MCF7 and MDA-MB-231 cells, we have clues based on a recent published manuscript by Dias and colleagues (2019). The authors demonstrated that overloading the cell stress pathway in Y1 adrenocortical mouse tumor cell line under the effect of FGF-2 growth factor disrupted the cell homeostasis and sensitized the Y1 tumor cells to stress-oriented therapeutic inhibitors. Dias concludes that further stimulation of the same signaling pathways may further increase mobilization and dependence on stress response pathways in tumor cells, improving the efficacy and selectivity of therapeutic interventions [146]. This data suggests that *B. jararaca* snake venom or some of its content may be used to down-modulate already known overexpressed proteins in cancer or overexpress oncogenic proteins that lead cells to stress, by disrupting the tumor homeostasis leading cells to death. This is particularly interesting for cancer types that are more resistant to the chemotherapeutic agents, such as the MCF7 cells. In this case, *B. jararaca* snake venom would work as an adjuvant treatment of cancer, making cells more sensitive to the cytotoxic agents.

Moreover, due to the complexity of *B. jararaca* venom and the complex response of different cell lines, this snake venom is also a promising candidate in the prognostic

aid of different tumors, assisting in the assessment of tumor level, as highlighted for the several overexpressed proteins. For example, targeted-knockdown of some of these proteins may result in tumor growth inhibition. In addition, *B. jararaca* venom has induced overexpression of proteins related to pathways that impairs antitumor activity such as the protein metabolism pathways, proteasome, and cellular stress response pathways.

It is possible that many responses observed here were due to specific or multiple venom components. Nevertheless, the current approach of applying nLC-MS/MS proteomics to cancer cells treated with crude snake venom is a promising strategy for the identification of proteins with potential application in cancer cell therapy. Overall, this study was able to identify several cancer-related proteins that undergo significant changes upon venom treatment of MCF7 and MDA-MB-231 cells. Future studies should address specific mechanisms by which the snake venom and some of its content may contribute to MCF7 and MDA-MB-231 cell death and survival.

4. Conclusions

Quantitative proteomic analysis of breast cancer cell lines allowed us to identify several proteins whose abundance (FC) increased more than 1.5×, and proteins that abundance decreased less than 0.67×, after 24 h treatment with *B. jararaca* at either low sub-toxic dose of 0.63 μg/mL or high sub-toxic dose of 2.5 μg/mL. Most of these proteins identified suggest that the treatment with the venom may activate mitochondrial apoptotic pathways leading cells to death. In addition, several of the identified proteins play important roles related to cell proliferation, invasion, metastasis, apoptosis, and stress response. Therefore, these data show that *B. jararaca* venom or some of its toxin or components can inhibit tumor cell proliferation and survival and can potentially be used to identify novel targets for cancer therapy.

5. Materials and Methods

5.1. Cell Culture and Maintenance

MCF7 and MDA-MB-231 breast cancer cell lines were previously acquired from ATCC (Manassas, VA, USA) and maintained at our laboratory cell bank. Cells were thawed and cultured at 37 °C in 5% CO_2 in RPMI 1640 culture medium (Gibco, Life Technologies, Grand Island, NY, USA) supplemented with 10% inactivated fetal bovine serum (Cultilab, Campinas, Brazil) and 25 mg/mL ampicillin and 100 mg/mL streptomycin antibiotics. Cells were split when the confluence reached 80%.

5.2. Bothrops jararaca Venom

The venom of *B. jararaca* (lot 01/09-2) used in this study was a pool made from the extraction of 697 snakes collected at various Brazilian locations (in the states of São Paulo, Paraná, and Santa Catarina). Extracted venom were pooled and lyophilized at the department of herpetology at Butantan Institute under the coordination of Dr. Marisa Maria Teixeira da Rocha, and assigned for use and testing at the Laboratory of Applied Toxinology at Butantan Institute. The methods and use of venom in this work were approved by Butantan Institute Ethics Committee under the certification CEUAIB #9766150719 (2019).

5.3. Cell Viability Assay

The cytotoxicity assays were carried out by treating the cells with different concentrations of venom in the range from 0.1 μM to 20 μM. The cytotoxicity tests were performed using the colorimetric method of cell viability analysis using the WST-1 cell proliferation reagent kit (Roche, Mannheim, Germany) according to manufacturer's instructions. Briefly, 10^4 cells were plated in each well of a flat bottom 96-well microtiter plate. Cells were cultured at 37 °C in 5% CO_2 and on the day prior to analysis (70–80% confluency), culture medium from each well was exchanged to 100 μL of medium in the absence or presence of venom in different concentrations. After 24 h, 10 μL of the WST-1 reagent previously dissolved into an Electro Coupling Solution (ECS) were added to each well and incubated

for 4 h at 37 °C in 5% CO_2. The absorbance at 450 nm of each well was measured using a microplate reader FlexStation 3 spectrophotometer (Molecular Devices, San Jose, CA, USA). The determination of the absorbance and the quantification of viable cells were calculated using SoftMax Pro (version 5.1, Molecular Devices) and Microsoft Excel software.

5.4. Cell Treatment with B. jararaca Venom

In a six-well plate, 2×10^5 cells were plated and after the cells had reached a confluence of 70–80% (2–3 days), different concentrations of *B. jararaca* venom were added to the culture medium, starting from the cell cytotoxicity threshold up to a 1000-fold dilution for 24 h. For mass spectrometry analysis, cells were washed with ice-cold PBS and lysed with 1 mL ice-cold 8 M urea supplemented with cOmplete^{TM} protease and phosphatase inhibitors cocktail (Merck Millipore, Burlington, MA, USA). Fifty microliters of the cell lysate were separated for protein quantification using BCA (Bicinchoninic acid assay, Thermo Pierce, Walthan, MA, USA) and the lysate were stocked at −80 °C until further preparation of the sample for mass spectrometry analysis. Both cytotoxicity and proteomics experiments were performed in three biological replicates.

5.5. Sample Preparation for Proteomic Analysis

To the cell lysates, four microliters of 10 mM dithiothreitol (DTT) were added to reduce the disulfide bonds and incubated at 56 °C for 1 h. After incubation with DTT, 40 µL of iodoacetamide (IAA) was added for the alkylation of the cysteines for 1 h in the dark at room temperature. After incubation, 2.5 mL of ammonium acetate and 20 µL of trypsin (Sigma Aldrich, St. Louis, MO, USA) were added enough to have an enzyme:protein ratio of 1:50 and incubated at 37 °C overnight. The reaction was stopped by adding 30 µL of 100% acetic acid. Samples volume were reduced in a SpeedVac (Hetovac VR-1, Heto Lab Equipment, Allerød, Denmark) until the volume has lowered to 50 µL and were further desalted on in-house manufactured stop-and-go extraction tips (Stage-Tip) with three SDB-XC (styrene-divinylbenzene, Empore, 3M, Royersford, PA, USA) membranes as previously described [147]. The stage-tips were initially conditioned with 100% methanol followed by 0.1% formic acid. Samples were applied to the stage-tips and the peptides bound to the membranes were eluted with 50% acetonitrile, 0.1% formic acid. The eluate was lyophilized for further analysis in the mass spectrometer.

5.6. Mass Spectrometry Analysis

Dried samples were resuspended in 0.1% formic acid and analyzed on LTQ-Orbitrap Velos mass spectrometer (Thermo Scientific, Bremen, Germany) coupled to an EASY II nano liquid chromatographer (Thermo Scientific) using the shotgun approach. The spectrometer was equipped with a nanospray source connected to an in-house prepared analytical column (10 cm × ID 75 µm × OD 360 µm) packaged with 7 cm of 5 µm C18 resin (Jupiter, Phenomenex, Torrance, CA, USA). Precolumn (7 cm × ID 75 µm × OD 360 µm) was also prepared in-house packed with 5 cm of 10 µm C18 resin (Acqua, Phenomenex). The LC-MS/MS analyses were carried out by injecting 5 µg of the peptide extract and the peptides eluted from the column with a gradient of 5–40% in 100 min of solvent B (acetonitrile 90%, formic acid 0.1%) at a flow rate of 200 nL/min. The nanospray source was operated at 1.8 kV. The peptide mixture was analyzed by the acquisition of spectra in the full scan mode at a resolution of 30,000 for the determination of molecular masses (MS) of up to 10,000 Da. The 10 most intense peaks were automatically selected via data dependent acquisition (DDA) for the subsequent acquisition of spectra of the ions product to MS/MS for amino acid sequence determination at a resolution of 7500, a maximum injection time of 30 ms, a range of 200 to 2000 m/z, and a dynamic exclusion of 70 s. Protein identification was performed using Mascot (Matrix Science, version 2.4.0, Boston, MA, USA), MaxQuant (version 1.4.1.2, www.maxquant.net accessed on 1 October 2019), and Peaks Studio (version 10, Bioinformatic Solutions Inc, Toronto, Canada) against the *Homo sapiens* database downloaded from the Uniprot in March 2019 (www.uniprot.org

accessed on 1 October 2019). As search parameters, oxidation of methionine was set as a variable modification and carbamidomethylation of cysteine was set as a fixed modification. Searches were performed with mass error tolerance of 10 ppm for MS and 0.3 Da for MS/MS, and trypsin was selected as the proteolytic enzyme used in the digestion of proteins, and up to two miscleavages were allowed. Mass spectrometry-based proteomic analysis of MCF7 and MDA-MB-231 cell lysates, treated or not treated with low or high doses of *B. jararaca* venom were performed in triplicate. All raw data files for these analyses were uploaded and are available at: http://massive.ucsd.edu/MSV000084138/ accessed on 5 July 2021.

5.7. Proteome Functional and Enrichment Analysis

The entire proteome was analyzed to classify protein profiles by biological processes, molecular function, cellular components, and cellular pathways using Gene Ontology (geneontology.org accessed on 1 October 2019) and PantherDB (pantherdb.org accessed on 1 October 2019). The proteins presenting different profiles in the venom conditions were also analyzed using KEGG (www.genome.jp/kegg accessed on 1 October 2019) canonical pathways to determine the protein group or pathways that have undergone changes with different concentrations of the venom treatment. The PANTHER Classification System (Protein ANalysis THrough Evolutionary Relationships) is a research tool that covers evolutionary and functional information on protein family genes and has been widely used to understand protein evolution and its functional classification [148,149]. We conducted the functional classification for the molecular function, cell component, biological process, and protein family classification profiles [150,151] of the different proteins in each cell line and treatment at low and high *B. jararaca* venom that presented FC $\geq$ 1.5 in order to identify an enrichment pattern of protein families and pathways affected by the venom in the cell lines.

5.8. Semi-Quantitative Proteomics Analysis

Semi-quantitative protein analysis was performed using the Label Free Quantification MaxLFQ algorithm from MaxQuant software with an FDR rate of $\leq$1% to compare relative abundance of proteins in each of the cell lines [152]. Data generated by MaxQuant were entered into the Perseus program to further perform statistical and bioinformatics analyzes [153]. Proteins identified in the contaminant database and the decoy database were removed. As a protein identification criterion, it was considered that only peptides identified with the posterior error probability (PEP) $\leq$ 0.01 in at least one biological replicate, the minimum identification of eight ions belonging to the b and y ion series in the MS/MS spectra, and the occurrence of at least one unique peptide. We considered the intensity values of the LFQ that are normalized by the Maxquant software based on the sum of the intensity of all peptides of all identified proteins. LFQ data was considered for calculation, when the intensity data were present in at least two out of three replicates. Protein abundance or fold change (FC) analysis was performed using Microsoft Excel software. In addition, proteins that had a zero value in two of the three conditions were analyzed separately. The breast cancer cell lines treated with the whole *B. jararaca* venom for two different doses were compared according to the differentially expressed proteins with FC $\geq$ 1.5 by hierarchical clustering using as variables the average log2 fold change for the three replicates for each treatment, normalized with mean-centering. The Clustering analysis was performed using R statistical software version 3.6.3 (http://www.R-project.org accessed on 1 October 2019). The set of protein dissimilarities were computed using the "Euclidean" distance with the function "dist" to the hierarchical clustering based on the package and function "hclust". There was employed the agglomerative method with "ward.D2". The fold change and the protein–protein interactions provided by information from the String database [154] was used to explore the biological interactions of proteins identified as differentially abundant between control and cells treated with *B. jararaca* venom using the *Homo sapiens* reference genome.

5.9. Principal Component Analysis

Principal component analysis (PCA) was applied to find which linear combinations of the differentially expressed proteins with ≥1.5 would explain most of the variability for the different cell lineage conditions. The PCA analysis was performed using the R-statistics packages FactoMineR (accessed on 1 November 2020) [155] and Factoextra (http://www.sthda.com/english/rpkgs/factoextra accessed on 1 November 2020) for graphical visualization.

Supplementary Materials: The following are available online at https://www.mdpi.com/article/10.3390/toxins13080519/s1, Figure S1: Optical microscopy analysis of breast cancer cell lines treated with different concentrations of *B. jararaca* snake venom. MCF7 (a) and MDA-MB-231 (b) cell lines (10× magnification), Figure S2: Functional classification of the proteins presenting fold change (FC) ≥ 1.5 according to Molecular Function GO enrichment analysis. (a) MCF7 cell line. (b) MDA-MB-231 cell line, Figure S3: Functional classification of the proteins presenting FC ≥ 1.5 according to the Biological Process GO enrichment analysis. (a) MCF7 cell line. (b) MDA-MB-231 cell line, Figure S4: Functional classification of the proteins presenting FC ≥ 1.5 according to the Cellular Component GO enrichment analysis. (a) MCF7 cell line. (b) MDA-MB-231 cell line, Figure S5: Functional classification of the proteins presenting FC ≥ 1.5 according to Protein Family Classification GO enrichment analysis. (a) MCF7 cell line. (b) MDA-MB-231 cell line, Figure S6a: Protein-protein interaction of proteins identified in MCF7 cell line presenting FC ≤ 0.67 in cells treated with 2.5 µg/mL of *B. jararaca* venom compared to control, Figure S6b: Protein-protein interaction of proteins identified in MCF7 cell line presenting FC ≥ 1.5 in cells treated with 0.67 µg/mL of *B. jararaca* venom compared to control, Figure S6c: Protein-protein interaction of proteins identified in MCF7 cell line presenting FC ≤ 0.67 when in cells treated with 0.63 µg/mL of *B. jararaca* venom compared to control, Supplemental Figure S7a: Protein-protein interaction of proteins identified in MDA-MB-231 cell line presenting FC ≤ 0.67 in cells treated with 2.5 µg/mL of *B. jararaca* venom compared to control, Figure S7b: Protein-protein interaction of proteins identified in MDA-MB-231 cell line presenting FC ≤ 0.67 in cells treated with 0.63 µg/mL of *B. jararaca* venom compared to control, Figure S7c: Protein-protein interaction of proteins identified in MDA-MB-231 cell line presenting FC ≥ 2.5 in cells treated with 0.63 µg/mL of *B. jararaca* venom compared to control, Figure S8: Intensity plots of proteins identified exclusively in one or two of the conditions tested (Control, 0.63 µg/mL or 2.5 µg/mL of *B. jararaca* venom) in both MCF7 and MDA-MB-231 cell lines (Values presented in Table S4). (a) Proteins identified exclusively in the control group. (b) Proteins identified exclusively in the 0.63 µg/mL of venom treatment. (c) Proteins identified exclusively in the 2.5 µg/mL of venom treatment. (d) Proteins identified exclusively in the 0.63 and 2.5 µg/mL of venom treatments. (e) Proteins identified exclusively in the control group and 2.5 µg/mL of venom treatments. (f) Proteins identified exclusively in the control group and 0.63 µg/mL of venom treatment, Table S1a: Mass spectrometry-based proteomics analysis of MCF7 cell line treated with PBS (CTRL), 0.63 µg/mL and 2.5 µg/mL of *B. jararaca* snake venom, Table S2a: Mass spectrometry-based proteomics analysis of MCF7 cell lines treated with PBS (CTRL), 0.63 mg/mL and 2.5 µg/mL of *B. jararaca* snake venom. Fold change based on the control LFQ intensity, Table S1b: Mass spectrometry-based proteomics analysis of MDA-MB-231 cell line treated with PBS (CTRL), 0.63 µg/mL, and 2.5 µg/mL of *B. jararaca* snake venom, Table S2b: Mass spectrometry-based proteomics analysis of MDA-MB-231 cell lines treated with PBS (CTRL), 0.63 µg/mL and 2.5 µg/mL of *B. jararaca* snake venom. Fold change based on the control LFQ intensity, Table S3: Protein list of each of the seven clusters corresponding to Figure 3, Table S4a: MCF7 proteins identified exclusively at one or two of the conditions tested: PBS (CTRL), 0.63 µg/mL and 2.5 µg/mL of *B. jararaca* snake venom, Table S4b: MDA-MB-231 proteins identified exclusively at one or two of the conditions tested: PBS (CTRL), 0.63 µg/mL and 2.5 µg/mL of *B. jararaca* snake venom.

Author Contributions: Conceptualization, L.K.I.; methodology, L.K.I.; validation, C.Y.K. and S.S.S.A.; formal analysis, C.Y.K., S.S.S.A., F.M., W.d.S.S., H.M.C., D.C.-C., E.S.F., M.Y.N.-J. and L.K.I., investigation, C.Y.K., S.S.S.A., I.F.L., and D.C.-C.; resources, L.K.I.; data curation, M.Y.N.-J.; writing—original draft preparation, C.Y.K., S.S.S.A., E.S.F., M.Y.N.-J. and L.K.I.; writing—review and editing, C.Y.K., E.S.F., M.Y.N.-J. and L.K.I.; supervision, E.S.F., M.Y.N.-J. and L.K.I.; project administration, L.K.I.; funding acquisition, E.S.F. and L.K.I. All authors have read and agreed to the published version of the manuscript.

Funding: This work was supported by grants 2013/07467-1, 2016/04000-3, and 2017/17943-6 from the São Paulo Research Foundation (FAPESP). C.Y.K. was supported by FAPESP master's degree program fellowship 2017/06496-9. E.S.F. was supported by Erna and Jakob Michael "Visiting Professorship", Department of Biological Regulation, Weizmann Institute of Science, Rehovot, Israel and grant 302809/2016-3 from the Brazilian National Council for Scientific and Technological Development, CNPq, Brazil. F.M., W.d.S.S. and S.S.S.A. were supported by the Coordination for the Improvement of Higher Education Personnel (CAPES, Brazil) and CNPq institutional fellowship #88882.442313/2019-01 (Butantan Institute, Brazil) for W.d.S.S. and # 131408/2019-4 for S.S.S.A. (University of São Paulo, Brazil).

Institutional Review Board Statement: The methods and use of venom in this work were approved by Butantan Institute Ethics Committee under the certification CEUAIB #9766150719 (2019).

Informed Consent Statement: Not Applicable.

Data Availability Statement: All generated raw files for these analyses were uploaded and are available at: http://massive.ucsd.edu/MSV000084138/ (acccessed on 5 July 2021).

Acknowledgments: We thank Solange M.T. Serrano, Hugo A. Armelin and Zhibin Chen for useful discussion.

Conflicts of Interest: The authors declare that there is no conflict of interest.

References

1. Brazilian Ministry of Health. Accidents at Work by Venomous Animals among Workers at the Countryside, Forest, and Water in Brazil from 2007 to 2017 (Port). 2019; Volume 50. Available online: https://portalarquivos2.saude.gov.br/images/pdf/2019/marco/29/2018-059.pdf (accessed on 1 March 2021).
2. Ribeiro, L.A.; Jorge, M.T. Bites by snakes in the genus Bothrops: A series of 3139 cases. *Rev. Soc. Bras. Med. Trop.* **1997**, *30*, 475–480. [CrossRef]
3. Tanjoni, I.; Weinlich, R.; Della-Casa, M.S.; Clissa, P.B.; Saldanha-Gama, R.F.; de Freitas, M.S.; Barja-Fidalgo, C.; Amarante-Mendes, G.P.; Moura-da-Silva, A.M. Jararhagin, a snake venom metalloproteinase, induces a specialized form of apoptosis (anoikis) selective to endothelial cells. *Apoptosis* **2005**, *10*, 851–861. [CrossRef] [PubMed]
4. Calvete, J.J.; Juarez, P.; Sanz, L. Snake venomics. Strategy and applications. *J. Mass Spectrom.* **2007**, *42*, 1405–1414. [CrossRef] [PubMed]
5. Fox, J.W.; Serrano, S.M. Exploring snake venom proteomes: Multifaceted analyses for complex toxin mixtures. *Proteomics* **2008**, *8*, 909–920. [CrossRef] [PubMed]
6. Doley, R.; Kini, R.M. Protein complexes in snake venom. *Cell. Mol. Life Sci.* **2009**, *66*, 2851–2871. [CrossRef]
7. Serrano, S.M.; Shannon, J.D.; Wang, D.; Camargo, A.C.; Fox, J.W. A multifaceted analysis of viperid snake venoms by two-dimensional gel electrophoresis: An approach to understanding venom proteomics. *Proteomics* **2005**, *5*, 501–510. [CrossRef]
8. Jin, H.; Varner, J. Integrins: Roles in cancer development and as treatment targets. *Br. J. Cancer* **2004**, *90*, 561–565. [CrossRef]
9. White, J. Snake venoms and coagulopathy. *Toxicon* **2005**, *45*, 951–967. [CrossRef]
10. Gay, C.; Sanz, L.; Calvete, J.J.; Pla, D. Snake Venomics and Antivenomics of Bothrops diporus, a Medically Important Pitviper in Northeastern Argentina. *Toxins* **2015**, *8*, 9. [CrossRef]
11. Sanz, L.; Perez, A.; Quesada-Bernat, S.; Diniz-Sousa, R.; Calderon, L.A.; Soares, A.M.; Calvete, J.J.; Caldeira, C.A.S. Venomics and antivenomics of the poorly studied Brazil's lancehead, Bothrops brazili (Hoge, 1954), from the Brazilian State of Para. *J. Venom. Anim. Toxins Incl. Trop. Dis.* **2020**, *26*, e20190103. [CrossRef]
12. Tashima, A.K.; Zelanis, A.; Kitano, E.S.; Ianzer, D.; Melo, R.L.; Rioli, V.; Sant'anna, S.S.; Schenberg, A.C.; Camargo, A.C.; Serrano, S.M. Peptidomics of three Bothrops snake venoms: Insights into the molecular diversification of proteomes and peptidomes. *Mol. Cell. Proteom.* **2012**, *11*, 1245–1262. [CrossRef]
13. Gren, E.C.K.; Kitano, E.S.; Andrade-Silva, D.; Iwai, L.K.; Reis, M.S.; Menezes, M.C.; Serrano, S.M.T. Comparative analysis of the high molecular mass subproteomes of eight Bothrops snake venoms. *Comp. Biochem. Physiol. Part D Genom. Proteom.* **2019**, *30*, 113–121. [CrossRef]

14. Zelanis, A.; Tashima, A.K.; Pinto, A.F.; Paes Leme, A.F.; Stuginski, D.R.; Furtado, M.F.; Sherman, N.E.; Ho, P.L.; Fox, J.W.; Serrano, S.M. Bothrops jararaca venom proteome rearrangement upon neonate to adult transition. *Proteomics* **2011**, *11*, 4218–4228. [CrossRef]
15. Farias, I.B.; Morais-Zani, K.; Serino-Silva, C.; Sant'Anna, S.S.; Rocha, M.; Grego, K.F.; Andrade-Silva, D.; Serrano, S.M.T.; Tanaka-Azevedo, A.M. Functional and proteomic comparison of Bothrops jararaca venom from captive specimens and the Brazilian Bothropic Reference Venom. *J. Proteom.* **2018**, *174*, 36–46. [CrossRef]
16. Augusto-de-Oliveira, C.; Stuginski, D.R.; Kitano, E.S.; Andrade-Silva, D.; Liberato, T.; Fukushima, I.; Serrano, S.M.; Zelanis, A. Dynamic Rearrangement in Snake Venom Gland Proteome: Insights into Bothrops jararaca Intraspecific Venom Variation. *J. Proteome Res.* **2016**, *15*, 3752–3762. [CrossRef]
17. Laing, G.D.; Clissa, P.B.; Theakston, R.D.; Moura-da-Silva, A.M.; Taylor, M.J. Inflammatory pathogenesis of snake venom metalloproteinase-induced skin necrosis. *Eur. J. Immunol.* **2003**, *33*, 3458–3463. [CrossRef]
18. Azevedo-Marques, M.M.; Cupo, P.; Hering, S.E. Acidentes Por Animais PeÇonhentos: Serpentes PeÇonhentas. *Medicina* **2003**, *36*. [CrossRef]
19. Bjarnason, J.B.; Fox, J.W. Hemorrhagic metalloproteinases from snake venoms. *Pharmacol. Ther.* **1994**, *62*, 325–372. [CrossRef]
20. Cidade, D.A.; Simao, T.A.; Davila, A.M.; Wagner, G.; Junqueira-de-Azevedo, I.L.; Ho, P.L.; Bon, C.; Zingali, R.B.; Albano, R.M. Bothrops jararaca venom gland transcriptome: Analysis of the gene expression pattern. *Toxicon* **2006**, *48*, 437–461. [CrossRef]
21. Pereira, L.M.; Messias, E.A.; Sorroche, B.P.; Oliveira, A.D.N.; Arantes, L.; de Carvalho, A.C.; Tanaka-Azevedo, A.M.; Grego, K.F.; Carvalho, A.L.; Melendez, M.E. In-depth transcriptome reveals the potential biotechnological application of Bothrops jararaca venom gland. *J. Venom. Anim. Toxins Incl. Trop. Dis.* **2020**, *26*, e20190058. [CrossRef]
22. Serrano, S.M.; Maroun, R.C. Snake venom serine proteinases: Sequence homology vs. substrate specificity, a paradox to be solved. *Toxicon* **2005**, *45*, 1115–1132. [CrossRef]
23. Fox, J.W.; Serrano, S.M. Insights into and speculations about snake venom metalloproteinase (SVMP) synthesis, folding and disulfide bond formation and their contribution to venom complexity. *FEBS J.* **2008**, *275*, 3016–3030. [CrossRef]
24. Matsui, T.; Fujimura, Y.; Titani, K. Snake venom proteases affecting hemostasis and thrombosis. *Biochim. Biophys. Acta (BBA)-Protein Struct. Mol. Enzym.* **2000**, *1477*, 146–156. [CrossRef]
25. Da Silva Cunha, K.C.; Fuly, A.L.; de Araujo, E.G. A phospholipase A(2) isolated from Lachesis muta snake venom increases the survival of retinal ganglion cells in vitro. *Toxicon* **2011**, *57*, 580–585. [CrossRef]
26. Jain, D.; Kumar, S. Snake venom: A potent anticancer agent. *Asian Pac. J. Cancer Prev.* **2012**, *13*, 4855–4860. [CrossRef] [PubMed]
27. Tan, N.; Fung, S.Y. Snake Venom L-Amino Acid Oxidases potential biomedical applications. *Mal. J. Biochem. Mol. Biol.* **2008**, *16*, 1–10.
28. Tan, K.K.; Bay, B.H.; Gopalakrishnakone, P. L-amino acid oxidase from snake venom and its anticancer potential. *Toxicon* **2018**, *144*, 7–13. [CrossRef]
29. Pawelek, P.D.; Cheah, J.; Coulombe, R.; Macheroux, P.; Ghisla, S.; Vrielink, A. The structure of L-amino acid oxidase reveals the substrate trajectory into an enantiomerically conserved active site. *EMBO J.* **2000**, *19*, 4204–4215. [CrossRef]
30. Phillips, D.R.; Scarborough, R.M. Clinical Pharmacology of Eptifibatide. *Am. J. Cardiol.* **1997**, *80*, 11B–20B. [CrossRef]
31. Ferreira, S.H. A Bradykinin-Potentiating Factor (Bpf) Present in the Venom of Bothrops Jararca. *Br. J. Pharmacol. Chemother.* **1965**, *24*, 163–169. [CrossRef]
32. Camargo, A.C.; Ianzer, D.; Guerreiro, J.R.; Serrano, S.M. Bradykinin-potentiating peptides: Beyond captopril. *Toxicon* **2012**, *59*, 516–523. [CrossRef]
33. Fox, J.W.; Serrano, S.M. Approaching the golden age of natural product pharmaceuticals from venom libraries: An overview of toxins and toxin-derivatives currently involved in therapeutic or diagnostic applications. *Curr. Pharm. Des.* **2007**, *13*, 2927–2934. [CrossRef]
34. Marsh, N.; Williams, V. Practical applications of snake venom toxins in haemostasis. *Toxicon* **2005**, *45*, 1171–1181. [CrossRef]
35. Vyas, V.K.; Brahmbhatt, K.; Bhatt, H.; Parmar, U. Therapeutic potential of snake venom in cancer therapy: Current perspectives. *Asian Pac. J. Trop. Biomed.* **2013**, *3*, 156–162. [CrossRef]
36. da Silva, R.J.; da Silva, M.G.; Vilela, L.C.; Fecchio, D. Antitumor effect of Bothrops jararaca venom. *Mediat. Inflamm.* **2002**, *11*, 99–104. [CrossRef]
37. Yamazaki, Y.; Morita, T. Snake venom components affecting blood coagulation and the vascular system: Structural similarities and marked diversity. *Curr. Pharm. Des.* **2007**, *13*, 2872–2886. [CrossRef] [PubMed]
38. Dias, M.H.; Kitano, E.S.; Zelanis, A.; Iwai, L.K. Proteomics and drug discovery in cancer. *Drug Discov. Today* **2016**, *21*, 264–277. [CrossRef] [PubMed]
39. Hanahan, D.; Weinberg, R.A. Hallmarks of cancer: The next generation. *Cell* **2011**, *144*, 646–674. [CrossRef] [PubMed]
40. Mora, R.; Valverde, B.; Diaz, C.; Lomonte, B.; Gutierrez, J.M. A Lys49 phospholipase A(2) homologue from Bothrops asper snake venom induces proliferation, apoptosis and necrosis in a lymphoblastoid cell line. *Toxicon* **2005**, *45*, 651–660. [CrossRef] [PubMed]
41. Bateman, E.; Venning, M.; Mirtschin, P.; Woods, A. The effects of selected Australian snake venoms on tumour-associated microvascular endothelial cells (TAMECs) in vitro. *J. Venom. Res.* **2013**, *4*, 21–30.
42. Moreira, V.; Lomonte, B.; Vinolo, M.A.; Curi, R.; Gutierrez, J.M.; Teixeira, C. An Asp49 phospholipase A2 from snake venom induces cyclooxygenase-2 expression and prostaglandin E2 production via activation of NF-kappaB, p38MAPK, and PKC in macrophages. *Mediat. Inflamm.* **2014**, *2014*, 105879. [CrossRef]

43. Leiguez, E.; Giannotti, K.C.; Moreira, V.; Matsubara, M.H.; Gutierrez, J.M.; Lomonte, B.; Rodriguez, J.P.; Balsinde, J.; Teixeira, C. Critical role of TLR2 and MyD88 for functional response of macrophages to a group IIA-secreted phospholipase A2 from snake venom. *PLoS ONE* **2014**, *9*, e93741. [CrossRef]
44. Frejno, M.; Meng, C.; Ruprecht, B.; Oellerich, T.; Scheich, S.; Kleigrewe, K.; Drecoll, E.; Samaras, P.; Hogrebe, A.; Helm, D.; et al. Proteome activity landscapes of tumor cell lines determine drug responses. *Nat. Commun.* **2020**, *11*, 3639. [CrossRef] [PubMed]
45. Ruprecht, B.; Di Bernardo, J.; Wang, Z.; Mo, X.; Ursu, O.; Christopher, M.; Fernandez, R.B.; Zheng, L.; Dill, B.D.; Wang, H.; et al. A mass spectrometry-based proteome map of drug action in lung cancer cell lines. *Nat. Chem. Biol.* **2020**, *16*, 1111–1119. [CrossRef] [PubMed]
46. Furtado, C.M.; Marcondes, M.C.; Sola-Penna, M.; de Souza, M.L.; Zancan, P. Clotrimazole preferentially inhibits human breast cancer cell proliferation, viability and glycolysis. *PLoS ONE* **2012**, *7*, e30462. [CrossRef] [PubMed]
47. Hui, L.; Zheng, Y.; Yan, Y.; Bargonetti, J.; Foster, D.A. Mutant p53 in MDA-MB-231 breast cancer cells is stabilized by elevated phospholipase D activity and contributes to survival signals generated by phospholipase D. *Oncogene* **2006**, *25*, 7305–7310. [CrossRef]
48. Neve, R.M.; Chin, K.; Fridlyand, J.; Yeh, J.; Baehner, F.L.; Fevr, T.; Clark, L.; Bayani, N.; Coppe, J.P.; Tong, F.; et al. A collection of breast cancer cell lines for the study of functionally distinct cancer subtypes. *Cancer Cell* **2006**, *10*, 515–527. [CrossRef]
49. Lv, M.; Shen, Y.; Yang, J.; Li, S.; Wang, B.; Chen, Z.; Li, P.; Liu, P.; Yang, J. Angiomotin Family Members: Oncogenes or Tumor Suppressors? *Int. J. Biol. Sci.* **2017**, *13*, 772–781. [CrossRef]
50. Zhang, H.; Fan, Q. MicroRNA-205 inhibits the proliferation and invasion of breast cancer by regulating AMOT expression. *Oncol. Rep.* **2015**, *34*, 2163–2170. [CrossRef]
51. Couderc, C.; Boin, A.; Fuhrmann, L.; Vincent-Salomon, A.; Mandati, V.; Kieffer, Y.; Mechta-Grigoriou, F.; Del Maestro, L.; Chavrier, P.; Vallerand, D.; et al. AMOTL1 Promotes Breast Cancer Progression and Is Antagonized by Merlin. *Neoplasia* **2016**, *18*, 10–24. [CrossRef] [PubMed]
52. Song, K.H.; Kim, J.H.; Lee, Y.H.; Bae, H.C.; Lee, H.J.; Woo, S.R.; Oh, S.J.; Lee, K.M.; Yee, C.; Kim, B.W.; et al. Mitochondrial reprogramming via ATP5H loss promotes multimodal cancer therapy resistance. *J. Clin. Investig.* **2018**, *128*, 4098–4114. [CrossRef] [PubMed]
53. Qiu, Z.; Oleinick, N.L.; Zhang, J. ATR/CHK1 inhibitors and cancer therapy. *Radiother. Oncol.* **2018**, *126*, 450–464. [CrossRef] [PubMed]
54. Karnitz, L.M.; Zou, L. Molecular Pathways: Targeting ATR in Cancer Therapy. *Clin. Cancer Res.* **2015**, *21*, 4780–4785. [CrossRef] [PubMed]
55. O'Kelly, J.; Chung, A.; Lemp, N.; Chumakova, K.; Yin, D.; Wang, H.J.; Said, J.; Gui, D.; Miller, C.W.; Karlan, B.Y.; et al. Functional domains of CCN1 (Cyr61) regulate breast cancer progression. *Int. J. Oncol.* **2008**, *33*, 59–67. [CrossRef] [PubMed]
56. Huang, Y.T.; Lan, Q.; Lorusso, G.; Duffey, N.; Ruegg, C. The matricellular protein CYR61 promotes breast cancer lung metastasis by facilitating tumor cell extravasation and suppressing anoikis. *Oncotarget* **2017**, *8*, 9200–9215. [CrossRef]
57. Hayes, J.D.; Flanagan, J.U.; Jowsey, I.R. Glutathione transferases. *Annu. Rev. Pharmacol. Toxicol.* **2005**, *45*, 51–88. [CrossRef] [PubMed]
58. Meding, S.; Balluff, B.; Elsner, M.; Schone, C.; Rauser, S.; Nitsche, U.; Maak, M.; Schafer, A.; Hauck, S.M.; Ueffing, M.; et al. Tissue-based proteomics reveals FXYD3, S100A11 and GSTM3 as novel markers for regional lymph node metastasis in colon cancer. *J. Pathol.* **2012**, *228*, 459–470. [CrossRef] [PubMed]
59. Saucedo-Cuevas, L.P.; Ruppen, I.; Ximenez-Embun, P.; Domingo, S.; Gayarre, J.; Munoz, J.; Silva, J.M.; Garcia, M.J.; Benitez, J. CUL4A contributes to the biology of basal-like breast tumors through modulation of cell growth and antitumor immune response. *Oncotarget* **2014**, *5*, 2330–2343. [CrossRef]
60. Lan, F.; Shi, Y. Histone H3.3 and cancer: A potential reader connection. *Proc. Natl. Acad. Sci. USA* **2015**, *112*, 6814–6819. [CrossRef]
61. Ayoubi, H.A.; Mahjoubi, F.; Mirzaei, R. Investigation of the human H3.3B (H3F3B) gene expression as a novel marker in patients with colorectal cancer. *J. Gastrointest. Oncol.* **2017**, *8*, 64–69. [CrossRef]
62. Roberts, E.L.; Newton, R.P.; Axford, A.T. Plasma purine nucleoside phosphorylase in cancer patients. *Clin. Chim. Acta* **2004**, *344*, 109–114. [CrossRef]
63. Vareed, S.K.; Bhat, V.B.; Thompson, C.; Vasu, V.T.; Fermin, D.; Choi, H.; Creighton, C.J.; Gayatri, S.; Lan, L.; Putluri, N.; et al. Metabolites of purine nucleoside phosphorylase (NP) in serum have the potential to delineate pancreatic adenocarcinoma. *PLoS ONE* **2011**, *6*, e17177. [CrossRef]
64. Dummer, R.; Duvic, M.; Scarisbrick, J.; Olsen, E.A.; Rozati, S.; Eggmann, N.; Goldinger, S.M.; Hutchinson, K.; Geskin, L.; Illidge, T.M.; et al. Final results of a multicenter phase II study of the purine nucleoside phosphorylase (PNP) inhibitor forodesine in patients with advanced cutaneous T-cell lymphomas (CTCL) (Mycosis fungoides and Sezary syndrome). *Ann. Oncol.* **2014**, *25*, 1807–1812. [CrossRef]
65. Tan, E.; Besant, P.G.; Zu, X.L.; Turck, C.W.; Bogoyevitch, M.A.; Lim, S.G.; Attwood, P.V.; Yeoh, G.C. Histone H4 histidine kinase displays the expression pattern of a liver oncodevelopmental marker. *Carcinogenesis* **2004**, *25*, 2083–2088. [CrossRef]
66. Besant, P.G.; Attwood, P.V. Histone H4 histidine phosphorylation: Kinases, phosphatases, liver regeneration and cancer. *Biochem. Soc. Trans.* **2012**, *40*, 290–293. [CrossRef]

67. Long, M.; Sun, X.; Shi, W.; Yanru, A.; Leung, S.T.C.; Ding, D.; Cheema, M.S.; MacPherson, N.; Nelson, C.J.; Ausio, J.; et al. A novel histone H4 variant H4G regulates rDNA transcription in breast cancer. *Nucleic. Acids Res.* **2019**, *47*, 8399–8409. [CrossRef] [PubMed]
68. Nacev, B.A.; Feng, L.; Bagert, J.D.; Lemiesz, A.E.; Gao, J.; Soshnev, A.A.; Kundra, R.; Schultz, N.; Muir, T.W.; Allis, C.D. The expanding landscape of 'oncohistone' mutations in human cancers. *Nature* **2019**, *567*, 473–478. [CrossRef] [PubMed]
69. Bell, J.L.; Wachter, K.; Muhleck, B.; Pazaitis, N.; Kohn, M.; Lederer, M.; Huttelmaier, S. Insulin-like growth factor 2 mRNA-binding proteins (IGF2BPs): Post-transcriptional drivers of cancer progression? *Cell. Mol. Life Sci.* **2013**, *70*, 2657–2675. [CrossRef]
70. Fakhraldeen, S.A.; Clark, R.J.; Roopra, A.; Chin, E.N.; Huang, W.; Castorino, J.; Wisinski, K.B.; Kim, T.; Spiegelman, V.S.; Alexander, C.M. Two Isoforms of the RNA Binding Protein, Coding Region Determinant-binding Protein (CRD-BP/IGF2BP1), Are Expressed in Breast Epithelium and Support Clonogenic Growth of Breast Tumor Cells. *J. Biol. Chem.* **2015**, *290*, 13386–13400. [CrossRef]
71. Kim, T.; Havighurst, T.; Kim, K.; Albertini, M.; Xu, Y.G.; Spiegelman, V.S. Targeting insulin-like growth factor 2 mRNA-binding protein 1 (IGF2BP1) in metastatic melanoma to increase efficacy of BRAF(V600E) inhibitors. *Mol. Carcinog.* **2018**, *57*, 678–683. [CrossRef] [PubMed]
72. Han, W.; Hu, C.; Fan, Z.J.; Shen, G.L. Transcript levels of keratin 1/5/6/14/15/16/17 as potential prognostic indicators in melanoma patients. *Sci. Rep.* **2021**, *11*, 1023. [CrossRef]
73. Palko, E.; Poliska, S.; Sziklai, I.; Penyige, A. Analysis of KRT1, KRT10, KRT19, TP53 and MMP9 expression in pediatric and adult cholesteatoma. *PLoS ONE* **2018**, *13*, e0200840. [CrossRef]
74. Hitzerd, S.M.; Verbrugge, S.E.; Ossenkoppele, G.; Jansen, G.; Peters, G.J. Positioning of aminopeptidase inhibitors in next generation cancer therapy. *Amino Acids* **2014**, *46*, 793–808. [CrossRef]
75. Tian, S.Y.; Chen, S.H.; Shao, B.F.; Cai, H.Y.; Zhou, Y.; Zhou, Y.L.; Xu, A.B. Expression of leucine aminopeptidase 3 (LAP3) correlates with prognosis and malignant development of human hepatocellular carcinoma (HCC). *Int. J. Clin. Exp. Pathol.* **2014**, *7*, 3752–3762.
76. He, X.; Huang, Q.; Qiu, X.; Liu, X.; Sun, G.; Guo, J.; Ding, Z.; Yang, L.; Ban, N.; Tao, T.; et al. LAP3 promotes glioma progression by regulating proliferation, migration and invasion of glioma cells. *Int. J. Biol. Macromol.* **2015**, *72*, 1081–1089. [CrossRef] [PubMed]
77. Zhang, S.; Yang, X.; Shi, H.; Li, M.; Xue, Q.; Ren, H.; Yao, L.; Chen, X.; Zhang, J.; Wang, H. Overexpression of leucine aminopeptidase 3 contributes to malignant development of human esophageal squamous cell carcinoma. *J. Mol. Histol.* **2014**, *45*, 283–292. [CrossRef]
78. Liu, Y.; Yuan, Z.; Song, C. Methylcrotonoyl-CoA carboxylase 2 overexpression predicts an unfavorable prognosis and promotes cell proliferation in breast cancer. *Biomark. Med.* **2019**, *13*, 427–436. [CrossRef] [PubMed]
79. Arco, A.D.; Satrustegui, J. New mitochondrial carriers: An overview. *Cell. Mol. Life Sci.* **2005**, *62*, 2204–2227. [CrossRef] [PubMed]
80. Hao, J.M.; Chen, J.Z.; Sui, H.M.; Si-Ma, X.Q.; Li, G.Q.; Liu, C.; Li, J.L.; Ding, Y.Q.; Li, J.M. A five-gene signature as a potential predictor of metastasis and survival in colorectal cancer. *J. Pathol.* **2010**, *220*, 475–489. [CrossRef] [PubMed]
81. Arigoni, M.; Barutello, G.; Riccardo, F.; Ercole, E.; Cantarella, D.; Orso, F.; Conti, L.; Lanzardo, S.; Taverna, D.; Merighi, I.; et al. miR-135b coordinates progression of ErbB2-driven mammary carcinomas through suppression of MID1 and MTCH2. *Am. J. Pathol.* **2013**, *182*, 2058–2070. [CrossRef]
82. De Palma, G.; Sallustio, F.; Curci, C.; Galleggiante, V.; Rutigliano, M.; Serino, G.; Ditonno, P.; Battaglia, M.; Schena, F.P. The Three-Gene Signature in Urinary Extracellular Vesicles from Patients with Clear Cell Renal Cell Carcinoma. *J. Cancer* **2016**, *7*, 1960–1967. [CrossRef]
83. Nunes, F.D.; de Almeida, F.C.; Tucci, R.; de Sousa, S.C. Homeobox genes: A molecular link between development and cancer. *Pesquisa Odontol. Bras.* **2003**, *17*, 94–98. [CrossRef]
84. Samuel, S.; Naora, H. Homeobox gene expression in cancer: Insights from developmental regulation and deregulation. *Eur. J. Cancer* **2005**, *41*, 2428–2437. [CrossRef]
85. Pyper, S.R.; Viswakarma, N.; Jia, Y.; Zhu, Y.J.; Fondell, J.D.; Reddy, J.K. PRIC295, a Nuclear Receptor Coactivator, Identified from PPARalpha-Interacting Cofactor Complex. *PPAR Res.* **2010**, *2010*, 173907. [CrossRef]
86. Viswakarma, N.; Jia, Y.; Bai, L.; Gao, Q.; Lin, B.; Zhang, X.; Misra, P.; Rana, A.; Jain, S.; Gonzalez, F.J.; et al. The Med1 subunit of the mediator complex induces liver cell proliferation and is phosphorylated by AMP kinase. *J. Biol. Chem.* **2013**, *288*, 27898–27911. [CrossRef]
87. Ahmed, N.; Escalona, R.; Leung, D.; Chan, E.; Kannourakis, G. Tumour microenvironment and metabolic plasticity in cancer and cancer stem cells: Perspectives on metabolic and immune regulatory signatures in chemoresistant ovarian cancer stem cells. *Semin. Cancer Biol.* **2018**, *53*, 265–281. [CrossRef]
88. Levin, A.; Minis, A.; Lalazar, G.; Rodriguez, J.; Steller, H. PSMD5 Inactivation Promotes 26S Proteasome Assembly during Colorectal Tumor Progression. *Cancer Res.* **2018**, *78*, 3458–3468. [CrossRef] [PubMed]
89. Chai, F.L.Y.; Bi, J.; Chen, L.Z.F.; Cui, Y.; Bian, X.; Jiang, J. High expression of REGγ is associated with metastasis and poor prognosis of patients with breast cancer. *Int. J. Clin. Exp. Pathol.* **2014**, *7*, 7834. [PubMed]
90. Chai, F.; Liang, Y.; Bi, J.; Chen, L.; Zhang, F.; Cui, Y.; Jiang, J. REGgamma regulates ERalpha degradation via ubiquitin-proteasome pathway in breast cancer. *Biochem. Biophys. Res. Commun.* **2015**, *456*, 534–540. [CrossRef]
91. Wang, X.; Tu, S.; Tan, J.; Tian, T.; Ran, L.; Rodier, J.F.; Ren, G. REG gamma: A potential marker in breast cancer and effect on cell cycle and proliferation of breast cancer cell. *Med. Oncol.* **2011**, *28*, 31–41. [CrossRef] [PubMed]

92. Coppock, D.; Kopman, C.; Gudas, J.; Cina-Poppe, D.A. Regulation of the quiescence-induced genes: Quiescin Q6, decorin, and ribosomal protein S29. *Biochem. Biophys. Res. Commun.* **2000**, *269*, 604–610. [CrossRef]
93. Notterman, D.A.; Alon, U.; Sierk, A.J.; Levine, A.J. Transcriptional gene expression profiles of colorectal adenoma, adenocarcinoma, and normal tissue examined by oligonucleotide arrays. *Cancer Res.* **2001**, *61*, 7.
94. Lv, Z.; Wang, Z.; Luo, L.; Chen, Y.; Han, G.; Wang, R.; Xiao, H.; Li, X.; Hou, C.; Feng, J.; et al. Spliceosome protein Eftud2 promotes colitis-associated tumorigenesis by modulating inflammatory response of macrophage. *Mucosal Immunol.* **2019**, *12*, 1164–1173. [CrossRef]
95. Sato, N.; Maeda, M.; Sugiyama, M.; Ito, S.; Hyodo, T.; Masuda, A.; Tsunoda, N.; Kokuryo, T.; Hamaguchi, M.; Nagino, M.; et al. Inhibition of SNW1 association with spliceosomal proteins promotes apoptosis in breast cancer cells. *Cancer Med.* **2015**, *4*, 268–277. [CrossRef] [PubMed]
96. Pons, V.; Luyet, P.P.; Morel, E.; Abrami, L.; van der Goot, F.G.; Parton, R.G.; Gruenberg, J. Hrs and SNX3 functions in sorting and membrane invagination within multivesicular bodies. *PLoS Biol.* **2008**, *6*, e214. [CrossRef]
97. Mendelsohn, J. The epidermal growth factor receptor as a target for cancer therapy. *Endocr. Relat. Cancer* **2001**, *8*, 3–9. [CrossRef]
98. John, A.S.; Rothman, V.L.; Tuszynski, G.P. Thrombospondin-1 (TSP-1) Stimulates Expression of Integrin alpha6 in Human Breast Carcinoma Cells: A Downstream Modulator of TSP-1-Induced Cellular Adhesion. *J. Oncol.* **2010**, *2010*, 645376. [CrossRef] [PubMed]
99. Jayachandran, A.; Anaka, M.; Prithviraj, P.; Hudson, C.; McKeown, S.J.; Lo, P.H.; Vella, L.J.; Goding, C.R.; Cebon, J.; Behren, A. Thrombospondin 1 promotes an aggressive phenotype through epithelial-to-mesenchymal transition in human melanoma. *Oncotarget* **2014**, *5*, 5782–5797. [CrossRef]
100. Tzeng, H.T.; Tsai, C.H.; Yen, Y.T.; Cheng, H.C.; Chen, Y.C.; Pu, S.W.; Wang, Y.S.; Shan, Y.S.; Tseng, Y.L.; Su, W.C.; et al. Dysregulation of Rab37-Mediated Cross-talk between Cancer Cells and Endothelial Cells via Thrombospondin-1 Promotes Tumor Neovasculature and Metastasis. *Clin. Cancer Res.* **2017**, *23*, 2335–2345. [CrossRef]
101. Shi, H.; Hayes, M.; Kirana, C.; Miller, R.; Keating, J.; Macartney-Coxson, D.; Stubbs, R. TUFM is a potential new prognostic indicator for colorectal carcinoma. *Pathology* **2012**, *44*, 506–512. [CrossRef]
102. Weng, X.; Zheng, S.; Shui, H.; Lin, G.; Zhou, Y. TUFM-knockdown inhibits the migration and proliferation of gastrointestinal stromal tumor cells. *Oncol. Lett.* **2020**, *20*, 250. [CrossRef]
103. He, K.; Guo, X.; Liu, Y.; Li, J.; Hu, Y.; Wang, D.; Song, J. TUFM downregulation induces epithelial-mesenchymal transition and invasion in lung cancer cells via a mechanism involving AMPK-GSK3beta signaling. *Cell. Mol. Life Sci.* **2016**, *73*, 2105–2121. [CrossRef] [PubMed]
104. Kulawiec, M.; Arnouk, H.; Desouki, M.M.; Kazim, L.; Still, I.; Singh, K.K. Proteomic analysis of mitochondria-to-nucleus retrograde response in human cancer. *Cancer Biol. Ther.* **2006**, *5*, 967–975. [CrossRef] [PubMed]
105. Li, W.; Wubulikasimu, G.; Zhao, X.; Wang, C.; Liu, R.; Wang, L.; Zhu, X.; Chen, Z. UQCRC1 downregulation is correlated with lymph node metastasis and poor prognosis in CRC. *Eur. J. Surg. Oncol.* **2019**, *45*, 1005–1010. [CrossRef]
106. Wang, Q.; Li, M.; Gan, Y.; Jiang, S.; Qiao, J.; Zhang, W.; Fan, Y.; Shen, Y.; Song, Y.; Meng, Z.; et al. Mitochondrial Protein UQCRC1 is Oncogenic and a Potential Therapeutic Target for Pancreatic Cancer. *Theranostics* **2020**, *10*, 2141–2157. [CrossRef] [PubMed]
107. Mazure, N.M. VDAC in cancer. *Biochim. Biophys. Acta Bioenerg.* **2017**, *1858*, 665–673. [CrossRef]
108. Sotgia, F.; Fiorillo, M.; Lisanti, M.P. Mitochondrial markers predict recurrence, metastasis and tamoxifen-resistance in breast cancer patients: Early detection of treatment failure with companion diagnostics. *Oncotarget* **2017**, *8*, 68730–68745. [CrossRef]
109. Camara, A.K.S.; Zhou, Y.; Wen, P.C.; Tajkhorshid, E.; Kwok, W.M. Mitochondrial VDAC1: A Key Gatekeeper as Potential Therapeutic Target. *Front. Physiol.* **2017**, *8*, 460. [CrossRef]
110. Magri, A.; Reina, S.; De Pinto, V. VDAC1 as Pharmacological Target in Cancer and Neurodegeneration: Focus on Its Role in Apoptosis. *Front. Chem.* **2018**, *6*, 108. [CrossRef] [PubMed]
111. Thul, P.J.; Akesson, L.; Wiking, M.; Mahdessian, D.; Geladaki, A.; Ait Blal, H.; Alm, T.; Asplund, A.; Bjork, L.; Breckels, L.M.; et al. A subcellular map of the human proteome. *Science* **2017**, *356*. [CrossRef]
112. Uhlen, M.; Fagerberg, L.; Hallstrom, B.M.; Lindskog, C.; Oksvold, P.; Mardinoglu, A.; Sivertsson, A.; Kampf, C.; Sjostedt, E.; Asplund, A.; et al. Tissue-based map of the human proteome. *Science* **2015**, *347*, 1260419. [CrossRef] [PubMed]
113. Uhlen, M.; Zhang, C.; Lee, S.; Sjostedt, E.; Fagerberg, L.; Bidkhori, G.; Benfeitas, R.; Arif, M.; Liu, Z.; Edfors, F.; et al. A pathology atlas of the human cancer transcriptome. *Science* **2017**, *357*. [CrossRef]
114. Doncheva, N.T.; Morris, J.H.; Gorodkin, J.; Jensen, L.J. Cytoscape StringApp: Network Analysis and Visualization of Proteomics Data. *J. Proteome Res.* **2019**, *18*, 623–632. [CrossRef]
115. Essex, H.E.; Priestley, J.T. Effect of Rattlesnake Venom on Flexner-Jobling's Carcinoma in the White Rat (Mus Norvegicus Albinus.). *Exp. Biol. Med.* **1931**, *28*, 550–551. [CrossRef]
116. Ferreira, S.H.; Greene, L.H.; Alabaster, V.A.; Bakhle, Y.S.; Vane, J.R. Activity of various fractions of bradykinin potentiating factor against angiotensin I converting enzyme. *Nature* **1970**, *225*, 379–380. [CrossRef] [PubMed]
117. Cushman, D.W.; Ondetti, M.A. History of the design of captopril and related inhibitors of angiotensin converting enzyme. *Hypertension* **1991**, *17*, 589–592. [CrossRef] [PubMed]
118. Smith, C.G.; Vane, J.R. The discovery of captopril. *FASEB J.* **2003**, *17*, 788–789. [CrossRef] [PubMed]
119. Ma, R.; Mahadevappa, R.; Kwok, H.F. Venom-based peptide therapy: Insights into anti-cancer mechanism. *Oncotarget* **2017**, *8*, 100908–100930. [CrossRef]

120. Li, L.; Huang, J.; Lin, Y. Snake Venoms in Cancer Therapy: Past, Present and Future. *Toxins* **2018**, *10*, 346. [CrossRef] [PubMed]
121. Sukocheva, O.; Menschikowski, M.; Hagelgans, A.; Yarla, N.S.; Siegert, G.; Reddanna, P.; Bishayee, A. Current insights into functions of phospholipase A2 receptor in normal and cancer cells: More questions than answers. *Semin. Cancer Biol.* **2019**, *56*, 116–127. [CrossRef]
122. Peng, Z.; Chang, Y.; Fan, J.; Ji, W.; Su, C. Phospholipase A2 superfamily in cancer. *Cancer Lett.* **2021**, *497*, 165–177. [CrossRef]
123. Cathcart, J.; Pulkoski-Gross, A.; Cao, J. Targeting Matrix Metalloproteinases in Cancer: Bringing New Life to Old Ideas. *Genes Dis.* **2015**, *2*, 26–34. [CrossRef]
124. Di Cara, G.; Marabeti, M.R.; Musso, R.; Riili, I.; Cancemi, P.; Pucci Minafra, I. New Insights into the Occurrence of Matrix Metalloproteases-2 and -9 in a Cohort of Breast Cancer Patients and Proteomic Correlations. *Cells* **2018**, *7*, 89. [CrossRef] [PubMed]
125. Quintero-Fabian, S.; Arreola, R.; Becerril-Villanueva, E.; Torres-Romero, J.C.; Arana-Argaez, V.; Lara-Riegos, J.; Ramirez-Camacho, M.A.; Alvarez-Sanchez, M.E. Role of Matrix Metalloproteinases in Angiogenesis and Cancer. *Front. Oncol.* **2019**, *9*, 1370. [CrossRef]
126. Bezerra, P.H.A.; Ferreira, I.M.; Franceschi, B.T.; Bianchini, F.; Ambrosio, L.; Cintra, A.C.O.; Sampaio, S.V.; de Castro, F.A.; Torqueti, M.R. BthTX-I from Bothrops jararacussu induces apoptosis in human breast cancer cell lines and decreases cancer stem cell subpopulation. *J. Venom. Anim. Toxins Incl. Trop. Dis.* **2019**, *25*, e20190010. [CrossRef] [PubMed]
127. Murray, A.S.; Hyland, T.E.; Sala-Hamrick, K.E.; Mackinder, J.R.; Martin, C.E.; Tanabe, L.M.; Varela, F.A.; List, K. The cell-surface anchored serine protease TMPRSS13 promotes breast cancer progression and resistance to chemotherapy. *Oncogene* **2020**, *39*, 6421–6436. [CrossRef] [PubMed]
128. Krasny, L.; Huang, P.H. Data-independent acquisition mass spectrometry (DIA-MS) for proteomic applications in oncology. *Mol. Omics* **2021**, *17*, 29–42. [CrossRef] [PubMed]
129. Zhao, W.; Li, J.; Chen, M.M.; Luo, Y.; Ju, Z.; Nesser, N.K.; Johnson-Camacho, K.; Boniface, C.T.; Lawrence, Y.; Pande, N.T.; et al. Large-Scale Characterization of Drug Responses of Clinically Relevant Proteins in Cancer Cell Lines. *Cancer Cell* **2020**, *38*, 829–843.e4. [CrossRef]
130. Klaeger, S.; Heinzlmeir, S.; Wilhelm, M.; Polzer, H.; Vick, B.; Koenig, P.A.; Reinecke, M.; Ruprecht, B.; Petzoldt, S.; Meng, C.; et al. The target landscape of clinical kinase drugs. *Science* **2017**, *358*. [CrossRef]
131. Qi, Z.; Zhang, L.; Chen, Y.; Ma, X.; Gao, X.; Du, J.; Zhang, F.; Cheng, X.; Cui, W. Biological variations of seven tumor markers. *Clin. Chim. Acta* **2015**, *450*, 233–236. [CrossRef]
132. Lamond, A.I.; Mann, M. Cell biology and the genome projects a concerted strategy for characterizing multiprotein complexes by using mass spectrometry. *Trends Cell Biol.* **1997**, *7*, 139–142. [CrossRef]
133. Tavares, C.; Maciel, T.; Burin, S.; Ambrosio, L.; Ghisla, S.; Sampaio, S.; Castro, F. l-Amino acid oxidase isolated from Calloselasma rhodostoma snake venom induces cytotoxicity and apoptosis in JAK2V617F-positive cell lines. *Rev. Bras. Hematol. Hemoter.* **2016**, *38*, 128–134. [CrossRef]
134. Zakraoui, O.; Marcinkiewicz, C.; Aloui, Z.; Othman, H.; Grepin, R.; Haoues, M.; Essafi, M.; Srairi-Abid, N.; Gasmi, A.; Karoui, H.; et al. Lebein, a snake venom disintegrin, suppresses human colon cancer cells proliferation and tumor-induced angiogenesis through cell cycle arrest, apoptosis induction and inhibition of VEGF expression. *Mol. Carcinog.* **2017**, *56*, 18–35. [CrossRef] [PubMed]
135. Bernardes-Oliveira, E.; Gomes, D.L.; Martelli Palomino, G.; Juvenal Silva Farias, K.; da Silva, W.D.; Rocha, H.A.; Goncalves, A.K.; Fernandes-Pedrosa, M.F.; Crispim, J.C. Bothrops jararaca and Bothrops erythromelas Snake Venoms Promote Cell Cycle Arrest and Induce Apoptosis via the Mitochondrial Depolarization of Cervical Cancer Cells. *Evid. Based Complement. Altern. Med.* **2016**, *2016*, 1574971. [CrossRef]
136. Knorre, D.G.; Kudryashova, N.V.; Godovikova, T.S. Chemical and functional aspects of posttranslational modification of proteins. *Acta Nat.* **2009**, *1*, 23.
137. Freed, E.F.; Bleichert, F.; Dutca, L.M.; Baserga, S.J. When ribosomes go bad: Diseases of ribosome biogenesis. *Mol. Biosyst* **2010**, *6*, 481–493. [CrossRef]
138. Ruggero, D.; Pandolfi, P.P. Does the ribosome translate cancer? *Nat. Rev. Cancer* **2003**, *3*, 179–192. [CrossRef]
139. Bilanges, B.; Stokoe, D. Mechanisms of translational deregulation in human tumors and therapeutic intervention strategies. *Oncogene* **2007**, *26*, 5973–5990. [CrossRef] [PubMed]
140. Hershko, A. Ubiquitin: Roles in protein modification and breakdown. *Cell* **1983**, *34*, 11–12. [CrossRef]
141. Hershko, A.; Ciechanover, A. The ubiquitin system. *Annu. Rev. Biochem.* **1998**, *67*, 425–479. [CrossRef]
142. Jankowska, E.; Stoj, J.; Karpowicz, P.; Osmulski, P.A.; Gaczynska, M. The proteasome in health and disease. *Curr. Pharm. Des.* **2013**, *19*, 19.
143. Pajonk, F.; McBride, W.H. The Proteasome in Cancer Biology and Treatment. *Radiat. Res.* **2001**, *156*, 447–459. [CrossRef]
144. Teicher, B.A.; Ara, G.; Herbst, R.; Palombella, V.J.; Adams, J. The proteasome inhibitor PS-341 in cancer therapy. *Clin. Cancer Res.* **1999**, *5*, 2638–2645. [PubMed]
145. Thul, P.J.; Lindskog, C. The human protein atlas: A spatial map of the human proteome. *Protein Sci.* **2018**, *27*, 233–244. [CrossRef]
146. Dias, M.H.; Fonseca, C.S.; Zeidler, J.D.; Albuquerque, L.L.; da Silva, M.S.; Cararo-Lopes, E.; Reis, M.S.; Noel, V.; Dos Santos, E.O.; Prior, I.A.; et al. Fibroblast Growth Factor 2 lethally sensitizes cancer cells to stress-targeted therapeutic inhibitors. *Mol. Oncol.* **2019**, *13*, 290–306. [CrossRef] [PubMed]

147. Montoni, F.; Andreotti, D.Z.; Eichler, R.; Santos, W.D.S.; Kisaki, C.Y.; Arcos, S.S.S.; Lima, I.F.; Soares, M.A.M.; Nishiyama-Jr, M.Y.; Nava-Rodrigues, D.; et al. The impact of rattlesnake venom on mice cerebellum proteomics points to synaptic inhibition and tissue damage. *J. Proteom.* **2020**, *221*, 103779. [CrossRef]
148. Mi, H.; Muruganujan, A.; Huang, X.; Ebert, D.; Mills, C.; Guo, X.; Thomas, P.D. Protocol Update for large-scale genome and gene function analysis with the PANTHER classification system (v.14.0). *Nat. Protoc.* **2019**, *14*, 703–721. [CrossRef] [PubMed]
149. Mi, H.; Poudel, S.; Muruganujan, A.; Casagrande, J.T.; Thomas, P.D. PANTHER version 10: Expanded protein families and functions, and analysis tools. *Nucleic Acids Res.* **2016**, *44*, D336–D342. [CrossRef]
150. Thomas, P.D.; Campbell, M.J.; Kejariwal, A.; Mi, H.; Karlak, B.; Daverman, R.; Diemer, K.; Muruganujan, A.; Narechania, A. PANTHER: A library of protein families and subfamilies indexed by function. *Genome Res.* **2003**, *13*, 2129–2141. [CrossRef]
151. Thomas, P.D.; Kejariwal, A.; Campbell, M.J.; Mi, H.; Diemer, K.; Guo, N.; Ladunga, I.; Ulitsky-Lazareva, B.; Muruganujan, A.; Rabkin, S.; et al. PANTHER: A browsable database of gene products organized by biological function, using curated protein family and subfamily classification. *Nucleic Acids Res.* **2003**, *31*, 334–341. [CrossRef]
152. Cox, J.; Hein, M.Y.; Luber, C.A.; Paron, I.; Nagaraj, N.; Mann, M. Accurate proteome-wide label-free quantification by delayed normalization and maximal peptide ratio extraction, termed MaxLFQ. *Mol. Cell Proteom.* **2014**, *13*, 2513–2526. [CrossRef] [PubMed]
153. Tyanova, S.; Temu, T.; Sinitcyn, P.; Carlson, A.; Hein, M.Y.; Geiger, T.; Mann, M.; Cox, J. The Perseus computational platform for comprehensive analysis of (prote)omics data. *Nat. Methods* **2016**, *13*, 731–740. [CrossRef] [PubMed]
154. Szklarczyk, D.; Franceschini, A.; Wyder, S.; Forslund, K.; Heller, D.; Huerta-Cepas, J.; Simonovic, M.; Roth, A.; Santos, A.; Tsafou, K.P.; et al. STRING v10: Protein-protein interaction networks, integrated over the tree of life. *Nucleic Acids Res.* **2015**, *43*, D447–D452. [CrossRef]
155. Lê, S.; Josse, J.; Husson, F. FactoMineR: AnRPackage for Multivariate Analysis. *J. Stat. Softw.* **2008**, *25*. [CrossRef]

ANEXO B. ARTIGOS EM PREPARAÇÃO

Arcos SSS, Evangelista KB, Santos WS, Portaro FCV, Chen Z, Iwai LK. Scorpion venom as a potential source for cancer drug: diagnosis and therapy.
Short review. A ser submetido para *Toxicon*

Abukawa FM, **Arcos SSS**, Ishihara MA, Castro FS, Santos WS, Iwai LK, Nishiyama Jr MY. A hybrid approach for identification and classification of arachnids venom components.
A ser submetido para *Frontiers in Pharmacology*

Toxicon: X

Scorpion venom as a potential source for cancer drug: diagnosis and therapy

--Manuscript Draft--

Manuscript Number:	
Article Type:	Short review
Section/Category:	Translational applications of toxins
Keywords:	Scorpion venom; cancer; drug discovery
Corresponding Author:	Leo Kei Iwai, PhD Instituto Butantan Sao Paulo, Sao Paulo BRAZIL
First Author:	Stephanie Santos Suehiro Arcos
Order of Authors:	Stephanie Santos Suehiro Arcos
	Kimberly Borges Evangelista
	Wellington da Silva Santos
	Fernanda Calheta Vieira Portaro, PhD
	Zhibin Chen, MD, PhD
	Leo Kei Iwai, PhD
Abstract:	Cancer is defined as abnormal cells that divide without control and can invade nearby tissues, causing a disruption in the body's homeostasis and may spread to other parts of the body becoming a metastasis. Surgery, chemotherapy and immune therapy have saved many lives but the limits of their efficacy are also well known. As such, the search for innovative treatments against cancer has been an ongoing endeavor. Alternative therapies using medical applications of animal venoms are not commonly discussed for effective cancer treatment. Venoms are a cocktail of complex mixtures of proteins, peptides, amino acids, mucoproteins, enzymes, inorganic salts and ions. Scorpion venom toxins are known for their negative and deleterious effects on cells, tissues and organisms. Moreover, some components of scorpion venoms have shown antimicrobial, anticancer and immunomodulatory activities. In this review, we describe the biomedical and immunological action of different scorpion venoms in cancer and their mechanisms of action with a potential to be explored for the development of new drugs for cancer therapy and treatment.
Suggested Reviewers:	Matheus Freitas Fernandes Pedrosa, PhD Associate Professor, Federal University of Rio Grande do Norte: Universidade Federal do Rio Grande do Norte mpedrosa@ufrnet.br; mffpedrosa@gmail.com He has experience in biotechnology, with emphasis on scorpion peptides (transcriptomics, proteomics, structural characterization and biological activity), snake proteins (biological activity and natural anti-venom products), inflammation and immunobiological production.
	Maria Elena de Lima, PhD Full professor, Universidade Federal de Minas Gerais Instituto de Ciências Biológicas: Universidade Federal de Minas Gerais Instituto de Ciencias Biologicas melenalima@icb.ufmg.br Expert in arthropod venoms such as Phoneutria, Tityus, and Lycosa with an emphasis on identification and analysis of peptides with antimicrobial, anticancer, insecticide, antinociceptive, erectile function applications in health and biotechnology.
Opposed Reviewers:	

Cover Letter

Secretaria de Estado da Saúde
Coordenadoria de Ciência, Tecnologia e Insumos Estratégicos de Saúde
Instituto Butantan
Laboratório Especial de Toxinologia Aplicada

21 December 2021

Prof Glenn King and Prof Ray Norton
Co-Editors-in-Chief
Toxicon: X

Re: Scorpion venom as a potential source for cancer drug: diagnosis and therapy

Dear Profs Glenn King and Ray Norton,

We would be grateful if you would consider our enclosed manuscript entitled "Scorpion venom as a potential source for cancer drug: diagnosis and therapy" by Arcos et al as a short review article in Toxicon: X.

It is known that scorpion venom of several species is a source of drug for both diagnosis and therapy of different diseases including cancer. In this short review, we describe the biomedical and immunological action of different scorpion venoms in cancer and their mechanisms of action with a potential to be explored for the development of new drugs for cancer therapy and treatment.

We hope the Editors will find the manuscript appropriate to be published in Toxicon: X.

Thank you for your consideration of this manuscript.

Sincerely yours,

Dr Leo Kei Iwai
Laboratory of Applied Toxinology (LETA)
Center of Toxins, Immune-response and Cell Signaling (CeTICS)
Butantan Institute

Av. Vital Brasil, 1.500 – Butantã – São Paulo – SP – 05503-900
Tel. (55 11) 2627-9502 / 9504
e-mail: instituto@butantan.gov.br
www.butantan.gov.br

Declaration of Interest Statement

Declaration of interests

☒ The authors declare that they have no known competing financial interests or personal relationships that could have appeared to influence the work reported in this paper.

☐The authors declare the following financial interests/personal relationships which may be considered as potential competing interests:

Scorpion venom as a potential source for cancer drug: diagnosis and therapy

Stephanie Santos Suehiro Arcos, Kimberly Borges Evangelista, Wellington da Silva Santos, Fernanda Calheta Vieira Portaro, Zhibin Chen, Leo Kei Iwai

Ethical statement:

The authors guarantee that the works presented in this show review manuscript follow the rules of ethics and respect the duties of authors presented in the Elsevier´s Ethical Guidelines for Journal Publication

Credit Author Statement

Scorpion venom as a potential source for cancer drug: diagnosis and therapy

CRediT author statement

Stephanie Santos Suehiro Arcos: Conceptualization, Writing-Original draft, Writing-Review & Editing

Kimberly Borges Evangelista: Writing-Original draft, Writing-Review & Editing

Wellington da Silva Santos: Writing-Review & Editing

Fernanda Calheta Vieira Portaro: Conceptualization, Writing-Original draft, Writing-Review & Editing, Supervision, Funding acquisition

Zhibin Chen: Conceptualization, Writing-Original draft, Writing-Review & Editing, Supervision, Funding acquisition

Leo Kei Iwai: Conceptualization, Writing-Original draft, Writing-Review & Editing, Supervision, Funding acquisition

Graphical Abstract

Scorpion venom as a potential source for cancer drug: diagnosis and therapy

Stephanie Santos Suehiro Arcos, Kimberly Borges Evangelista, Wellington da Silva Santos, Fernanda Calheta Vieira Portaro, Zhibin Chen, Leo Kei Iwai

Graphical Abstract

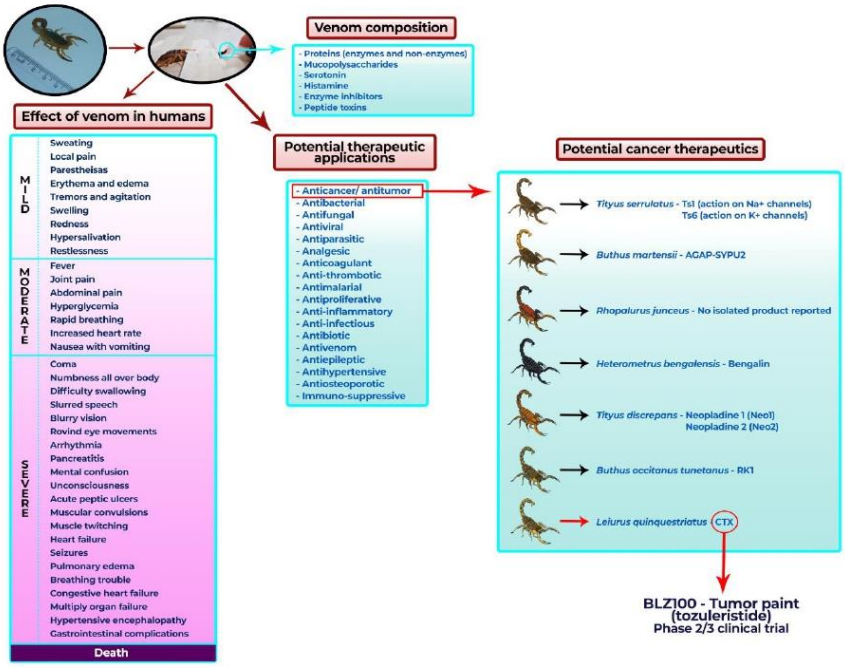

Scorpion venom as a potential source for cancer drug: diagnosis and therapy

Stephanie Santos Suehiro Arcos, Kimberly Borges Evangelista, Wellington da Silva Santos, Fernanda Calheta Vieira Portaro, Zhibin Chen, Leo Kei Iwai

Highlights:

- Cancer is one of the leading causes of death in the world
- Surgery, chemotherapy, radiotherapy, and immune therapy have saved many lives but their efficacy is limited
- Animal venoms are a rich source of natural compounds that may be used to treating diseases including cancer
- Scorpion venom contain toxins that have been used for the treatment of several diseases including cancer
- More effective drugs for therapeutics and diagnosis of cancer may be developed from scorpion venom

Scorpion venom as a potential source for cancer drug: diagnosis and therapy

Stephanie Santos Suehiro Arcos[1], Kimberly Borges Evangelista[1], Wellington da Silva Santos[1], Fernanda Calheta Vieira Portaro[2], Zhibin Chen[3], Leo Kei Iwai[1*]

1. Laboratory of Applied Toxinology (LETA) and Center of Toxins, Immune-Response and Cell Signaling (CeTICS), Butantan Institute, São Paulo, 05503-900, Brazil

2. Laboratory of Structure and Functions of Biomolecules, Butantan Institute, São Paulo, 05503-900, Brazil

3. Department of Microbiology and Immunology, University of Miami Miller School of Medicine, Miami, FL 33136, USA.

Running Title: **Scorpion venom as a source for cancer drug**

***Corresponding author**

Dr. Leo K. Iwai, Av. Vital Brasil, 1500, São Paulo, SP, 05503-900, Brazil

Phone: +55 11 2627 9731

E-mail: leo.iwai@butantan.gov.br

Abstract

Cancer is defined as abnormal cells that divide without control and can invade nearby tissues, causing a disruption in the body's homeostasis and may spread to other parts of the body becoming a metastasis. Surgery, chemotherapy and immune therapy have saved many lives but the limits of their efficacy are also well known. As such, the search for innovative treatments against cancer has been an ongoing endeavor. Alternative therapies using medical applications of animal venoms are not commonly discussed for effective cancer treatment. Venoms are a cocktail of complex mixtures of proteins, peptides, amino acids, mucoproteins, enzymes, inorganic salts and ions. Scorpion venom toxins are known for their negative and deleterious effects on cells, tissues and organisms. Moreover, some components of scorpion venoms have shown antimicrobial, anticancer and immunomodulatory activities. In this review, we describe the biomedical and immunological action of different scorpion venoms in cancer and their mechanisms of action with a potential to be explored for the development of new drugs for cancer therapy and treatment.

Keywords: Scorpion venom, cancer, drug discovery.

1. Introduction

Cancer is a comprehensive term for a large cluster of diseases that can affect any part of the body. It is one of the most deadly diseases worldwide, accounting for nearly 10 million deaths only in 2020, according to the World Health Organization [1]. There are several types of cancer. In terms of new cases, the most common types of cancer in 2020 were: breast (2.26 million cases), lung (2.21 million cases), colon and rectum (1.93 million cases), prostate (1.41 million cases), skin (non-melanoma) (1.20 million cases), and stomach (1.09 million cases); and the most common causes of cancer death in 2020 were lung (1.80 million deaths), colon and rectum (935.000 deaths), liver (830.000 deaths), stomach (769.000 deaths), and breast (685.000 deaths) [1].

Cancer is defined as abnormal cells that divide without control and can invade nearby tissues, causing a disruption in the body's homeostasis. It can also spread to other parts of the body through the blood and lymph systems, becoming a metastasis, which are the primary cause of death from cancer [2]. The incidence rate of cancer rises dramatically with age. It happens because there is a tendency for cellular repair mechanisms to be less effective as a person grows older. Still, the causes of cancer are very comprehensive, since there is no pattern for the cancer to manifest and it can be due to genetic and/or environmental factors. Cancer is the result of the interaction between inherited genetic mutation of an individual and environmental factors such as physical carcinogens (ultraviolet and ionizing radiation), chemical carcinogens (asbestos, components of tobacco smoke, aflatoxin - a food contaminant -, and arsenic - a drinking water contaminant -), and biological carcinogens (infections from certain viruses, bacteria, or parasites) [3].

Although there are preventive ways to avoid the cancer development, once it starts to grow inside the body, it will demand some kind of treatment. Early detection or diagnosis of cancer is crucial for the patient survival. A correct cancer diagnosis is essential for appropriate and effective treatment since every cancer type requires a specific treatment regimen.

Alternative therapies using medical applications of animal venoms are not commonly mentioned when discussing effective ways for cancer treatment. Traditional Medicine is often recognized as “complementary”, “alternative” or “non-conventional” medicine [4]. Some examples of these traditional medicines are the use of larvae (*Vespa manchuria* Smith) in South Korea, eaten daily during winter in order to feel less

cold; adult vespids and larvae commonly seen in various bottled spirits offered for sale and used as a fortifying in Taiwan [5 6]; products derived from the *Varanus bengalensis* lizard used to treat hemorrhoids, rheumatism, body pain and burns, as well as spider and snake bites in India [7]; rattlesnake venom pills used for curing a wide variety of ailments, including skin blotches, cancer, sores, rashes, pimples, welts, itching, rheumatism, varicose veins, face blotches, acne, blackheads, stress, heart disease, diabetes, hemorrhoids, and sexual impotence in Mexico [8]. It has been described over 165 species of reptiles used in traditional folk medicine, where the groups with the largest numbers of species were snakes (60 species), followed by lizards (51), turtles and tortoises (43), and crocodilians (11) [9]. There are currently several drugs derived from animal venom that have been approved by the Food and Drug Administration of several countries such as the Captopril, commonly used to treat high blood pressure (hypertension) and it is derived from a peptide present in the *Bothrops jararaca* snake venom. It was the first orally active inhibitor of angiotensin-converting enzyme responsible for conversion of inactive angiotensin I to the potent suppressor peptide angiotensin II [10 11]. In addition, Eptifibatide derived from the *Echis carinatus* snake venom developed as an antiplatelet drug [12], Zoconotide derived from *Conus magus* marine snail venom used for pain therapeutics [13], and Exenatide derived from *Heloderma suspectum* gila monster venom used for type 2 diabetes treatment [14].

Venoms are a cocktail of complex mixtures of proteins, peptides, amino acids, mucoproteins, enzymes and non-protein inclusions such as inorganic salts and ions. Many organisms are capable of producing venom, such as scorpions, snakes, spiders, centipedes, frogs, fishes and even birds.

Toxins related to the scorpion venom are known for their negative and deleterious effects on cells, tissues and organisms. However, despite their toxicity, scorpion venoms are also a rich mixture of bioactive compounds, which are a natural source of molecules that have been used for the benefit of human health. Thus, antagonistically, some components of scorpion venoms have shown antimicrobial, anticancer, and immunosuppressive activities with potential for the development of pharmaceutical drugs [15]. Scorpion venom is composed by a mixture of several different proteins (enzymes and non-enzymes), mucopolysaccharides, serotonin, histamine, enzyme inhibitors, and peptide toxins [16].

109 Studies that permeate anticancer activities have shown that venom molecules
110 of some scorpions inhibited the growth of human glioma [17], prevented proliferation,
111 induced apoptosis in leukemic cells [18], inhibited growth and induced apoptosis in
112 human prostate cancer cells (DU145) [19] and have differential and selective toxicity
113 against epithelial cancer cells [20]. In addition, Soroceanu and colleagues (1998)
114 showed that the use of chlorotoxin, a 36 amino acid peptide derived from the *Leiurus*
115 *quinquestriatus* scorpion venom, was efficient in marking primary brain tumors
116 (gliomas) [21]. A direct application of this toxin is the Tumor Paint BLZ-100, which has
117 been in the clinical phase 2, and is used in neurosurgery to promote almost complete
118 resection of gliomas [22]. In addition, a study involving the action of two peptide
119 components from the venom of a scorpion from the genus *Tityus* (neopladine 1 and
120 neopladine 2) revealed that these molecules induce apoptosis in human breast
121 carcinoma cells (SKBR3) by inducing the expression of FasL and BcL-2 apoptosis-
122 related ligands [23]. Also, a few scorpion enzymes have been reported to have
123 anticancer activities in breast cancer, such as the serine proteinase-like protein BMK-
124 CBP [24] and a hyaluronidase BmHYA1 [25], both isolated from the *Buthus martensii*
125 scorpion venom. Moreover, a short peptide from *Buthus occitanus tunetanus* scorpion
126 venom was recently shown to present potential to inhibit tumor cell migration,
127 proliferation and angiogenesis [26 27].
128 In this review, we describe the biomedical and immunological action of different
129 scorpion venoms in cancer and their mechanisms of action that can be explored for
130 the development of drugs against cancer (Figure 1)
131

132 .

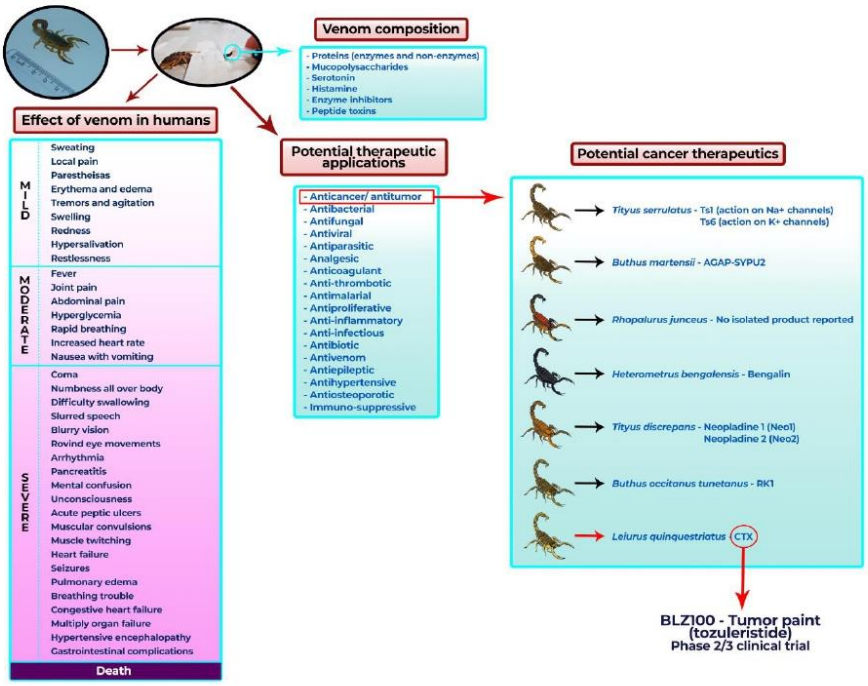

133

134 Figure 1. Scorpion venom composition, effect in humans, potential therapeutic
135 applications, and potential cancer therapeutics application.

136

137

138 **1.1. *Tityus serrulatus* scorpion venom induction of inflammation and immune**
139 **responses**

140 The *Tityus serrulatus* scorpion, popularly known as the "Brazilian yellow
141 scorpion", is one of the most medical and scientific relevant in Brazil due to the severe
142 clinical manifestations in injured victims.

143 Magalhães et al., (1999) and Fukuhara et al., (2003) analyzed the production
144 of inflammatory mediators in envenomed patients by *T. serrulatus*, and these showed
145 high levels of pro-inflammatory cytokines, such as interleukin 1 alpha (IL-1α) found in
146 mild and moderate cases, while high levels of IL-1β, IL-6, IL-8, interferon gamma (IFN-
147 γ) and granulocyte macrophage colony stimulating factor (GM-CSF) were related to
148 the severe cases, indicating a worse prognosis [28 29]. In murine macrophages, *T.*
149 *serrulatus* venom (TsV) and isolated neurotoxins - Ts1 (acting on Na+ channels) and

Ts6 (acting on K+ channels) - also increase the pro-inflammatory mediators IL-6, TNF-α and IFN-γ [16 30]. The production of these mediators is induced by the interaction of TsV and Ts1 with Toll-like 2 (TLR2) and CD14/TLR4 receptors that activate the NF-κβ and MAPK pathways [31]. It was also reported that the neurotoxin called Ts2 causes increased production of the anti-inflammatory cytokine, IL-10 [30].

Scorpion envenomation has an inflammatory response that lasts over 24 h after the accident, although the symptoms' evolution starts 5 h after the envenomation [32]. Generally, reports in mild and moderate cases are local pain, sweating, nausea, and vomiting. In severe cases, there is an evolution to systemic inflammation of the body, leading to arterial hypertension, tachycardia or bradycardia, which can lead to cardiac shock or pulmonary edema [32]. The way the immune system is activated by the scorpion venom is still not completely elucidated, however, two hypothesis are being studied: 1) Activation through depolarization and repolarization of nerve cells, leading to the release of neuropeptides that bind to inflammatory cell receptors, which in turn leads to the release of inflammatory mediators; and 2) Venom neurotoxins having direct action on inflammatory cells, which leads to the activation of macrophages and lymphocytes, generating the inflammatory process [32].

From the moment of the scorpion accident, several immune and inflammatory changes occur, which can be detected through specific blood tests. For example, after 30 minutes of scorpion sting, there is an increase in serum levels of the tumor necrosis factor TNF-∝, a pro-inflammatory cytokine that induces an immune system response, promoting systemic or local inflammation leading to vasodilation and stimulation of other cytokines and chemokines. After 120 minutes of the accident, it is observed an increase in the number of neutrophils, increase in IL-6 and a drop in spleen cells number. IL-6 is a pro-inflammatory cytokine that signals the multiplication and differentiation of B cells into antibody-forming cells and causes an exacerbation of acute inflammation signs. Within 360 minutes of the envenomation, it is observed a reduction in the amount of TNF-∝ and IL-6, and an increase in the amount of IL-10, and an increase in the number of lymph nodes, spleen cells and mast cells. IL-10 is an anti-inflammatory cytokine that acts by inhibiting the synthesis of pro-inflammatory cytokines, gradually reducing acute inflammation. IL-10 also acts as a co-stimulator of mast cells production, which acts directly on inflammation and may be a risk factor for pulmonary edema [16 33].

1.2. *Buthus martensii* Karsch scorpion venom against cancer and pain

The Asian *Buthus martensii* Karsch (BmK), also known as gold scorpion or Chinese scorpion, is a very common species in China, Mongolia, Korea, and Japan. Its venom has been used in traditional Chinese medicine to treat a variety of diseases for over 2000 years especially as a painkiller such as migraine, rheumatism-related pain, and cancer pain. Prostate cancer is an invasive type of cancer that can easily lead the patient to death. The prostate cancer progression has potential to develop from a small latent carcinoma to originate a high-grade metastasis [34 35]. The growth and development of prostate cancer is frequently androgen-dependent, making androgen-deprivation one of the most used therapies against this type of cancer [35 36]. However, there are androgen-independent carcinoma cells, making this type of treatment usually not 100% efficient [37]. As an alternative to prostate cancer treatment, Zhang and colleagues (2009) have been studying the use of a Polypeptide Extract from BmK Scorpion Venom (PESV), which is composed of a major biologically active polypeptide component of 50-60 amino acids extracted from the venom and have been reported to have anticancer activities [19]. PESV has been described as a potent anti-proliferative and anti-apoptosis induced activity against HUVEC cells, inhibition of neovascularization, and tumor growth suppression of S180 sarcoma and H22 hepatocellular carcinoma in mice [38]. Also, it has been hypothesized that PESV could be effective as a chemoprevention or intervention agent against prostate cancer, inducing DU145 cells to a cell cycle arrest, inhibiting tumor growth and inducing apoptosis [19]. PESV has also been shown to strongly induce the expression of Kip1/p27 and decrease cyclin E expression, increasing interaction with CDKIs and CDK, probably causing inhibition of kinase activity of CDKs. The uncontrolled CDKs activity is one of the major causes of cancer progression and their functions are regulated by CDKIs [39]. Still, more studies are required to support this hypothesis and to identify the exact mechanism of action of the venom in modulating mitogenic and survival signaling cascade in human prostate cancer using different prostate cancer cells and animal models [19].

In breast cancer cells, the nonsulfated glycosaminoglycan hyaluronan has been shown to be up-regulated and often correlated to tumor aggressiveness. Moreover, it has been described that hyaluronan has important physiological and pathological functions [40]. Feng and colleagues (2008) have shown that hyaluronidase isolated from BmK scorpion venom was able to completely remove hyaluronan from the triple

218 negative MDA-MB-231 breast cancer cell line [25]. Hyaluronan has shown to be
219 important in cancer cell migration, invasion, adhesion and metastasis by interacting
220 with CD44 [41], which is also expressed in high levels in cancer cells, generating CD44
221 variants (CD44v) by alternative splicing of a gene [42]. CD44v6 has been suggested
222 to be down-regulated after treatment of MDA-MB-231 with hyaluronidase, confirming
223 that the CD44 variant of cancer cells can be modulated by external signaling by
224 hyaluronidase treatment [25]. In addition, another study reported a 33 kDa serine
225 proteinase-like from the BmK (BMK-CBP) binding specifically in a dose-dependent
226 manner to the MCF-7 cancer cell membrane, although the receptor was not described
227 [24].
228 Another peptide isolated from BmK scorpion venom is AGAP-SYPU2. Shao
229 and collaborators (2014) purified AGAP-SYPU2 via bioassay-driven chromatographic
230 route, and this peptide has shown analgesic and antitumor activities in animal tests
231 Peptide GAP-SYPU2 exhibited strong analgesic effects against visceral and somatic
232 pain, and its primary sequence has high homology to sodium channel (Na^+) inhibitors
233 [43]. Scorpion α-toxins bind to sodium channels, blocking neuronal transmission [44].
234 Although BmK AGAP-SYPU2 has shown it effectiveness, its potency was slower
235 compared to the positive control painkiller, morphine [43]. Moreover, the anticancer
236 activity shown by BmK AGAP-SYPU2 prolonged the survival of 36.05% Ehrlich ascites
237 tumor mouse model and reduced the tumor weight of 46.3% S180 fibrosarcoma
238 mouse model [43]. In another work, Zhao and colleagues (2011) has demonstrated
239 that BmK AGAP can inhibit the proliferation and migration of Suzhou Human Glioma-
240 44 (SHG-44) cells derived from lymph node metastatic site, where sodium channels
241 play an important role in the proliferation and migration of cancer cells [45]. Because
242 of the high sequence identity between BmK AGAP and BmK AGAP-SYPU2, the
243 anticancer activity of BmK AGAP-SYPU2 was described to possibly involve sodium
244 channels [43]. The dual-function shown by BmK AGAP-SYPU2 as a pain reliever and
245 antitumor effects is clinically valuable, since it improves patient survival without
246 compromising the patient's quality of life [43].
247
248 **1.3. Effects of *Rhopalurus junceus* scorpion venom on cancer cells and cancer**
249 **mouse models**
250 The *Rhopalurus junceus* scorpion is an endemic species from Cuba belonging
251 to the Buthidae family. *R. junceus* venom has been used in Cuban traditional medicine

for the treatment of some illnesses, including cancer. Díaz-García and collaborators (2013) evaluated the anticancer effect of *R. junceus* scorpion venom on different cancer cell lines: HeLa, SiHa, Hep-2, NCI-H292, A549, MDA-MB-231, MDA-MB-468, and HT-29, hematopoietic cells lines: U937, K562, and Raji and normal cells: MRC-5, MDCK, and Vero. They verified that the venom induced a significant viability effect on HeLa and A549 cancer cell lines without affecting normal cells [20]. In HeLa cells, the venom induced apoptotic cell death involving p53 up-regulation, which influences the activation of pro-apoptotic genes, such as bax, and suppression of anti-apoptotic genes, such as bcl-2, which plays an important role in the activation of caspases and dominates intrinsic pathways of apoptosis [46]. These results indicate that mitochondria-mediated apoptosis is involved in scorpion venom-induced cell death in HeLa cells [20]. A more recent study showed that combinations of this scorpion venom with low concentrations of chemotherapy drugs such as 5-FU, CDDP, and DOX increased the cytotoxic effect in the HeLa cells [47].

In the adenocarcinomic human alveolar basal epithelial A549 cell line, the *R. junceus* venom induced necrotic cell death involving p53 and bcl-2 mRNA down-regulation, while bax expression level remained the same. Bcl-2 overexpression is responsible for many drug-resistant or apoptotic-resistant cancers, such as in B-cell lymphoma and small cell lung cancer [48], and it could be also responsible to mediate programmed necrosis [48 49]. Higher venom concentration, over the IC50, lead A549 cells to necrosis, while lower concentration, below IC50, lead HeLa cells to apoptosis, showing that the necrosis and apoptosis could be venom concentration dependent [20].

The investigation of the *R. junceus* scorpion venom effect in triple negative-MDA-MB-231 breast cancer cells showed that the venom has a notable anticancer activity with minimal effects on normal cells [50]. Cell morphology analysis through fluorescent DAPI staining showed that the cells treated with the scorpion venom presented shrunken and marginated nuclei in cancer cells, while the non-treated cells presented large nuclei. The authors noticed formation of apoptotic nuclei, chromatin condensation, apoptotic bodies and cell membrane blebbing, providing evidence of the apoptotic potential in those cancer cells. At the molecular level, the scorpion venom treatment induced an up-regulation of p53 gene and several pro-apoptotic genes such as bax, noxa and puma, and down-regulation of anti-apoptotic genes, such as bcl-2

and bcl-xL, possibly inducing apoptosis through the mitochondrial-apoptotic pathway [50].

In a pharmacokinetic study, investigating the biodistribution of *R. junceus* scorpion venom in tumor-bearing mice after intravenous or oral administration showed that the *R. junceus* scorpion venom has a long lasting presence in tumor tissue compared to other main organs. Both intravenous and oral administration of the *R. junceus* venom were able to reach all tissues in the body, however, the scorpion venom presence was momentary. Although the oral administration showed low bioavailability of *R. junceus* scorpion venom at all organs, suggesting high degradation of venom components, it was observed that the venom kept targeting the tumor [51].

1.4. *Heterometrus bengalensis* Koch scorpion venom and apoptosis induction in leukemic cells

Heterometrus bengalensis Koch is a scorpion that is highly prevalent in the state of West Bengal of Eastern India. Gupta and collaborators (2007) studied the *H. bengalensis* Koch venom cytotoxic profile by investigating the antiproliferative and apoptotic efficacy of *H. bengalensis* Koch venom against two human leukemic cell lines, U937 and K562. Nuclear fragmentation and margination were found in treated U937 and K562 cells in comparison with the untreated control cells, and fluorescence microscopic observations indicated nuclear disintegration when stained by ethidium bromide and acridine orange, characterizing an apoptotic event [52]. Apoptosis usually presents several morphological changes such as membrane blebbing, cell shrinkage, chromatin condensation, nuclear fragmentation and formation of apoptotic bodies [53]. Evidence from morphological changes, comet assay, and flow cytometry analysis indicated that *H. bengalensis* venom has antiproliferative and apoptogenic effects on both U937 and K562 tumor cell lines [52].

Another study from the same group isolated a component present in *H. bengalensis* venom responsible for the action described in the earlier study [18]. They isolated and purified a protein named Bengalin, which may have anticancer activity against human leukemic U937 and K562 cells. Bengalin induced U937 and K562 cell death promoting apoptosis mediated by the mitochondrial pathway where HSP70, HSP90, telomerase activity suppression and initiation of DNA damage were important features in Bengalin mediated apoptosis [18]. However, more studies are needed to

investigate the exact mechanisms of action of this compound and perform *in vivo* assays to confirm this anti-tumorigentic activity.

1.5. Effects of Neopladine 1 and Neopladine 2 from *Tityus discrepans* scorpion venom in breast cancer

As *Tityus serrulatus*, *T. discrepans* belongs to the genus *Tityus*, and is found in countries in the North and Northwest of South America, such as Brazil, Suriname, Venezuela, Guyana and Trinidad and Tobago. Breast cancer is one of the most common type of cancer worldwide. Although it has many therapies available, advanced breast cancer remains with poor alternatives. D'Suze and colleagues (2010) studied the action of *Tityus discrepans* scorpion venom and two purified peptides on human breast cancer cells (SKBR3) and on non-malignant epithelial monkey kidney cell line (MA104). They isolated the peptides Neopladine 1 (Neo1) and Neopladine 2 (Neo2), which presented active effects against SKBR3 cells via the activation of Fas signaling by induction of FasL expression [23]. The apoptotic effects were similar to those caused by *B. martensii* Karsch scorpion venom on human glioma and by Bengalin from *H. bengalensis* venom on leukemic cells [17 18]. Neopladines are a new kind of antineoplastic peptides, which are interesting as tools or as templates for novel antineoplastic drugs [23]. Olvera and colleagues have recently cloned the gene coding nNeo2 looking for the best experimental condition to express rNeo2 with high activity [54]. They found a set of eleven isoforms with potential antineoplastic properties, and some of them with a more potent activity when compared to the original peptide. These peptides have been studied to be used for biotechnological and biomedical applications. Given that chlorotoxin succeeds in better removing glioma tumors [55], neopladines should be also further studied to test their function, since they exhibit a significant selectivity for breast cancer cells [23].

1.6. RK1, a short peptide from *Buthus occitanus tunetanus* scorpion venom, inhibits tumor cell migration, proliferation, and angiogenesis

The *Buthus occitanus tunetanus* scorpion, belonging to the Buthidae family, is responsible for accidents in Middle Eastern countries such as Tunisia. RK1 is a short 14 amino acid peptide purified from the *B. o. tunetanus* scorpion venom capable of inhibiting cell proliferation, migration and angiogenesis of U87 glioblastoma cell line and IGR39 human malignant melanoma cell line. RK1 showed to have a potential anti-

tumoral activity without manifesting toxicity *in vitro* and *in vivo*, as well as a capacity to form a disulfide bond, increasing stability in physiological conditions, reducing toxic effects of chemotherapy and radiotherapy, although it strongly inhibits neoangiogenesis. In addition, due to RK1 small size, it may possibly be less immunogenic when compared to other larger molecules [26].

In another study by the same group, Khamessi and collaborators (2018b) analyzed the anti-tumoral activity of a disintegrin-like homologous peptide RK isolated from the *Buthus occitanus tunetanus* scorpion venom as a targeting molecule for cancer cell adhesion by its potential interaction with different integrins *in vivo* and *in silico* [27]. Compared to the RK1 peptide, RK has a sequence identity of 47%, where the conserved residues are localized mainly at the C- and N-terminal ends, including the disulfide bridge forming cysteines. RK has dual disintegrin activity on α1β1 and αvβ3 integrins, due to the presence of contiguous motifs ECD and KSS. This selective blockade of α1β1 and αvβ3 integrins is a desirable target for cancer therapy and tumor angiogenesis [27].

1.7. Effects of scorpion venom on gliomas: apoptosis induction and tumor paint BLZ-100

Glial cells are non-neuronal cells that do not produce electrical impulses. Glia surround and support nerve cells, protecting neurons and forming myelin in the peripheral nervous system and glioma is a type of brain cancer that affects glial cells [56]. Malignant gliomas are notoriously resistant to currently available therapies, since they fail to undergo apoptosis upon any anticancer treatment [17].

Several early studies have shown that polypeptidyl toxins purified from the venom from *Buthus martensii* Karsch (BmK) scorpion specifically interfere with several ion channels, altering their functional properties [57-61]. Later, Wang and collaborators (2005) showed that BmK venom induces human glioblastoma astrocytoma U251-MG cell death, although it did not induce apoptosis in non-glioma control cells lineages such as the BEL7404 human hepatocellular carcinoma cells and the CHOC400 Chinese hamster ovary cells, leading to the conclusion that BmK venom specifically triggers glioma cell death *in vitro*. Moreover, they observed that BmK were able to inhibit glioma tumor growth *in vivo*. Authors showed that Na^+, K^+ and Cl^- ion channels play a key role in the processes of glioma cell proliferation, swelling, migration, invasion, and apoptosis. The dysfunction of these channels by the BmK venom may

386 be the key for the negative effects on the gliomas, however, more studies are still
387 needed to investigate the key factor that induce glioma apoptosis by the BmK venom
388 [17].
389 Soroceanu and colleagues (1998) have studied a glioma-specific chloride ion
390 channel that is sensitive to chlorotoxin (CTX), which is derived from *Leiurus*
391 *quinquestriatus* scorpion venom [21]. CTX is a 36 amino acid peptide that specifically
392 binds to MMP-2 and small conductance Cl^- channels [21 62 63]. The CTX peptide
393 shows a specificity as a tumor-targeting agent in a diversity of forms, including
394 radiolabeled, conjugated to fluorescent tags, or incorporated into nanoparticles [64-
395 66].
396 Many clinical trials demonstrated that CTX toxicity to humans is low, making
397 this peptide attractive as a targeted imaging agent for cancer [22]. The Tumor Paint
398 BLZ-100 has been developed by Blaze Bioscience and is derived from CTX peptide.
399 It has been studied as a new agent to assist in tumor brain surgeries, specifically
400 gliomas. BLZ-100 is a tumor ligand made of synthetic CTX conjugated to ICG. The
401 potential of BLZ-100 as a targeted contrast agent is still being tested on animals and
402 humans. However, many studies have already shown successful results on painting
403 gliomas and even other types of injuries, and it is being evaluated in a phase 2/3
404 clinical study in pediatric CNS tumors [22 67-70].
405 In mouse models studies of glioma, medulloblastoma, prostate cancer,
406 sarcoma, and colorectal cancer, the CTX conjugated to Cy5.5 (a fluorescent molecular
407 beacon that emits photons in the near-IR or NIR spectrum) showed a binding to both
408 primary tumor and metastasis [55]. NIR beacons suit better for intraoperative imaging,
409 since photons of this wavelength are minimally absorbed by water or hemoglobin.
410 Studies on mouse models revealed that BLZ-100 was successfully administered and
411 used as an aid during tumor brain surgery removal [22 67].
412 A clinical study testing the BLZ-100 in canine patients with spontaneously
413 occurring tumors was also successfully and safely applied [68]. In addition, the value
414 of comparative oncology studies in drug development between humans and dogs is
415 well-recognized, since their cancers have features similar to those seen in human
416 tumors [71 72]. Therefore, the agents developed for use in humans are frequently used
417 in the veterinary field, making these comparative oncology studies also beneficial to
418 animals [72].

Fidel and collaborators (2015) found that BLZ-100 was safe and effective in detecting tumors using real-time fluorescence imaging during surgery in dogs, providing key information to support clinical translation of the product. Many studies reached a safety profile as a human product candidate, testing BLZ-100 with success in CD-1 mice, Sprague Dawley rats, beagle dogs and other species of dogs, and cynomolgus monkeys [68 69].

In a recent study in humans revealed that BLZ-100 also has the potential to "paint" other tissues beyond tumors. Kobets and colleagues (2021) found an unexpected binding of BLZ-100 to cerebral vascular malformations while participating in a phase 2/3 study of intraoperative near infrared fluorescence detection of pediatric primary central nervous system tumors in patients receiving BLZ-100 intravenously [70]. Two patients were diagnosed with intracranial lesions, suspected of being gliomas, although these lesions proved to be cavernous vascular malformations during the surgery. The drug was administered by an IV bolus injection at least 1h and no more than 36 h preoperatively, at a dose of 15 mg/mL. Both patients (a 12 year old boy and a 15 year old girl) were randomized to receive BLZ-100, administered intravenously before surgery. Canvas imaging showed avid fluorescence of their lesion, making the surgical resection easier to perform [70].

More recently, Yamada and colleagues (2021) described the use of BLZ-100 in 21 adult patients with known or suspected non-metastatic basal cell or squamous cell carcinoma or non-metastatic melanoma to assess its safety, tolerability, and pharmacokinetics. The BLZ-100 showed to be safe at doses up to 18 mg with an effective and accurate imaging at doses between 3 and 12 mg after 15 min to 2 h post injection [73]. Further investigation is still ongoing to determine if BLZ-100 may have a wider range application in identifying pathologies beyond cancer and vascular malformations.

2. Conclusions

Cancer is one of the most deadly diseases worldwide, despite the various breakthroughs that have saved many lives, together with standard treatments to cancer, such as tumor removal by surgery, or chemotherapy and radiotherapy. The scientific community has always been on the journey searching for innovative medications to cure or to attenuate symptoms and prolong the lifespan of the patient.

452 The study of natural products, especially venoms from different kinds of species
453 aiming at the treatment of cancer is a relatively new field. In particular, studies involving
454 scorpion venom, which presents several toxins and potential anti-cancer compounds,
455 have been increasing along with the years. One example is the BLZ-100 that is a
456 promising tool that has been developed to help in medical surgeries to remove tumors.
457 We expect that other promising tools or drugs derived from scorpion venom may be
458 developed in the near future since venom from these animals may contain several
459 molecules able to treat cancer.
460
461
462 **Funding**
463 This work was supported by the grants 2013/07467-1, 2016/04000-3, 2017/17943-6, and
464 2019/20832-7 from the São Paulo Research Foundation (FAPESP). SSSA was supported by
465 CNPq # 131408/2019-4 (University of São Paulo, Brazil). ZC was supported in part a grant
466 from the National Cancer Institute (NCI) of National Institutes of Health (NIH) R01CA245673.
467
468
469 **Author contributions**
470 SSSA: Conceptualization, Writing-Original draft, Writing-Review & Editing; KBE: Writing-
471 Original draft, Writing-Review & Editing; WSS: Writing-Review & Editing; FCVP:
472 Conceptualization, Writing-Original draft, Writing-Review & Editing, Supervision, Funding
473 acquisition; ZC: Conceptualization, Writing-Original draft, Writing-Review & Editing,
474 Supervision, Funding acquisition; LKI: Conceptualization, Writing-Original draft, Writing-
475 Review & Editing, Supervision, Funding acquisition
476
477
478 **Declaration of competing interest**
479 The authors have no conflict of interest.
480
481
482 **References**
483
484 1. World Health Organization. WHO Cancer. Secondary Cancer 2021.
485 https://www.who.int/news-room/fact-sheets/detail/cancer. Last accessed in August
486 2021
487 2. Ferlay JE, M.; Lam, F.; Colombet, M; Mery, L.; Piñeros, M.; Znaor, A.; Soerjomataram, I.;
488 Bray, F. Global Cancer Observatory: Cancer Today. Lyon, France: International

Agency for Research on Cancer. Secondary Global Cancer Observatory: Cancer Today. Lyon, France: 2020. https://gco.iarc.fr/today.
3. de Martel C, Georges D, Bray F, Ferlay J, Clifford GM. Global burden of cancer attributable to infections in 2018: a worldwide incidence analysis. The Lancet Global Health 2020;**8**(2):e180-e90 doi: 10.1016/s2214-109x(19)30488-7 .
4. Qiu J. Traditional medicine: a culture in the balance. Nature 2007;**448**(7150):126-8 doi: 10.1038/448126a .
5. Posey DA. Topics and issues in ethnoentomology with some suggestions for the development of hypothesis-generation and testing in ethnobiology. J. Ethnobiol 1986;**6**(1):21
6. Pemberton RW. Insects and other arthropods used as drugs in Korean traditional medicine. Journal of Ethnopharmacology 1999;**65**(3):207-16 doi: 10.1016/s0378-8741(98)00209-8 .
7. Kakati LN, Ao B, Doulo V. Indigenous Knowledge of Zootherapeutic Use of Vertebrate Origin by the Ao Tribe of Nagaland. Journal of Human Ecology 2017;**19**(3):163-67 doi: 10.1080/09709274.2006.11905874 .
8. Rubio M. *Rattlesnake: portrait of a predator*. 1st Edition ed. Springfield, VA, USA: Smithsonian Books, 1998.
9. da Nóbrega Alves RR, da Silva Vieira WL, Santana GG. Reptiles used in traditional folk medicine: conservation implications. Biodiversity and Conservation 2008;**17**(8):2037-49 doi: 10.1007/s10531-007-9305-0 .
10. Ferreira SH. A Bradykinin-Potentiating Factor (Bpf) Present in the Venom of Bothrops Jararca. Br J Pharmacol Chemother 1965;**24**:163-9 doi: 10.1111/j.1476-5381.1965.tb02091.x .
11. Vidt DG, Bravo EL, Fouad FM. Medical intelligence drug therapy: captopril. N Engl J Med 1982;**306**(4):214-9 doi: 10.1056/NEJM198201283060405 .
12. Phillips DR, Scarborough RM. Clinical Pharmacology of Eptifibatide. The American Journal of Cardiology 1997;**80**(4):11B-20B doi: 10.1016/s0002-9149(97)00572-9 .
13. McIntosh M, Cruz LJ, Hunkapiller MW, Gray WR, Olivera BM. Isolation and structure of a peptide toxin from the marine snail *Conus magus*. Archives of Biochemistry and Biophysics 1982;**218**(1):329-34 doi: 10.1016/0003-9861(82)90351-4 .
14. Eng J, Kleinman WA, Singh L, Singh G, Raufman JP. Isolation and characterization of exendin-4, an exendin-3 analogue, from Heloderma suspectum venom. Further evidence for an exendin receptor on dispersed acini from guinea pig pancreas. Journal of Biological Chemistry 1992;**267**(11):7402-05 doi: 10.1016/s0021-9258(18)42531-8 .
15. Ortiz E, Gurrola GB, Schwartz EF, Possani LD. Scorpion venom components as potential candidates for drug development. Toxicon 2015;**93**:125-35 doi: 10.1016/j.toxicon.2014.11.233 .
16. Petricevich VL. Scorpion venom and the inflammatory response. Mediators Inflamm 2010;**2010**:903295 doi: 10.1155/2010/903295 .
17. Wang WX, Ji YH. Scorpion venom induces glioma cell apoptosis in vivo and inhibits glioma tumor growth in vitro. J Neurooncol 2005;**73**(1):1-7 doi: 10.1007/s11060-004-4205-6 .
18. Gupta SD, Gomes A, Debnath A, Saha A, Gomes A. Apoptosis induction in human leukemic cells by a novel protein Bengalin, isolated from Indian black scorpion venom: through mitochondrial pathway and inhibition of heat shock proteins. Chem Biol Interact 2010;**183**(2):293-303 doi: 10.1016/j.cbi.2009.11.006 .
19. Zhang YY, Wu LC, Wang ZP, et al. Anti-proliferation Effect of Polypeptide Extracted from Scorpion Venom on Human Prostate Cancer Cells in vitro. J Clin Med Res 2009;**1**(1):24-31 doi: 10.4021/jocmr2009.01.1220 .
20. Diaz-Garcia A, Morier-Diaz L, Frion-Herrera Y, et al. In vitro anticancer effect of venom from Cuban scorpion Rhopalurus junceus against a panel of human cancer cell lines. J Venom Res 2013;**4**:5-12
21. Soroceanu LG, Y.; Khazaeli, M.B.; Sontheimer, H. Use of chlorotoxin for targeting of primary brain tumors. Cancer Res 1998;**58**(21):9

22. Butte PV, Mamelak A, Parrish-Novak J, et al. Near-infrared imaging of brain tumors using the Tumor Paint BLZ-100 to achieve near-complete resection of brain tumors. Neurosurg Focus 2014;**36**(2):E1 doi: 10.3171/2013.11.FOCUS13497 .
23. D'Suze G, Rosales A, Salazar V, Sevcik C. Apoptogenic peptides from Tityus discrepans scorpion venom acting against the SKBR3 breast cancer cell line. Toxicon 2010;**56**(8):1497-505 doi: 10.1016/j.toxicon.2010.09.008 .
24. Gao R, Zhang Y, Gopalakrishnakone P. Purification and N-terminal sequence of a serine proteinase-like protein (BMK-CBP) from the venom of the Chinese scorpion (Buthus martensii Karsch). Toxicon 2008;**52**(2):348-53 doi: 10.1016/j.toxicon.2008.06.003 .
25. Feng L, Gao R, Gopalakrishnakone P. Isolation and characterization of a hyaluronidase from the venom of Chinese red scorpion Buthus martensi. Comp Biochem Physiol C Toxicol Pharmacol 2008;**148**(3):250-7 doi: 10.1016/j.cbpc.2008.06.003 .
26. Khamessi O, Ben Mabrouk H, ElFessi-Magouri R, Kharrat R. RK1, the first very short peptide from Buthus occitanus tunetanus inhibits tumor cell migration, proliferation and angiogenesis. Biochem Biophys Res Commun 2018;**499**(1):1-7 doi: 10.1016/j.bbrc.2018.01.133 .
27. Khamessi O, Ben Mabrouk H, Othman H, et al. RK, the first scorpion peptide with dual disintegrin activity on alpha1beta1 and alphavbeta3 integrins. Int J Biol Macromol 2018;**120**(Pt B):1777-88 doi: 10.1016/j.ijbiomac.2018.09.180 .
28. Magalhães MM, Pereira MES, Amaral CFS, et al. Serum levels of cytokines in patients envenomed by Tityus serrulatus scorpion sting. Toxicon 1999;**37**(8):1155-64 doi: 10.1016/s0041-0101(98)00251-7 .
29. Fukuhara YDM, Reis ML, Dellalibera-Joviliano R, Cunha FQC, Donadi EA. Increased plasma levels of IL-1β, IL-6, IL-8, IL-10 and TNF-α in patients moderately or severely envenomed by Tityus serrulatus scorpion sting. Toxicon 2003;**41**(1):49-55 doi: 10.1016/s0041-0101(02)00208-8 .
30. Zoccal KF, Bitencourt Cda S, Secatto A, et al. Tityus serrulatus venom and toxins Ts1, Ts2 and Ts6 induce macrophage activation and production of immune mediators. Toxicon 2011;**57**(7-8):1101-8 doi: 10.1016/j.toxicon.2011.04.017 .
31. Zoccal KF, Bitencourt Cda S, Sorgi CA, et al. Ts6 and Ts2 from Tityus serrulatus venom induce inflammation by mechanisms dependent on lipid mediators and cytokine production. Toxicon 2013;**61**:1-10 doi: 10.1016/j.toxicon.2012.10.002 .
32. Monica S-F, Orlando R, Nancy S, et al. Mice selected for acute inflammatory response display a higher lung inflammation induced by Tityus serrulatus scorpion venom. Frontiers in Immunology 2013;**4** doi: 10.3389/conf.fimmu.2013.02.01051 .
33. Fialho EM, Maciel MC, Silva AC, et al. Immune cells recruitment and activation by Tityus serrulatus scorpion venom. Toxicon 2011;**58**(6-7):480-5 doi: 10.1016/j.toxicon.2011.08.006 .
34. De Marzo AM, Meeker AK, Zha S, et al. Human prostate cancer precursors and pathobiology. Urology 2003;**62**(5 Suppl 1):55-62 doi: 10.1016/j.urology.2003.09.053 .
35. Nelson WG, De Marzo AM, Deweese TL, et al. Preneoplastic prostate lesions: an opportunity for prostate cancer prevention. Ann N Y Acad Sci 2001;**952**:135-44 doi: 10.1111/j.1749-6632.2001.tb02734.x .
36. Bostwick DG, Qian J. Effect of androgen deprivation therapy on prostatic intraepithelial neoplasia. Urology 2001;**58**(2):91-93 doi: 10.1016/s0090-4295(01)01248-1 .
37. Feldman BJ, Feldman D. The development of androgen-independent prostate cancer. Nat Rev Cancer 2001;**1**(1):34-45 doi: 10.1038/35094009 .
38. Zhang WDC, Y. Z.; Yao, C. F.; Jia, Q.; Song, S. Q.; Wang, Z. X.; Dong, Q. Polypeptide extract from scorpion venom inhibits angiogenesis and angiogenesis-dependent tumor growth. Chin. Pharmacol. Bull. 2005;**21**(6):4
39. Marak BN, Dowarah J, Khiangte L, Singh VP. A comprehensive insight on the recent development of Cyclic Dependent Kinase inhibitors as anticancer agents. Eur J Med Chem 2020;**203**:112571 doi: 10.1016/j.ejmech.2020.112571 .

40. Anttila MA, Tammi RH, Tammi MI, Syrjanen KJ, Saarikoski SV, Kosma VM. High levels of stromal hyaluronan predict poor disease outcome in epithelial ovarian cancer. Cancer Res 2000;**60**(1):150-5
41. Delpech B, Girard N, Bertrand P, Courel MN, Chauzy C, Delpech A. Hyaluronan: fundamental principles and applications in cancer. J Intern Med 1997;**242**(1):41-8 doi: 10.1046/j.1365-2796.1997.00172.x .
42. Naor D, Sionov RV, Ish-Shalom D. CD44: structure, function, and association with the malignant process. Adv Cancer Res 1997;**71**:241-319 doi: 10.1016/s0065-230x(08)60101-3 .
43. Shao JH, Cui Y, Zhao MY, Wu CF, Liu YF, Zhang JH. Purification, characterization, and bioactivity of a new analgesic-antitumor peptide from Chinese scorpion Buthus martensii Karsch. Peptides 2014;**53**:89-96 doi: 10.1016/j.peptides.2013.10.023 .
44. Catterall WA. Binding of scorpion toxin to receptor sites associated with sodium channels in frog muscle. Correlation of voltage-dependent binding with activation. J Gen Physiol 1979;**74**(3):375-91 doi: 10.1085/jgp.74.3.375 .
45. Zhao Y, Cai X, Ye T, et al. Analgesic-antitumor peptide inhibits proliferation and migration of SHG-44 human malignant glioma cells. J Cell Biochem 2011;**112**(9):2424-34 doi: 10.1002/jcb.23166 .
46. Edlich F. BCL-2 proteins and apoptosis: Recent insights and unknowns. Biochem Biophys Res Commun 2018;**500**(1):26-34 doi: 10.1016/j.bbrc.2017.06.190 .
47. Yglesias AS, H.; Diaz Garcia, A.; Garrudi, G. Synergistic effect of Rhopalurus junceus scorpion venom combined with conventional cytostatics in cervical cancer cell line HeLa. J. Pharm Pharmacogn 2019;**7**(1):10
48. Sasi N, Hwang M, Jaboin J, Csiki I, Lu B. Regulated cell death pathways: new twists in modulation of BCL2 family function. Mol Cancer Ther 2009;**8**(6):1421-9 doi: 10.1158/1535-7163.MCT-08-0895 .
49. Poliseno L, Bianchi L, Citti L, et al. Bcl2-low-expressing MCF7 cells undergo necrosis rather than apoptosis upon staurosporine treatment. Biochem J 2004;**379**(Pt 3):823-32 doi: 10.1042/BJ20031538 .
50. Diaz-Garcia A, Ruiz-Fuentes JL, Rodriguez-Sanchez H, Fraga Castro JA. Rhopalurus junceus scorpion venom induces apoptosis in the triple negative human breast cancer cell line MDA-MB-231. J Venom Res 2017;**8**:9-13
51. Diaz-Garcia A, Pimentel Gonzalez G, Basaco Bernabeu T, et al. Pharmacokinetics and Biodistribution of Rhopalurus junceus Scorpion Venom in Tumor-Bearing Mice after Intravenous and Oral Administration. Iran Biomed J 2019;**23**(4):287-96
52. Das Gupta S, Debnath A, Saha A, et al. Indian black scorpion (Heterometrus bengalensis Koch) venom induced antiproliferative and apoptogenic activity against human leukemic cell lines U937 and K562. Leuk Res 2007;**31**(6):817-25 doi: 10.1016/j.leukres.2006.06.004 .
53. D'Arcy MS. Cell death: a review of the major forms of apoptosis, necrosis and autophagy. Cell Biol Int 2019;**43**(6):582-92 doi: 10.1002/cbin.11137 .
54. Olvera F, Rosales A, Olvera A, et al. An efficient approach to clone and express active Neopladine 2, an anticancer peptide from Tityus discrepans scorpion venom. Process Biochemistry 2016;**51**(5):624-31 doi: 10.1016/j.procbio.2016.02.013 .
55. Veiseh M, Gabikian P, Bahrami SB, et al. Tumor paint: a chlorotoxin:Cy5.5 bioconjugate for intraoperative visualization of cancer foci. Cancer Res 2007;**67**(14):6882-8 doi: 10.1158/0008-5472.CAN-06-3948 .
56. Weller M, Wick W, Aldape K, et al. Glioma. Nat Rev Dis Primers 2015;**1**:15017 doi: 10.1038/nrdp.2015.17 .
57. Li YJ, Ji YH. Binding characteristics of BmK I, an alpha-like scorpion neurotoxic polypeptide, on cockroach nerve cord synaptosomes. J Pept Res 2000;**56**(4):195-200 doi: 10.1034/j.1399-3011.2000.00750.x .
58. Li Y-J, Liu Y, Ji Y-H. BmK AS: New scorpion neurotoxin binds to distinct receptor sites of mammal and insect voltage-gated sodium channels. Journal of Neuroscience

650 Research 2000;**61**(5):541-48 doi: 10.1002/1097-4547(20000901)61:5<541::Aid-
651 jnr9>3.0.Co;2-# .
652 59. Tong Q-C, Zhang Y, Li D-P, Zhou Z-N, Ji Y-H. The blocking effect of BmP02, one novel
653 short-chain scorpion peptide on transient outward K+ channel of adult rat ventricular
654 myocyte. Regulatory Peptides 2000;**90**(1-3):85-92 doi: 10.1016/s0167-
655 0115(00)00116-6 .
656 60. Tan Z-Y, Xiao H, Mao X, Wang C-Y, Zhao Z-Q, Ji Y-H. The inhibitory effects of BmK IT2,
657 a scorpion neurotoxin on rat nociceptive flexion reflex and a possible mechanism for
658 modulating voltage-gated Na+ channels. Neuropharmacology 2001;**40**(3):352-57 doi:
659 10.1016/s0028-3908(00)00168-4 .
660 61. Ji Y-H, Wang W-X, Wang Q, Huang Y-P. The binding of BmK abT, a unique neurotoxin,
661 to mammal brain and insect Na+ channels using biosensor. European Journal of
662 Pharmacology 2002;**454**(1):25-30 doi: 10.1016/s0014-2999(02)02363-4 .
663 62. El-Ghlban S, Kasai T, Shigehiro T, et al. Chlorotoxin-Fc fusion inhibits release of MMP-2
664 from pancreatic cancer cells. Biomed Res Int 2014;**2014**:152659 doi:
665 10.1155/2014/152659 .
666 63. Cohen G, Burks SR, Frank JA. Chlorotoxin-A Multimodal Imaging Platform for Targeting
667 Glioma Tumors. Toxins (Basel) 2018;**10**(12) doi: 10.3390/toxins10120496 .
668 64. Mamelak AN, Jacoby DB. Targeted delivery of antitumoral therapy to glioma and other
669 malignancies with synthetic chlorotoxin (TM-601). Expert Opin Drug Deliv
670 2007;**4**(2):175-86 doi: 10.1517/17425247.4.2.175 .
671 65. Sun C, Fang C, Stephen Z, et al. Tumor-targeted drug delivery and MRI contrast
672 enhancement by chlorotoxin-conjugated iron oxide nanoparticles. Nanomedicine
673 (Lond) 2008;**3**(4):495-505 doi: 10.2217/17435889.3.4.495 .
674 66. Stroud MR, Hansen SJ, Olson JM. In vivo bio-imaging using chlorotoxin-based conjugates.
675 Curr Pharm Des 2011;**17**(38):4362-71 doi: 10.2174/138161211798999375 .
676 67. Kittle DS, Mamelak MDA, Parrish-Novak JE, et al. Fluorescence-guided Tumor
677 Visualization Using the Tumor Paint BLZ-100. Cureus 2014 doi: 10.7759/cureus.210 .
678 68. Fidel J, Kennedy KC, Dernell WS, et al. Preclinical Validation of the Utility of BLZ-100 in
679 Providing Fluorescence Contrast for Imaging Spontaneous Solid Tumors. Cancer Res
680 2015;**75**(20):4283-91 doi: 10.1158/0008-5472.CAN-15-0471 .
681 69. Parrish-Novak J, Byrnes-Blake K, Lalayeva N, et al. Nonclinical Profile of BLZ-100, a
682 Tumor-Targeting Fluorescent Imaging Agent. Int J Toxicol 2017;**36**(2):104-12 doi:
683 10.1177/1091581817697685 .
684 70. Kobets AJ, Nauen D, Lee A, Cohen AR. Unexpected Binding of Tozuleristide "Tumor
685 Paint" to Cerebral Vascular Malformations: A Potentially Novel Application of
686 Fluorescence-Guided Surgery. Neurosurgery 2021;**89**(2):204-11 doi:
687 10.1093/neuros/nyab106 .
688 71. Gordon I, Paoloni M, Mazcko C, Khanna C. The Comparative Oncology Trials Consortium:
689 using spontaneously occurring cancers in dogs to inform the cancer drug development
690 pathway. PLoS Med 2009;**6**(10):e1000161 doi: 10.1371/journal.pmed.1000161.
691 72. Paoloni MC, Khanna C. Comparative oncology today. Vet Clin North Am Small Anim Pract
692 2007;**37**(6):1023-32 doi: 10.1016/j.cvsm.2007.08.003 .
693 73 Yamada, M. Yamada M, Miller DM, Lowe M, Rowe C, Wood D, Soyer HP, Byrnes-Blake
694 K, Parrish-Novak J, Ishak L, Olson JM, Brandt G, Griffin P, Spelman L, Prow TW.
695 (2021) A first-in-human study of BLZ-100 (tozuleristide) demonstrates tolerability and
696 safety in skin cancer patients. *Contemp Clin Trials Commun*. 2021 Aug 4;23:100830,
697 1-6. doi: 10.1016/j.conctc.2021.100830.

Figure

Click here to access/download;Figure;Arcos et al - Figure 1.tif